Experimental and Analytical Study of Concrete Structures Reinforced With GFRP Bars

DOCTORAL THESIS

Patrícia Carlota Costa Escórcio
DOCTORATE IN CIVIL ENGINEERING

UNIVERSIDADE da MADEIRA
A Nossa Universidade
www.uma.pt

March | 2015

Experimental and Analytical Study of Concrete Structures Reinforced With GFRP Bars

DOCTORAL THESIS

Patrícia Carlota Costa Escórcio
DOCTORATE IN CIVIL ENGINEERING

SUPERVISOR
Paulo Miguel Macedo França

Title: Experimental and Analytical Study of Concrete Structures Reinforced With GFRP Bars

Keywords: Full-scale beams; GFRP bars; GFRP shear reinforcement; GFRP bent bar; GFRP stirrups; GFRP double headed bars; shear behaviour; flexural behaviour; rehabilitation solution; finite element model

Author: Patrícia Carlota Costa Escórcio

UMa – University of Madeira
FCEE – Faculty of Exact Sciences and Engineering
Campus Universitário da Penteada
9020-105 Funchal – Portugal
Telephone +351 291 705 000

Jury:

Chairperson:	Doctor Maria Teresa Alves Homem Gouveia, President of the Faculty of Exact Sciences and Engineering of Universidade da Madeira
Members of the Committee:	Doctor José Manuel Matos Noronha da Câmara, Associate Professor in IST, Lisboa
	Doctor João Pedro Ramôa Ribeiro Correia Associate Professor in IST, Lisboa
	Doctor José Manuel da Sena Cruz, Associate Professor in Universidade do Minho
	Doctor Paulo Miguel Macedo de França, Assistent Professor in Universidade da Madeira, Madeira

Defence on 8th July of 2016

Funchal, Portugal

“There is gold, and a multitude of rubies: but the lips of knowledge are a precious jewel.”

Proverbs 20:15

Acknowledgments

I would like to start by expressing my gratitude to my family, in general, and to my parents, in particular, for having me, for believing in me and for all the support and understanding, which were essential for the progress of the present work. To my sister Filipa for her support. A special acknowledgement to my grandparents, in particular to Carlota, Inês and Teresa for enriching my childhood and my life. To Jose, my uncle, for the help with the experimental work.

To my supervisor, the Professor Paulo Macedo França, I express my gratitude for the huge effort to make this research work possible, for his availability, for the several interesting discussions, ideas and suggestions, and for the support, guidance and friendship.

The experimental campaign of the present work was entirely carried out at the civil engineering laboratory of Madeira Island (LREC). I gratefully acknowledge this institution in general for providing the necessary equipment and manpower and, in particular, its Regional Director at the time this work was performed, the Professor Paulo Macedo França (my supervisor), for providing the clearance for all the necessary means to be at my disposal, and for all the authorizations to adjust the laboratory for the tests, including the demolition of a wall to facilitate the manoeuvres of the 1 ton full-scale specimens. Additionally, the contributions of the engineers and the lab technicians are appreciated.

I would like to acknowledge all the companies that provided equipment and materials. Among them, I would like to express my gratitude to Schöck Ltd for the support of 50% of the GFRP bars used in this work, to *Beto Madeira* and *Cimentos Madeira* for providing all the concrete used in the tests, to *Labirinto dos Talentos* for the help on making the metallic structure for the tests and to *Construmadeira* for the availability.

My gratitude to the University of Madeira in general for affording me the opportunity to make this research work, and in particular to Professor José do Carmo for all the support. I am also grateful to my colleagues and friends, in particular, to João Gonçalves and Luís Correia for the help and the interesting discussions.

I also would like to thank to Filipe Gonçalves, for his availability, rapid response and for the effort in reviewing the English writing. Finally, I also would like to thank all the anonymous reviewers of the scientific papers for their contribution to enhance the final version of this work.

Abstract

The rational use of natural, economic and social resources in order to ensure the sustainability and a long-term balance has become one of the largest global concerns. In the civil engineering field, the limited durability of steel reinforced concrete structures, especially in aggressive environments, and the high costs of the repair and maintenance operations have motivated the search for alternative materials and solutions to steel. One of these alternative reinforcements is the glass fibre reinforced polymer (GFRP) bars due to their immunity to corrosion, which is an important advantage when comparing to steel. However, several factors such as the novelty in the market, the high fabrication costs, the different design philosophies and the uncertainties of its behaviour with the concrete have been delaying the use of the GFRP bars in a larger scale.

This thesis aims to contribute to the scientific knowledge of the GFRP reinforced concrete, as it studies its behaviour and design. The research work is mainly experimental and is based on a campaign with 24 full-scale reinforced concrete (RC) beams 4.30 m long and rectangular cross-section of 0.25 x 0.40 m^2, divided into two groups with different purposes:

- 18 beams to study the performance of different GFRP bar layouts as shear reinforcement;
- 6 beams to assess the behaviour of a rehabilitation solution with GFRP bars to replace the deteriorated flexural steel reinforcement.

The specimens of the first group were designed to fail due to shear with four different GFRP shear reinforcement solutions: 1) closed hoop GFRP stirrups, 2) two C shaped GFRP bars forming a stirrup, 3) two double headed GFRP bars and 4) two simple straight GFRP bars. Two shear reinforcement ratios with different spacing were also tested with the closed hoop GFRP stirrups. For each GFRP shear reinforcement layout, three different longitudinal stiffnesses were considered using steel and GFRP bars with different ratios. The beam specimens were tested until failure under a four point loading set-up and both the serviceability and the ultimate performance were analysed. The results were reported in terms of deflections, crack pattern, crack width, strains in the longitudinal and shear reinforcements, ultimate load capacity and failure modes. The different shear layouts were compared regarding their load carrying performance and their field implementation easiness. The design of the beams and their result predictions were made according to the existing guidelines and codes. It was concluded that the closed hoop stirrups and the C-stirrups were the most efficient and that the beams load capacity was highly underestimated by the GFRP codes. To improve the design formulas of these codes, different values for the limit strains and for the strut angle were

proposed. The double headed bars as shear reinforcement were also efficient in the cases with higher longitudinal stiffness because it contributed to keep the integrity of the beam by exhibiting low deflections and crack widths. It was observed that a wide crack at the end of these bars highly compromises the anchorage function of the head. The solution of the simple straight bars was not effective because of the lack of anchorage length.

The idea for the second group of beams was inspired on the RC structures with deteriorated bottom concrete due to the corrosion of the longitudinal steel reinforcement. Actually, no steel corrosion was considered in these specimens, but they were concreted in two phases to simulate the replacement of the deteriorated concrete, starting at the stage after its complete removal. The rehabilitation procedure consisted on the insertion of the longitudinal GFRP bars and the concreting of a new bottom layer in the beam. Two solutions with different GFRP longitudinal cross-section areas were designed according to the existing guidelines, one to restore the ultimate load capacity of the original beam, and the other to maintain the deflection of the original beam. The ends of the GFRP bars were conic heads to compensate their lower anchorage length. The rehabilitated beam specimens were subjected to 3 point bending tests until failure, and their service and ultimate behaviour were analysed. Results are presented in terms of deflection, crack pattern, mid-span crack width, reinforcement strains, ultimate flexural capacity and failure modes. It was concluded that this technique was effective for both the serviceability and ultimate limit states of the rehabilitated beam, as it was able to restore the deflection and the load capacity of the original beam, and that the existing GFRP design documents can be used.

Although this was mainly an experimental research work, a simple but reliable two-dimensional finite element (FE) model was defined using ATENA software to simulate the tests, which helped to better understand some issues regarding the specimens behaviour and enabled to extrapolate some results of non-tested possibilities. The linear and nonlinear behaviour of all materials was adequately modelled by appropriate constitutive laws. Furthermore, numerical results were compared with the experimental results. Results show that, in general there was a good agreement between the overall modelling results and the experimental ones. The constructed models were able to predict the experimental behaviour in terms of ultimate capacity and load-deflection curves.

Regarding the first group of beams, two additional stirrups spacing were modelled in order to clarify its influence in the shear capacity. It was simulated different longitudinal reinforcement ratios to assess its influence in the shear capacity.

As a final remark, the results of the present work show that the use of GFRP bars is viable in RC structures, which contributes to more durable structures in long-term. This material can be used as

longitudinal and shear reinforcement of new structures and as a rehabilitation solution to replace the corroded steel in deteriorated structures.

Key words:

Full-scale beams; GFRP bars; GFRP shear reinforcement; GFRP bent bar; GFRP stirrups; GFRP double headed bars; shear behaviour; flexural behaviour; rehabilitation solution; finite element model.

Resumo

O uso racional dos recursos naturais, económicos e sociais, para assegurar a sustentabilidade e o equilíbrio a longo prazo, tornou-se numa das maiores preocupações globais. No domínio da Engenharia Civil, a durabilidade limitada das estruturas de betão com aço, em especial em ambientes agressivos, e os custos elevados das operações de reparação e de manutenção, motivaram a procura de materiais e soluções alternativas ao aço. Uma dessas alternativas são varões de FRP (*Fibre Reinforced Polymer*) devido à sua resistência à corrosão, que é uma vantagem importante destes materiais comparativamente ao aço. No entanto, a coexistência de vários fatores, tais como a novidade no mercado, os elevados custos no seu fabrico, diferentes filosofias de dimensionamento e as incertezas relativas ao seu comportamento no betão armado, têm atrasado o seu uso como armaduras em grande escala.

Este trabalho visa contribuir para o conhecimento científico do betão armado com varões GFRP (*Glass Fibre Reinforced Polymer*) estudando o seu comportamento e dimensionamento. O trabalho de investigação é maioritariamente experimental e é baseado numa campanha experimental com 24 vigas de betão armado à escala real, de secção retangular com 0,25 x 0,40 m^2 e com 4,30 m de comprimento, divididas em dois grupos com propósitos diferentes:

- 18 vigas para estudar o desempenho de diferentes soluções com varões de GFRP como armaduras de esforço transverso;
- 6 vigas para avaliar o comportamento de uma solução de reabilitação com varões de GFRP a substituir a armadura longitudinal de aço deteriorada.

Os provetes do primeiro grupo foram dimensionados para a rotura ao corte e foram consideradas quatro soluções diferentes: 1) estribos fechados em GFRP, 2) estribos fechados formados a partir de dois varões de GFRP com a forma de C, 3) dois varões de GFRP retos com cabeça de ancoragem, 4) dois varões de GFRP retos simples. Na solução com estribos fechados de GFRP, duas percentagens de armadura transversal, pela variação do espaçamento, foram também testadas. Para cada solução de armadura transversal de GFRP, foram consideradas três rigidezes longitudinais diferentes. As vigas foram testadas até a rotura com quatro pontos de carga e foram avaliados, quer o comportamento em serviço quer a capacidade última. Os resultados foram relatados em termos de deformações, padrão de fendilhação, aberturas de fendas, extensões na armadura longitudinal e de esforço transverso, capacidade de carga e modos de rotura. A comparação entre as diferentes soluções de armadura transversal em GFRP foi feita relacionando

a facilidade de execução e implementação em obra com o desempenho em termos de capacidade de carga. O dimensionamento das vigas e as previsões dos seus resultados foram feitos de acordo com os regulamentos e códigos de dimensionamento existentes. Concluiu-se que os estribos fechados de GFRP e os estribos formados com os dois varões de GFRP em C foram os mais eficientes e, para esses casos, a capacidade de carga foi muito subestimada pelos principais códigos de dimensionamento. Para diminuir a subestimação, foi proposta uma modificação aos valores das extensões limite e do ângulo da escora de betão propostos pelos principais códigos. A solução com os dois varões com cabeça de ancoragem como armadura de esforço transverso foi eficiente nos casos em que a rigidez longitudinal permitiu à viga manter a integridade por apresentar deformações e abertura de fendas pequenas. Observou-se que uma fenda no lugar certo pode comprometer a função da cabeça de ancoragem e causar o escorregamento do varão. A solução de varões retos simples não foi eficaz por falta de comprimento de amarração.

A ideia para o segundo grupo de vigas foi inspirada nas estruturas de betão armado com camada inferior de betão deteriorada devido à corrosão do aço da armadura longitudinal. Na verdade, não se considerou a corrosão do aço nos provetes mas as vigas foram betonadas em duas fases para simular a substituição do betão deteriorado, começando na etapa a seguir à completa remoção desta. O processo de reabilitação consistiu na inserção de varões longitudinais de GFRP e na betonagem de uma camada na zona inferior da viga. Foram executadas duas soluções com varões longitudinais de GFRP com áreas transversais diferentes, dimensionados de acordo com os regulamentos existentes, uma para restaurar a capacidade última das vigas de referência e outra para manter a flecha das vigas de referência. As terminações dos varões de GFRP foram constituídas por cabeças cónicas usadas para compensar o menor comprimento de ancoragem. As vigas reabilitadas foram testadas à flexão com três pontos de carga e o seu comportamento em serviço e último foi analisado. Os resultados foram apresentados em termos de flechas, desenvolvimento da fendilhação, largura de fendas a meio vão, extensões nos varões longitudinais, capacidade última e modos de rotura. Foi concluído que a técnica de reabilitação apresentada é efetiva quer do ponto de vista do comportamento em serviço quer em estado limite último, tendo capacidade para restaurar os níveis de deformação e capacidade de carga da viga de referência, e que os códigos gerais de dimensionamento com GFRP podem ser aplicados.

Apesar de este estudo incidir sobretudo num trabalho de investigação experimental definiu-se um modelo simples bidimensional de elementos finitos (FE) com recurso ao software ATENA que permitiu compreender algumas questões sobre o comportamento das vigas que surgiram durante os testes e extrapolar alguns resultados de soluções não testadas possíveis. O comportamento linear e não-linear de todos os materiais foi modelado adequadamente por relações constitutivas

apropriadas. Além disto, os resultados numéricos foram comparados com os resultados experimentais e com as previsões dos códigos de dimensionamento. Os resultados mostraram que em geral houve uma boa concordância entre os resultados da modelação e os experimentais. Os modelos construídos permitiram a previsão do comportamento experimental em termos de capacidade última e das curvas de carga-deformação.

Em relação ao primeiro grupo de vigas, dois outros espaçamentos da armadura transversal foram também modelados para clarificar a influência na capacidade ao corte. Foram simulados diferentes percentagens de armadura longitudinal para analisar a sua relação com a capacidade ao corte.

Uma solução de reabilitação adicional foi simulada, considerando um aumento da altura total da viga de forma a obter-se os níveis de deformação das vigas de referência mas considerando apenas a armadura longitudinal em GFRP necessária para se obter a mesma capacidade resistente da viga de referência.

Como observação final, os resultados mostraram que a aplicação de varões de GFRP é fiável em estruturas de betão armado, o que contribui para estruturas com maior durabilidade a longo prazo. Este material pode ser usado como armadura longitudinal e de corte de novas estruturas, ou mesmo em soluções de reabilitação como substituição da armadura em aço corroída em estruturas deterioradas.

Palavras-chave:

Viga à escala real; varão de GFRP; armadura de esforço transverso em GFRP; varão dobrado de GFRP; estribo de GFRP; varão de GRP com cabeça de ancoragem; comportamento ao corte; comportamento à flexão; solução de reabilitação; corrosão; modelo de elementos finitos.

Contents

Acknowledgments ..... **iii**

Abstract ..... **v**

Resumo ..... **ix**

Contents ..... **xiii**

List of figures ..... **xix**

List of tables ..... **xxvii**

Notation ..... **xxxi**

1. Introduction **1**

1.1 The FRP material and the GFRP bars **1**

1.2 Scope, motivations and objectives **6**

1.3 Organization of the thesis **8**

1.4 List of the intended publications **9**

1.5 Original contributions **11**

2. Study of GFRP shear reinforced concrete beams **13**

2.1 Experimental programme **16**

2.1.1 Material properties 16

2.1.1.1 Concrete 16

2.1.1.2 Steel 17

2.1.1.3 GFRP 18

2.1.2 Test set-up 21

2.1.2.1 Beams specimens 21

2.1.2.2 Instrumentation 25

2.1.2.3 Loading History 27

2.2 Performance of four different GFRP shear reinforcement solutions in reinforced concrete beams 28

2.2.1 Results and discussion 28

2.2.1.1 Ultimate capacity 29

2.2.1.2 Cracking pattern 32

2.2.1.3 Failure modes 34

2.2.1.4 Mid-span deflection 38

2.2.1.5 Reinforcement strains 40

2.2.1.6 Shear crack width 45

2.2.2 Conclusions 45

2.3 Experimental analysis of different GFRP transverse reinforcement solutions in reinforced concrete beams with GFRP longitudinal bars 48

2.3.1 Results and discussion 49

2.3.1.1 Ultimate capacity 49

2.3.1.2 Cracking pattern and failure modes 52

2.3.1.3 Mid-span defection 58

2.3.1.4 Reinforcement strains 60

2.3.2 Conclusions 66

2.4 Influence of the GFRP longitudinal bar ratio on the behaviour of reinforced concrete beams with GFRP shear reinforcement 68

2.4.1 Results and discussion 69

2.4.1.1 Ultimate capacity 69

2.4.1.2 Cracking pattern 74

2.4.1.3 Failure modes 77

2.4.1.4 Deflection 82

2.4.1.5 Reinforcement strains 85

2.4.1.6 Shear crack width 89

2.4.2 Conclusions 90

2.5 Experimental performance comparison of reinforced concrete beams with different GFRP transverse reinforcement solutions and different longitudinal bar material and ratios 92

2.5.1 Results and discussion 93

2.5.1.1 Ultimate capacity 93

2.5.1.2 Cracking pattern 101

2.5.1.3 Failure modes 105

2.5.1.4 Deflection 108

2.5.1.5 Deflection at mid-span 108

2.5.1.6 Reinforcement strains 111

2.5.1.7 Shear crack width 117

2.5.2 Conclusions 118

2.6 Effect of the longitudinal stiffness on the performance of reinforced concrete beams with GFRP stirrups spaced between d/2 and d 121

2.6.1 Results and discussion 121

2.6.1.1 Capacity and mode of failure 122

2.6.1.2 Deflection 124

2.6.1.3 Flexural strains 124

2.6.1.4 Strain in stirrups 124

2.6.2 Comparison of experimental results and predicted capacity 125

2.6.2.1 Shear capacity 125

2.6.2.2 Maximum spacing of stirrups 127

2.6.3 Conclusions 127

2.7 Influence of the shear reinforcement ratio and the longitudinal stiffness on the behaviour of reinforced concrete beams with GFRP stirrups 128

2.7.1 Results and discussion 129

2.7.1.1 Ultimate capacity 129

2.7.1.2 Failure modes 135

2.7.1.3 Mid-span deflection 142

2.7.1.4 Reinforcement strains 144
2.7.1.5 Cracking behaviour 148
2.7.1.6 Shear crack widths 151
2.7.2 Conclusions 152
3. Experimental study of a solution that uses GFRP bars to replace the steel bars of reinforced concrete beams 155
3.1 Introduction 156
3.2 Experimental program 159
3.2.1 Material properties 160
3.2.1.1 Concrete 160
3.2.1.2 Steel reinforcement bars 161
3.2.1.3 GFRP reinforcement bars 162
3.2.1.4 Filling resin for the anchorage of the reinforcement in the rehabilitation beams 165
3.2.2 Test set-up 165
3.2.2.1 Beam specimens 165
3.2.2.2 Tests instrumentation 168
3.2.2.3 The production of the beam specimens and the rehabilitation procedure 170
3.2.2.4 Tests loading history 172
3.2.3 Results and discussion 173
3.2.3.1 Theoretical predictions 173
3.2.3.2 Cracking moment 173
3.2.3.3 Flexural capacity 174
3.2.3.4 Deflection 176
3.2.3.5 Mid-span strain 176
3.2.4 Experimental results 176
3.2.4.1 Cracking moment and deflection at service load 176
3.2.4.2 Flexural capacity and failure modes 178

3.2.4.3 Tensile reinforcement strain 186
3.2.4.4 Deflection behaviour 189
3.2.4.5 Crack development 191
3.2.4.6 Mid-span crack width 192
3.3 Conclusions 194
4. Numerical Simulation 197
4.1 Non-linear finite element program, ATENA 197
4.2 Reinforced concrete beams with GFRP shear reinforcement 200
4.2.1 Simulation of tested beams 200
4.2.2 Parametric study 208
4.2.2.1 Beam reinforced with 8 mm GFRP stirrups 209
4.2.2.2 Shear reinforcement ratio 210
4.2.2.3 Longitudinal reinforcement ratio 210
4.3 GFRP longitudinally rehabilitated beams 212
4.4 Conclusions 215
5. Conclusions, final remarks and future research 217
5.1 Conclusions 217
5.2 Final remarks 221
5.3 Future Research 221
References 223

List of figures

Figure 1 – GFRP straight bars: a) each diameter sample; b) Pure tension test set-up 19
Figure 2 - Stress-strain diagram of the tested samples of GFRP bars [43] 20
Figure 3 - Tests set-up and instrumentation scheme: a) Beam specimens with stirrups spaced at 0.175 m; b) beams specimens with stirrups spaced at 0.250 m 21
Figure 4 – Cross-section of the beams specimens 22
Figure 5 – GFRP shear reinforcement proposed and tested solutions 23
Figure 6 – LVDTs scheme during tests 26
Figure 7 – Positioning of the LVDTs: a) front view; b) side view 26
Figure 8 – Instrumentation used in the tests: a) Lens used for the crack width measure; b) Load-cell; c) LVDT 27
Figure 9 – Cracking pattern at failure of: a) REF250; b) REFB250 33
Figure 10 – Cracking pattern at failure: a) BS250; b) BC250 33
Figure 11 – Cracking pattern at failure: a) BB250; b) BDHB250 33
Figure 12 – REF250 beam failure: a) front view of the support; b) overall view of the failure; c) bottom reinforcement; d) broken stirrup 35
Figure 13 – REFB250 beam failure: a) overall view of one of the sides of the support; b) overall view of the other side of the support; c) slip of stirrup; d) slip of stirrup 35
Figure 14 – BB250 beam failure: a) overall view of one side of the support; b) overall view of the other side of the support; c) pull-out of the shear reinforcement in compression zone; d) pull out of the shear reinforcement in bottom zone 36
Figure 15 – BDHB250 beam failure: a) overall view; b) view near the support; c) pull-out of longitudinal reinforcement; d) fractured lower head 36
Figure 16 – BC250 beam failure: a) overall view; b) mid-span; c) top of mid-span; d) disintegration of mid-span stirrup 37
Figure 17 – BS250 beam failure: a) overall view from one side; b) overall view from the other side; c) mid-span; d) top of mid-span 38
Figure 18 - Load-deflection curves 39
Figure 19 - Strain of tensile reinforcement: a) REF250; b) REFB250 40
Figure 20 -Strain of tensile reinforcement: a) BS250; b) BC250; c) BDHB250; d) BB250 41
Figure 21 – Comparison of strains 42
Figure 22 - Distribution of strains in the shear span of: a) REF250; b) REFB250 43

Figure 23 – Distribution of strains in the shear span of: a) BS250; b) BC250 43
Figure 24 - Distribution of strains in the shear span of: a) BB250; b) BDHB250 44
Figure 25 – Width of shear cracks 45
Figure 26 – Cracking pattern until failure of: a) REF250; b) REFB250 52
Figure 27 – Cracking pattern of: a) BS250GFRP1; b) BC250GFRP1 53
Figure 28 – Cracking pattern of: a) BDHB250GFRP1; b) BB250GFRP1 53
Figure 29 – REF250 beam failure: a) front view of the support; b) overall view of the failure; c) bottom reinforcement; d) broken stirrup 54
Figure 30 – REFB250 beam failure: a) overall view of one of the sides of the support; b) overall view of the other side of the support; c) slip of stirrup; d) slip of stirrup 55
Figure 31 – BB250GFRP1 beam failure: a) overall view of the failure; b) other side; c) pull-out of the shear reinforcement at the bottom; d) bottom longitudinal reinforcement pull-out 56
Figure 32 – BDHB250GFRP1 beam failure: a) overall view near the support; b) fractured top and bottom heads; c) bottom reinforcement pull-out; d) detachment of the section near the bottom reinforcement 57
Figure 33 – BC250GFRP1 beam failure: a) overall view; b) near the support; c) stirrup disintegration; d) pull-out of bottom reinforcement 57
Figure 34 – BS250GFRP1 beam failure: a) overall view; b) near the support; c) crushing of concrete under the loading point; d) slip of longitudinal reinforcement near the support 58
Figure 35 - Load-deflection curves GFRP 2φ16+2φ25 reinforced beams 59
Figure 36 - Strain of tensile reinforcement: a) REF250; b) REFB250 61
Figure 37 – Strain of tensile reinforcement: a) BS250GFRP1; b) BC250GFRP1; c) BDHB250GFRP1; d) BB250GFRP1 62
Figure 38 – Comparison of the strains of most stressed stirrup of each beam specimen 63
Figure 39 – Distribution of strains along the shear span of: a) REF250; b) REFB250 63
Figure 40 – Distribution of the strains along the shear span of: a) BS250GFRP1; b) BC250GFRP1 . 64
Figure 41 – Distribution of the strains along the shear span of: a) BB250GFRP1; b) BDHB250GFRP1 65
Figure 42 – Variation of the shear crack width with the load 66
Figure 43 - Comparison between the experimental and the predicted values for the parameter k72
Figure 44 – Cracking pattern of: a) REF250; b) REFB250. 74
Figure 45 – Cracking pattern of: a) BS250GFRP1; b) BC250GFRP1 75
Figure 46 – Cracking pattern of: a) BS250GFRP2; b) BC250GFRP2 75
Figure 47 – Cracking pattern of: a) BDHB250GHFRP1; b) BB250GFRP1 76

Figure 48 - Cracking pattern of: a) BDHB250GFRP2; b) BB250GFRP2 76
Figure 49 – REF250 beam failure: a) front view of the support; b) broken stirrup 78
Figure 50 – REFB250 beam failure: a) overall view of one of the sides of the support; b) slip of stirrup 78
Figure 51 – BC250GFRP1 beam failure: a) overall view near the support; b) stirrup disintegration 79
Figure 52 – BDHB250GFRP1 beam failure: a) overall view near the support; b) fractured top and bottom heads 79
Figure 53 – BDHB250GFRP2 beam failure: a) overall view; b) fractured head 79
Figure 54 – BB250GFRP1 beam failure: a) overall view of the failure; b) pull-out of the shear reinforcement at the bottom 80
Figure 55 – BB250GFRP2 beam: a) overall view of the support; b) crushing of the concrete rod; d) pull-out of the shear reinforcement on the top 80
Figure 56 – BS250GFRP2 beam failure: a) overall view o from one side of the support; b) overall view from the other side of the support 81
Figure 57 – BC250GFRP2 beam failure: a) one side of the support; b) stirrups disintegration 81
Figure 58 – BS250GFRP1 beam failure: a) overall view near the support; b) slip of longitudinal reinforcement near the support 82
Figure 59 – Load-deflection curves at mid-span: a) BS group beams; b) BC group beams; c) BB group beams; d) BDHB group beams 83
Figure 60 – Load deflection curves at mid-span deflection: a) in the GFRP1 beams; b) in the GFRP2 beams 84
Figure 61 - Strain of tensile reinforcement: a) REF250; b) REFB250 86
Figure 62 – Strain of tensile reinforcement: a) BS250GFRP1; b) BC250GFRP1; c) BDHB250GFRP1; d) BB250GFRP1 86
Figure 63 - Strain of tensile reinforcement: a) BS250GFRP2; b) BC250GFRP2; c) BDHB250GFRP2; d) BB250GFRP2 87
Figure 64 – Shear reinforcement strains for: a) BS- beams; b) BC- beams; c) BDHB- beams; d) BB-beams 89
Figure 65 – Shear crack width with the loading 90
Figure 66 – Comparison between C-stirrups and closed hoop stirrups: a) C-stirrups horizontal branch opening; C-stirrups disintegration; c) closed hoop stirrups behaviour at failure of one of the beams; d) closed hoop stirrups behaviour at failure 98
Figure 67 – Comparison of the experimental to predictions ratios for different methods 101
Figure 68 – Cracking pattern of: a) REF250; b) REFB250 102

Figure 69 - Cracking pattern of: a) BS250; b) BC250 103
Figure 70 - Cracking pattern of: a) BB250; b) BDHB250 103
Figure 71 - Cracking pattern of: a) BS250GFRP1; b) BC250GFRP1 103
Figure 72 - Cracking pattern of: a) BDHB250GFRP1; b) BB250GFRP1 104
Figure 73 - Cracking pattern of: a) BS250GFRP2; b) BC250GFRP2 104
Figure 74 - Cracking pattern of: a) BDHB250GFRP2; b) BB250GFRP2 104
Figure 75 – Concrete crushing in: a) BS250; b) BC250 105
Figure 76 - Shear diagonal tension failure in: a) REF250; b) REFB250 106
Figure 77 - Shear diagonal tension failure in: a) BB250; b) BDHB250 106
Figure 78 – Shear diagonal tension failure in: a) BDHB250GFRP1; BDHB250GFRP2 106
Figure 79 - Shear diagonal tension failure in: a) BB250GFRP1; b) BB250GFRP2; c) BC250GFRP1 . 107
Figure 80 – Shear failure due to the crushing of the concrete rod: a) BS250GFRP2; b) BC250GFRP2 107
Figure 81 - Shear failure due to the failure of the bond of the longitudinal reinforcement at support of BS250GFRP1 a) overall view; b) slip of the reinforcement at support 107
Figure 82 - Load-deflection curves: a) steel 2φ16+2φ25 reinforced beams; b) GFRP 2φ16+2φ25 reinforced beams; c) GFRP 5φ25 reinforced beams d) average of beams with same longitudinal reinforcement 111
Figure 83 – Longitudinal reinforcement strains at mid-span: a) BS beams; b) BC beams; c) BDHB beams-, d) BB beams 112
Figure 84 – Distribution of the shear reinforcement strain with the loading: a) BS250; b) BC250; c) BDHB250; d) BB250 114
Figure 85 - Distribution of the shear reinforcement strain with the loading: a) BS250GFRP1; b) BC250GFRP1; c) BDHB250GFRP1; d) BB250GFRP1 115
Figure 86 - Distribution of the shear reinforcement strain with the loading: a) BS250GFRP2; b) BC250GFRP2; c) BDHB250GFRP2; d) BB250GFRP2 116
Figure 87 – Maximum shear reinforcement strains development 117
Figure 88 – Variation of the shear crack widths with load 118
Figure 89 – Cracking pattern at failure for test specimens: a) REF250; b) BS250; c) BS250GFRP1; d) BS250GFRP2 122
Figure 90 –Failure of test specimens: a) REF250; b) BS250 123
Figure 91 - Failure of test specimens: a) BS250GFRP1; b) slip of the longitudinal reinforcement in BS250GFRP1; c) stirrups after failure in BS250GFRP1; d) BS250GFRP2 123
Figure 92 - Force-deflection relationship for the tested beams 124

Figure 93 – Development of stirrups strains along the shear span: a) REF250; b) BS250; BS250GFRP1; d) BS250GFRP2 125
Figure 94 – Experimental to predicted ratio according to the several formulations 135
Figure 95 – REF175 beam failure: a) overall view immediately before failure; b) view of the support after failure; c) bottom reinforcement; d) broken stirrup 136
Figure 96 – REF250 beam failure: a) front view of the support; b) overall view of the failure; c) bottom reinforcement; d) broken stirrup 137
Figure 97 – BS175 beam failure: a) view of shear cracks at failure; b) mid-span; c) overall view; d) top of mid-span 137
Figure 98 – BS250 beam failure: a) overall view from one side; b) overall view from the other side; c) mid-span; d) top of mid-span 138
Figure 99 – BS250GFRP1 beam failure: a) shear span before failure; b) overall view before failure; c)overall view after failure; d) shear span after failure; e) shear cracks under loading point; f) slip of longitudinal reinforcement 139
Figure 100 – BS175GFRP1 beam failure: a) overall view before failure; b) shear span before failure; c) shear-span after failure; d) concrete crushing; e) no-slip of longitudinal reinforcement; f) disintegrated stirrup at loading-point 140
Figure 101 – BS250GFRP2 failure: a) overall view before the testing; b) shear-span after failure; c) stirrup disintegration; d) concrete crushing under the loading point 141
Figure 102 – BS175GFRP2 failure: a) shear-span before failure; b) shear-span after failure; c) concrete crushing over the loading point; d) stirrups disintegrated at bottom 141
Figure 103 – Load-deflection curves at mid-span location 143
Figure 104 – Longitudinal reinforcement strains: a) REF250; b) REF175 144
Figure 105 - Longitudinal reinforcement strains: a) BS250; b) BS175 144
Figure 106 – Longitudinal reinforcement strains: a) BS250GFRP1; b) BS175GFRP2 145
Figure 107 – Longitudinal reinforcement strains: a) BS250GFRP2; b) BS175GFRP2 145
Figure 108 – Shear reinforcement strain distribution along shear span of beam BS175GFRP2 ... 147
Figure 109 - Shear reinforcement strain distribution along shear span of beam BS250GFRP2 147
Figure 110 – Strains in shear reinforcement: a) BS250 beams; b) BS175 beams 148
Figure 111 – Cracking pattern of: a) REF250; b) REF175 149
Figure 112 – Cracking pattern of: a) BS250; b) BS175 150
Figure 113 - Cracking pattern of: a) BS250GFRP1; b) BS175GFRP1 151
Figure 114 – Cracking pattern of: a) BS250GFRP2; b) BS175GFRP2 151
Figure 115 – Variation of the shear crack widths with the load 152

Figure 116 – Procedures to simulate real conditions: a) original layer after surface picking and drilled holes; b) filling the holes with resin; c) anchorage areas after reinforcement insertion and the filling of the holes 160
Figure 117 – Sample of GFRP bar with polymeric conic head at the end 162
Figure 118 – Pure tension tests on GFRP bars: a) Solution developed to test GFRP bars in pure tension; b) Test set-up with video extensometer; c) GFRP bar failure 164
Figure 119 - Stress-strain diagram of the tested GFRP bars [43] 165
Figure 120 – Test set-up and specimens configuration 167
Figure 121 –Beam test set-up 169
Figure 122 – Instrumentation used in the tests: a) Lens used for the crack width measure; b) Load-cell; c) LVDT 169
Figure 123 - Steps of the beam specimen production and its rehabilitation procedure: 1 – Concreting of the first layer; 2 – Insertion of the GFRP tension reinforcement; 3 – Concreting of the second layer; 4 – Rotation of the beam 170
Figure 124 - First stage of the specimen's production: a) filling the formworks with concrete until it reaches the tension reinforcement level; b) insertion of the negatives at the supports; c) filling with concrete the support areas 171
Figure 125- Steps of the rehabilitation stage: a) enlargement of the holes, concrete surface pricking and reinforcement insertion; b) and c) sealing of the anchorage holes; d) rehabilitation layer concreting 172
Figure 126 - Ratio between the experimental and the predicted values in function of deflection. Where REF – REF beam; RS – REHABSTEEL; RG1A – REHABGFRP1A; RG1B – REHABGFRP1B; RG2A – REHABGFRP2A; RG2B – REHABGFRP2B 178
Figure 127 - GFRP beams ratio between the experimental and the predicted values as a function of: a) Experimental ultimate moment; b) Design moment 180
Figure 128 –Main cracking at failure: a) REF; b) REHABSTEEL; c) REHABGFRP1A; d) REHABGFRP1B; e) REHABGFRP2A; f) REHABGFRP2B 180
Figure 129 - REF beam failure: a) immediately before; b) after 181
Figure 130 – REHABSTEEL beam failure: a) at mid-span; b) mid-span cross section detail; c) left support; d) right support 182
Figure 131 – REHABGFRP1A beam failure: a) general view; b) mid-span detail; c) left support; d) right support 183
Figure 132 – REHABGFRP1B: a) front general view; b) back general view mid-span detail d) concrete layers detail 183

Figure 133 - REHABGFRP2A: a) general view b) mid-span detail; c) support detail; d) reinforcement slip detail 184
Figure 134 - REHABGFRP2B: a) mid-span detail; b) right support front detail; c) right support back detail; d) left support detail 185
Figure 135 – Bottom reinforcement mean tensile strain of each beam at the supports (end 1 and 2) 186
Figure 136 – Bottom reinforcement mean tensile strain of each beam at the mid-span (ms) 187
Figure 137 – Load-deflection curves at mid-span for all beams 189
Figure 138 - Load-Deflection at mid-span: (a) REF and REHABSTEEL; (b) REHABGFRP1 A and B; (c) REHABGFRP2 A and B 190
Figure 139 - Width progression of the bottom mid-span crack of the beam with load increase.. 193
Figure 140 - a). Variation of mid-span reinforcement strain width the mid-span crack width. b). Variation of mid-span deflection with mid-span crack width 194
Figure 141 – Unixaial stress-strain relationship for concrete [25] 198
Figure 142 – Macro-elements and FE mesh 201
Figure 143 – Load-deflection curves of REF175 202
Figure 144 – Load-deflection curves for REF250 202
Figure 145 – Comparison between the crack patterns obtained in the models near the failure and in the experimental tests: a) REF175; b) REF250 203
Figure 146 – a) REF175 failure; b) Reinforcement stress obtained in the numerical model before the failure 204
Figure 147 – Load-deflection curves of BS175 205
Figure 148 – Load-deflection curves of BS250 205
Figure 149 – Comparison of the FE model and the actual failure of BS175 205
Figure 150 - Comparison of the FE model and the actual failure of BS250 206
Figure 151 – Load deflection curves of BS250GFRP1 206
Figure 152 -– Load deflection curves of BS250GFRP2 207
Figure 153 - - Load deflection curves of BS175GFRP1 207
Figure 154 - Load deflection curves of BS175GFRP2 207
Figure 155 - Behaviour comparison between the REF250 and BS250-8 mm 209
Figure 156 – Comparison between BS150, BS175, BS250 and BS250 210
Figure 157 – Load-displacement curves for different GFRP longitudinal reinforcement ratios 211
Figure 158 – Shear capacity vs. GFRP longitudinal reinforcement ratio 211
Figure 159 – Macro-elements and FE mesh 212

Figure 160 - Behaviour comparison between the REF, REHABSTEEL and the FE model..... 213
Figure 161 - Behaviour comparison between the REHABGFRPGFRP1A, REHABGFRP1B and the FE model..... 213
Figure 162 – FE model crack pattern of REHAB beams..... 213
Figure 163 – Experimental crack pattern of REHAB beams 214
Figure 164 - Behaviour comparison between the REHABGFRP2A, REHABGFRP2B and the FE model 214

List of tables

Table 1 – Composition of concrete 16
Table 2 – Concrete properties 17
Table 3 - Steel reinforcement properties 18
Table 4 – GFRP bars properties according to the producer[84] 19
Table 5 - GFRP bar properties [43] 20
Table 6 – Beams with closed stirrups spaced at 0.250 m reinforcement details 24
Table 7 – Beams with vertical bars spaced at 0.250 m as shear reinforcement details 25
Table 8 – Beams with stirrups spacing of 0.175 m reinforcement details 25
Table 9 – Non-design capacity of all beams specimens 29
Table 10 – Shear design equations of FRP RC beams 30
Table 11 - Non-design values varying the strains and the angle of the strut 31
Table 12 – Summary of experimental and design values of shear capacity 32
Table 13 – Summary of mid-span deflections at service and ultimate loads 40
Table 14 – Summary of ultimate strain values 44
Table 15 – Experimental and non-design theoretical capacities 49
Table 16 – ACI 440.1R-06 [2] and FIB 40 [22] shear design equations 49
Table 17 - Non-design capacity varying the strain limits 51
Table 18 – Summary of experimental and design values of shear capacity 51
Table 19 – Summary of mid-span deflections at service and ultimate loads 60
Table 20 – Summary of ultimate strain values 65
Table 21 – ACI 440.1R-06 [2] and FIB 40 [22] shear design equations 69
Table 22 – Non-design capacity of the beams 70
Table 23 – Summary of experimental and design values of shear capacity 73
Table 24 – Non-design capacity of the beams considering various strains and angle of strut 74
Table 25 – Summary of mid-span deflections at service and ultimate loads 85
Table 26 – Summary of ultimate strain values 87
Table 27 – Shear design equations accordingly to ACI 440.1R-06 [2], JSCE design guidelines[35] and FIB 40 [22] 93
Table 28 – Shear design equations accordingly to CSA S806-02[13]and CSA S6-09 Addendum[65] 94

Table 29 – Shear design equations accordingly to CNR DT-203[27], Fico et al. [35], Nehdi et al. [65], Oller et al.[75] and Schöck [84] 95
Table 30 – Summary of experimental and predicted ultimate shear and bending capacity with ACI 440.1R-06 [2] / ACI 318 -11[3] and EC2 [23]/FIB 40 [22] 96
Table 31 – Non-design capacity of beams in accordance with ACI 440.1R-06[2] and FIB 40[22] varying the strain limit and the angle 99
Table 32 – Ultimate shear capacity accordingly to several models 100
Table 33 – Summary of mid-span deflections at service and ultimate loads 109
Table 34 – Summary of ultimate strain values 113
Table 35 – Summary of test results 122
Table 36 – Shear design equations according to ACI 440.1R-06 [2] and FIB 40 [22] 126
Table 37 – Summary of experimental and predicted ultimate shear and bending capacity with ACI 440.1R-06 [2] / ACI 318-11 [3] and EC2 [23]/FIB 40 [22] 126
Table 38 – Shear design equations according to ACI 440.1R-06 [2], JSCE design guidelines[35] and FIB 40 [22] 129
Table 39 – Shear design equations according to CSA S806-02[13] and CSA S6-09 Addendum[65] 130
Table 40 - Shear design equations according to CNR DT-203[27], Fico et al. [35], Nehdi et al. [65], Oller et al.[75] and Schöck [84] 131
Table 41 – Non-design capacity of the beams 132
Table 42 –Summary of experimental and predicted ultimate shear capacity values 134
Table 43 – Summary of deflection values 143
Table 44 – Summary of strain values 146
Table 45 – Concrete composition according to BETOMADEIRA information 160
Table 46 – Concrete properties 161
Table 47 - Yield stress, tensile strength and elasticity modulus of the steel reinforcement bars . 162
Table 48 – GFRP bars properties according to the producer [85] 163
Table 49 – Dimensions of L-shaped gutters according to the diameter of GFRP bar [43] 163
Table 50 - Mechanical properties obtained at pure tension test [43]. 164
Table 51 – Beams reinforcement 168
Table 52 – Summary of the experimental-to-predicted values of the cracking moment and the deflection at service load 177
Table 53 –Summary of the experimental and the predicted ultimate moments for the tests with the corresponding design values 179

Table 54 – Description of failure modes 186
Table 55 – Mean load and anchorage length at failure side of REHABGFRP2 beams 188
Table 56 – The mean spacing between cracks of beams 191
Table 57 – Comparison of the experimental and numerical ultimate loads 208
Table 58 – Comparison between the experimental and numerical values 214

Notation

a	[m]	Shear span length
A_f	[m^2]	Longitudinal reinforcement area of GFRP
A_{fv}	[m^2]	Area of shear GFRP reinforcement
b	[m]	Width of the rectangular cross-section
C_E	[-]	Environmental factor
d	[m]	Distance from the extreme compression fibre to the centroid of the tension reinforcement
d_b	[mm]	Diameter of FRP reinforcement bar
E	[GPa]	Elasticity modulus
E_{fl}	[GPa]	Elasticity modulus of GFRP bars
f_{bd}	[MPa]	Bond strength design value
f_c'	[MPa]	Concrete compressive strength
f_{cd}	[MPa]	Concrete compressive strength design value
f_{cm}	[MPa]	Mean value of concrete compressive strength
f_{ctm}	[MPa]	Mean value of tensile strength
f_f	[MPa]	GFRP bars tensile strength
f_{fb}	[MPa]	Strength of bent portion of FRP shear reinforcement
f_{fk}	[MPa]	Characteristic value of the FRP reinforcement tensile strength
f_{fu}	[MPa]	Ultimate FRP tensile strength
$f_{fu}{}^*$	[MPa]	Guaranteed tensile strength of an FRP bar
f_{fv}	[MPa]	Ultimate value of FRP shear reinforcement tensile strength
f_t	[MPa]	Maximum tensile
f_y	[MPa]	Yield stress
h	[m]	Cross-section depth
l_b	[m]	Anchorage length
I_e	[m^4]	Branson's effective moment of inertia
I_g	[m^4]	Cross-section gross moment of inertia
M_a	[kNm]	Bending moment at a considered load

M_{cr}	[Nm]	Cracking moment
M_f	[kNm]	Bending moment at a considered load
M_n	[kNm]	Moment capacity (nominal moment)
M_u	[kNm]	Ultimate moment resistance
r_b	[mm]	Internal radius of bent in FRP reinforcement
s	[m]	Shear reinforcement spacing
V_C	[kN]	Shear resistance provided by concrete
V_{fv}	[kN]	Shear resistance provided by GFRP reinforcement
V_s	[kN]	Shear resistance provided by steel reinforcement
z	[m]	Internal lever arm

β_1	[-]	Reduction factor that dependent of the concrete strength
β_d	[-]	Reduction factor used on the deflection calculation
δ	[-]	Service deflection
ε	[MPa]	Mean strain
ε_{cu}	[MPa]	Concrete ultimate strain
ε_f	[MPa]	FRP reinforcement tensile strain
ρ_{fb}	[-]	Balanced reinforcement area
ρ_{fl}	[-]	Longitudinal reinforcement area of GFRP
ρ_{sl}	[-]	Longitudinal reinforcement area of steel

Chapter 1.

Introduction

This chapter presents a general description of the thesis. It starts by reporting the FRP (Fibre Reinforced Polymer) material in general and the GFRP (Glass Fibre Reinforced Polymer) bars in particular, followed by the scope, motivation and objectives of the present research work. Then it outlines the organization of the document and lists the intended publications in peer reviewed journals produced from this scientific work, some of which already submitted. It ends mentioning the original contributions to the scientific knowledge.

1.1 The FRP material and the GFRP bars

This section describes in short the current knowledge about the Fibre Reinforced Polymers (FRP) in general. It starts with a brief note about the historical evolution of the material, followed by the description of its physical, chemical and mechanical properties, and ends pointing out the main differences between the FRP and the steel reinforced concretes.

To overcome the well-known steel corrosion problem in reinforced concrete (RC) structures [66], several repairing, rehabilitation and preventive methods have been developed, such as the use of galvanized protection, stainless steel, or impregnated polymers in concrete and epoxy coatings. Because many of these solutions are expensive and have a limited time duration [45, 67, 70, 71], the search for more attractive solutions with non-corrosive materials, such as fibre reinforced polymers (FRPs), has increased significantly in the 80s and early 90s [22, 70]. These FRP products were introduced in the construction industry in the forms of profiles, tubes, grids, rebars, fabrics, plates and strips in the 60s [17], after being primarily developed and applied to the aerospace and shipbuilding industries since the World War II [16, 17, 95].

A composite is a combination of two or more component materials, different of the molecular level, that are mixed to obtain a new material. In this sense, FRP composites are a combination of fibres bonded together by a polymeric matrix [22, 41]. The FRP composite characteristics are affected by the type of fibres, matrix and content volumes of the mixture.

The reinforcing fibres are the load-carrying element and determine the FRP strength and stiffness in the direction of the fibres. For the construction industry application, the fibres with high strength and stiffness, stable properties, high durability and acceptable costs are chosen. The glass, the aramid and the carbon are the most commonly used materials nowadays but there are others more recently developed, such as the basalt fibres.

Although the glass fibres are the least expensive and their tensile strength can be similar to the aramid and carbon fibres, they exhibit the lowest modulus of elasticity. Other disadvantages of the glass fibres are the high sensitivity to handling abrasion and a lower fatigue resistance. The tensile strength is reduced with the increase of temperature, but it is known that it happens for temperature ranges that also cause stability problems to the majority of the matrices [61]. Generally, three types of glass can be used: E-glass, S-glass and Alkali-resistant glass (AR-G). The E-glass is the most common one due to its lowest cost, but the S-glass has the highest tensile strength and modulus of elasticity. The main advantage of the AR-glass is its higher durability in alkali environments, as it is the case of the concrete [22].

The carbon fibres are essentially of two types: carbon and graphite. In general, these fibres are stable with the temperature, have high strength and modulus of elasticity, and are resistant to fatigue and to aggressive environment elements. However, their cost can be 10 to 30 times higher than the E-glass [22].

The aramid fibres have high strength, high stiffness, good fatigue resistance and a brittle tension failure similarly to the carbon and glass fibres, but are ductile in compression, which gives them better impact resistance and dumping. Their major disadvantages are the sensitivity to the UV light and the fact that they are hygroscopic and can be damaged by the water absorption [39, 94].

The basalt fibres are a more recent research and they are obtained by melting crushed volcanic lava deposits. They exhibit better properties than glass, are cheaper than carbon and have the better fire behaviour [33] than the others.

The matrix bonds the fibres together, is responsible for the load transfer among them and protects the fibres against aggressive environment agents and mechanical abrasion. It also affects the failure mechanism, the fracture toughness and the stress-strain behaviour of the resulting composite[32].

The most common polymeric matrices are the thermoset resins such as the epoxies, the vinylesters and the polyesters. These resins exhibit good bond and adhesive properties, high capacity to impregnate the fibres, good resistance to solvents and low viscosity and cost. However, they are not reprocessable because when cured, the chemical reaction of their formation is irreversible [87]. Some minor constituent materials (fillers) are generally added to these matrices to reduce the manufacturing costs and to enhance several properties, such as the impact strength, the UV and fire protections and the shrinkage control [80].

The thermoplastic resins are being used more recently such as the polypropylene, the polyamide and the polyethylene. They are different from the thermosets since their formation reaction process is reversible upon heating and cooling, which makes them capable of being reshaped. This is an advantage because it becomes possible to bend the reinforcement bars after their production. These matrices are also attractive from the sustainability point of view since they are recyclable and can be used for other ends such as PET bottles, while the thermosetting resins can only be reused as a filler material. However, the bond behaviour, the mechanical properties and the performance needs at high temperatures are for now a disadvantage and require further research [19].

Nowadays the structural applications of FRP materials are finding wider acceptance due to their inherent advantages over steel: the corrosion resistance, the electromagnetic neutrality, the low thermal expansion, the high strength-to-weight ratio and the good fatigue resistance [22]. Their versatility in construction material forms such as laminates, sheets, bars and profiles, also contributes for their wider application in civil engineering.

The benefits of using FRP bars as internal reinforcement in structural concrete go beyond their corrosion resistance as they are lighter and easier to assemble than steel. Although the market offers a high variety of FRP bars to use as internal reinforcement, the glass fibre reinforced polymer (GFRP) bars are the least expensive and therefore the most used. Some of the application examples are partial constructions of pedestrian and road bridges, hospitals with magnetic resonance equipment, nuclear power stations, airport runways, underground works and a wide variety of marine structures, where the harsh environment such as the sea causes the corrosion of the steel reinforcement [14].

The FRP bars are often manufactured by a mechanical automated process called pultrusion. The reinforcing fibres, in the form of rovings or fabrics, are continuously pulled and wetted in a resin bath and then they pass through a heated die, where the resin is cured [39].

The differences between the properties of the FRP and the steel bars influence the RC behaviour, especially its linear-elastic performance until rupture, which justifies the study and the adoption of different design philosophies. Several traditional assumptions of the steel RC design must be reassessed and eventually changed in the design of the FRP RC structures. Many advances have been made in this field, with the development of several codes and guidelines such as the ACI440.1R-06 [2] in the United States of America, the FIB 40 [22] in Europe, the CSA S806-02 [13] in Canada, the JSCE design guidelines [35] in Japan, among others. However, it is consensual that these documents tend to be conservative because in most cases they propose penalized and restrictive adaptations of the steel RC formulas instead of presenting design methodologies based in the actual FRP RC behaviour [31, 48].

The bond between concrete and the GFRP bars is of the utmost importance as it influences the service and the ultimate behaviour of RC structures [42]. The bond characteristics vary with the FRP materials, in particularly with the resin, and also with the surface treatment. There are bars with smooth, rough, dimpled, sand coated, helically grooved and other surface forms to increase the bond between the concrete and the reinforcement [78]. This wide variety of surfaces makes it harder to establish the bond-slip relationships to use in design [67].

In the FRP RC structures design it is common that the serviceability limit state controls the design [2]. The lower elasticity modulus of the FRP bars and their different bond characteristics in comparison to the steel bars are responsible for higher deflections and wider cracks in the RC members. Since the corrosion is not an issue, the maximum cracks width and deflection are imposed only to keep the elements integrity and for an aesthetic and appearance concern [61]. Additionally, according to Pilakoutas [77], despite the almost linear moment-curvature and load-deflection relationships under pure-bending, the FRP RC beams are capable of achieving deformations comparable to the steel RC beams.

Regarding the flexural design of FRP RC elements, the under-reinforced cross-section possibility, as usual in steel RC elements, corresponds to a brittle tensile rupture of the FRP bar. This failure depends on several factors such as the type, the strength to stiffness ratio and the bond characteristics. To avoid this uncertainty it is preferable to design over reinforced cross-sections to force the concrete crushing, despite its also brittle failure.

The shear behaviour of FRP RC elements is still a subject of discussion due to its complexity [75]. It is distinct from the steel RC elements due to the different interaction between the concrete and the FRP reinforcement, which directly and/or indirectly affects the performance of the internal shear carrying components: the un-cracked compression concrete zone, the aggregate interlock,

the dowel action and the shear reinforcement [22]. Despite the complexity to quantify each of these mechanisms that depend on the concrete and FRP characteristics, when comparing to steel it is known that the dowel-strength is lower due to the lower shear resistance of the bars. Also, the shear cracks are larger as a consequence of the lower modulus of elasticity that results in a reduction of the shear carrying portion given by the aggregate interlock and by the smaller compression zone[61].

After a deep search it was possible to conclude that there are only a few research studies [5, 6, 29, 86] about the use of FRP bars as shear reinforcement and that the closed stirrup is the most mentioned solution. The most common manufacturing process for the FRP closed stirrup with a thermoset matrix is to wrap the pultruded material around a mandrel with the desired dimensions before curing. An alternative process is the use of a unidirectional fibre bundles covered by a plastic tube that is injected with resin and cured after moulded with the desired dimensions. The advantage of a thermoplastic FRP may be the possibility to create a stirrup by heating the bar on site [61]. One important issue related to the use of FRP closed stirrups is the loss of strength near the bents due to the stress concentrations and to the thickness reduction. This lower capacity at the bents was found to be related to the bend radius / bar diameter ratio, to the type of fibres and matrices materials and to the fabrication processes [5, 22, 61, 75].

The long-term durability issue of the FRP RC is yet a knowledge gap to be filled, not only due to the different properties of the FRPs but also due to the FRP bars – concrete interaction uncertainties [24, 34]. Since the use of FRP bars as concrete reinforcement is a recent technique, there is limited amount of data to verify its behaviour during the design working life of 50-100 years. The majority of the existing data regarding this subject was obtained from accelerated tests [28, 93] and therefore the conclusion that the reduction in ultimate flexural strength of FRP RC is minimal remain yet to be validated by actual structures.

The production of the GFRP bars requires approximately 4 times less energy than the steel, which makes it a better solution from a sustainability point of view. Although the production of the resins depends on the oil industry, the amount of fossil fuels used is very low. Despite the fact that the thermoset resins are the most widely used and can only be reused as a filler material, new recyclable thermoplastic resins are currently being developed. Additionally, the fibres are practically an inexhaustible resource because they are made of a combination of various recyclable products [70].

Regardless of all the benefits of using FRP bars as reinforcement in concrete, their widespread application delay may be justified by the relatively high initial cost, the non-ductile behaviour, the

yet insufficient knowledge about the response of FRP RC structures and the lack of design codes [45]. Currently, the FRP RC solution is only considered in the cases where there are distinct and remarkable advantages due to its higher initial costs in comparison to the steel RC solution. A greater use of the FRP bars will contribute to reduce the costs.

All the potential and advantages of the FRPs described before justify the importance to fulfil the scientific knowledge gaps, through proper research to contribute for their wide and current use in the civil engineering structures.

1.2 Scope, motivations and objectives

A large amount of the total costs to repair and maintain RC structures worldwide is spent in durability issues, most of them caused by the steel susceptibility to the phenomenon of corrosion, especially in harsh environments [22]. It was estimated by Keller [58] that it is spent about 11 billion dollars to repair partially one third of the total US bridges every year. At early stages of the degradation development, it is possible to repair the structures and restore their safety with a relatively low budget but, in many cases, due to the advanced deteriorated state of the structure, deeper and much more expensive rehabilitations are needed [102]. Moreover, the sustainability issue and the need to reduce the ecological footprint, made the durability of RC structures an important concern in civil engineering nowadays [81].

In this context, the FRP RC alternative has a huge potential for the increasing demand of solutions to enable the reduction of maintenance and repairing costs in RC structures. However, because it is a relatively recent solution, the available data from actual structures with FRP material is scarce and many uncertainties about its behaviour remain to be answered. As a consequence, the few existing design codes and guidelines are restrictive in many aspects. The main motivation of this thesis is to provide a practical contribution to fulfil some of these gaps. It is intended to extent the scientific knowledge about several issues within two different specific domains of the FRP RC:

1) The performance of RC members with GFRP shear reinforcement;
2) The rehabilitation of steel RC elements through the replacement of the deteriorated reinforcement by GFRP bars.

The contribution is fully supported by an experimental campaign carried out with full-scale GFRP reinforced concrete beam specimens.

The first domain of the research is focused on the shear behaviour of concrete beams with vertical and longitudinal GFRP reinforcement, and the main objectives are:

- Test, compare the performance and conclude about the viability of four GFRP shear reinforcement solutions in RC beams;
- Analyse the assembling easiness of all solutions;
- Discuss the influence of each shear reinforcement anchorage length;
- Assess the effect of the GFRP closed stirrup spacing on the crack angle;
- Determine the influence of the longitudinal reinforcement stiffness on the shear behaviour of the GFRP RC beams;
- Design and predict the behaviour of all the GFRP RC specimens according to European and North American reference guidelines and technical documents, and conclude about their adequacy to the test results;
- Propose new and better adjusted parameters to the shear design formulas of the guidelines and technical documents used.

The second domain of the work is dedicated to the study of a rehabilitation proposal for deteriorated steel RC beams. The main idea for this research was inspired by the need to repair a significant amount of degraded RC structures in Madeira Island due to steel corrosion, as a consequence of the exposure to seawater chlorides. Another motivation is to propose a technique with a better cost to long-term durability ratio as an alternative to the expensive rehabilitation interventions with limited durability reported by several researchers [30, 66]. The replacement of the corroded steel reinforcement by GFRP bars, which are immune to corrosion, offers the possibility to solve this problem in the structure until the end of its design working life without having any more expenses. The technique is tested on RC beams and the main objectives are:

- To simulate the rehabilitation intervention, including the constructive restrictions and difficulties;
- To assess the structural behaviour of the rehabilitated beams in terms of flexural capacity, failure modes, deflections and crack widths;
- To discuss the ability of the rehabilitated beams to restore the serviceability and ultimate capacity of the original beams;
- To conclude about the performance of the GFRP bar anchorages at the supports of the beams;

- To analyse if the rehabilitated solution can be designed according to the general FRP design guidelines.

Finally, a 2D numerical analysis is carried out to reproduce and simulate some of the beam specimen tests from both parts of the present work. The main objectives are:

- To help the understanding of some hard to explain issues about the performance of the beams during the tests;
- To allow the modelling of non-tested possibilities and draw more conclusions about RC beams with GFRP shear reinforcement and the proposed rehabilitation solution.

The best and the most important way to disseminate the knowledge achieved in a research work is to publish it in international peer reviewed scientific journals. Hence, the publication of several papers describing the present work, its results and main conclusions is also an objective.

1.3 Organization of the thesis

The current research was planned to be published in various international scientific journals. Therefore, the document of this thesis is a compilation of all the intended papers for publication and is organized in five chapters.

This introductory chapter 1 presents a general description of the thesis and starts by reporting the FRP material in general and the GFRP bars in particular. Then it outlines the scope, motivation and objectives of the work followed by the organization of the document. Finally, it lists the intended publications in peer reviewed journals and ends reporting the original contributions to scientific knowledge.

The following two chapters describe all the experimental component of the research work.

The chapter 2 presents the shear study of the concrete beams with GFRP shear reinforcement. The section 2.1 mentions the full experimental programme prepared, illustrates the specimen details and the test instrumentation layout, and points out the material properties. Since several parameters were tested within the scope of this chapter, for a better organization and presentation of the results, each of the following sections discusses a specific behaviour comparison with precise and distinct objectives and conclusions of the study. Therefore, every section corresponds to a single paper intended for publication, has the same title as the submitted manuscript and is

constituted by a brief introduction to enumerate the objectives, the presentation of the tests, the discussion of the results and the conclusions.

The chapter 3 reports the performed work about the proposed solution to rehabilitate deteriorated steel reinforced concrete beams with GFRP bars. As the entire chapter is a submitted scientific paper for publication, it has an introduction with the state of the art about the topic, followed by the description of all the beam specimens, tests, results, analyses and conclusions.

The chapter 4 describes the finite element models created using the ATENA software to simulate some tested beams and to extrapolate for some non-tested possibilities. It ends with additional conclusions drawn from these analyses.

The chapter 5 starts with general remarks about the work and provides only a summary of the main findings because all the conclusions are described in detail at the end of each section that corresponds to an individual paper. The chapter ends with some proposals for future research.

Finally, all the references cited along the document are listed at the end of the thesis.

As a consequence of assembling the thesis document based on individual scientific papers intended for publication, and because some specimens, materials and tests are common to various papers, it is possible that some repetitions and / or resemblance may occur from one section / chapter to another.

1.4 List of the intended publications

As mentioned, this thesis is a compilation of several original papers, intended to be published in international scientific journals to spread the extension of knowledge achieved from the developed research. Bellow, it is listed all the papers and mentioned the actual situation regarding its publication by the time this document was written.

From chapter 2:

- Escórcio, Patrícia; França, Paulo M., *"**Performance of four different GFRP shear reinforcements solution in reinforced concrete beams**"*, preparing the manuscript for submission.
- Escórcio, Patrícia; França, Paulo M., *"**Experimental analysis of different GFRP transverse reinforcement solutions in reinforced concrete beams with GFRP longitudinal bars**"*, preparing the manuscript for submission.

- Escórcio, Patrícia; França, Paulo M., ***"Influence of the GFRP longitudinal bar ratio on the behaviour of reinforced concrete beams with GFRP shear reinforcement"***, preparing the manuscript for submission.
- Escórcio, Patrícia; França, Paulo M., ***"Experimental performance comparison of the reinforced concrete beams with different GFRP transverse reinforcement solutions and different longitudinal bar material and ratios"***, preparing the manuscript for submission.
- Escórcio, Patrícia; França, Paulo M., ***"Performance assessment of reinforced concrete beams with GFRP stirrups considering different shear reinforcement ratios"***, preparing the manuscript for submission.
- Escórcio, Patrícia; França, Paulo M., ***"Effect of the shear reinforcement ratio on the behaviour of reinforced concrete beams with GFRP stirrups and longitudinal bars"***, preparing the manuscript for submission.
- Escórcio, Patrícia; França, Paulo M., ***"Influence of the transverse and the longitudinal bar ratios on the performance of the GFRP reinforced concrete beams"***, preparing the manuscript for submission.
- Escórcio, Patrícia; França, Paulo M., ***"Effect of the longitudinal stiffness on the performance of reinforced concrete beams with GFRP stirrups spaced between d/2 and d"***, preparing the manuscript for submission.
- Escórcio, Patrícia; França, Paulo M., ***"Performance evaluation of reinforced concrete beams with d/2 spaced GFRP stirrups and different longitudinal stiffness"***, preparing the manuscript for submission.
- Escórcio, Patrícia; França, Paulo M., ***"Influence of the shear reinforcement ratio and the longitudinal stiffness on the behaviour of reinforced concrete beams with GFRP stirrups"***, preparing the manuscript for submission.

From chapter 3:

- Escórcio, Patrícia; França, Paulo M., ***"Experimental analysis of a rehabilitation solution using GFRP bars in corroded steel reinforced beams"***, submitted in publication in Engineering Structures Journal.

From chapter 4:

- Escórcio, Patrícia; França, Paulo M., ***"Modelling of GFRP reinforced beams with ATENA"***, preparing the manuscript for submission.

Finally, the following papers were also submitted for the national conference *"BE2016: Encontro Nacional de Betão Estrutural 2016"*:

- Escórcio, Patrícia; França, Paulo M., ***"Reabilitação de vigas de betão armado com varões de GFRP"***, abstract submitted.

Escórcio, Patrícia; França, Paulo M., ***"Estudo experimental de vigas de betão armado com varões de GFRP com cabeça de ancoragem como armadura de esforço transverso"***, abstract submitted.

1.5 Original contributions

At the end of the current research work, it is expected to have contributed to improve the scientific knowledge about the use of GFRP reinforcement in concrete members and, consequently, to its wider application in actual structures. The main original contributions extracted are:

- The collected data from tests of full-scale specimens is always more reliable concerning the actual behaviour of a structural member. The tests of 24 RC beams have contributed to reduce the lack of serviceability and ultimate behaviour results of RC beams with GFRP bars as longitudinal and shear reinforcement;
- The study of four GFRP shear reinforcement configurations provided the knowledge about the viability of each solution and its advantages and disadvantages. The conclusion about the performance and influence of every tested anchorage type and length of the bars is always a very important subject. Additionally, the conclusion that the double C stirrup has a similar performance to the traditional closed loop stirrup, turns it into a more versatile solution in the way that it is possible to adjust its width in situ. From a production perspective, this possibility is less restrictive than the closed loop stirrup with the exact dimensions, which contributes to broaden the horizons of using the GFRP as shear reinforcement;
- The tests of several different variables, including various longitudinal stifnesses, enabled a much deeper and consistent understanding about the use of GFRP shear reinforcement in RC structures;
- The proposal of new and better adjusted parameters for the GFRP shear design formulas is also an important contribution for the improvement of the design codes and consequently the use of this material in actual structures;
- It has been proved that the proposed rehabilitation technique to replace the deteriorated steel reinforcement by GFRP bars can be implemented, not only from a construction perspective but also from a structural point of view. It was demonstrated that the method is feasible and that it can restore the serviceability and the ultimate capacities of the

original structural element. This way, a new immune to corrosion rehabilitation solution becomes available to the market, which is a significant contribution to solve the long term corrosion problems of the steel RC structures in harsh environments, such as the marine structures or the ones near the sea.

Chapter 2.

Study of GFRP shear reinforced concrete beams

This chapter describes the part of the experimental campaign whose purpose was to study the behaviour and performance of beams with four GFRP shear reinforcement solutions. This chapter is based on the scientific manuscripts from the author, related to this part of the experimental campaign. In order to avoid repetitions, section 2.1 describes the experimental programme: the material properties, the beam specimens, the test set-up, the instrumentation and the loading history of all the specimens of this part. Then, each section from 2.2 to 2.7 corresponds to a different paper and it is organized as follows: introduction, results and conclusion, without the experimental programme details.

Nowadays corrosion is one of the major concerns of civil engineering. Particularly on aggressive environments [65], corrosion can spread rapidly inside of steel RC (reinforced concrete) structures and cause severe structural deterioration, leading to costly repairs and maintenance operations, catastrophic failures [6, 29], and reducing the expected service life of structures [72, 74]. Many methods have been applied and tested to prevent and delay the corrosion of steel RC [70, 98]. However, many of these are difficult to apply and have a limited durability. Thus, the demand for cost-effective solutions has increased the interest for non-corrodible reinforcement types, such as the fibre reinforced polymers (FRP) bars, as they are easy to apply, eliminate the corrosion problem and have the potential to reduce the life cycle costs of structures [31].

The durability, light weight, high tensile strength in longitudinal direction when compared to steel, and the electromagnetic transparency of FRP bars [70] make them attractive to the civil engineering structures. They have started being used in the 80's and early 90's [22, 70]. Among the several types of FRP bars, the most widely used is the GFRP (glass fibre reinforced polymer) due to its competitive life cycle cost.

FRP bars have been used as longitudinal reinforcement in structures in which the flexural strength is the most important mark or the shear strength is mainly assured by the concrete, such as floor slabs, decks and wall type structures [98]. The flexural behaviour of RC elements with FRP bars has been studied by many researchers [50, 92]. Also, the shear behaviour of FRP RC elements without shear reinforcement has been experimentally studied by several researchers [11, 12, 74], and several models and formulas have been proposed to evaluate the shear strength [35, 57, 60, 69, 89]. Several authors concluded [47, 98] that similar shear failure modes were developed in FRP RC beams and in steel RC beams. They have suggested that for the modes of failure investigated, the shear carrying mechanisms are mobilized in a similar manner, thereby justifying the extension of the design principles adopted for steel RC to FRP RC elements. El-Sayed and Soudki [31] compared the predictions from existing design methods with the experimental data of 149 beams and one-way slabs tested by other investigators. He concluded that the average predictions of the shear strength by the several methods varied by more than 70% from one another. Moreover, the differences in the mechanical properties of FRP comparing to steel – namely the lower modulus of elasticity, the linear stress-strain relationship up to failure without yielding, the different bond characteristics, the anisotropic behaviour with low stiffness and strength in the lateral direction – are responsible for a distinct shear behaviour (although with the same shear mechanisms) and strength of RC elements with FRP bars when compared to RC elements with steel and substantiate the need to validate the existing equations and models or even develop different design methodologies and procedures [10, 11, 62].The complexity of the RC members shear behaviour and of its mechanisms makes the shear capacity harder to evaluate and quantify [22].

Besides that, the number of studies on the shear behaviour of RC elements with FRP shear reinforcement is limited [29]. As a result, most of shear design provisions, codes and guidelines come from existing formulas developed for steel RC, and for the traditional Mörsch truss model [6], adding several safety factors, to take into account the uncertainties about the shear behaviour of FRP RC elements. Concerning existing codes, it is consensual that the values of shear strength are very conservative. Guadagnini, Pilakoutas*, et al.* [47] found that both the concrete shear strength and the strength of the stirrups were almost 200% higher than estimated by the current design equations and that the maximum strain values at stirrups were higher than 10‰ for GFRP exceeding the limit of 4‰ imposed by ACI 440.1R-06[2]. Ehab A. Ahmed and Brahim [29] found that GFRP stirrups behave like steel stirrups enhancing the concrete shear strength due to the confinement. He also found that at shear failure, the inclination angle of the shear crack was in agreement with the traditional 45-degree truss model. However, it is known that there is a reduction of the strength at bent portions of GFRP stirrups, given the stress concentration at the

bend caused by the curvature and the lower strength of the fibres at the perpendicular direction to their axis [2, 22, 29]. In the past, the tensile strength at bents was reported as varying from 30% to 60% of the straight portions [5, 63] and it is related to the type of fibres, the bending process and the ratio of bend radius to the bar diameter [2, 64]. Recently, several other researchers [7, 29, 30, 55, 63] stated that with recent improvements on the bending of FRP bars at production, the previously mentioned problems of the FRPs as shear reinforcement are being overcome, and as a result the GFRP bent stirrups are able to develop the full tensile strength of bars.

Although extensive research has been carried out to study the performance of FRP bars as longitudinal reinforcement, the number of studies conducted on the shear behaviour of RC elements with FRP bars as shear reinforcement is limited. The main conclusions seems to suggest that existing codes and guidelines are overly conservative conducting to congestion of reinforcement and non-cost-efficient solutions and their predictions are not in agreement with each other, as mentioned above. Furthermore, for being located as an outer reinforcement related to the longitudinal reinforcement, the use of FRP bars as the shear reinforcement is even more relevant to prevent corrosion. Thus, it is of paramount importance to explore FRP shear reinforcement solutions and adapt the existing equations and models. Additionally, it is mandatory to investigate the behaviour of the shear reinforcement obtained by the new different techniques of bending of GFRP bars and test other shear reinforcement solutions like the double headed bars.

Within this context, the research work developed and described in this chapter is intended to fill some of these gaps, which led to the following main objectives: 1) to evaluate the shear strength and the overall behaviour of full-scale RC beams with four different solutions of GFRP shear reinforcement, combined with different longitudinal reinforcement ratios and materials (GFRP and steel); 2) to evaluate the shear strength and the overall behaviour of full-scale RC beams reinforced with bent GFRP stirrups with different spacing combined with different longitudinal reinforcement ratios and materials; 3) to propose different values and formulas to better predict the shear resistance of a RC beam with GFRP stirrups.

To this end, beam specimens were tested until failure by four-point bending, and the ultimate capacity, the load-deflection, the stirrup strains, crack patterns and crack widths were analysed and compared with the reference beams and with theoretical predictions.

2.1 Experimental programme

This part of the experimental campaign was constituted by 18 full-scale RC beams with a rectangular cross-section of 0.25 m x 0.40 m and a free span of 4.30 m. These beams were designed to fail due to shear and constructed to test different layouts of GFRP shear reinforcement (bent and straight bars with and without headed ends) and different GFRP shear reinforcement ratios while considering different materials (steel and GFRP) and ratios of longitudinal reinforcement.

2.1.1 Material properties

In this section, the properties of the following materials are described: concrete, steel bars and GFRP reinforcement bars.

2.1.1.1 Concrete

A self-compacting concrete (SCC) C30/37 was used in the specimens with the composition indicated in Table 1.

Table 1 – Composition of concrete

SCC –C30/37 XC4 (P) Cl 0.2 D16 SF2 SR2 EN 206-9[51]

Material	Water	Cement	Clinker	Fly Ash	Limestone filler	Additional minority constituents (EN-197)	Gravel 8/16	Gravel 4/10	Stone dust - AB 0/4	Sand 0/2	G SKy 548 (adjuvant)	Pozolith 390N (adjuvant)
Kg/m^3	185	350	280	100	47.5	22.5	200	575	661	402	5.8	3.5

The concrete compression strength was determined at 28 days by compression tests on three cylinders of 0.15 m diameter and 0.30 m depth, and on three cubic samples with 0.15 m edge (Table 2) according to NP EN 12390-3: 2011 [52]. The compression strength was also determined at the day of the test. Likewise, the elasticity modulus E_c was also experimentally determined on three cylinders of 0.15 m diameter and 0.30 m depth according to NP EN 12390-13:2014 [54]. The results are presented in Table 2.

Table 2 – Concrete properties

Beam designation	Cylinder/cube strength, $f_{cm,28}$	Elasticity Modulus, $E_{cm\ 28}$	Concrete age at test	Cylinder strength, $f_{c,test}$	Elasticity Modulus, $E_{c,test}$
	[MPa]	[GPa]	[Days]	[MPa]	[GPa]
REF250	37.1/42.2	28	148	42.7	31
REFB250	39.9	23	40	41.6	26
BS250	44.5	28	226	47.9	28
BS250GFRP1	37.1/42.2	28	203	43.4	31
BS250GFRP2	37.1/42.2	28	210	43.5	31
BC250	44.5/47.6	28	259	52.6	28
BC250GFRP1	44.5/47.6	28	269	52.7	28
BC250GFRP2	44.5/47.6	28	267	52.7	28
BB250	39.9/41.5	23	41	41.7	26
BB250GFRP1	39.9/41.5	23	35	41.0	26
BB250GFRP2	39.9/41.5	23	29	40.1	26
BDHB250	39.9/41.5	23	34	40.8	26
BDHB250GFRP1	39.9/41.5	23	39	41.5	26
BDHB250GFRP2	39.9/41.5	23	33	40.7	26
REF175	37.1/42.2	28	198	43.4	31
BS175	39.9/41.5	23	36	41.1	26
BS175GFRP1	40.4/46.9	27	248	47.7	29
BS175GFRP2	40.4/46.9	27	252	47.7	29

2.1.1.2 Steel

The grade of steel reinforcement was A500 according to EC2[23]. The values of yield strength (f_{sy}), tensile strength (f_{st}) and elasticity modulus (E_s) were experimentally determined through pure tension tests on three samples of each diameter, according to the standard NP EN ISO 6892-1:2012[53]. The results are presented in Table 3. The 16 mm and 25 mm diameter bars were used as longitudinal bottom reinforcement, the 12 mm diameter bars were used as longitudinal top reinforcement and the 8 mm diameter bars were used as shear reinforcement of the reference beams.

Table 3 - Steel reinforcement properties

Φ [mm]	Yield strength, f_y [MPa]		Tensile strength, f_t [MPa]		Elasticity modulus, E_s [GPa]	
	Sample	Mean	Sample	Mean	Sample	Mean
8	763.0	670	834.4	743	251.2	230
	603.7		674.5		210.4	
	644.8		717.2		227.4	
12	628.3	605	749.0	721	202.7	209
	540.7		660.7		208.8	
	648.7		762.9		214.0	
16	718.2	682	844.6	820	206.3	218
	648.8		810.8		206.0	
	680.4		805.8		241.9	
25	634.0	613	750.6	737	237.8	226
	589.4		729.6		213.2	
	617.7		731.0		226.2	

2.1.1.3 GFRP

Three different types of GFRP bars were used: bent bars, straight bars and double headed straight bars. The bars were from the same producer and have a helically grooved surface forming ribs (Figure 1 a)).

The straight bars with 16 mm and 25 mm diameter were used as longitudinal reinforcement, and the 12 mm diameter as shear reinforcement. The properties indicated by the producer [84] are summarized in Table 4. Nevertheless, three samples of each diameter were tested in pure tension (Figure 1 b)) to determine the stress-strain relationship and the tensile strength (f_f) in order to compare the values with those presented by the producer. The stress-strain relationship was linear until failure with no yielding (Figure 2) and the results are presented in Table 5. They are similar to the ones indicated by the producer, except for the 25 mm bars, which were lower than expected due to a deficiency in the tests which led to a premature failure at the clamped ends.

Table 4 – GFRP bars properties according to the producer[84]

ComBAR	Exterior diameter	Interior diameter	Cross-sectional area	Specific mass	Tensile strength, f_f	Elasticity modulus, E_f	Bond strength, f_{bd}
	[mm]	[mm]	[mm2]	[Kg/m]	[MPa]	[GPa]	[MPa]
Bent bars (Stirrups)							
12	15.5	11.6	106	0.30	1000/700[1]	55	2.3 (For C30/37)
Straight bars and straight bars with end head							
12	13.5	12	113	0.30	1350	60	3.0 (For C30/37)
16	18	16	201	0.52	1200		
25	27	25	491	1.22	1100		
1 - The lower value at the bends							

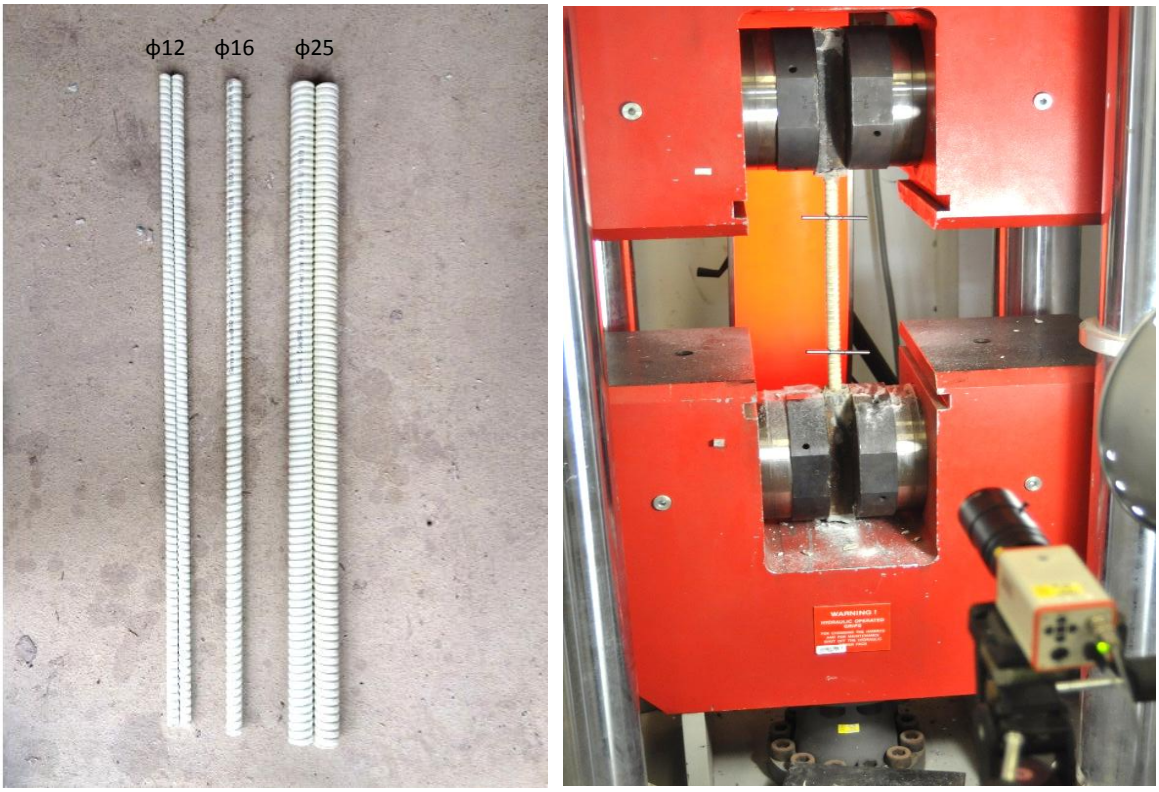

a) **b)**

Figure 1 – GFRP straight bars: a) each diameter sample; b) Pure tension test set-up

The straight bars with end heads and bent bars were also used as shear reinforcement, both with 12 mm diameter. The conic heads casted at the ends of the straight bars are made of polymeric concrete [84].

The bent bars have different properties compared to the straight ones due to its manufacturing process. They have a lower modulus of elasticity of 55 GPa and the tensile strength (f_f) is 1000 MPa and 700 MPa for the straight and the bent parts, respectively [84].

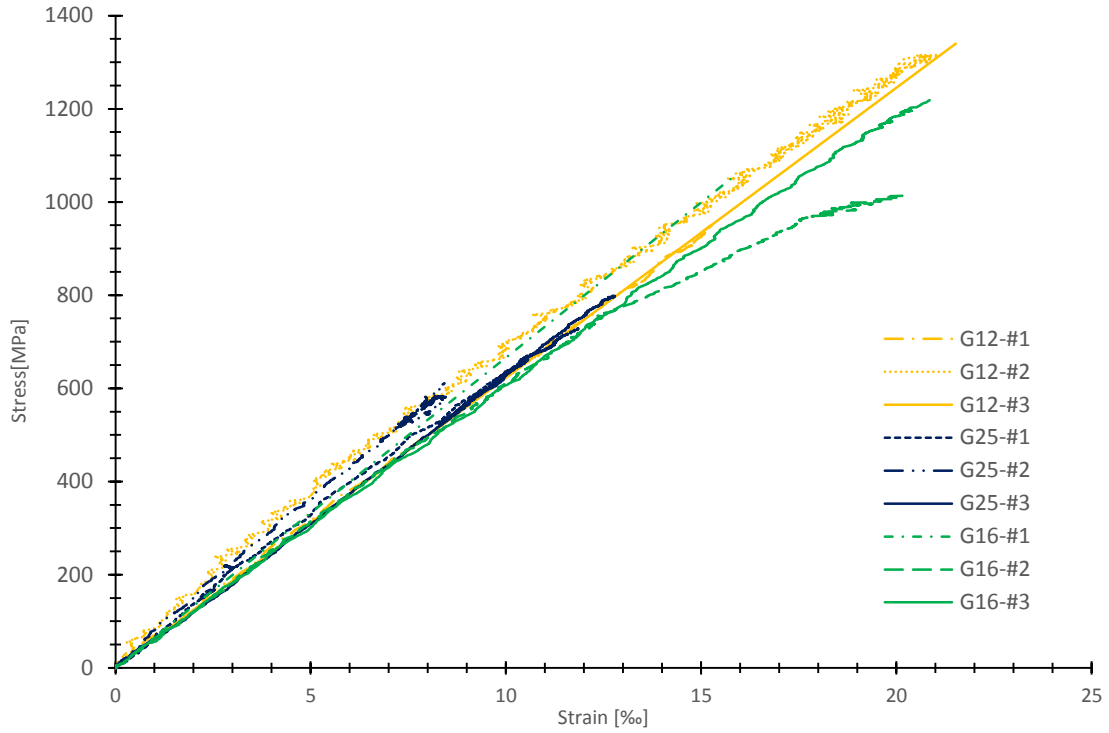

Figure 2 - Stress-strain diagram of the tested samples of GFRP bars [43]

Table 5 - GFRP bar properties [43]

ComBAR [mm]	Tensile strength [MPa]		Modulus of elasticity [GPa]		Ultimate strain [‰]	
	Sample	Mean	Sample	Mean	Sample	Mean
12	949.6	1200.0	61.8	60.0	15.4	19.0
	1315.3		61.3		21.5	
	1336.8		61.3		21.5	
16	1051.7	1094.7	66.6	62.3	15.8	17.6
	1013.7		60.7		16.7	
	1218.6		59.7		20.4	
25	777.3	729.0	59.3	64.0	13.1	11.0
	610.9		68.7		8.9	
	798.5		65.0		12.3	

2.1.2 Test set-up

2.1.2.1 Beams specimens

A total of 18 full-scale RC beams with intermediate length ($2.5 \leq a/d \leq 6$) designed to fail due to shear were tested until failure. The specimens were 4.30 m long, weighed approximately 1 ton and had a rectangular cross-section area of the 0.25 x 0.40 m^2. The free span was 4.0 m and the beams were subjected to a four-point loading with two applied loads at 1.0 m from the supports. A schematic representation of the test set-up is shown in Figure 3 and the instrumentation used is presented in the next section.

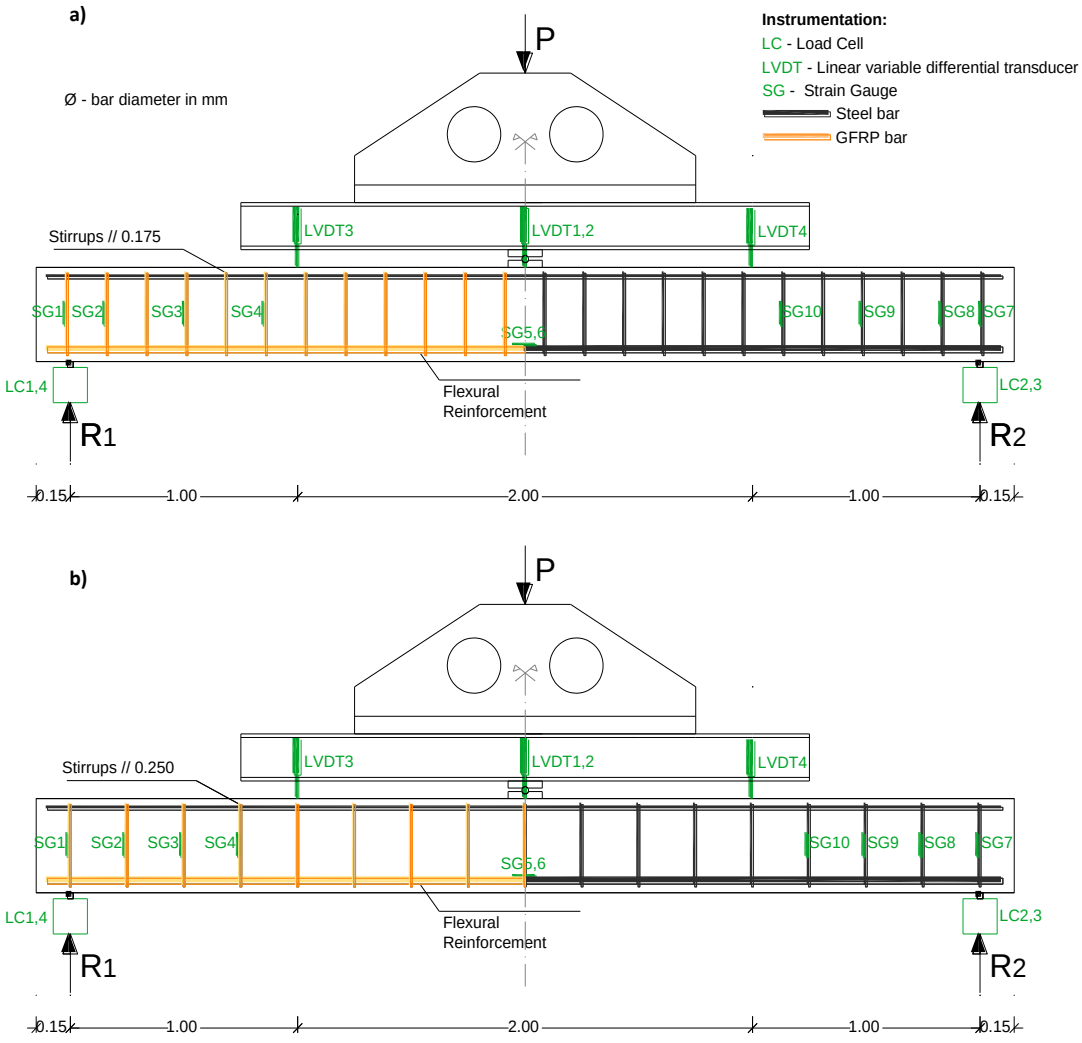

Figure 3 - Tests set-up and instrumentation scheme: a) Beam specimens with stirrups spaced at 0.175 m; b) beam specimens with stirrups spaced at 0.250 m

The different cross-sections of all the beam specimens are shown in Figure 4. The 18 beams were divided into 7 groups according to the type, ratio and material of the shear reinforcement:

1) 1 REF250: a reference RC beam with 8 mm conventional steel closed stirrups spaced at 0.250 m and steel longitudinal reinforcement;
2) 1 REFB250: a reference RC beam with two 8 mm steel straight bars (B) as shear reinforcement spaced at 0.250 m and steel longitudinal reinforcement;
3) 1 REF175: a reference RC beam with 8 mm conventional steel closed stirrups spaced at 0.175 m and steel longitudinal reinforcement;
4) 6 BS beams (S - closed GFRP stirrups): 3 with stirrups spaced at 0.250 m, BS250, BS250GFRP1 and BS250GFRP2; 3 with stirrups spaced at 0.175 m, BS175 BS175GFRP1 and BS175GFRP2;
5) 3 BC beams (C - two overlapped C-shaped GFRP bent bars): BC250, BC250GFRP1 and BC250GFRP2;
6) 3 BDHB beams (DHB - two double headed GFRP vertical straight bars): BDHB250, BDHB250GFRP1 and BDHB250GFRP2;
7) 3 BB beams (B - two GFRP vertical straight bars): BB250, BB250GFRP1 and BB250GFRP2.

The purpose of the 3 reference beams was to compare their behaviour, load capacity and deflections with the 15 GFRP shear RC beams. The reinforcement of these beams was entirely of steel material with a bottom longitudinal reinforcement of two 16 mm plus two 25 mm diameter bars (2ϕ16+2ϕ25) with a total cross-section area of 13.84 cm^2.

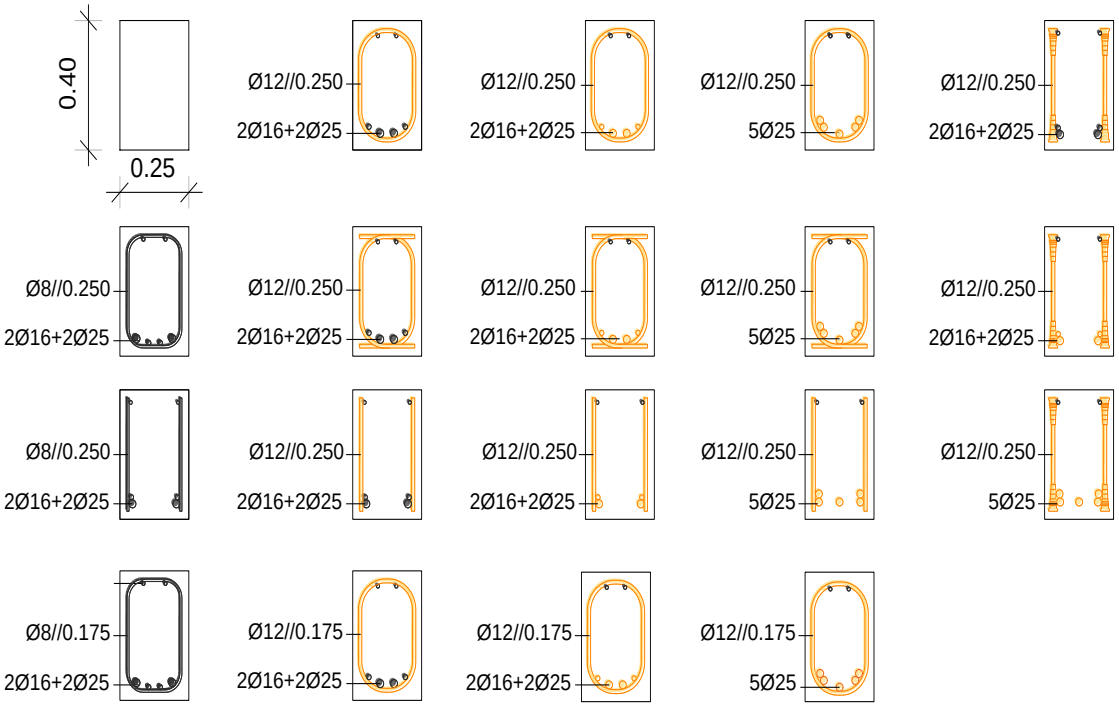

Figure 4 – Cross-section of the beams specimens

As shown in Figure 5, four different 12mm diameter GFRP shear reinforcement types were tested:

i) bent bars forming a closed hoop stirrup;

ii) two overlapped C-shaped bent bars to form a closed stirrup;

iii) two vertical straight bars;

iv) two double headed vertical straight bars.

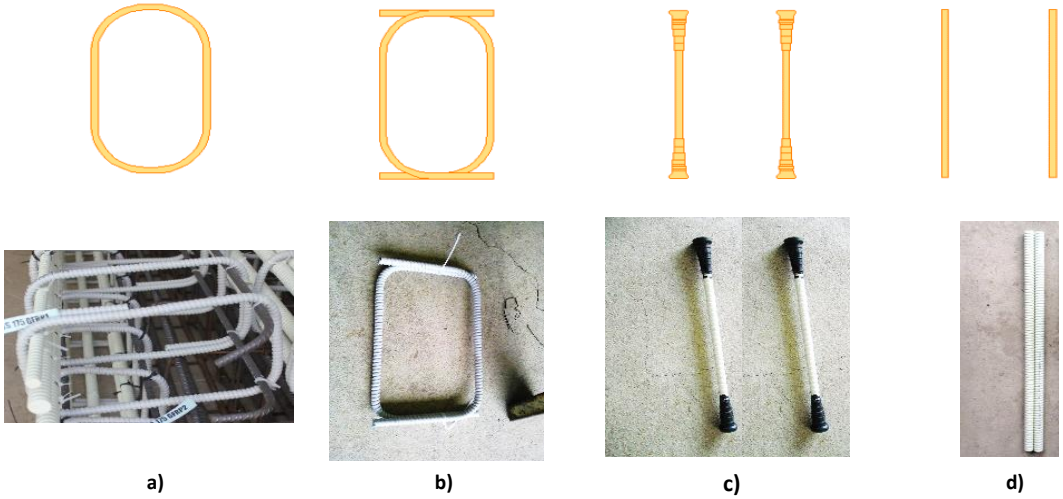

Figure 5 – GFRP shear reinforcement proposed and tested solutions

The GFRP closed hoop stirrups are similar to the traditional steel stirrups with the difference of having to be bent at the factory. The two overlapped C shaped bent GFRP bars to form a closed stirrup used is a solution more flexible to adjustments during the construction phase because it allows a width correction of the overlapped top and bottom branches within certain limits. The two double headed GFRP vertical bars used as shear reinforcement is a solution tested in this research work, especially because it does not require the bending process and also due to the simplicity of its assembly during the construction phase. According to the manufacturer[84] the heads at the ends of the straight bars compensate the lack of anchorage length when the bars are acting as shear reinforcement, which is meant to be confirmed within the scope of the present work. The two simple straight bars as shear reinforcement were tested mainly for two reasons: 1) to compare its shear behaviour with the double headed solution and demonstrate the enhancement provided by the heads at the ends of the bars; 2) to see how far it was possible to inflict load, deformation and cracks to these structural elements without failure due to shear, considering the huge lack of anchorage length of the shear reinforcement.

For each GFRP shear reinforcement solution, 3 different bottom longitudinal reinforcements were considered:

i) a steel reinforcement equal to the reference beams (2ϕ16 + 2ϕ25);

ii) a GFRP reinforcement of 13.84 cm^2 in a combination of two bars of 16 mm diameter (2ϕ16) and two bars of 25 mm diameter (2ϕ25). In this case, the beams were designed to keep similar dowel effect and to maintain the flexural capacity in order to evaluate only the material influence. Moreover, it was expected that this design enables the behaviour assessment between the four GFRP solutions and the influence of reducing the longitudinal stiffness when compared to the reference steel RC beams. This is mainly due to the GFRP lower modulus of elasticity when compared to the steel that gives lower longitudinal stiffness, thus increasing the expected deflection;

iii) a GFRP reinforcement of 25.54 cm^2 in a combination of five bars of 25 mm diameter (5ϕ25). In this case, the purpose was to maintain the deflection at mid-span in service conditions of the reference beam and to assess the influence of increasing the longitudinal stiffness.

The spacing of the shear reinforcement was 0.250 m. However, in the closed hoop stirrups solutions it was also considered a 0.175 m spacing in order to assess the effects of varying the shear reinforcement ratio, as well as to compare the cracking patterns and the shear capacity when the ratio of shear reinforcement increases.

The top longitudinal reinforcement of all beam specimens was two 12 mm diameter (2ϕ12) steel bars. Table 6, Table 7 and Table 8 summarizes the information about the full reinforcement of all specimens.

Table 6 – Beams with closed stirrups spaced at 0.250 m reinforcement details

Beam designation	Bottom longitudinal reinforcement				Transversal reinforcement			
	Material	Bars	ρ_{sl} or ρ_{fl}	$E_{sl}A$ or $E_{fl}A$	Type	Bars	ρ_{sv} or ρ_{fv}	$E_{sv}A$ or $E_{fv}A$
			(%)	(kN)			(%)	(kN)
REF250	Steel	2ϕ[1]16 + 2ϕ25 13.84 cm^2	1.58	304.48	Steel closed-hoop stirrup	ϕ8//0.250[2]	0.16	92.46
BS250	Steel	2ϕ[1]16 + 2ϕ25 13.84 cm^2	1.58	304.48	GFRP bent for a closed-hoop stirrup	ϕ12//0.250	0.36	49.72
BS250GFRP1	GFRP	2ϕ16 + 2ϕ25	1.58	83.04	GFRP bent for a closed-hoop stirrup	ϕ12//0.250	0.36	49.72
BS250GFRP2	GFRP	5ϕ25 24.55 cm^2	2.80	147.00	GFRP bent for a closed-hoop stirrup	ϕ12//0.250	0.36	49.72
BC250	Steel	2ϕ16 + 2ϕ25	1.58	304.48	GFRP bent for a C- stirrup	ϕ12//0.250	0.36	49.72
BC250GFRP1	GFRP	2ϕ16 + 2ϕ25	1.58	83.04	GFRP bent for a C- stirrup	ϕ12//0.250	0.36	49.72
BC250GFRP2	GFRP	5ϕ25	2.80	147.00	GFRP bent for a C- stirrup	ϕ12//0.250	0.36	49.72

1 – 2ϕ16 means 2 bars of 16 mm diameter
2 – ϕ8//0.250 means two vertical branches of 8mm stirrups spaced at 0.25 m

Table 7 – Beams with vertical bars spaced at 0.250 m as shear reinforcement details

Beam designation	Bottom longitudinal reinforcement				Transversal reinforcement			
	Material	Bars	ρ_{sl} or ρ_{fl}	$E_{sl}A$ or $E_{fl}A$	Type	Bars	ρ_{sv} or ρ_{fv}	$E_{sv}A$ or $E_{fv}A$
			(%)	(kN)			(%)	(kN)
REFB250	Steel	2ϕ[1]16 + 2ϕ25 13.84 cm²	1.58	304.48	Steel straight vertical bars	ϕ8//0.250	0.16	92.46
BDHB250	Steel	2ϕ16 + 2ϕ25	1.58	304.48	GFRP straight vertical bars with end heads	ϕ12//0.250	0.36	54.24
BDHB250GFRP1	GFRP	2ϕ16 + 2ϕ25	1.58	83.04	GFRP straight vertical bars with end heads	ϕ12//0.250	0.36	54.24
BDHB250GFRP2	GFRP	5ϕ25	2.80	147.00	GFRP straight vertical bars with end heads	ϕ12//0.250	0.36	54.24
BB250	Steel	2ϕ16 + 2ϕ25	1.58	304.48	GFRP straight vertical bars	ϕ12//0.250	0.36	54.24
BB250GFRP1	GFRP	2ϕ16 + 2ϕ25	1.58	83.04	GFRP straight vertical bars	ϕ12//0.250	0.36	54.4
BB250GFRP2	GFRP	5ϕ25	2.80	147.00	GFRP straight vertical bars	ϕ12//0.250	0.36	54.25

Table 8 – Beams with stirrups spacing of 0.175 m reinforcement details

Beam designation	Bottom longitudinal reinforcement				Transversal reinforcement			
	Material	Bars	ρ_{sl} or ρ_{fl}	$E_{sl}A$ or $E_{fl}A$	Type	Bars	ρ_{sv} or ρ_{fv}	$E_{sv}A$ or $E_{fv}A$
			(%)	(kN)			(%)	(kN)
REF175	Steel	2ϕ[1]16 + 2ϕ25 13.84 cm²	1.58	304.48	Steel closed-hoop stirrup	ϕ8//0.175	0.23	132.02
BS175	Steel	2ϕ16 + 2ϕ25	1.58	304.48	GFRP bent for a closed-hoop stirrup	ϕ12//0.175	0.51	77.52
BS175GFRP1	GFRP	2ϕ16 + 2ϕ25	1.58	83.04	GFRP bent for a closed-hoop stirrup	ϕ12//0.175	0.51	77.52
BS175GFRP2	GFRP	5ϕ25	2.80	147.00	GFRP bent for a closed-hoop stirrup	ϕ12//0.175	0.51	77.52

2.1.2.2 Instrumentation

All the instrumentation used during the tests is shown in Figure 3.

To measure deflections, four LVDTs (linear variable differential transducers) were placed on the beams. To prevent the beams from being damaged during the tests, the LVDTs were placed on the top sides, as shown on Figure 6 and Figure 7 a) and b): LVDT1 and LVDT2, with a maximum stroke of 100 mm and 50 mm, installed on both sides of the top of mid-span of the beams (Figure 8 c)) measured the mid-span deflection, and LVDT3 and LVDT4, with a maximum capacity of 50 mm,

measured the loading point's deflection. Four load cells with 200 kN of capacity each (Figure 8 b)), two for support, measured the reaction forces (LC1 and LC4; LC2 and LC3). The sum of the values from the four load cells is the applied load.

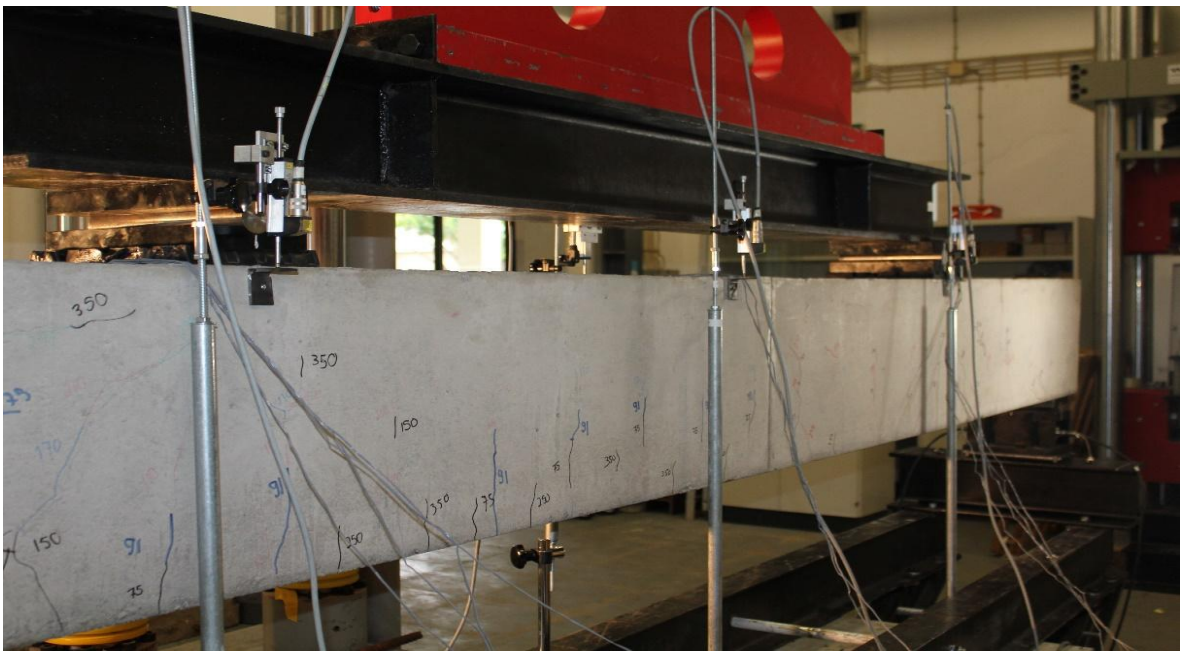

Figure 6 – LVDTs scheme during tests

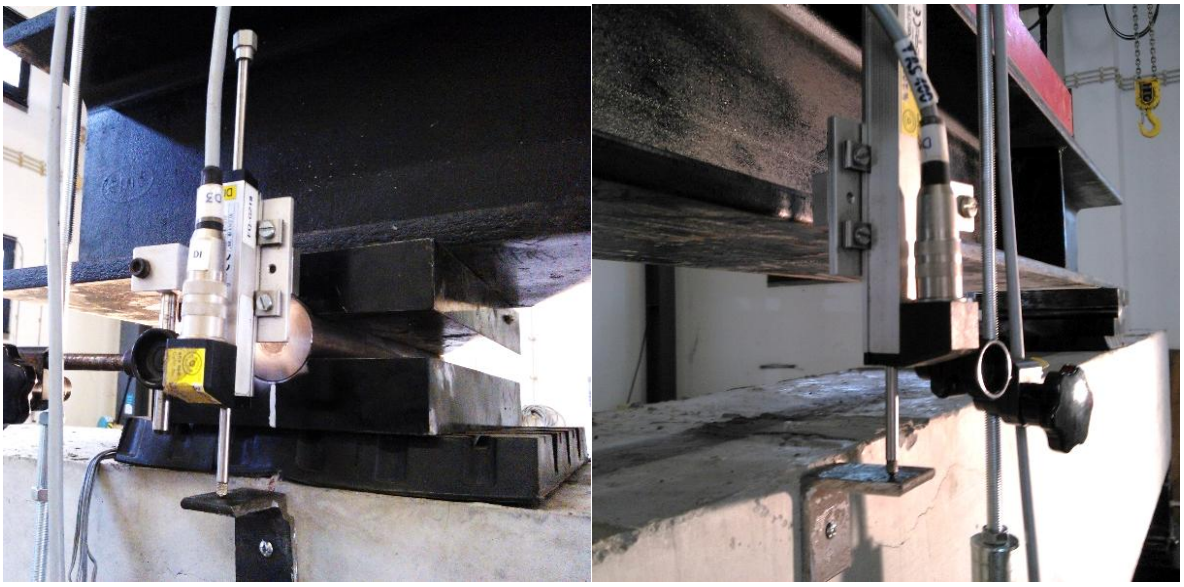

a) **b)**

Figure 7 – Positioning of the LVDTs: a) front view; b) side view

The mid-span strains of tension reinforcement were monitored by two strain gauges (SG5 and SG6), glued at half length of the bars. One strain gauge was placed on the middle bar and the other on

one of the extremity bars. The stirrups strains were also measured by eight strain gauges placed at middle height of stirrups to determine their behaviour. These strain gauges were placed as shown in Figure 3: for BS175, beams at first, second, fourth and sixth stirrups from the support; and for BS250, beams at the first four stirrups closer to the supports. The strain gauges applied are indicated for general use and their maximum strain capacity is of the order of 21 ± 1‰, the gauge factor (GF) is 2.13 ± 1% and the resistance is 120 ± 0.3 Ω[90].

The crack widths were manually measured using a monocular lens with an accuracy of 0.05 mm (Figure 8 a)).

(a) (b) (c)

Figure 8 – Instrumentation used in the tests: a) Lens used for the crack width measure; b) Load-cell; c) LVDT

2.1.2.3 Loading History

Beam specimens were tested under four point bending with the applied loads at 1.0 m from the supports and considering a free span of 4.0 m. The loading was controlled by force and the load was applied with a hydraulic actuator of 1500 kN maximum capacity. The loading history until failure was divided into several steps to allow the beam inspection: the cracking pattern was marked on beam sides, pictures were taken and the width of several shear cracks was measured. The load steps were defined according to the predicted load values for the different stages of the beam's behaviour. Also, for each beam specimen, three total discharges were considered to assess the deflection recovering behaviour at different loading stages. In order to continuously monitoring and recording the data, all the instrumentation and the hydraulic actuator were connected to a data acquisition system.

2.2 Performance of four different GFRP shear reinforcement solutions in reinforced concrete beams

The research work developed and described in this section is related to 6 of the beams part of the experimental programme and has the following main objectives: 1) propose and evaluate the performance of four different GFRP shear reinforcement solutions; 2) assess the shear strength and the overall behaviour of full-scale RC beams, with GFRP shear reinforcement and steel longitudinal reinforcement; 3) propose modifications to design codes to better predict the shear resistance of a RC beam with GFRP stirrups.

The four different GFRP solutions tested as shear reinforcement were: i) bent bars forming a closed hoop stirrup, ii) two C-shaped bent bars overlapped to form a closed stirrup, iii) two vertical straight bars, and iv) two double headed vertical straight bars.

The beams analysed in this section were REF250, REFB250, BS250, BC250, BDHB250 and BB250, and their properties and details were presented in the Experimental Programme from section 2.1. To achieve the defined goals, the beams were designed to fail due to the lack of shear capacity and were subjected to four point bending tests until failure. The load-deflection, the stirrups strains, the crack patterns and the crack widths of the beams were measured, analysed and compared with the reference beam and with the theoretical predictions of ACI 440.1R-06[2] and FIB40[22].

It was concluded that the bent GFRP stirrups (closed hoop stirrups and C-stirrups) are effective as shear reinforcement and that the bents of GFRP stirrups do not compromise the performance of the stirrups. The solution with double headed bars also exhibited a good performance. The general FRP design guidelines present overly conservative proposals to estimate the shear resistance. The GFRP straight bars as shear reinforcement led to a shear capacity lower than the predictions, being an inadequate solution.

Additionally, for being longitudinally reinforced with steel, these beams are an interesting solution since they are cost-effective and have a good overall performance with corrosion resistance.

2.2.1 Results and discussion

The experimental results as well as the theoretical predictions are described and compared in the following sections.

2.2.1.1 Ultimate capacity

The test results regarding the ultimate capacity of all beams and the corresponding failure modes are presented in Table 9. In order to establish a comparison, it was also indicated the theoretical values of the expected shear and bending load capacity (designated by non-design) obtained according to different codes ACI 318-11 [3], ACI 440.1R-06 [2], FIB-40 [22] and EC2 [23]. The non-design shear capacity was calculated with the mean values of the material properties, without safety factors and was always estimated as the sum of the concrete and reinforcement contributions ($V = V_c + V_{fv}$).

All the beam specimens were designed to fail due to shear, however BS250 and BC250 failed by compression of the concrete at top of mid-span at loads of about 85 % of the non-design prediction for the bending capacity of both ACI 440.1R-06 [2] and FIB-40 [21].To all the others beam specimens the experimental ultimate loads were always higher than the bending design capacity.

Table 10 summarizes the equations of the considered codes to calculate the shear capacity of FRP RC beams.

Table 9 – Non-design capacity of all beams specimens

Beam	Non-design Capacity					
	Experimental		ACI 440.1R-06 [2] / ACI 318 [3]		EC2 [23]/FIB 40 [22]	
	Type	Load (kN)	Shear (kN)	Bending (kN)	Shear Θ=45° (kN)	Bending (kN)
REF250	Shear	426.4	393.9	546.2	326.6	543.8
REFB250	Shear	257.4	391.3	544.0	325.3	541.5
BS250	Bending	488.2*	335.2	555.4	303.0	553.3
BC250	Bending	490.3*	344.4	562.1	308.0	560.2
BDHB250	Shear	422.3	325.5	542.3	294.8	539.8
BB250	Shear	217.6	327.5	544.2	295.9	541.7

* - Bending failure

Note: The values of shear capacity of the steel RC beams include the concrete contribution, because although EC2 [23] indicates that the shear capacity is given only by the stirrups contribution, more recent studies and codes [20] mentioned that better estimation can be achieved by adding the concrete contribution, V_c.

Considering that the strain in the concrete was the ultimate concrete compressive strain, ε_{cu}, 3.5‰, and that the strain in the longitudinal reinforcement , ε_{sl}, is 2.8‰ – which corresponds to the yield strain of the steel considered, achieved by the ratio between the values determined experimentally on the pure tension tests of the yield strength,f_{sy}, and the elasticity modulus, E_s – an ultimate bending capacity of 477,0 kN is obtained. As this value is close to the experimental capacity of the bending failure of BS250 and BC250 due to concrete crushing, it can explain these failures.

Moreover, the experimental longitudinal strain development (Figure 20 a) and b)) supports these calculations.

Table 10 – Shear design equations of FRP RC beams

Code	Shear equations	
ACI 440.1R-06 [2]	$V_c = \frac{2}{5} k \sqrt{f_c'} bd$	(1)
	$k = \sqrt{2\rho_{fl} n_f + (\rho_{fl} n_f)^2} - \rho_{fl} n_f$	(2)
	$n_f = \frac{E_{fl}}{E_c}$,	(3)
	$V_{fv} = \frac{A_{fv} \sigma_{fv} d}{s}$	(4)
	$\sigma_{fv} = 0.004 E_{fv} \leq f_{fb}$	(5)
	$f_{fb} = \frac{\left(\frac{0.05 r_b}{d_b} + 0.3\right)}{1.5} f_{fv} \leq f_{fv}$	(6)
FIB-40 [22]/ EC2 [23]	$V_c = 0.12 \left(1 + \sqrt{\frac{200}{d}}\right) \left(100 \rho_{fl} \frac{E_{fl}}{E_s} \phi_\varepsilon f'_c\right)^{1/3} bd$	(7)
	$V_{fv} = \frac{A_{fl}}{s} f_{fl} z \cot\theta^*$	(8)
	$\varepsilon_f = 0.0045$	(9)
	$\phi_\varepsilon = \varepsilon_f / \varepsilon_{sy}$	(10)

* - although a variable strut angle is possible, a fixed strut angle, $\theta = 45°$ is recommended in FIB-40 [22].

For the fact that both BC250 and BS250 failed by concrete crushing at mid-span and for a load higher than the beam REF250 failure load, it can be stated that their shear capacity was higher than REF250 in at least 15%.

The BB250, BDHB250 and REFB250 were designed to have the same shear strength. However, the ultimate capacity of BB250 was 16% lower than REFB250 while the ultimate capacity of BDHB250 was 200% of REFB250 failure load. This difference is justified by the lack of anchorage length of the shear reinforcement of BB250 and REFB250 when compared to BDHB250.

Comparing the experimental ultimate loads of beam specimens with the non-design predictions of the shear capacity it can be stated that with exception of BB250, codes are conservative. The underestimation is particularly high for the case of GFRP closed stirrups. For both BS250 and BC250, the experimental shear capacity was at least 45% higher than the ACI 440.1R-06 [2] values and at least 60% higher than FIB 40 [22] values. In the case of BDHB250 the experimental values were 130% and 143%, the predictions of ACI 440.1R-06 [2] and FIB 40 [22], respectively. BB250 shear capacity was only 66% and 74% of the predicted capacity of ACI 440.1R-06 [2] and FIB 40 [22], respectively.

In the case of ACI 440.1R-06 [2], the differences between the predictions and the experimental values are related to the 4‰ referred as limit to the shear reinforcement strains, which corresponds to 220 MPa in tension. In fact, as shown hereafter, the maximum strains on stirrups of BC and BS beams ranged from 7‰ to almost 10‰ (Figure 21). Table 11, presents the values of the shear capacity for a shear reinforcement strain of 4‰, 6‰ and 7 ‰. With the exception of the BB250, the predictions closer to the experimental results, although conservative, were obtained when considering the value of 7‰ for the strains. Guadagnini, Pilakoutas*, et al.* [47] had already proposed an increase of the strain limit.

Considering the FIB 40 [22], there are two variables that may be responsible for the difference between the experimental and the prediction values: the angle of 45 degrees for the strut and the limit of 4.5‰ for the reinforcement strain. The failure planes (Figure 9 to Figure 11) suggest that the angle for the strut can be lower, thus in the Table 11 there are the capacity values considering 30˚, 38˚, and 45˚. Fixing the strains at 4.5‰, the best predictions were obtained with the 30 ˚, however experimentally the best angle is 38˚. As the predictions for this value are still very conservative it was considered increasing the strains to 7‰, and the values of predictions were very similar to those achieved with ACI 440.1R-06 [2] and close, but conservative, to the experimental.

Table 11 - Non-design values varying the strains and the angle of the strut

Beam	Non-design Capacity								
	Experimental		ACI 440.1R-06[2] / ACI 318-11 [3]				FIB 40[22] / EC2[23]		
	Type	Load (kN)	Shear				Shear		
			ε_{fv} =4 ‰ (kN)	ε_{fv} =6 ‰ (kN)	ε_{fv} =7 ‰ (kN)	Θ=30˚ (kN)	Θ=38˚ ε_{fv} =4.5 ‰ (kN)	Θ=38˚ ε_{fv} =7 ‰ (kN)	Θ=45˚ (kN)
BS250	Bending	488.2	335.2	406.8	442.6	409.2	343.6	446.7	303.0
BC250	Bending	490.3	344.4	416.0	451.8	414.2	348.6	451.7	308.0
BDHB250	Shear	422.3	325.5	397.1	432.9	400.9	335.4	438.5	294.8
BB250	Shear	217.6	327.5	399.1	434.9	402.0	336.5	439.6	295.9

A comparison of the experimental results with the design values (with safety factors) is presented in Table 12. Both codes result in very conservative values. Excluding BB250, on average the experimental values were 2.5 and 3.1 times higher than design values, for ACI 440.1R-06 [2] and FIB 40 [22], respectively. Again, in the case of ACI 440.1R-06 [2], to decrease this ratio to a value

around 1.5, which is, in general, the global safety factor used when design with steel, the limit strain considered should be increased to a value between 6‰ to 7‰. For the case of FIB 40 [22], if adding the concrete contribution for the shear capacity, the prediction values goes up to 288.8 kN, and the ratio experimental to predicted decreases to around 1.6.

Table 12 – Summary of experimental and design values of shear capacity

Beam	Shear Capacity					
	Experimental		Design Values			
	Load	Type	ACI 440.1R-06[2] / ACI 318-11[3]	Experimental / Design	FIB 40[22] / EC2[23]	Experimental / Design
	(kN)		(kN)	(-)	(kN)	(kN)
REF250	426.4	Shear	253.0	1.7	190.9	2.2
REFB250	257.4	Shear	253.0	1.0	190.9	1.3
BS250	488.2*	Bending	190.0	2.6	150.0	3.3
BC250	490.3*	Bending	190.0	2.6	150.0	3.3
BDHB250	422.3	Shear	190.0	2.2	150.0	2.8
BB250	217.6	Shear	190.0	1.2	150.0	1.5

* Bending failure

2.2.1.2 Cracking pattern

In order to analyse the differences in the cracking behaviour, the crack development was marked on the beams with different colours after each load step. The cracking patterns are shown from Figure 9 to Figure 11. Initially, all beam specimens were uncracked. The cracks appeared firstly at the constant moment region, and grew vertically (absence of shear stresses). With the load increase, other flexural cracks appeared in the shear-span region, vertically but then propagating to the loading point direction. The failure starts with the formation of an inclined crack oriented perpendicular to the direction of the maximum principal stress. Generally, it was the shear crack closest to the support that leads to the failure of the beam, as reported by Yost, Gross*, et al.* [98] The slope of the plane of failure of beams that failed due to shear varies from 38˚ to 46˚, being in agreement with the 45˚applied in the truss model (including the plane followed by the shear cracks of BS250 and BC250). It can also be referred that the higher the failure load, the greater the number of shear cracks. This was also verified by Ehab A. Ahmed and Brahim [29].

Comparing the mean flexural crack spacing, it was similar for all the beam specimens, with the following fixed vertical development pattern: for REF250 it was 0.138 m, for REFB250 it was 0.104 m, for BC250 it was 0.112 m, for BS250 it was 0.110 m, for BDHB250 it was 0.131 m and for BB250 it was 0.114 m.

Another important data that can be obtained is the height of the compression zone (distance between the compression fibre and the neutral axis): steel reinforced beams, REF250 and REFB250, have the lowest neutral axis, with a mean height of 0.179 m and 0.185 m respectively. For BS250 and BC250 (bending failure) the mean height of the neutral axis was 0.118 m and 0.154 m, respectively, for BDHB250 was 0.127 m and for BB250 0.144 m.

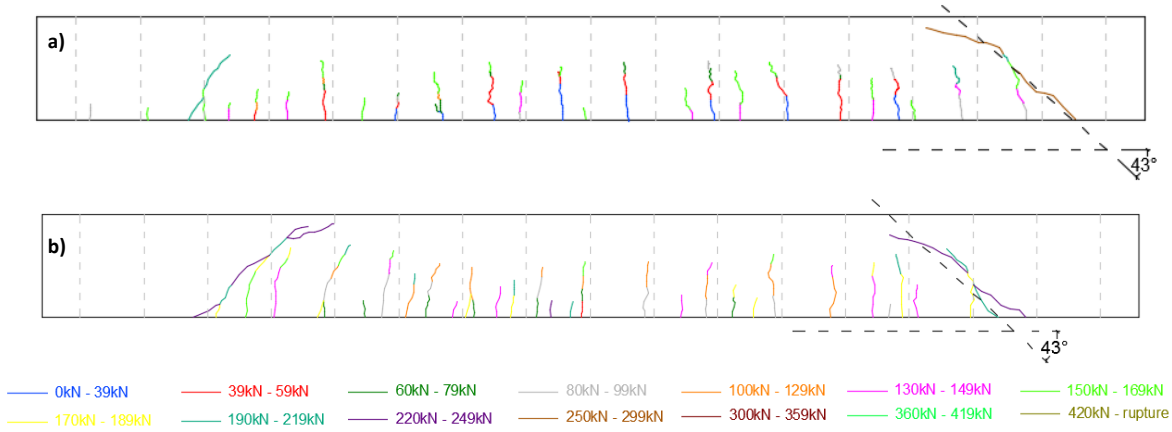

Figure 9 – Cracking pattern at failure of: a) REF250; b) REFB250

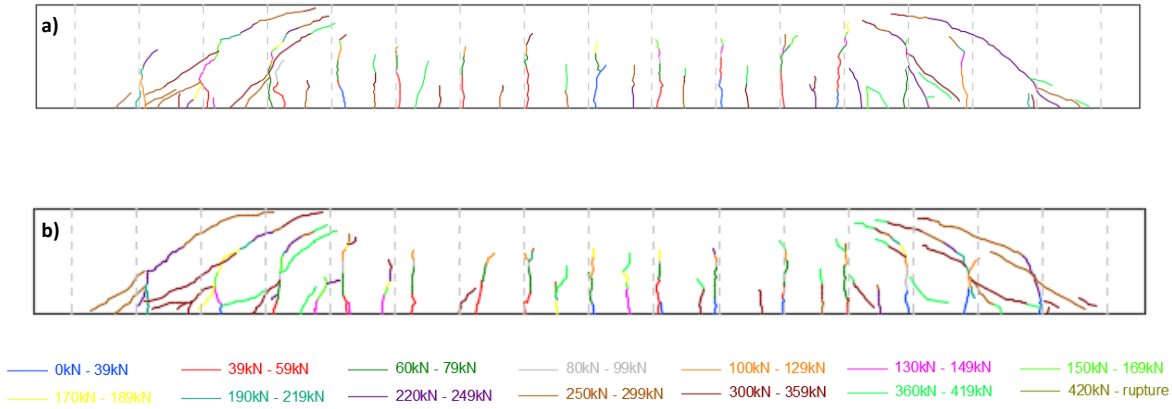

Figure 10 – Cracking pattern at failure: a) BS250; b) BC250

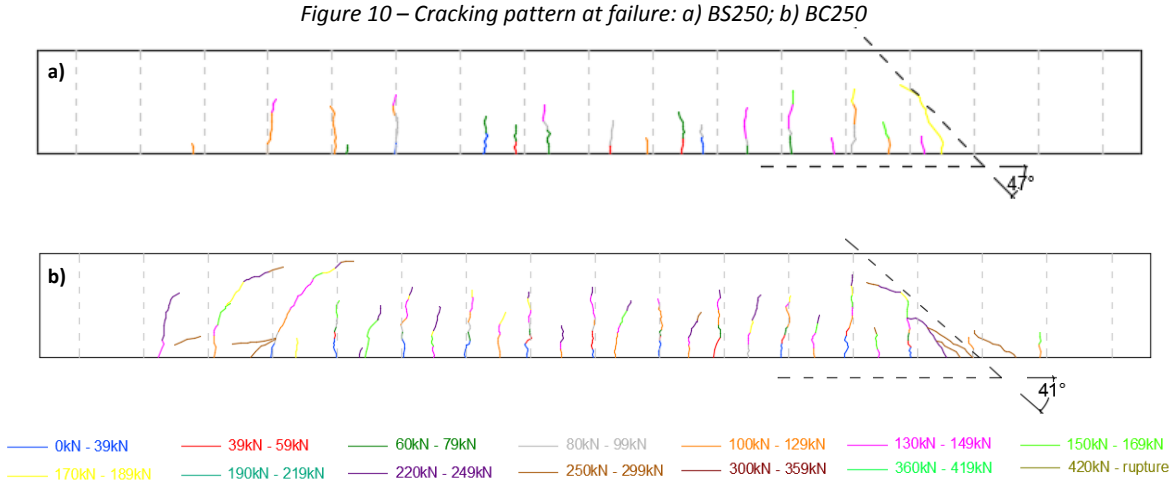

Figure 11 – Cracking pattern at failure: a) BB250; b) BDHB250

2.2.1.3 Failure modes

Comparing the reference beams with the GFRP shear reinforced beams it can be stated that there was no significant difference in the overall behaviour in terms of cracking pattern or failure modes. The failure modes of all specimens are presented from Figure 12 to Figure 17. Two distinct types of failure occurs:

- bending failure due to concrete crushing at top of mid-span (BS250 and BC250);
- shear diagonal tension failure by shear reinforcement failure (REF250; REFB250; BDHB250 and BB250).

The reference beam REF250 had a brittle shear failure mode of several stirrups. Several flexural cracks developed along the span, vertically as the load increased. For loads above 150 kN, cracks located between the loading points and the supports started to incline in the direction of the loading points. The failure occurs with the rupture of the third stirrup from support, followed by the ruptures of all the others stirrups along the shear crack (Figure 12 c) and d)), leading to an almost instantaneous failure of the beam at 426.4 kN (Figure 12 a) and b)). Regarding the strains in this stirrup (Figure 22 a)), it can be stated that the rupture occurred for a strain of approximately 2.8‰, which is the yield strain of the considered steel.

The REFB250 beam failed by the slip/pull-out of the shear reinforcement (Figure 13 a) and b)). Similarly to REF250, for loads under 130 kN, cracks develop along all the span vertically (Figure 9 b)). Above 130 kN, the cracks near the supports started to incline in the direction of the loading points. The failure occurred when the third bar of the shear reinforcement slipped, followed by others along the shear crack (Figure 13 c) and d)), leading to a quick failure of the beam at 257.4 kN. The strain development (Figure 22 b)) indicated that these bars did not reach the yield strain.

The failure of BB250 beam was similar to the failure of REFB250 (Figure 14 a) and b)). As shown by Figure 11 a), for loads above 130 kN the shear cracks developed leading to the slip of the third group of bars of the shear reinforcement (from the support) causing a brittle failure at 217.6 kN (Figure 14 c) and d)). Comparing the strains of the bars that slipped (Figure 23 a)) with the strains of the same bar in REFB250, it can be stated that the strains were higher on BB250 than REFB250, suggesting different bonding properties of the two materials: GFRP and steel.

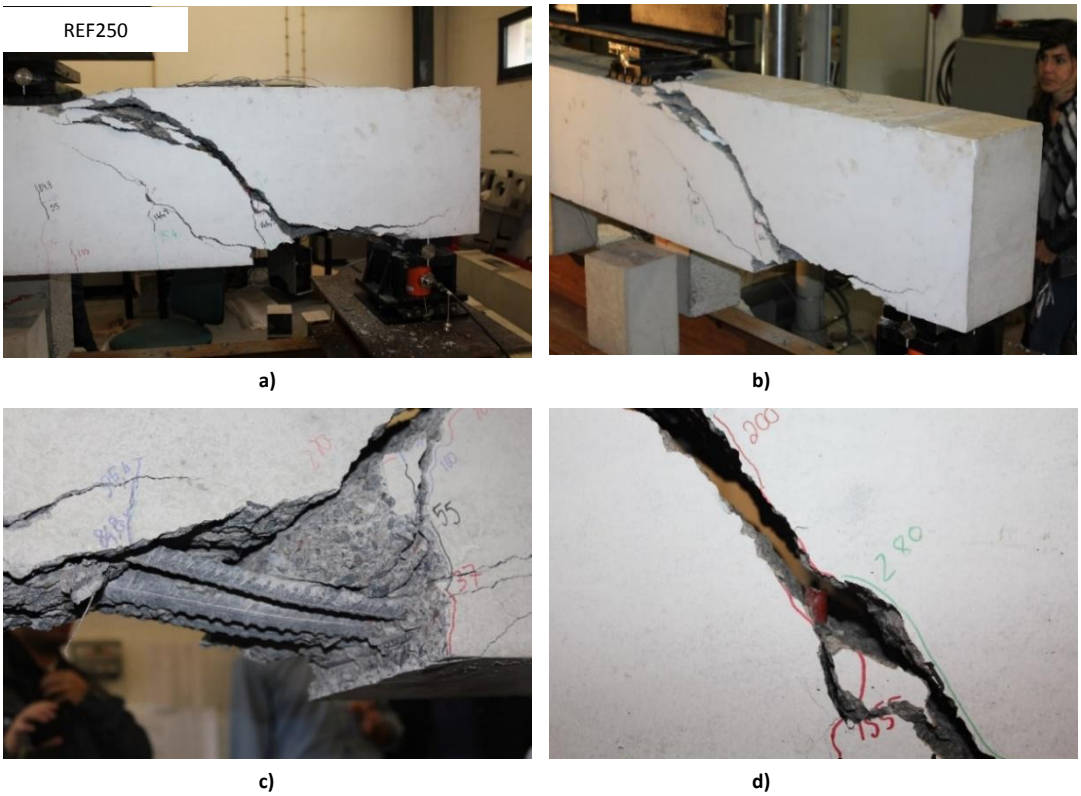

Figure 12 – REF250 beam failure: a) front view of the support; b) overall view of the failure; c) bottom reinforcement; d) broken stirrup

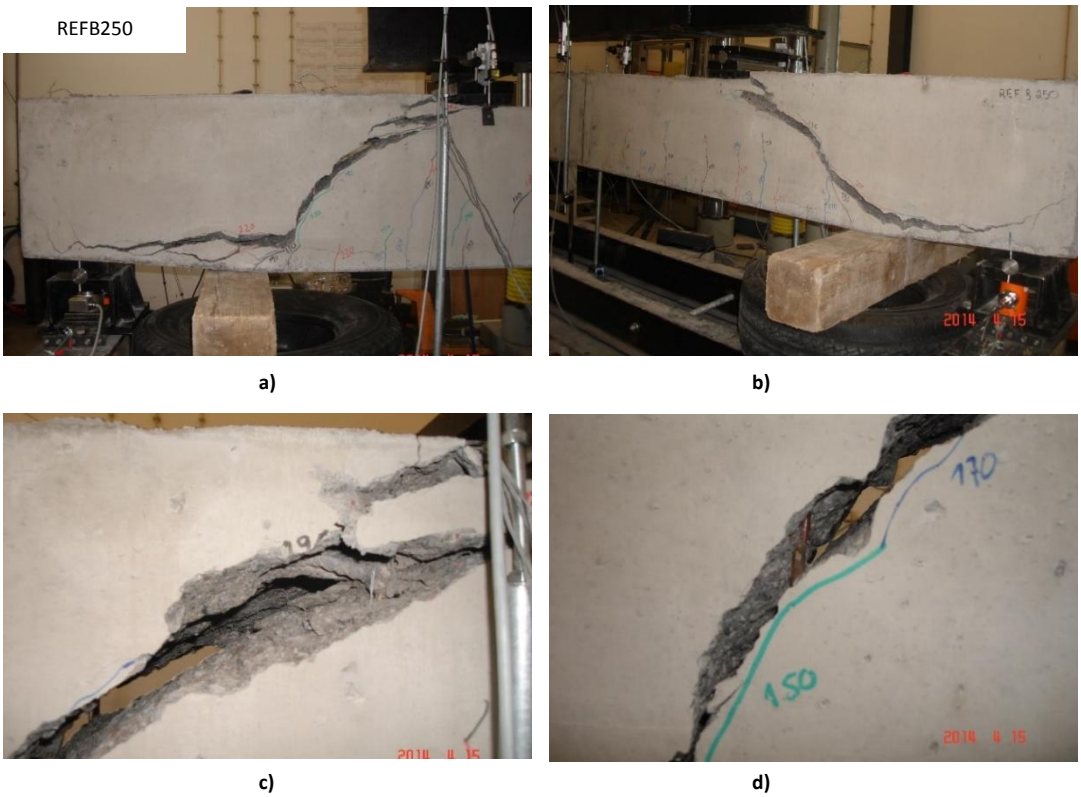

Figure 13 – REFB250 beam failure: a) overall view of one of the sides of the support; b) overall view of the other side of the support; c) slip of stirrup; d) slip of stirrup

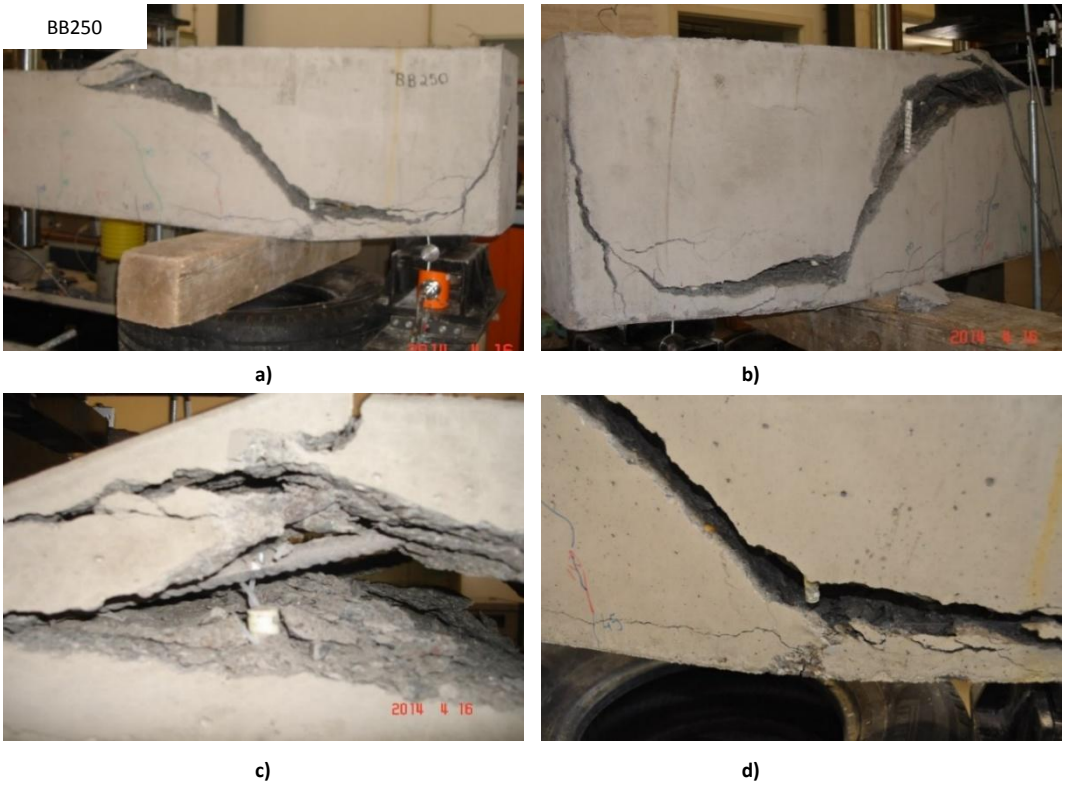

Figure 14 – BB250 beam failure: a) overall view of one side of the support; b) overall view of the other side of the support; c) pull-out of the shear reinforcement in compression zone; d) pull out of the shear reinforcement in bottom zone

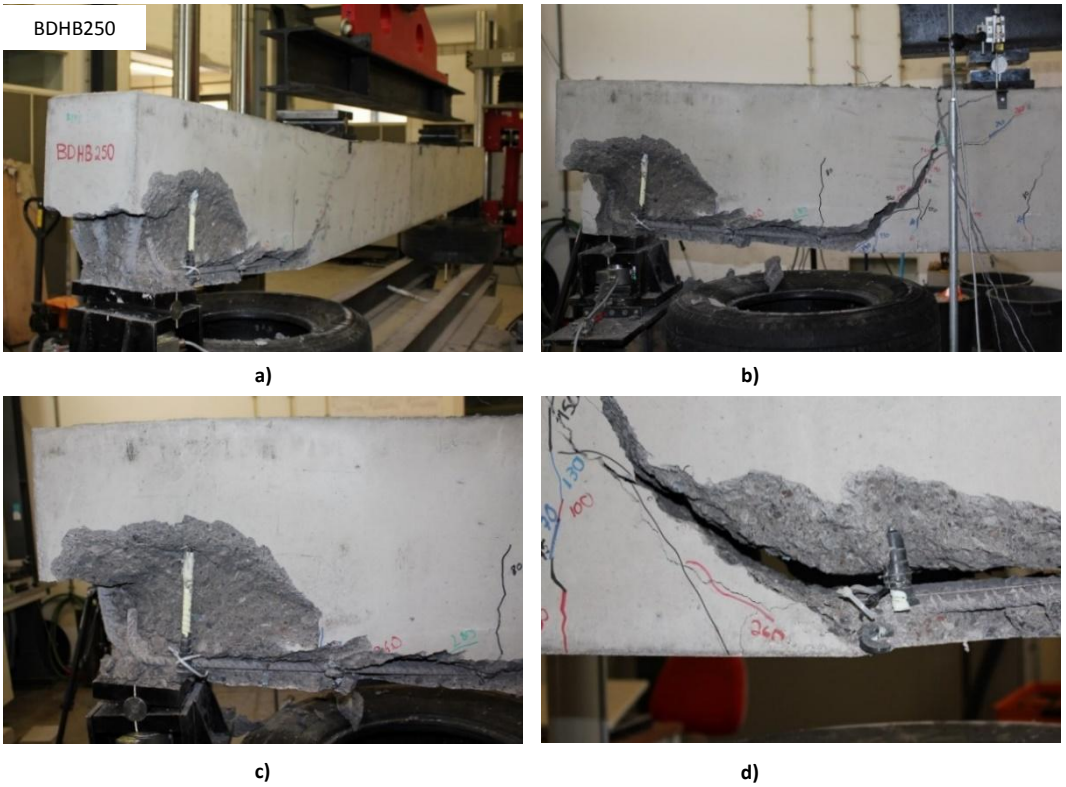

Figure 15 – BDHB250 beam failure: a) overall view; b) view near the support; c) pull-out of longitudinal reinforcement; d) fractured lower head

BDHB250 beam also exhibits a shear failure due to fracture of the end heads of the shear reinforcement bars (Figure 15 a) and b)). The shear cracks appeared above 150 kN (Figure 15 d)), causing the fracture of the end heads of the shear reinforcement (second and third group of bars from the support). This was followed by the pull-out of the longitudinal bars, although these bars were bent at supports increasing the embedded length (Figure 15 c) and d)). As a consequence, the beam failed at 422.3 kN. It can be noticed that when the fracture of the heads happens, these bars slipped and the stress was absorbed by the fourth bar, as indicated in the Figure 23 b).

The failure of BC250 and BS250 was a bending failure which occurred by the crushing of concrete at the top of mid-span, at 490.3 kN and 488.2 kN (Figure 16 and Figure 17) respectively. Although for loads above 190 kN several shear cracks appeared in both of the beam specimens, the flexural cracks at mid-span were still propagating vertically (Figure 10). Figure 16 c) and d) show that C-stirrups at the mid-span disintegrated, for BC250. This did not happen on BS250. Figure 17 c) and d)). Figure 20 a) and b) enhance the fact that the longitudinal reinforcement yielded at failure, indicating the failures occurred by the concrete crushing but with yielding of reinforcement.

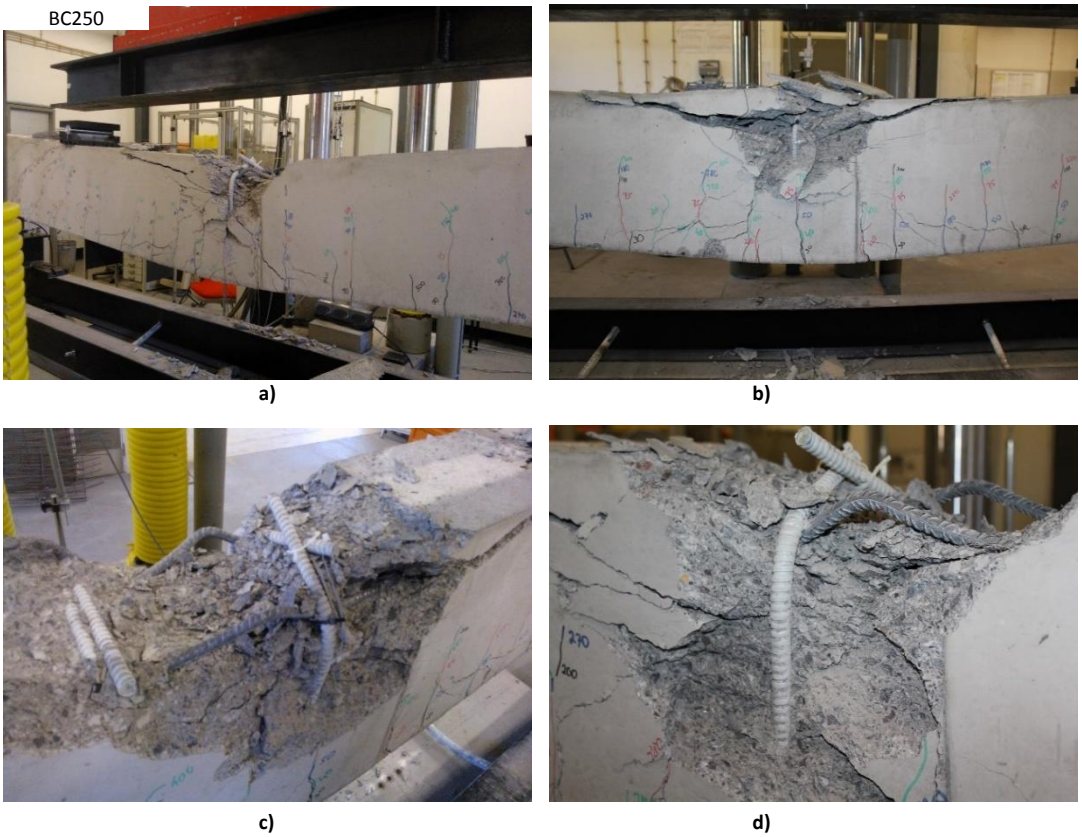

Figure 16 – BC250 beam failure: a) overall view; b) mid-span; c) top of mid-span; d) disintegration of mid-span stirrup

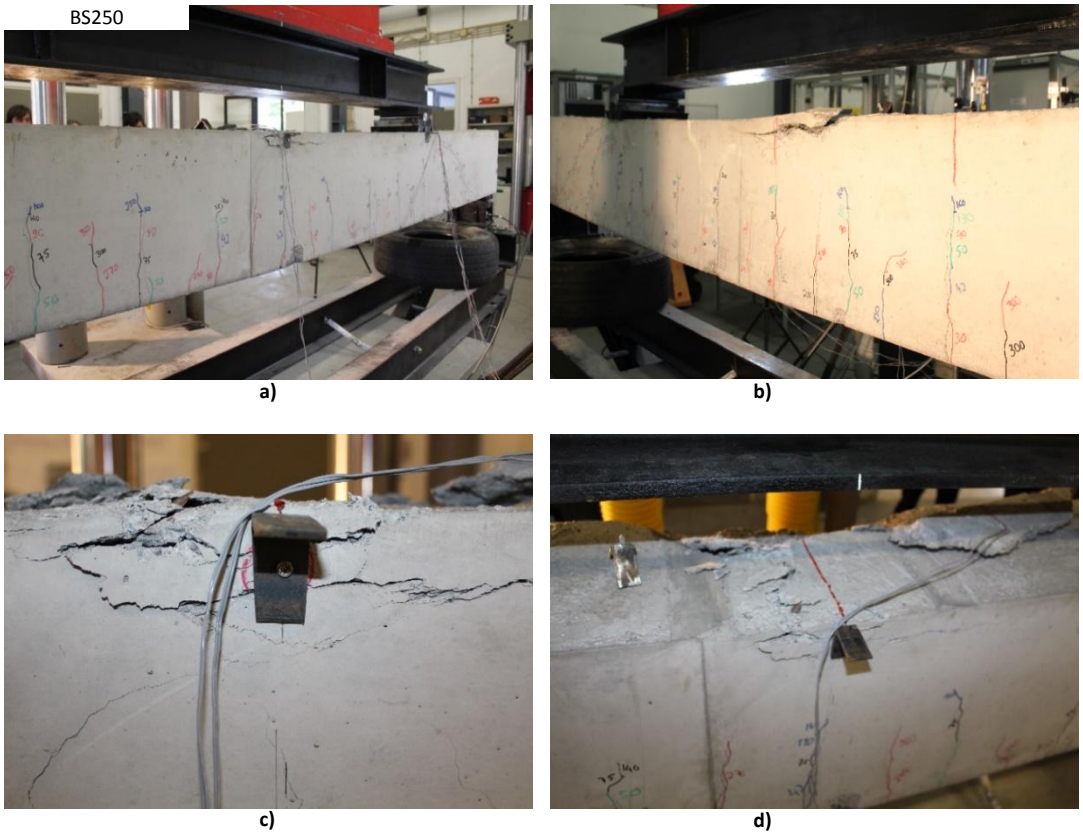

Figure 17 – BS250 beam failure: a) overall view from one side; b) overall view from the other side; c) mid-span; d) top of mid-span

2.2.1.4 Mid-span deflection

In order to assess the behaviour of the different shear reinforcement types, the load-deflection curves at mid-span are shown in the Figure 18. The REF250 and REFB250 curves were also plotted over the other curves for immediate comparison of the behaviour. Each curve represented is the average deflection obtained by the 100 mm LVDT mounted at mid-span. In general, for loads under the load of the cracking moment, all the specimens exhibit an initial elastic phase where the load-displacement relation was linear, followed by a cracked phase where the load-displacement relation is still linear but with lower slope. For all the beams, the load-displacement curves developed with only two distinct phases which were approximately linear, with no yielding and no ductile behaviour, with the exception of the beams BS250 and BC250, as these failed by mid-span concrete crushing. The load-deflection curves of these two beams had a third phase, where the deflection is still increasing for an almost constant load value, corresponding to a yielding phase, and thus exhibiting some ductility. REF250 has the highest stiffness and REFB250 has the lowest stiffness. For all others beams (BS250, BC250, BDHB250 and BB250) the load-deflections curves are

approximately coincident. In the case of BB250, for loads above 140 kN, the deflection increased for a stationary load value, creating horizontal landings in the figure. This reflects the lack of anchorage length of the shear reinforcement (even at a stationary load, the shear reinforcement bars slipped, forcing the beam to deform more to establish the internal equilibrium). Comparing the REF250 with REFB250, it is possible to notice that since the beginning of the loading the deflection was higher than on REFB250, showing lower stiffness when compared with the other steel beam.

In Table 13, it is possible to notice that there is no difference between the deflections of beam specimens for the service load values (50 kN). Comparing the service predicted deflections with the experimental deflections, the experimental deflections were on average 25% higher than predicted. For the reference beams: REF250, the experimental deflection was 10% lower than predictions, and for REFB250 the experimental displacement was 36% higher than predicted.

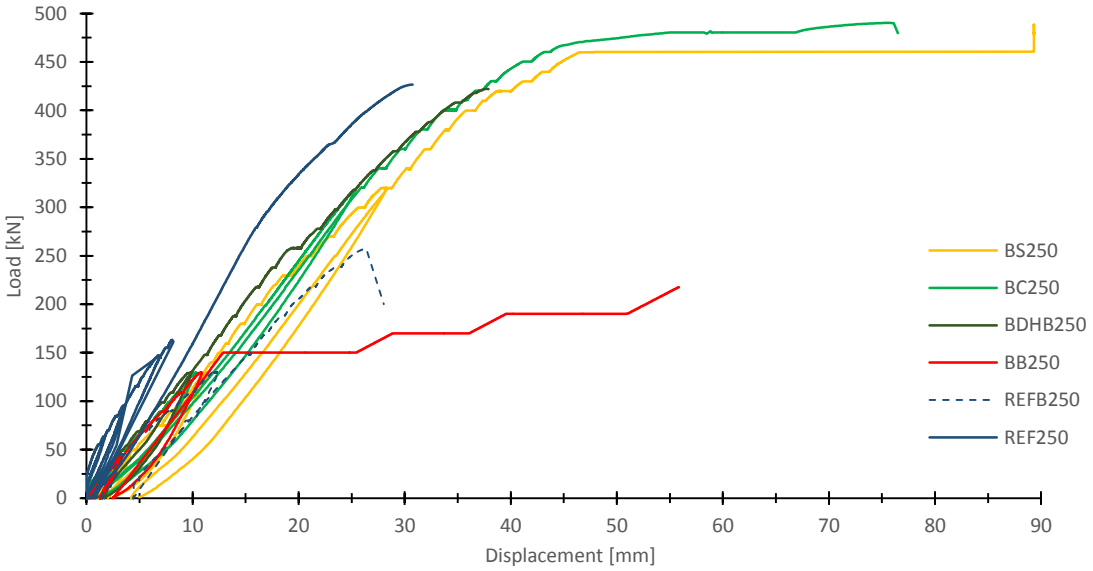

Figure 18 - Load-deflection curves

In Table 13 the ultimate mid-span deflections are also represented. In general, beams with closed stirrups, BS250 and BC250 exhibited higher ultimate deflections but also the highest ultimate loads. And if a fixed load value is considered, it can be stated that closed stirrups solutions exhibit higher stiffness.

Table 13 – Summary of mid-span deflections at service and ultimate loads

Beam	ρ_{sL}	Mid-span deflection			
		Service			Ultimate
		Exp.	Pred.	Exp /Pred	Exp.
	(%)	(mm)	(mm)	(-)	(mm)
REF250	1.58	4.5	5.0	0.90	31.1
REFB250		6.8	5.0	1.36	27.2
BS250		6.2	5.4	1.15	88.0
BC250		6.1	5.4	1.13	75.7
BDHB250		5.2	5.4	0.96	38.0
BB250		6.1	5.4	1.13	55.0

2.2.1.5 Reinforcement strains

2.2.1.5.1 Mid-span reinforcement strain

The strains at longitudinal reinforcement at mid-span measured by SG5 and SG6 are presented in Figure 19 and Figure 20. All beam specimens that failed for shear had a bilinear load-strain relationship with no evidence of yielding of longitudinal reinforcement or concrete crushing. BS250 and BC250 failed due to mid-span concrete crushing (bending failure) and exhibit load-strain relationship with a three-stage development: an elastic first phase until cracking, a second phase non-linear until the yielding and the yielded phase.

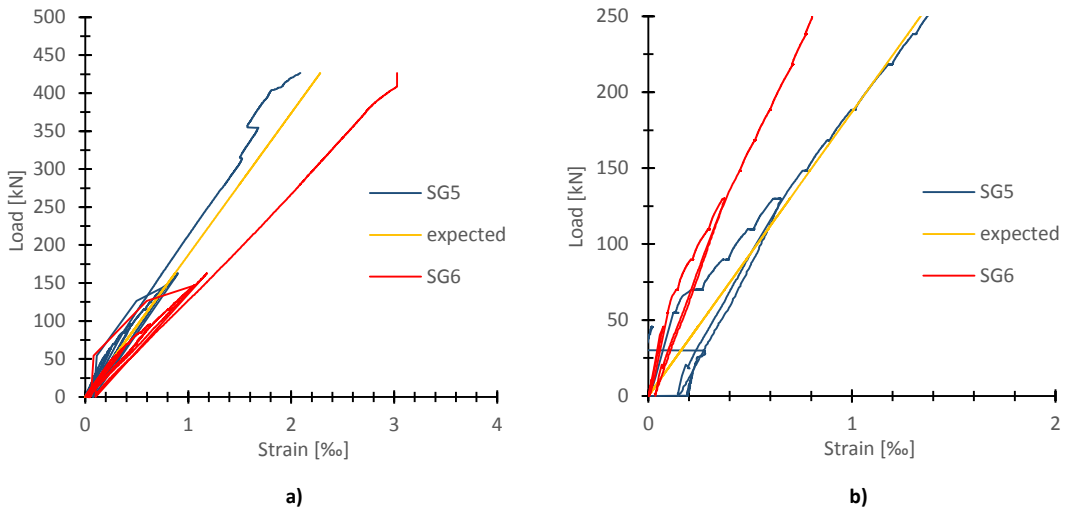

Figure 19 - Strain of tensile reinforcement: a) REF250; b) REFB250

A prediction of the strains of the bottom reinforcement by the “expected” curve was also presented in charts. These predictions were done by the equilibrium of forces in the section and relating the applied load with the reinforcement area. The strains were, in general, in accordance with predictions but for high load values. This enhances the importance of the contribution of the concrete to the tension stiffening at lower load levels when the beams are little cracked. As the load increases, the reinforcement becomes more responsible for supporting the load carrying, as assumed in a simplified form in the predictions. The strain values for the maximum load capacity are presented in Table 14. The variation of the measured values to the predictions is lower than ± 10%.

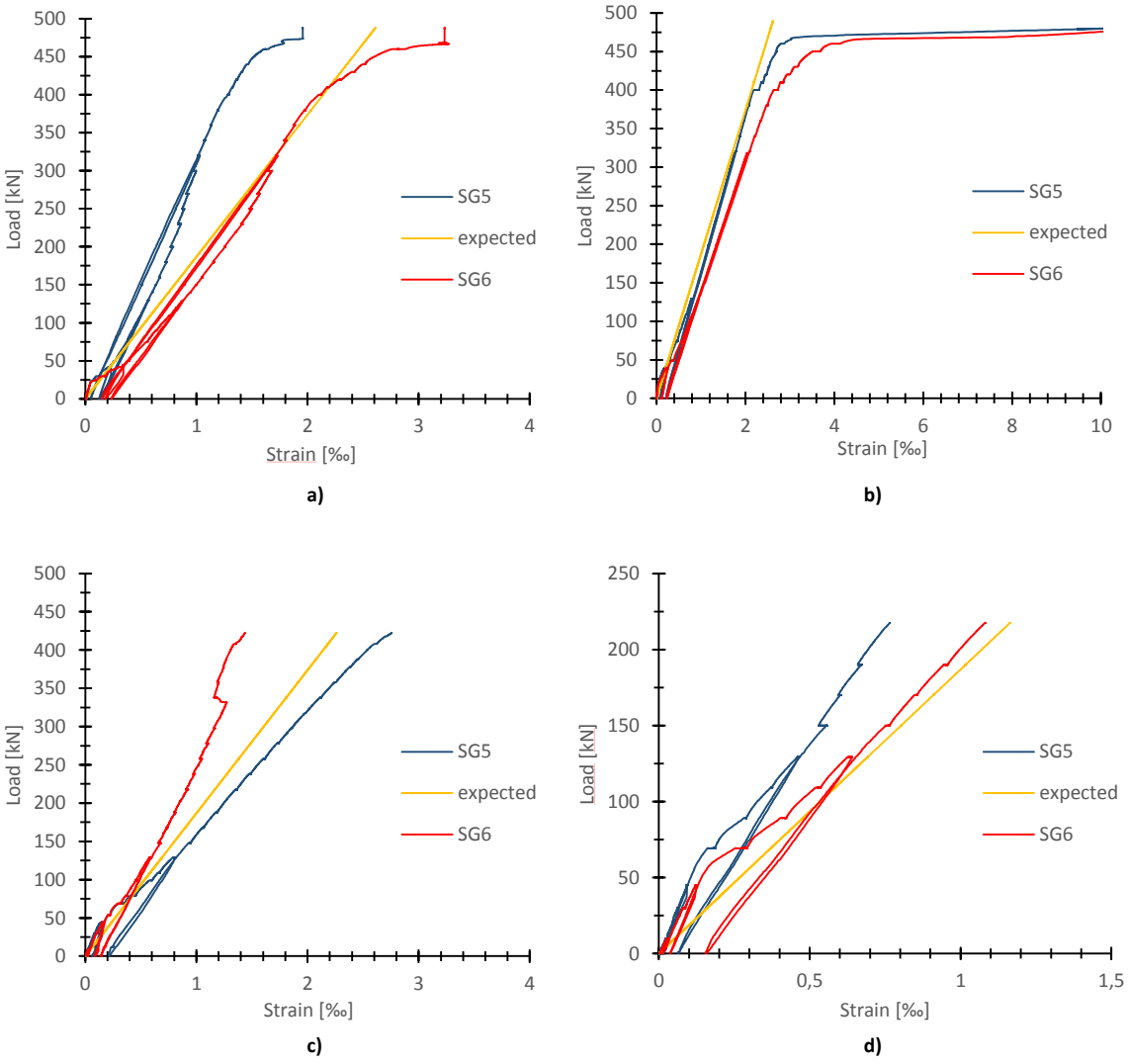

Figure 20 -Strain of tensile reinforcement: a) BS250; b) BC250; c) BDHB250; d) BB250

2.2.1.5.2 Shear reinforcement strain

The maximum shear reinforcement strains for the different beam specimens, as well as the predicted values, are presented in Table 14. Figure 21 shows, for each beam, the development of the strain at the most stressed stirrup, as well as a rough prediction of the strains expressed by the equation (11), as a function of the applied load, P, the reinforcement spacing, s , the area, A_{fv}, and the elasticity modulus, E_{fv}, of the shear reinforcement and the internal lever arm, z.

$$\varepsilon_{fv} = \frac{Ps}{2zE_{fv}A_{fv}} \tag{11}$$

In general, the strain values were close to expected near the failure, being in agreement with the typical behaviour of steel RC elements. Beams with closed stirrup or C-stirrup, BS250 and BC250, mobilized better the shear strength of the reinforcement, followed by BDHB250. Consequently, these beams had a higher shear load capacity than BB250.

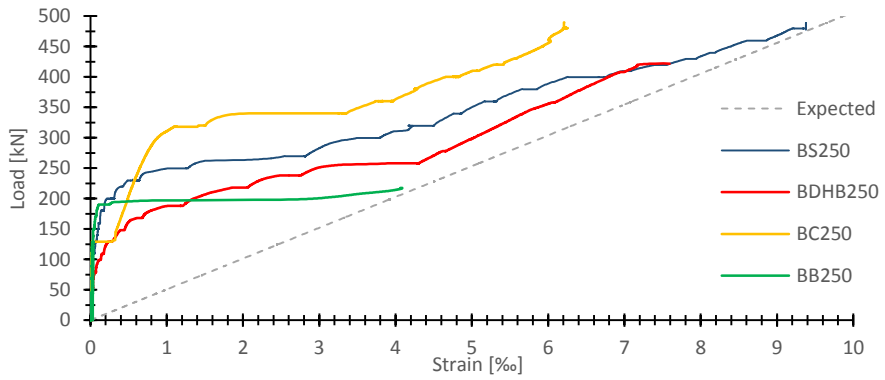

Figure 21 – Comparison of strains

The evolution of the shear reinforcement strain in the shear span during the tests is plotted from the Figure 22 to the Figure 24. It was found that this development varies from beam to beam, and helps to explain the shear failures. It can be noticed that the stirrup near the support has very small strain values, as expected. The strain in the stirrups along the shear span is affected by crack development with the load increase, and several stirrups, the third and the fourth stirrups from the support, were the most stressed at failure. In the case of the REF250, the third stirrup was the most stressed since the beginning of the loading and near the failure it yielded, followed by the fourth stirrup which also yielded. For REFB250, only the third group of bars exhibit some strain. However, the third group did not reach the yielding once it slipped. BB250 had a strain development similar to REFB250, where the third pair of bars was the most mobilized. For BDHB250, only the fourth pair of bars was mobilized. This can be explained by the fact that the first shear cracks appeared at the

bottom of the beam, breaking the head of the bars and causing them to slip. The cracks propagated in the direction of the fourth, however, as these pairs of bars were intercepted by the cracks at mid length, the anchorage length was guaranteed. The strains development on BS250 and BC250, followed a different pattern from all the other beams, because the second, the third and the fourth stirrups were mobilized from the beginning of the loading and reached strains in the order of 7‰. For all the beams, the highest strain levels were measured at the stirrups located at the middle of the shear span.

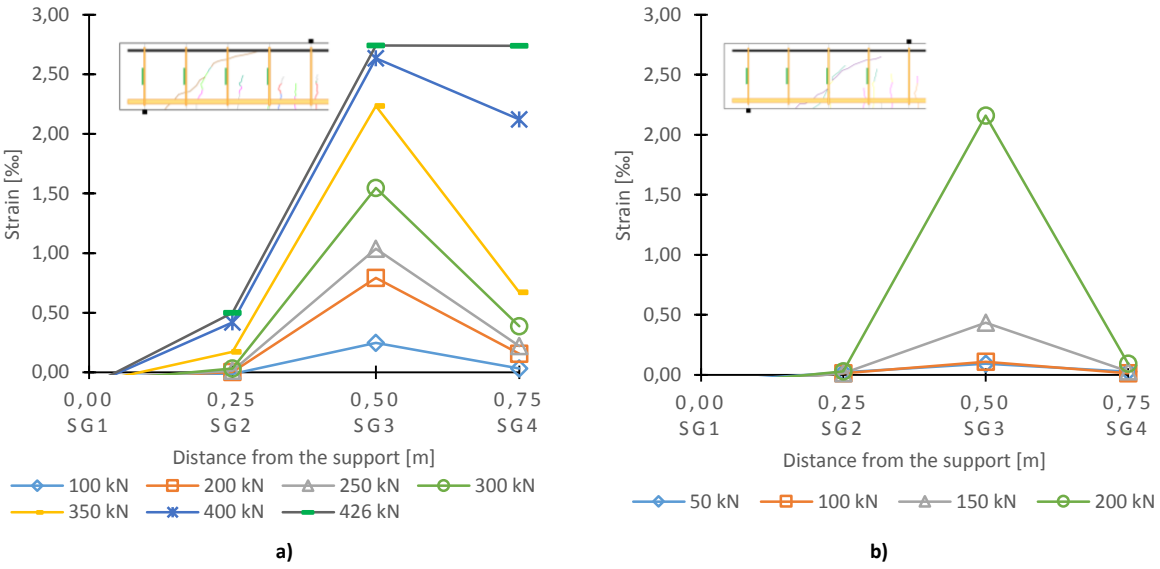

Figure 22 - Distribution of strains in the shear span of: a) REF250; b) REFB250

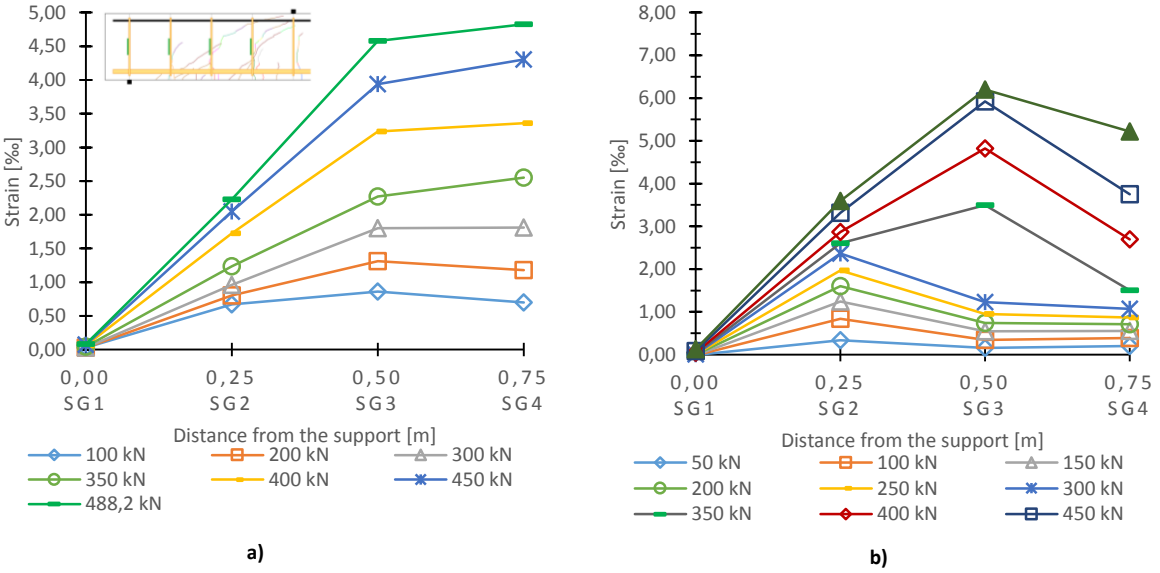

Figure 23 – Distribution of strains in the shear span of: a) BS250; b) BC250

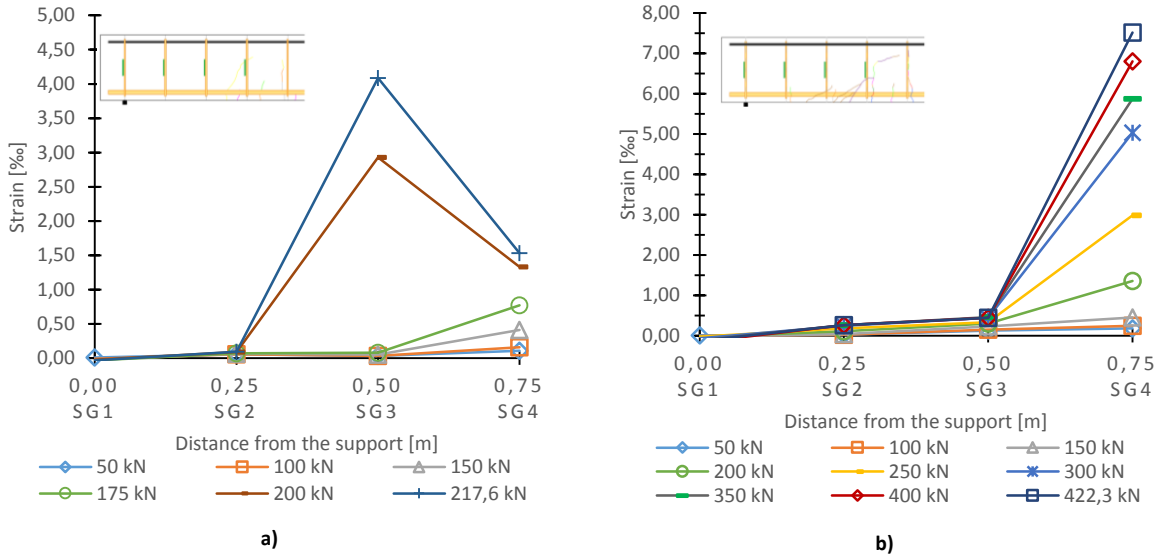

Figure 24 - Distribution of strains in the shear span of: a) BB250; b) BDHB250

Corresponding to an average of 4‰ strain in GFRP stirrups, which is the ACI 440.1R-06 [2] limit, the applied force was 305 kN for BS250, and represents 62.5% of the observed failure loads. For BC250, the applied force was 360 kN and represents approximately 62% of the ultimate capacity of the beam. Similar results were stated by [29].

Table 14 shows that the strains of shear reinforcement were, for all the beam specimens, higher than the ACI 440.1R-06[2] limit of 4‰, except for BB250. The maximum strains were reported in Table 14. The shear strains on BS250 and BC250 varied from 7‰ to 10‰, but as these two beams failed by compression of mid-span concrete, it is possible that the strains at shear failure could be higher.

Table 14 – Summary of ultimate strain values

Beam	ρ_{fL} or ρ_{sL}	ρ_{fv} or ρ_{sv}	Ultimate values					
			Mid-span strain			Shear reinforcement strain		
			Exp.	Pred.	Exp /Pred	Exp.	Pred.	Exp /Pred
	(%)	(%)	(‰)	(‰)	(-)	(‰)	(‰)	(-)
REF250	1.58	0.16	2.53	2.25	1.12	2.74	9.00	0.30
REFB250			1.04	1.30	0.80	2.14	4.00	0.54
BS250		0.36	2.08*	2.39	0.87	9.38	9.40	1.00
BC250			3.31*	2.50	1.34	6.25	9.15	0.68
BDHB250			2.05	2.25	0.90	6.82	7.20	0.95
BB250			1.08	1.16	0.93	4.00	5.20	0.77

- at yielding point

2.2.1.6 *Shear crack width*

Figure 25 presents the shear crack width evolution with the loading. It is not clear any relation between the stirrups solution and the shear crack widths. The larger crack widths developed on GFRP reinforced beams are responsible for the lower shear strength, although the characteristics of shear failure are similar to that of the steel RC beams.

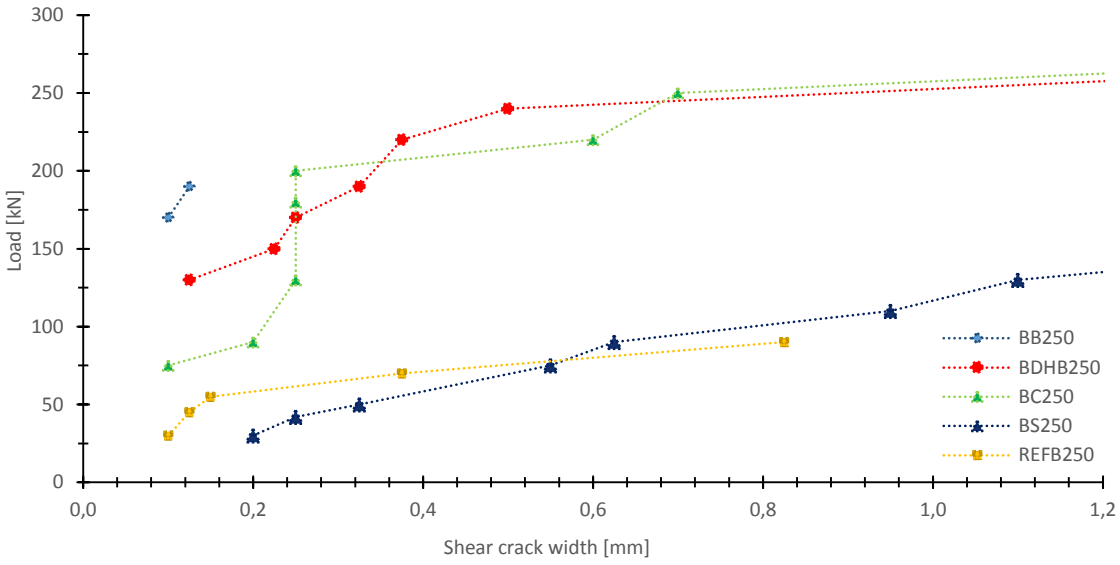

Figure 25 – Width of shear cracks

2.2.2 Conclusions

This study evaluated the performance of four GFRP shear reinforcement solutions by testing and comparing full-scale intermediate length GFRP shear RC beams with steel shear RC beams and with design provisions predictions. In general, the results show that GFRP shear reinforcement is efficient, and that the overall behaviour of GFRP reinforced beams is similar to steel reinforced beams on cracking pattern and failure mechanisms.

Although all the beam specimens had the same shear reinforcement amount, the four solutions had distinct performances. GFRP bent bars with closed stirrups (BS250 and BC250) had the higher shear capacity, followed by the BDHB250 and finally by the BB250. This behaviour can be explained by the anchorage length provided by the two horizontal branches on the stirrups which enhances

the capacity of the beam to mobilize the shear reinforcement. Thus, the best solutions were the closed stirrups (BS250 and BC250) followed by the bars with the end heads (BDHB250). BB250 and REFB250 exhibit lack of anchorage length when compared with the others solutions.

Beams with GFRP traditional stirrups and GFRP C-stirrups have a similar overall behaviour and shear strength that overcomes the different codes predictions. C-stirrups, being easier and more flexible to use in the field, represent an adequate solution.

Although the shear capacity of BDHB250 was lower than the capacity of BS250 and BC250, the overall behaviour was efficient and overcome the different codes predictions, being also an adequate solution to be applied. Furthermore, this solution is easier to use in the field.

The solution of using two straight vertical bars as shear reinforcement was proved to be inefficient, and had a shear strength lower than predictions. Considering the service load levels, BB250 behaviour was similar to the other beams. However, comparing the ultimate loads with the predictions the shear capacity was overestimated, and thus this solution is inefficient, and should not be applied.

Applying ACI 440.1R-06 [2] to determine the design shear capacity overly underestimates the beams capacity when using the limit of 4‰ for the maximum strain. The level of underestimation is particularly high for the solutions with GFRP bent bars. It was found that for this strain level, the beams were still at 60-70% of their shear capacity. It was showed that a more accurate prediction, although safe, can be achieved if the strain limit was increased to 7‰ when designing with GFRP bent closed stirrups and with the double headed bars.

Similarly, concerning the EC2 [23] modifications proposed by FIB40 [22] it was demonstrated that more accurate predictions can be obtained if the limit strain is increased to 7‰ and if the angle of strut is modified to 38° instead of 45°.

Also, from a design point of view, the predictions from both ACI 440.1R-06 [2] and FIB40 [22] were very restrictive resulting in ratio experimental to predicted from 2.5 to 3.3. An experimental to predicted ratio of around 1.5 can be achieved, resulting in a more rational but safe design, if the strain limit was increased for 7‰ and if the variable strut angle was considered instead of the fixed approach.

Applying ACI 440.1R-06 [2] to predict the short-term deflections at service load gives the predictions close to the experimental value.

It was found that the number of shear cracks is related to the shear capacity. The higher the failure load, the higher is the number of shear cracks. To all beams, the angle of shear failure was in good

agreement with the 45 degrees truss model. And generally, beams failed by the shear crack closest to the support.

From the four GFRP shear reinforcement solutions tested, only the simple vertical bars (BB250) was found to be inefficient. Moreover, the combination of GFRP as shear reinforcement and steel as longitudinal reinforcement is efficient and economical, and still adequate for use where the corrosion is the main concern because the shear reinforcement is the first to be corroded as it is located closer to the edge of the beams when comparing to the longitudinal reinforcement.

2.3 Experimental analysis of different GFRP transverse reinforcement solutions in reinforced concrete beams with GFRP longitudinal bars

This section has two main goals: to compare the behaviour of the four different GFRP transverse reinforcement solutions in RC beams with GFRP longitudinal reinforcement and the influence of reducing the longitudinal stiffness from the GFRP beams to the reference beams.

To accomplish these objectives, the performance of 4 GFRP shear and longitudinally reinforced (BS250GFRP1, BC250GFRP1, BDHB250GFRP1 BB250GFRP1) was compared with the performance of the two references (REF250 and REFB250).

The GFRP beams were longitudinally reinforced to keep the same area and, approximately, the same predicted ultimate capacity of the reference beams, to analyse the influence of the material and of the lower longitudinal stiffness. Within the GFRP beams group, the dowel effect and the longitudinal stiffness were unchanged, in order to evaluate only the influence of each transverse solution.

The four different GFRP bar solutions used as shear reinforcement were the following: bent bars forming a closed hoop stirrup; two C-shaped bent bars overlapped to form a closed stirrup; two vertical straight bars and two double headed vertical straight bars.

Specimens were designed to fail due to shear and subjected to four point bending tests until failure. The behaviour was analysed in terms of load-deflection response, ultimate load capacity, shear and flexural reinforcement strains, crack pattern and shear crack widths. Furthermore, a comparison with ACI 440.1R-06 [2] and FIB40 [22] predictions was also done.

The tests proved that the GFRP shear and longitudinally reinforced beams are reliable. Furthermore, solutions with GFRP bent bars are effective as shear reinforcement and that its bending process does not reduce the resistance performance of the material. It was also concluded that the general FRP design guidelines present overly conservative proposals to estimate the shear resistance. The solution with double headed bars had a disappointing performance in this case, with a shear resistance lower than predictions, showing that this solution is highly dependent on the longitudinal stiffness. Similarly, the beam with straight bars as shear reinforcement has proven to be an inadequate solution.

2.3.1 Results and discussion

2.3.1.1 Ultimate capacity

The experimental capacity of all beams and the corresponding failure modes are presented in Table 15. In order to establish a comparison, the theoretical values of the expected shear and bending load capacities according to ACI 440.1R-06 [2] / ACI 318-11 [3] and EC2 [23]/FIB 40 [22] are also indicated. The average material properties (without any safety factor) were considered for the calculation of the theoretical non-design capacities. The shear equations used are listed in Table 16.

Table 15 – Experimental and non-design theoretical capacities

	Non-design Capacity							
	Experimental		ACI 440.1R-06 [2] / ACI 318-11[3]			EC2 [23]/FIB 40 [22]		
Beam	Type	Load (kN)	Shear (kN)	E/P*	Bending (kN)	Shear (kN)	E/P	Bending (kN)
REF250	Shear	426.4	393.9	1.1	546.2	326.6	1.3	543.8
REFB250	Shear	257.4	391.3	0.7	544.0	325.3	0.8	541.5
BS250GFRP1	Shear	400.0	245.8	1.6	449.9	275.6	1.5	527.7
BC250GFRP1	Shear	318.5	261.4	1.2	507.5	284.3	1.1	595.2
BDHB250GFRP1	Shear	202.2	251.6	0.8	437.5	273.7	0.7	513.1
BB250GFRP1	Shear	293.9	250.9	1.2	434.2	273.1	1.1	509.2

*E/P – ratio between experimental and non-design predictions.

Table 16 – ACI 440.1R-06 [2] and FIB 40 [22] shear design equations

Model	Concrete shear equations		Reinforcement shear equations	
ACI 440.1R-06 [2]	$V_c = \frac{2}{5} k \sqrt{f_c'} b d$	(12)	$V_{fv} = \frac{A_{fv} \sigma_{fv} d}{s}$	(13)
	$k = \sqrt{2\rho_{fl} n_f + (\rho_{fl} n_f)^2} - \rho_{fl} n_f$	(14)	$\sigma_{fv} = 0.004 E_{fv} \leq f_{fb}$	(15)
	$n_f = \frac{E_{fl}}{E_c}$	(16)	$f_{fb} = \frac{\left(\frac{0.05 r_b}{d_b} + 0.3\right)}{1.5} f_{fv} \leq f_{fv}$	(17)
FIB 40 [22]	$V_c = 0.12 \left(1 + \sqrt{\frac{200}{d}}\right) \left(100 \rho_{fl} \frac{E_{fl}}{E_s} \phi_\varepsilon f'_c\right)^{1/3} b d$	(18)	$V_f = \frac{A_{fl}}{s} f_{fl} z \cot\theta$	(19)
	$\phi_\varepsilon = \varepsilon_f / \varepsilon_y$	(20)		
	$\varepsilon_f = 0.0045$	(21)		

All beam specimens failed by shear, as designed. The ratio between the experimental shear load and the non-design prediction is also referred in Table 15. Concerning the GFRP beams, with exception of BDHB250GFRP1, the experimental capacity was higher than theoretical non design values of both codes. The load capacity of BS250GFRP1 was highly underestimated by both codes. The capacity of this beam was 60% and 50% higher than non-design prediction values of ACI 440.1R-06[2] and FIB 40[22], respectively. It was expected that BC250GFRP1 and BS250GFRP1 would exhibit similar performance, but a problem during the test caused premature failure at the beginning of third load-discharge cycle. Nevertheless the load capacity was higher than non-design predictions. It was also expected that the experimental shear capacity of BDHB250GFRP1 was higher than the capacity of BB250GFRP1 due to lack of anchorage length of the latter, but a shear crack damaged and compromised the end heads of two pairs of GFRP bars, causing the immediate slip of the bars. As result, the capacity of BDHB250GFRP1 was only 80% and 70% of the non-design theoretical capacity, of ACI 440.1R-06 [2] and FIB 40 [22], respectively.

Comparing the beams with the respective reference, the ultimate capacities of the BS250GFRP1 and BC250GFRP1 were 94% and 75% of the ultimate capacity of REF250, respectively.

The BDHB250GFPR1 had 79% of the capacity of REFB250, while BB250GFRP1 had 114% of the capacity of REFB250, although they have been designed to have the same ultimate shear strength. The fact that none of the GFRP beams, with the exception of BB250GFRP1, exceeded the load capacity of the respective reference may be related to the influence of the lower longitudinal stiffness of the GFRP beams.

Comparing the different GFRP solutions, it was verified that beams with close shear reinforcement had higher shear failure loads: BS250GFRP1 had 2.1 times higher capacity than BDHB250GFRP1 and 1.45 times higher capacity than BB250GFRP1.

Table 17 has the values of shear capacity varying the limits of strains, and for the FIB 40[22] varying also the angle of the strut. The strains considered were the maximum values measured experimentally. For the BS250GFRP1, both codes give better predictions when the strain limit is increased to 6‰ which was the maximum strain measured by the gauges in the stirrups. The ratio experimental to theoretical in this case was 1.25 and 1.17 for ACI 440.1R-06 [2] and FIB 40 [22], respectively. For the FIB 40 [22], better predictions were achieved when the angle of the strut was approximated to the experimental value.

For the solutions with straight bars (BDHB250GFRP1 and BB250GFRP1), the maximum experimental strains (3‰ to 5‰), demonstrate that increasing the design strains isn’t conservative.

Table 17 - Non-design capacity varying the strain limits

Beam	Non-design Capacity								
	Experimental		ACI 440.1R-06 [2] / ACI 318-11 [3]			EC2 [23]/FIB 40 [22]			
	Type	Load	Shear			Shear			
						Θ=38˚			Θ=45˚
		(kN)	ε_{fv} = 4 ‰	ε_{fv} = 5 ‰	ε_{fv} = 6 ‰	ε_{fv} = 4.5 ‰	ε_{fv} = 5 ‰	ε_{fv} = 6 ‰	
			(kN)	(kN)	(kN)	(kN)	(kN)	(kN)	(kN)
BS250GFRP1	Shear	400.0	245.8	281.7	317.5	316.2	341.5	391.3	275.6
BC250GFRP1	Shear	318.5	261.4	297.2	333.1	324.9	350.6	400.9	284.3
BDHB250GFRP1	Shear	202.2	251.6	287.4	323.2	314.3	339.5	389.1	273.7
BB250GFRP1	Shear	293.9	250.9	286.7	322.6	313.8	338.9	388.6	273.1

As listed in Table 18, it was also established a comparison of the experimental capacities with the design values, calculated with ACI 440.1R-06 [2] and FIB 40 [22] but considering the safety factors. The experimental-design values ratio was higher than 1.5 for all the beams specimens, with the exception of BDHB250GFRP1. The value 1.5 is very often the global safety coefficient primarily used in steel RC, and therefore it was considered the comparison term. The experimental capacity of BS250GFRP1 was 2.2 times higher than the ACI 440.1R-06 [2] design value and 2.6 the FIB 40 [22]. Similarly, the experimental capacity of BC250GFRP1 was 1.8 and 2.1 times higher than the design values of ACI 440.1R-06 [2] and FIB 40 [22]. For BB250GFRP1 the experimental-design values ratio was 1.6 and 1.9, respectively for ACI 440.1R-06 [2] and FIB 40 [22] values. For the closed GFRP stirrup solutions, the experimental- design predicted values ratio can be approximated to 1.5 if the strain limit was increased to 6‰, which was the lowest maximum strain values verified during the tests.

Table 18 – Summary of experimental and design values of shear capacity

Beam	Shear Capacity					
	Experimental		Design Values			
	Load	Type	ACI 440.1R-06 [2] / ACI 318 -11[3]	Experimental/ Design	FIB 40 [22]/EC2 [23]	Experimental/ Design
	(kN)		(kN)	(-)	(kN)	(kN)
BS250GFRP1	400.0	Shear	180.2	2.2	151.0	2.6
BC250GFRP1	318.5	Shear	180.2	1.8	151.0	2.1
BDHB250GFRP1	202.2	Shear	180.2	1.1	151.0	1.3
BB250GFRP1	293.9	Shear	180.2	1.6	151.0	1.9

2.3.1.2 *Cracking pattern and failure modes*

In order to analyse the differences in the cracking behaviour, the crack development was marked with different colours on the beams after each load step. The cracking patterns were similar for both steel reinforced beams and GFRP beams, and are shown from Figure 26 to Figure 28. In the beginning of the testing, the beam specimens were uncracked .The first cracks appeared firstly at the constant moment region and grew vertically indicating the absence of shear stresses. With the loading, other flexural cracks appeared in the shear-span region. Although they are initially vertical, with the loading they propagated to the loading point. These inclined cracks - which were oriented perpendicularly to the direction of the maximum principal stress - were responsible for the failure. In all cases, the shear crack closest to the support was responsible for the failure of the beam. The slope of the plane of failure of beams varies from 37˚ to 43˚, which can be considered in agreement with the 45 degrees applied in the truss model. The angle of the failure plan was lower for the closed GFRP stirrups solutions. This explains the fact that for these two beams the best predictions with FIB 40 [22]/EC2 [23]were achieved when considering θ=38˚ (Table 17).

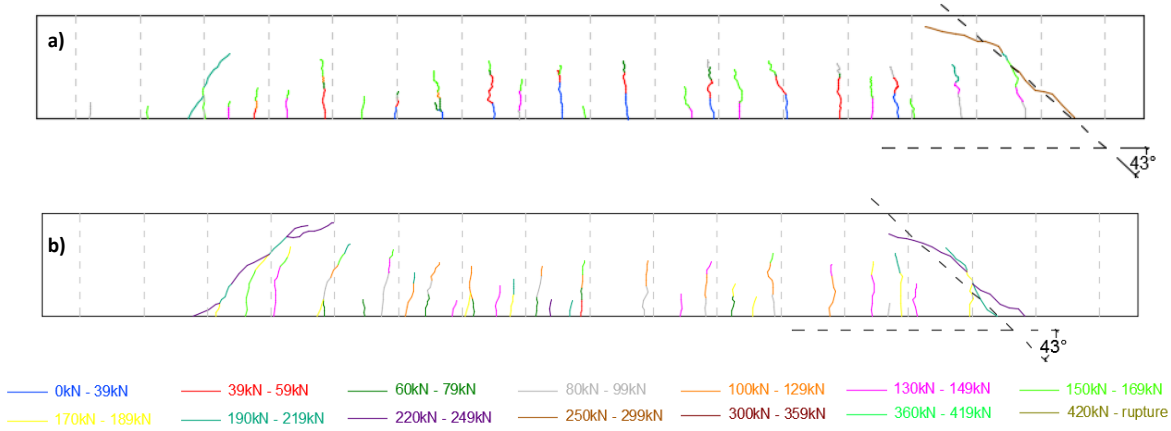

Figure 26 – Cracking pattern until failure of: a) REF250; b) REFB250

From the cracking pattern is also possible to estimate the height of the compression zone at failure (distance between the compression fibre and the neutral axis), which was measured considering the mean of the height from flexural cracks. All GFRP beam specimens exhibited the smaller compression zones, a mean height of 0.095m, while the reference beams exhibited a mean height of 0.150m. This shows that there was a rise of the neutral axis of the GFRP reinforced beams. This can be explained by the lower longitudinal stiffness of GFRP beams comparing to the steel, and consequently higher deflection, although the longitudinal reinforcement area remained the same.

For the GFRP beams, it can be stated that the higher the shear failure load, the more shear cracks appear, as shown by comparing the cracking pattern of BS250GFRP1 and BC250GFRP1 with the cracking pattern of BDHB250GFRP1 and BB250GFRP1.

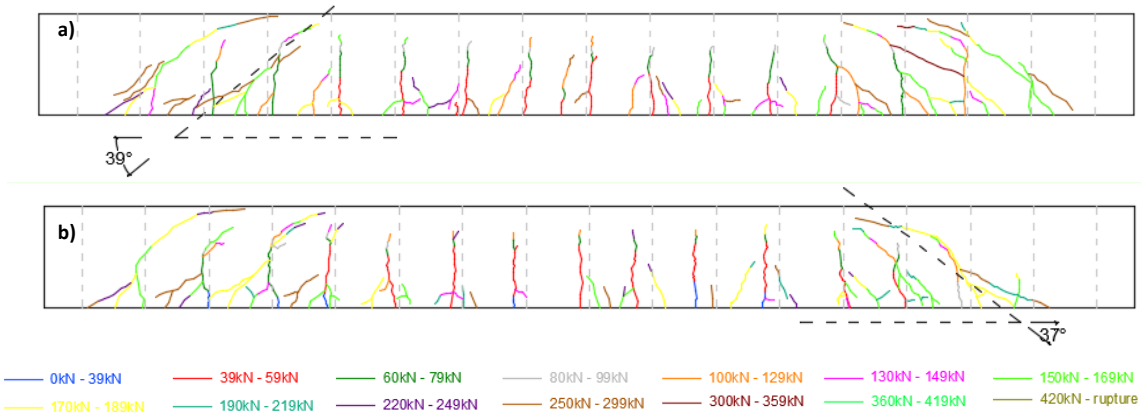

Figure 27 – Cracking pattern of: a) BS250GFRP1; b) BC250GFRP1

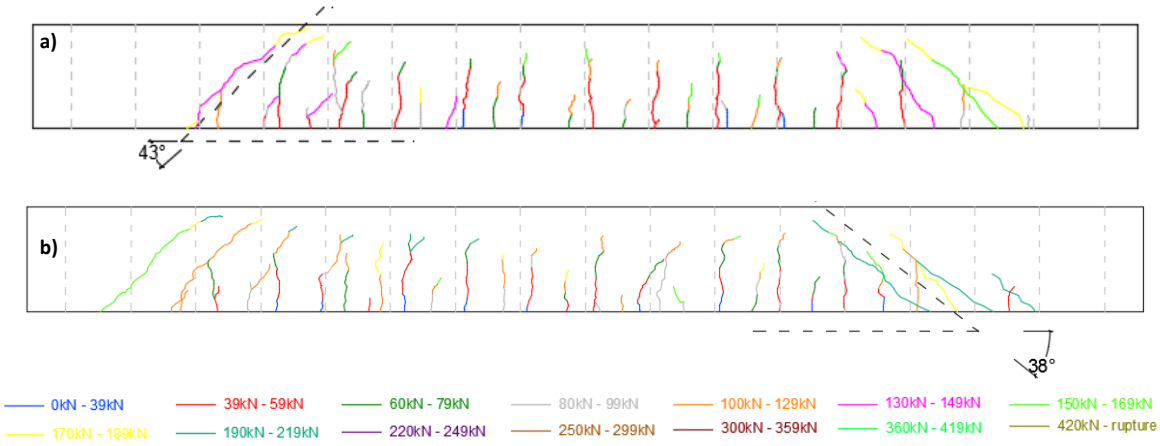

Figure 28 – Cracking pattern of: a) BDHB250GFRP1; b) BB250GFRP1

In terms of failure modes, there was no difference in the overall behaviour of the reference and the GFRP beams. The detailed failure of each beam specimen is presented from Figure 29 to Figure 34. Two distinct modes of failure occurs:

- shear diagonal tension failure by shear reinforcement failure (REF250; REFB250; BC250GFRP1, BDHB250GFRP1, BB250GFRP1);
- shear failure due to the failure of the bond of the longitudinal reinforcement at support (BS250GFRP1).

As shown in Figure 29, the reference beam REF250 had a brittle shear failure by the failure of third stirrup. With the loading, several flexural cracks developed vertically along the span (Figure 26 a)).

Above 150 kN, the cracks located between the loading points and the supports started to incline in the direction of the loading points. When the crack nearest to the support intersected the loading point, the crack width increased and the rupture of the third stirrup from support occured, followed by the rupture of all the others stirrups along the shear crack (Figure 29 c) and d)). This was responsible for the almost instantaneous failure of the beam at 426.4 kN (Figure 29 a) and b)). It was verified that these stirrup strains at failure was approximately 2.8‰, which is the yield strain of the considered steel.

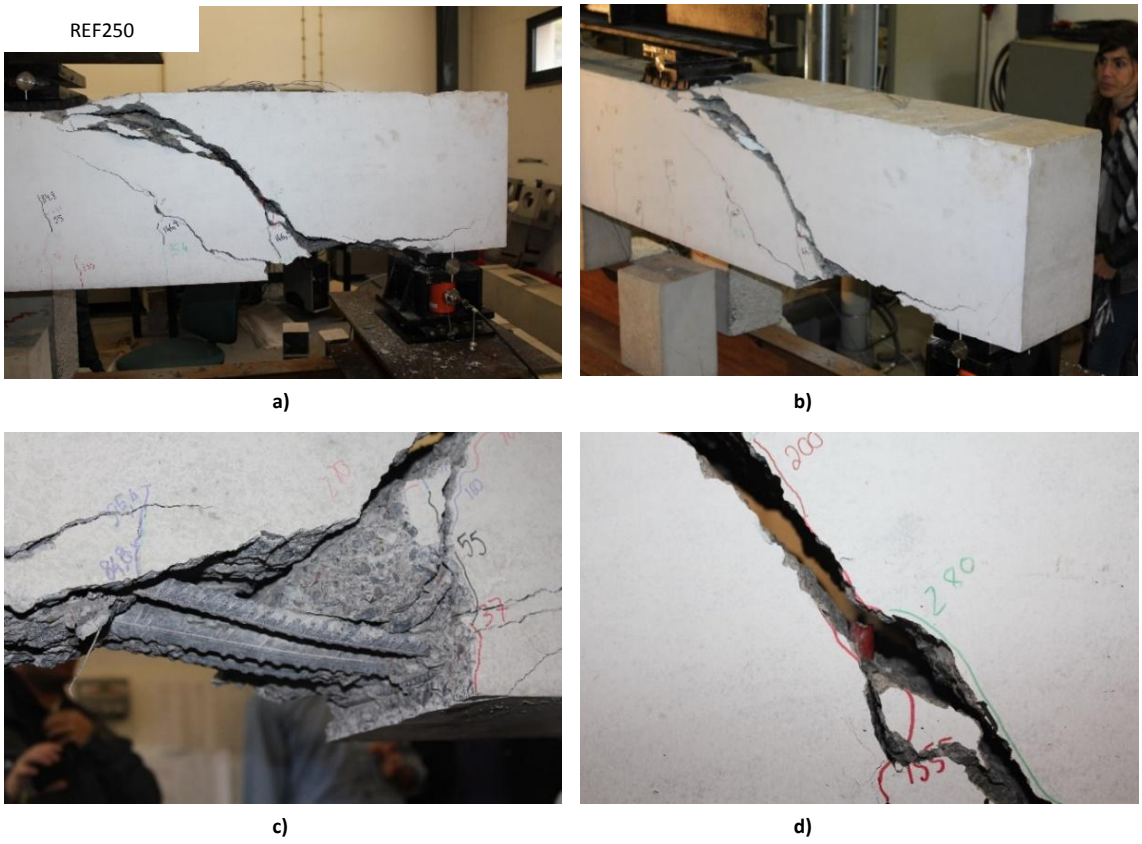

Figure 29 – REF250 beam failure: a) front view of the support; b) overall view of the failure; c) bottom reinforcement; d) broken stirrup

The REFB250 beam failed by the slip/pull-out of the shear reinforcement (Figure 30 a) and b)). Similarly to REF250, for loads under 130 kN, cracks develop vertically along all the span (Figure 26 b)). Above 130 kN the cracks near the supports started to incline in the direction of the loading points. The failure occurred when the third bar of the shear reinforcement slipped followed by others along the shear crack (Figure 30 c) and d)), leading to a quick failure of the beam at 257.4 kN. It was verified by the strain development that these bars did not reach the yield strain, they just slipped due to the lack of anchorage length.

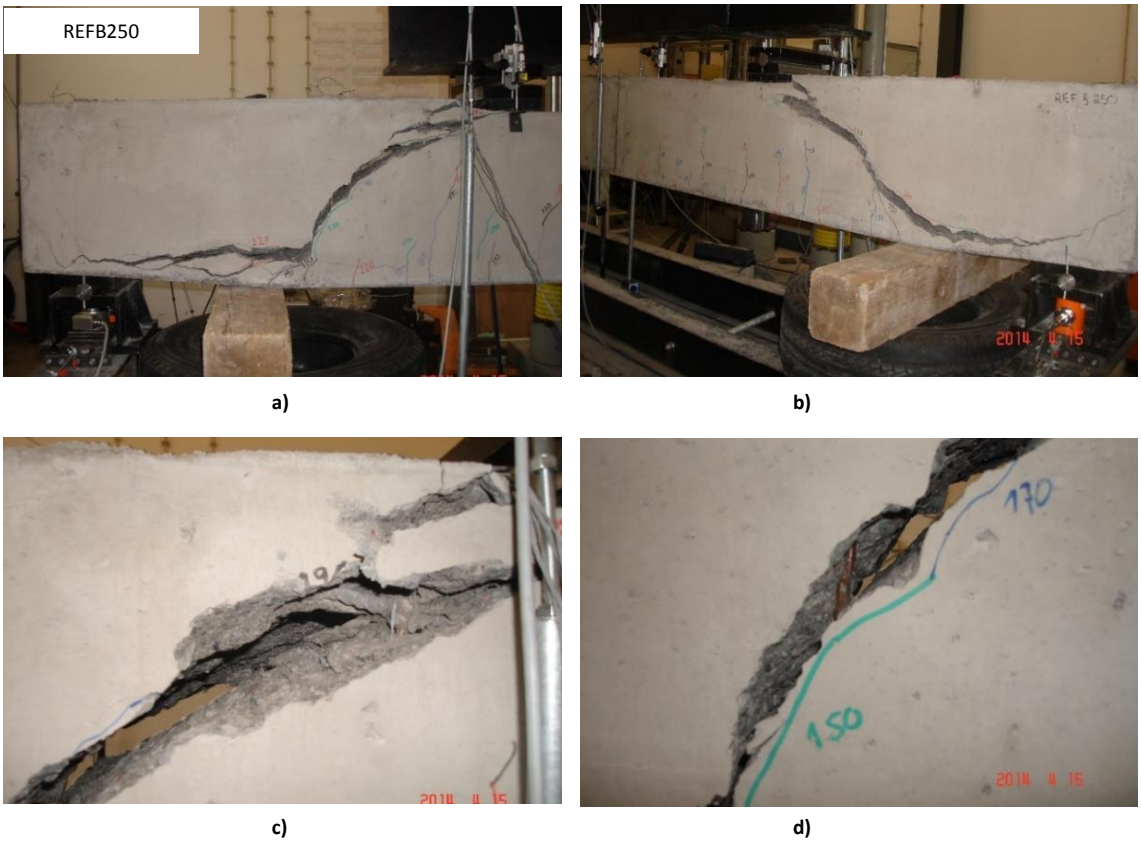

Figure 30 – REFB250 beam failure: a) overall view of one of the sides of the support; b) overall view of the other side of the support; c) slip of stirrup; d) slip of stirrup

As shown in Figure 31 a) and b) the failure of BB250GFRP1 beam was also a shear failure due to the slip of the shear reinforcement bars. For loads above 100 kN, the cracks on the shear span evolved on the direction of the loading points (Figure 28 b)). This was followed by the slip of the bars of the shear reinforcement along the shear crack, resulting in an increase of the crack width and the pull-out of the longitudinal bars near the support, leading to brittle failure at 293.9 kN (Figure 31 c) and d)).

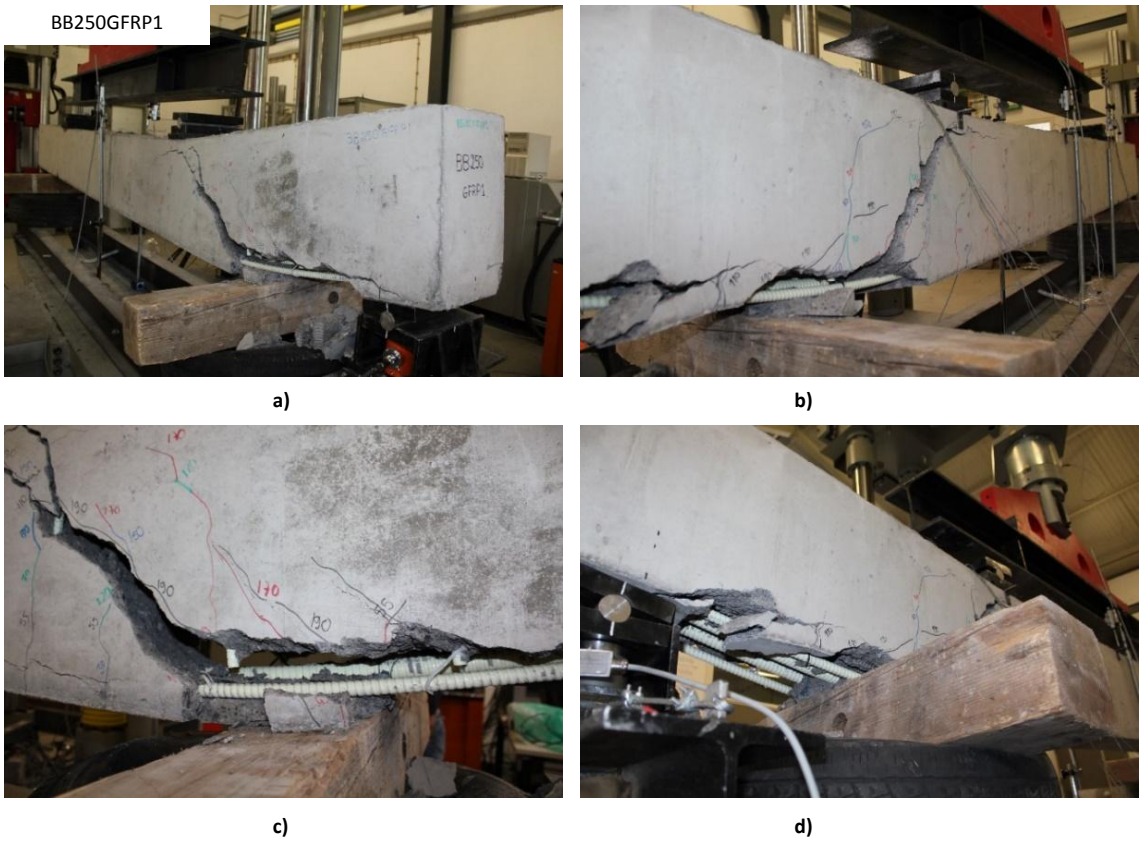

Figure 31 – BB250GFRP1 beam failure: a) overall view of the failure; b) other side; c) pull-out of the shear reinforcement at the bottom; d) bottom longitudinal reinforcement pull-out

The shear failure of BDHB250GFRP1 beam was due to the fracture of several end heads of the shear reinforcement bars (Figure 32 a) and b)). The shear cracks appeared above 130 kN (Figure 28 e)) and, a shear crack has damaged the end heads of GFRP of two pairs of bars at the bottom of the beams, compromising their function and causing the immediate slip of the bars. This was followed by a total separation of the beam's section at the longitudinal reinforcement level for the load of 202.2 kN (Figure 32 c) and d)).

The failure of BC250GFRP1 beam was a shear failure due to the disintegration of the C-stirrups followed by the pull-out of the longitudinal bars near the support (Figure 33). For loads above 180 kN the cracks on the shear span evolved on the direction of the loading points (Figure 27 e)). Due to a deficiency on the testing, this beam failed at the third charge-discharge cycle, but it was previously submitted to 318.5 kN. As shown in Figure 33 c), the helically grooved coating and the ribs of the stirrups were ripped out. The strains of the stirrups at the failure's side were lower than the strains of the opposite side of the beam: it was measured a maximum strain of almost 10‰ on the opposite side of the failure while the maximum strain was approximately 6‰ on the failure's side.

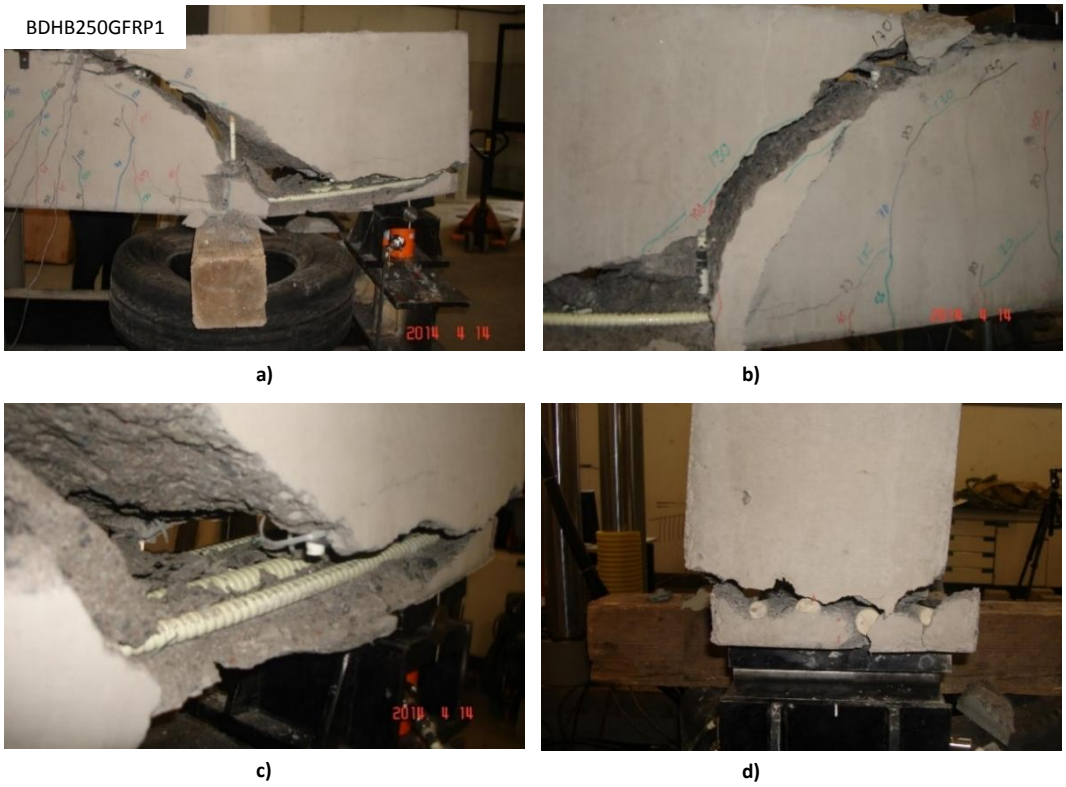

Figure 32 – BDHB250GFRP1 beam failure: a) overall view near the support; b) fractured top and bottom heads; c) bottom reinforcement pull-out; d) detachment of the section near the bottom reinforcement

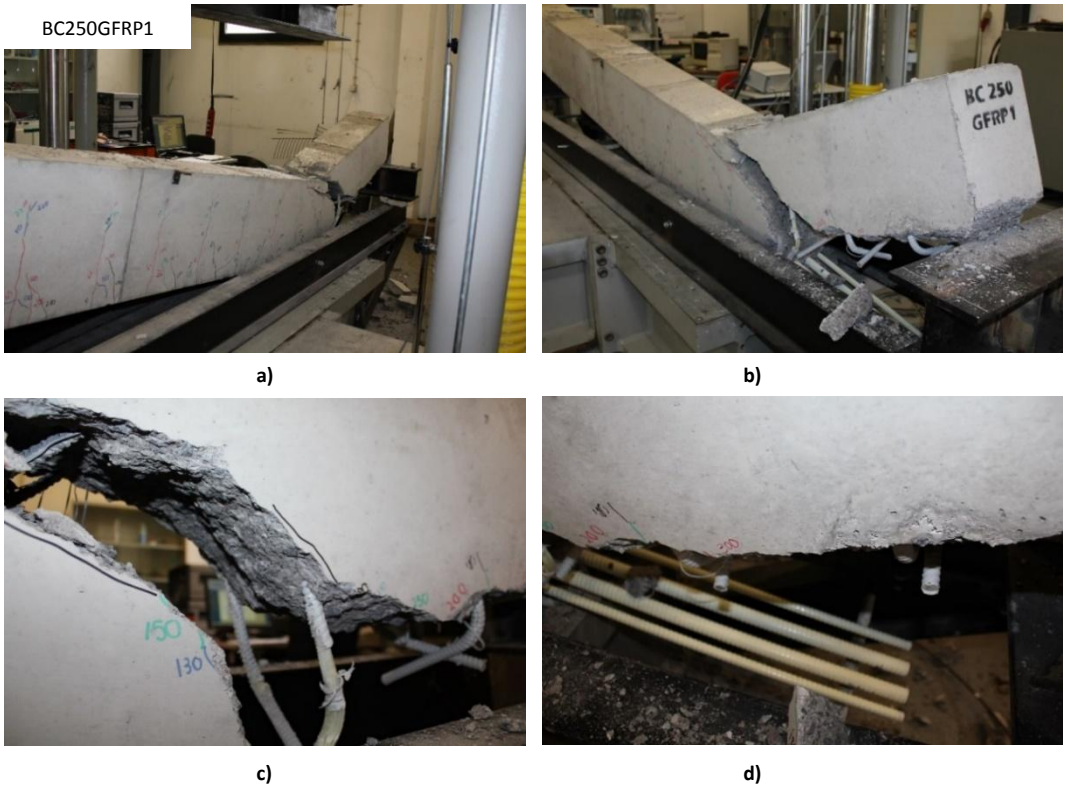

Figure 33 – BC250GFRP1 beam failure: a) overall view; b) near the support; c) stirrup disintegration; d) pull-out of bottom reinforcement

In Figure 34, there is the BS250GFRP1 beam failure which was also a brittle shear failure due to the pull-out of the longitudinal reinforcement at 400 kN. Figure 34 d) shows the pull-out of the longitudinal reinforcement, and Figure 34 c) shows a secondary concrete crushing. The shear cracks appeared for loads near the 150 kN (Figure 27 a)) and when failure was imminent, horizontal cracks appeared from the bottom of the shear cracks towards the supports. This can be explained by the loss of the aggregate interlock at the shear crack, when the failure is imminent. In order to keep the equilibrium at the section, the dowel action in the longitudinal reinforcement has to increase. This increase of the dowel action causes vertical tension stresses which combined with the existing splitting forces due to flexural bond can lead to the bond-anchorage failure [98], as happened at 400 kN.

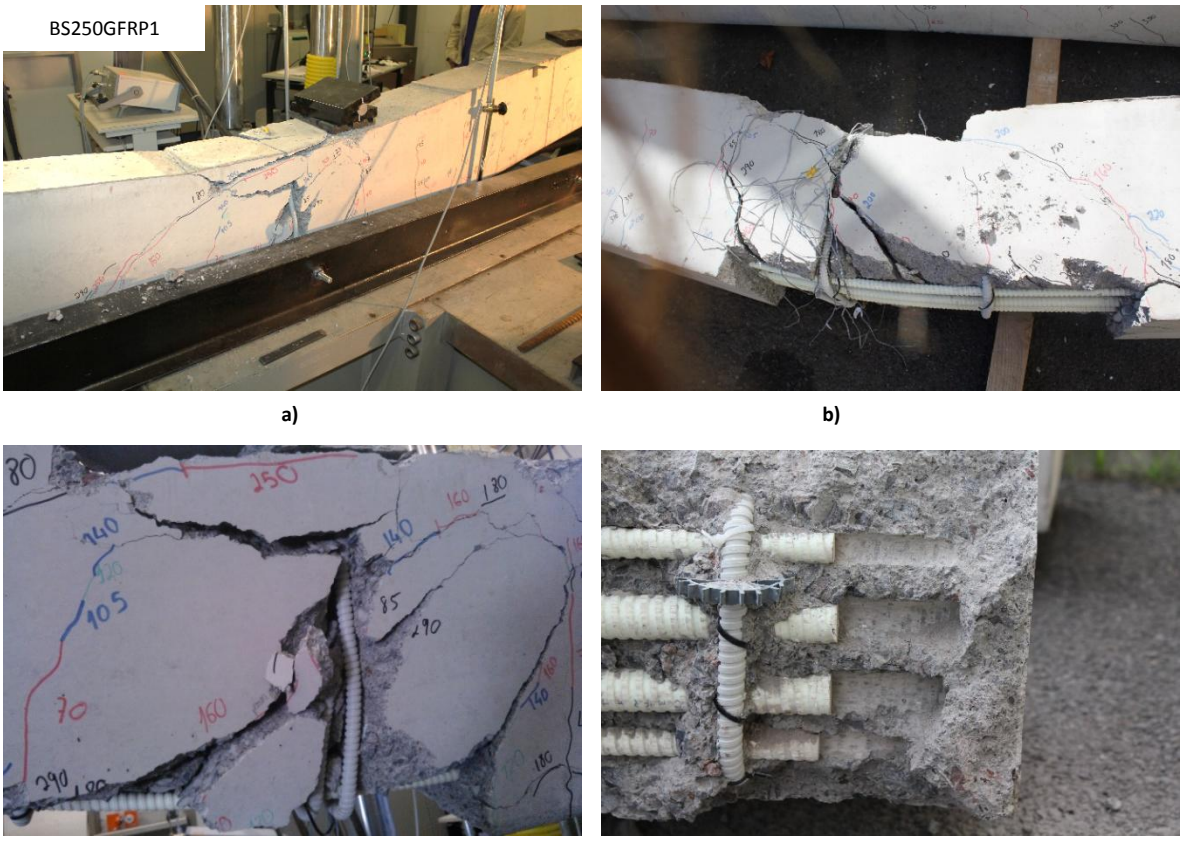

Figure 34 – BS250GFRP1 beam failure: a) overall view; b) near the support; c) crushing of concrete under the loading point; d) slip of longitudinal reinforcement near the support

2.3.1.3 Mid-span defection

The load-deflection curves at mid-span are shown in Figure 35. The REF250 and REFB250 curves were also plotted over the other curves for the immediate comparison of the behaviour and the

flexural stiffness. Each curve represented in Figure 35 is the deflection obtained by the 100 mm LVDT mounted at mid-span. In general, for loads under the load of the cracking moment, all the specimens exhibited an initial elastic phase where the load-displacement relation was linear, followed by a cracked phase where the load-displacement relation was still linear but with lower slope. For all the beams the load-displacement curves developed with only two distinct phases which were approximately linear, with no yielding and no ductile behaviour. Until failure, the load-deflection curves are approximately coincident for the beams with the same longitudinal stiffness (longitudinal reinforcement area and material), independently of the shear reinforcement solution. For GFRP beams (Figure 35) the stiffness was the lowest and, after the cracking load, the deflection was on average 1.5 times higher than REF250. Comparing the REF250 with REFB250, it is possible to notice that since the beginning of the loading the deflection was higher than on REFB250, showing lower stiffness when compared with the other steel beam. The reference REF250 exhibited the higher longitudinal stiffness.

From Table 19, it is possible to state that there is no difference between the deflections of beam specimens for the service load (50 kN). However, with the load increase, the GFRP beams exhibited the higher deflections due to their lower longitudinal stiffness. Comparing the service predicted deflections with the experimental deflections, the experimental deflections were on average 25% higher than predicted. For the reference beams: REF250, the experimental deflection was 10% lower than predictions, and for REFB250 the experimental displacement was 36% higher than predicted.

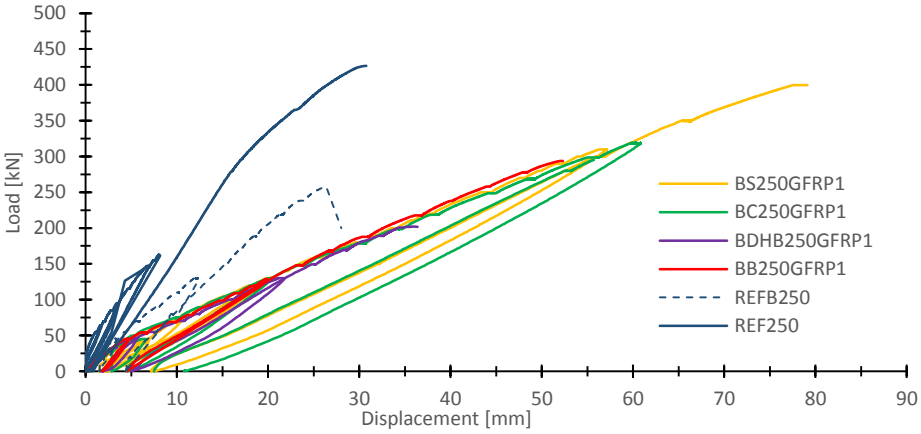

Figure 35 - Load-deflection curves GFRP 2ϕ16+2ϕ25 reinforced beams

Table 19 represents the ultimate mid-span deflections. In general, the beams with closed stirrups solutions exhibited higher ultimate loads but also higher ultimate deflections.

Table 19 – Summary of mid-span deflections at service and ultimate loads

Beam	ρ_{fL} or ρ_{sL}	$E_{sl}A$ or $E_{fl}A$	Mid-span deflection			
			Service			Ultimate
			Experimental	Predicted	Exp /Pred	Experimental
	(%)	(kN)	(mm)	(mm)	(-)	(mm)
REF250	1.58	304.48	4.5	5.0	0.90	31.1
REFB250			6.8	5.0	1.36	27.2
BS250GFRP1		83.04	8.0	6.1	1.31	78.0
BC250GFRP1			5.6	6.1	0.92	60.8
BDHB250GFRP1			7.8	6.1	1.28	36.4
BB250GFRP1			5.6	6.1	0.92	52.1

2.3.1.4 Reinforcement strains

2.3.1.4.1 Mid-span reinforcement tensile strains

The strains measured at the bottom of the longitudinal reinforcement at mid-span are presented from Figure 36 and Figure 37. All beam specimens that failed for shear had a bilinear load-strain relationship with no evidence of yielding of longitudinal reinforcement or concrete crushing (shear failure).

The strains in the longitudinal reinforcement were also predicted by the equilibrium of forces in the section, assuming that the entire applied load was carried by the longitudinal reinforcement. It is expected that the strain values of this approximation are closer to the experimental near the ultimate load, when the beam specimens are highly cracked. These predictions are also presented in charts by the “expected” curve. The average values of strains were, in general, in accordance with predictions for high load values. This was expected as the predictions were done assuming

that the load carrying capacity was assured by the reinforcement. For lower load values where beams are little cracked, the concrete contribution is important to the tension stiffening. The strain values, for the maximum load capacity, are presented in Table 14. The variation of the measured values to the predictions is lower than ± 10%.

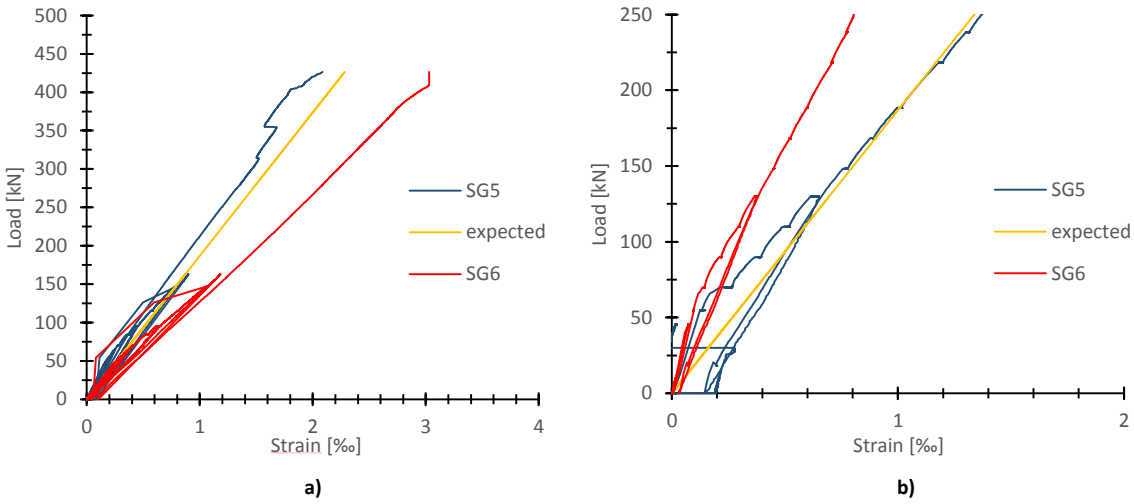

Figure 36 - Strain of tensile reinforcement: a) REF250; b) REFB250

By comparing steel reinforced beams, it is possible to see that the GFRP beams had the highest reinforcement strains. The curves differ from one stirrup to another, but the behaviour is similar. These differences are related to the cracking pattern, which is different on both sides of the beam. As the cracking patterns of the two faces of a beam are not exactly the same, the strain gauge on one side can be subjected to different strains in comparison to the opposite side. Moreover, it is known that the strains close to a crack are affected.

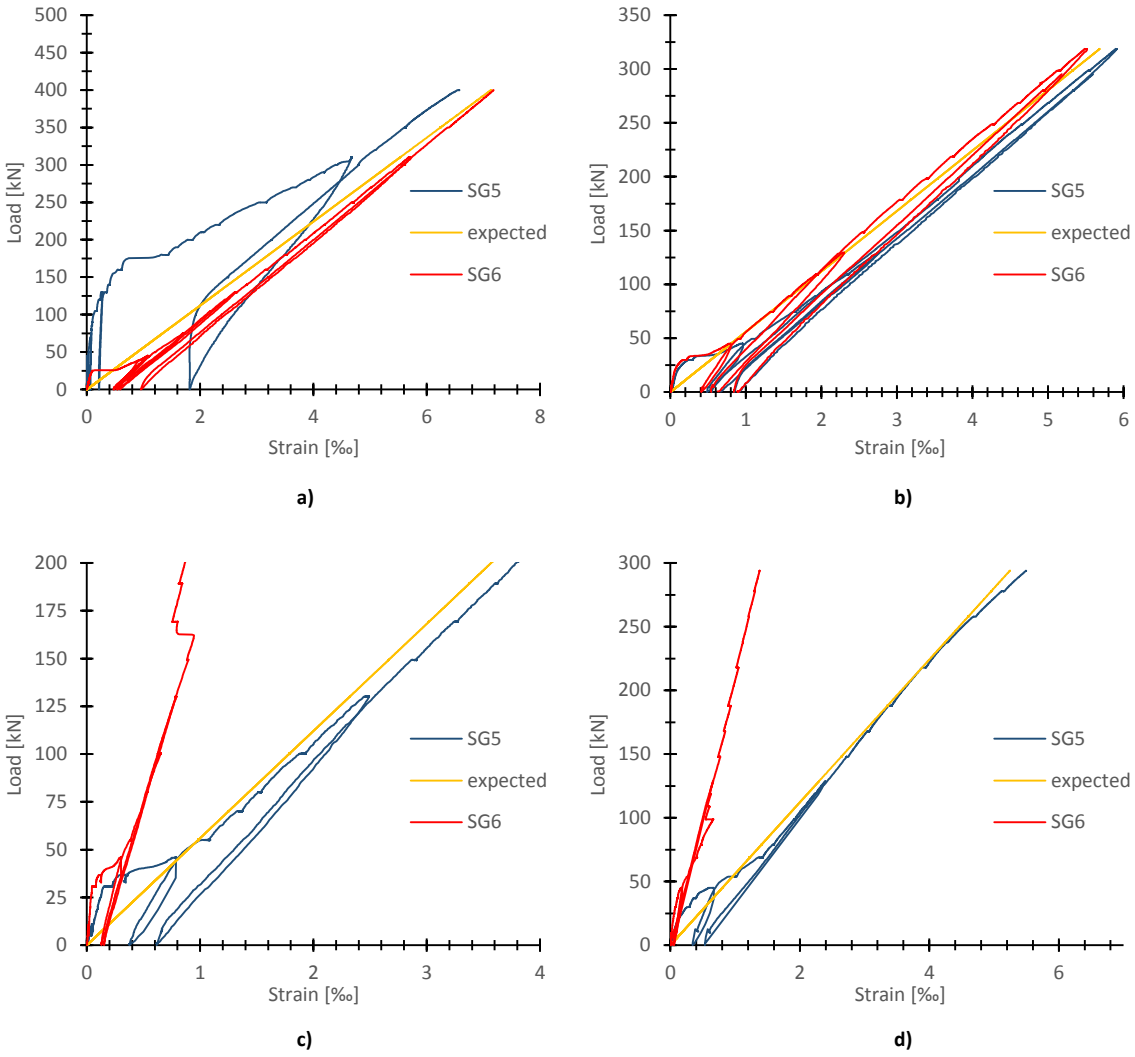

Figure 37 – Strain of tensile reinforcement: a) BS250GFRP1; b) BC250GFRP1; c) BDHB250GFRP1; d) BB250GFRP1

2.3.1.4.2 Shear reinforcement strain

The maximum shear reinforcement strains for the different beam specimens, as well as the predicted values, are presented in Table 20. Figure 38 represents the strains of the most stressed stirrup of each beam and their predictions according to Equation(22), where the strains are expressed as a function of the applied load, P, the reinforcement spacing, s , the area, A_{fv}, and the elasticity modulus, E_{fv}, of the shear reinforcement and the internal lever arm, z.

$$\varepsilon_{fv} = \frac{Ps}{2zE_{fv}A_{fv}} \tag{22}$$

Close to the failure, the strain values were in agreement with those roughly expected. As expected, this behaviour is similar to the typical tension-stiffening effect in tensile RC elements. For all the beam specimens, the development had a bilinear configuration. When compared with reference

beams, the GFRP beams had the higher stirrup strains, for the same load value. It is important to notice that the beams with the capacity to better mobilize the shear reinforcement were those with the closed stirrup or C-stirrup.

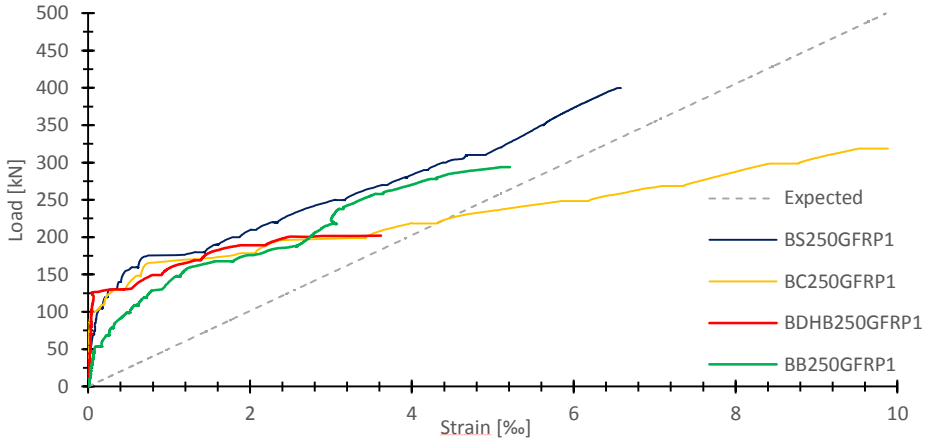

Figure 38 – Comparison of the strains of most stressed stirrup of each beam specimen

The distribution and evolution of the shear reinforcement strains in the shear-span of the failure side during the loading of all the beam specimens are indicated from Figure 39 to Figure 41.

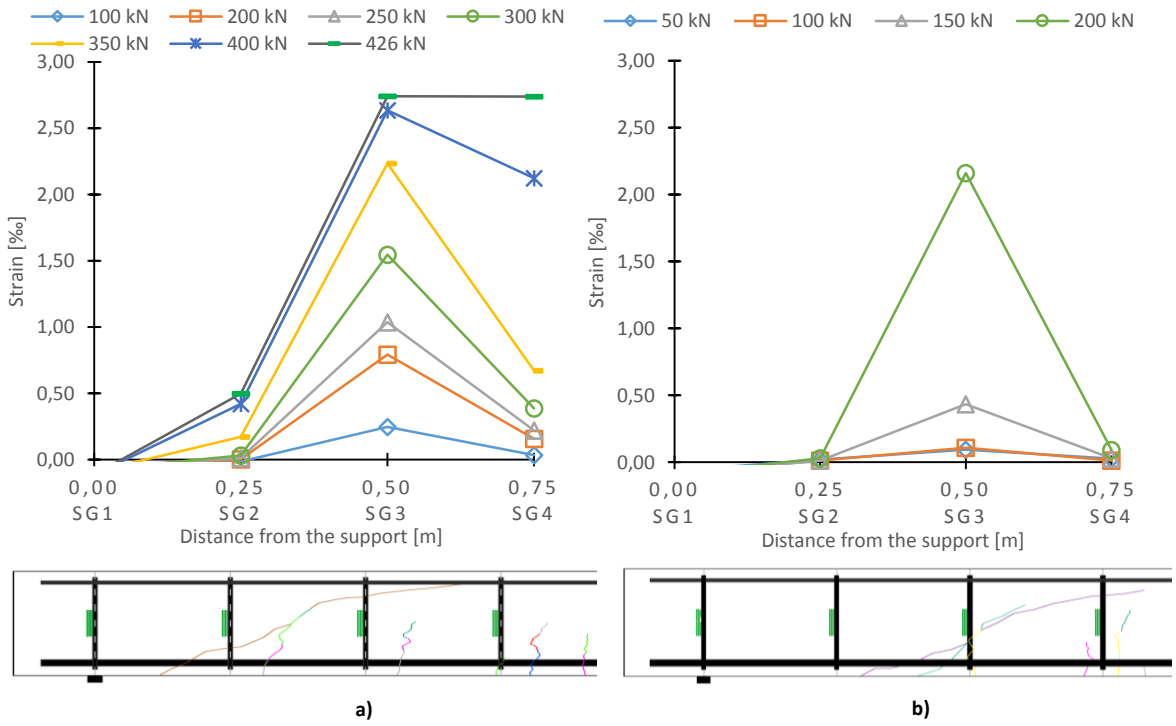

Figure 39 – Distribution of strains along the shear span of: a) REF250; b) REFB250

It can be noticed that the strain distribution varies from beam to beam, confirming the idea that the stirrup strains are affected by the development of the cracks, and helping to explain the shear failures. For all the beams, the stirrups near the support had very small strain values, as expected. For the reference beams, the stirrups located at 0.50 m from the support (SG3) had the higher strains, while for all the GFRP beams it was the stirrups located at 0.75 m from the support (SG4).

For the REF250 it was found that near the failure, due to the yielding of the third stirrup, the fourth stirrup also yielded. For the REFB250, only SG3 exhibited some strains, however it did not reach the yielding once the shear reinforcement slipped. The GFRP beams had a development similar among them only differing in the value of strains. For BDHB250GFRP1, once the first shear cracks damaged the head of the second and third shear reinforcement bars causing them to slip, the stresses were absorbed by the fourth one causing the slip 3‰.

Focusing the beams with the closed GFRP stirrups, corresponding to an average of 4‰ strain in GFRP stirrups, which is the ACI 440.1R-06 [2] limit, the applied forces were 268 kN for BS250GFRP1 and 200 kN for BC250GFRP1, representing 67% and 62% of the observed failure loads, respectively. Similar results were stated by [29]. Even BC250GFRP1 exhibited strains of nearly 9‰ on the shear span on the opposite site of the failure (Figure 38).

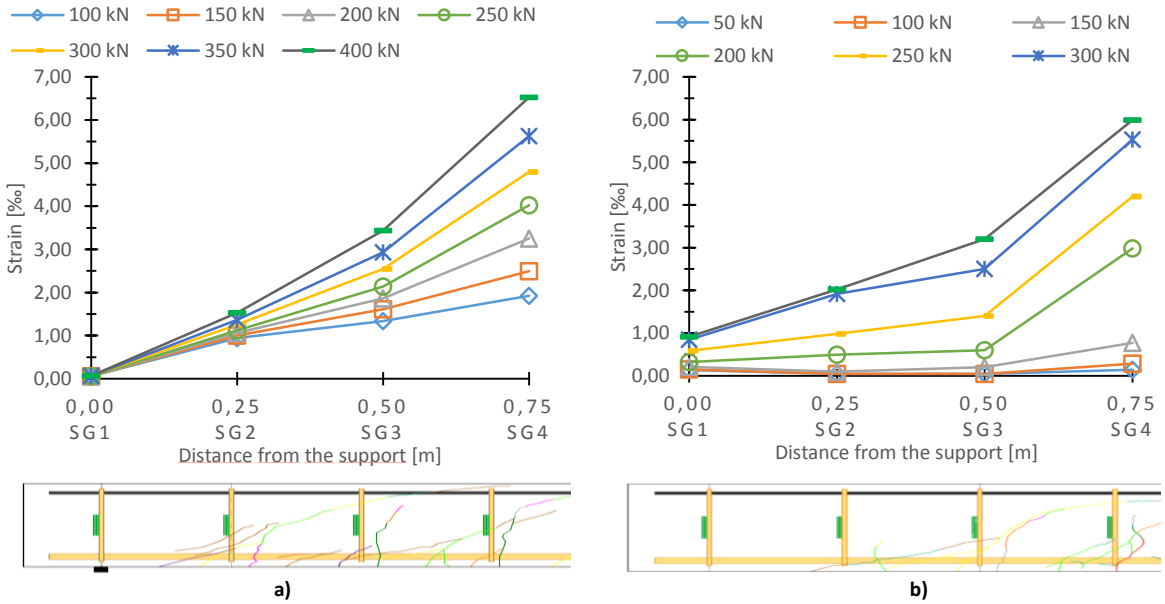

Figure 40 – Distribution of the strains along the shear span of: a) BS250GFRP1; b) BC250GFRP1

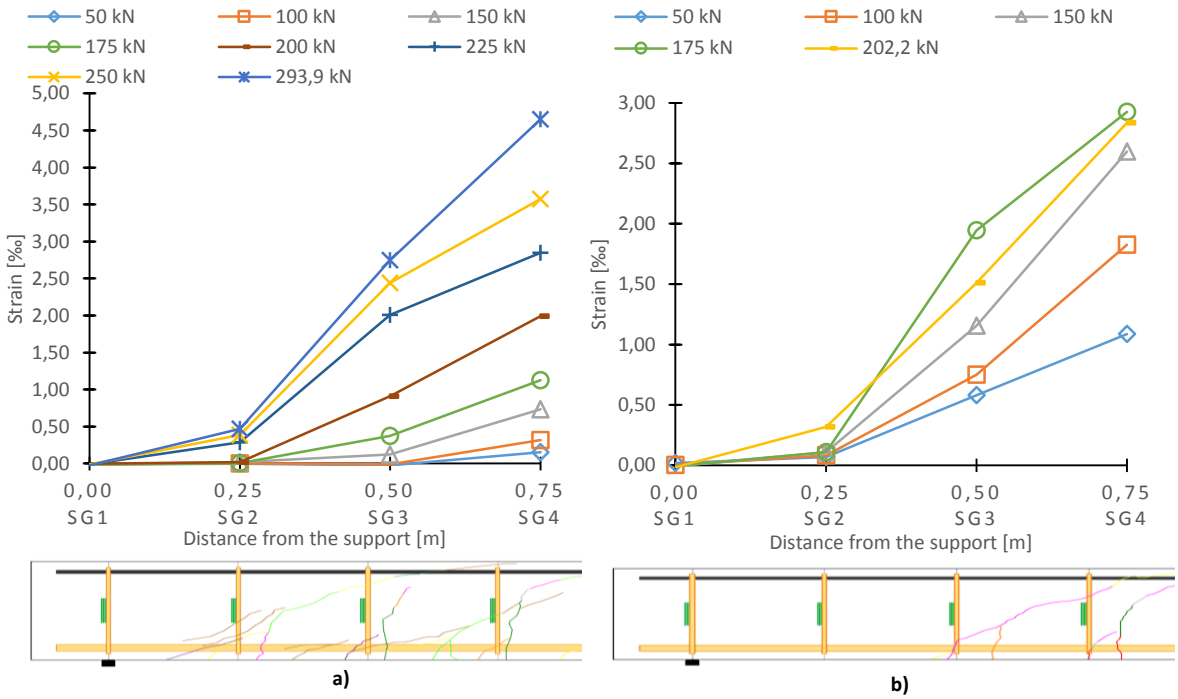

Figure 41 – Distribution of the strains along the shear span of: a) BB250GFRP1; b) BDHB250GFRP1

Table 20 – Summary of ultimate strain values

Beam	ρ_{fL} or ρ_{sL}	EA_{fL} or EA_{sL}	ρ_{fv} or ρ_{sv}	EA_{fv} or EA_{sv}	Ultimate values					
					Mid-span strain			Shear reinforcement strain		
					Exp.	Pred.	Exp /Pred	Exp.	Pred.	Exp /Pred
	(%)	(kN)	(%)	(kN)	(‰)	(‰)	(-)	(‰)	(‰)	(-)
REF250	1.58	304.48	0.16	92.46	2.53	2.25	1.12	2.74	9.00	0.30
REFB250					1.04	1.30	0.80	2.14	4.00	0.54
BS250GFRP1		83.04	0.36	49.72	6.80	7.15	0.95	6.56	9.40	0.70
BC250GFRP1					5.63	5.50	1.02	9.86*	9.15	1.02
BDHB250GFRP1				54.24	3.77	3.54	1.06	3.62	7.20	0.50
BB250GFRP1					5.24	5.09	1.03	5.21	5.20	1.00

* not on the failure side. On the failure side the maximum strain was 2.85‰

2.3.1.4.3 Shear crack width

Figure 42 shows the variation of the shear crack widths with the loading. It can be stated that the shear cracks appeared only for load levels above the service load and that it seems to be a correlation although it is not linear between the crack widths and the applied load. For REF250 it was not possible to measure the shear cracks during the testing.

The larger crack widths developed on GFRP reinforced beams are responsible for the lower shear strength, although the characteristics of shear failure are similar to that of steel RC beams. This may also indicate differences in the bonding of GFRP and steel with concrete.

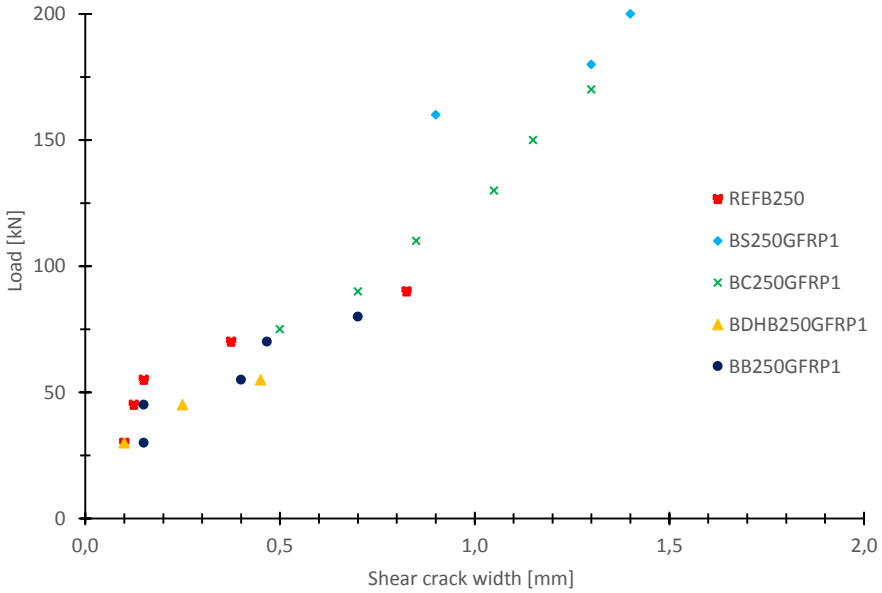

Figure 42 – Variation of the shear crack width with the load

2.3.2 Conclusions

In this study the performance of four GFRP shear reinforcement solutions were evaluated by testing full-scale intermediate length GFRP RC beams. The behaviour was then compared with similar steel RC beams and with predictions of design provisions. It was concluded that beams with GFRP shear and longitudinal reinforcement are a reliable solution, and their overall performance are similar to steel reinforced concrete beams. More detailed findings and results of this research can be summarized as follows:

1- Although all the beam specimens had the same shear reinforcement amount, the four solutions had distinct performances. GFRP bent bars with closed stirrups (BS and BC beams) had the highest shear capacity. Similar behaviour was found in the reference beams, REF250 exhibited a shear capacity twice times higher than REFB250. The main reason for this behaviour is the anchorage length provided by the two horizontal branches on the stirrups which enhances the capacity of the beam to mobilize the shear reinforcement.
2- With exception of BDHB250GFRP1, all GFRP beams had a shear strength that overcomes the different code predictions.
3- Despite the problem on the testing of BC250GFRP1, that conducted to its premature failure at the beginning of the third load cycling, the closed stirrup beams, BS250GFRP1 and BC250GFRP1, had a similar overall behaviour and shear strength that overcame the different codes predictions. As the C-stirrups solution is an easier and more flexible to use in the field, it represents an adequate solution.
4- The overall behaviour and performance of double headed bars solution, BDHB250GFRP1, was disappointing. Although this solution can improve the anchorage length, it is not a reliable solution because it is affected by the deflection and the cracking pattern, and a crack near the heads can significantly compromise the beams shear capacity.
5- With the exception of the BB250GRP1, none of the GFRP beams exceeded the load capacity of the respective reference. This means that the lower longitudinal stiffness of the GFRP beams in comparison to the reference beams, had a significant influence on the performance of the GFRP shear reinforcement.
6- Considering the service load levels, the behaviour of the BB250GRP1 and BDHB250GFRP1 beams were similar to the other beams.
7- Codes shear predictions were more accurate for steel beams than for GFRP beams. And it was also concluded that applying ACI 440.1R-06 [2] and FIB 40 [22] to determine the design shear capacity underestimates the GFRP closed stirrups beams capacity. It was found that for this strain level beams are about 60-70% of their shear capacity. More accurate predictions can be achieved when the strain limit is increased to 6‰.

2.4 Influence of the GFRP longitudinal bar ratio on the behaviour of reinforced concrete beams with GFRP shear reinforcement

This section describes the results of 10 of the beam specimens, which were designed to fail due to shear. In this particular case, the main objectives were to analyse the influence of the GFRP longitudinal bar ratio on the behaviour of RC beams with GFRP shear reinforcement, to compare the behaviour with the behaviour of the reference beams entirely reinforced with conventional steel, and to discuss how the codes take into consideration the longitudinal stiffness in the shear capacity. This influence was tested on four different layouts of GFRP shear reinforcement (closed hoop stirrups, 2 overlapped C-shaped bent bars to form a closed stirrup 2 straight bars with headed ends and 2 straight bars). Beams were divided into 3 groups:

1) The reference beams entirely reinforcement with steel (REF250 e REFB250);

2) The GFRP1 beams (BS250GFRP1; BC250GFRP1; BDHB250GFRP1; BB250GFRP1) with GFRP shear reinforcement and longitudinal reinforcement with the same longitudinal bar ratio and approximately the same flexural design capacity than the reference beams;

3) The GFRP2 beams (BS250GFRP2; BC250GFRP2; BDHB250GFRP2; BB250GFRP2) with GFRP shear and longitudinal reinforcement but with higher longitudinal reinforcement ratio to maintain the same deflection than the reference beams.

Within each group all beams had the same longitudinal reinforcement ratio in order to keep the dowel effect and the longitudinal stiffness unchanged.

The beam specimens were loaded until failure under four-point bending tests. The load-deflection, the stirrup strains, the crack patterns and the crack widths of the beams were measured, analysed and compared with the reference beam and with the theoretical predictions.

Results showed that all beams of the third group supported a significantly higher shear load, proving that the longitudinal stiffness has an important influence on the shear capacity. Solutions with closed GFRP stirrups had a higher shear capacity however, on the third group, the double headed bars exhibited a good performance explained by the higher longitudinal stiffness. The capacity of the reference beams were well predicted by the codes but are conservative to GFRP, particularly in the cases with closed stirrups and higher longitudinal stiffness.

2.4.1 Results and discussion

2.4.1.1 Ultimate capacity

It was designated by non-design, the values calculated considering the characteristic material properties without safety factors. The values applying the safety factors were designated as and the design values. The theoretical values of the shear ultimate capacity were calculated with the equations listed in Table 21.

Table 21 – ACI 440.1R-06 [2] and FIB 40 [22] shear design equations

Model	Concrete shear equations		Reinforcement shear equations	
ACI 440.1R-06 [2]	$V_c = \frac{2}{5} k \sqrt{f_c'} bd$	(23)	$V_{fv} = \frac{A_{fv} \sigma_{fv} d}{s}$	(24)
	$k = \sqrt{2\rho_{fl} n_f + (\rho_{fl} n_f)^2} - \rho_{fl} n_f$	(25)	$\sigma_{fv} = 0.004 E_{fv} \leq f_{fb}$	(26)
	$n_f = \frac{E_{fl}}{E_c}$	(27)	$f_{fb} = \frac{\left(\frac{0.05 r_b}{d_b} + 0.3\right)}{1.5} f_{fv} \leq f_{fv}$	(28)
FIB 40 [22]	$V_c = 0.12 \left(1 + \sqrt{\frac{200}{d}}\right) \left(100 \rho_{fl} \frac{E_{fl}}{E_s} \phi_\varepsilon f'_c\right)^{1/3} bd$	(29)		
			$V_f = \frac{A_{fl}}{s} f_{fl} z \cot\theta$	(30)
	$\phi_\varepsilon = \varepsilon_f / \varepsilon_y$	(31)		
	$\varepsilon_f = 0.0045$	(32)		

The ultimate capacity of all beams and the corresponding failure modes are presented in Table 22. It also indicates the expected non-design values of the shear and the bending load capacity obtained according to different codes ACI 318-11 [3], ACI 440.1R-06 [2], FIB-40 [22] and EC2 [23], as well as the experimental to predicted ratio. The non-design shear capacity was always estimated as the sum of the concrete and reinforcement contributions.

Table 22 – Non-design capacity of the beams

Beam	Non-design Capacity							
	Experimental		ACI 440.1R-06[2] / ACI 318-11[3]			EC2[23]/FIB 40[22]		
	Type	Load (kN)	Shear (kN)	Exp./Pred. (-)	Bending (kN)	Shear (kN)	Exp./Pred. (-)	Bending (kN)
REF250	Shear	426.4	393.9	1.1	546.2	454.4	0.9	543.8
REFB250	Shear	257.4	391.3	0.7	544.0	453.1	0.6	541.5
BS250GFRP1	Shear	400.0	245.8	1.6	449.9	275.6	1.5	527.7
BC250GFRP1	Shear	318.5	261.4	1.2	507.5	284.3	1.1	595.2
BDHB250GFRP1	Shear	202.2	251.6	0.8	437.5	273.7	0.7	513.1
BB250GFRP1	Shear	293.9	250.9	1.2	434.2	273.1	1.1	509.2
BS250GFRP2	Shear	506.0	268.5	1.9	527.7	297.1	1.7	619.1
BC250GFRP2	Shear	478.7	287.7	1.7	598.5	307.4	1.6	702.0
BDHB250GFRP2	Shear	319.7	273.7	1.2	504.8	293.7	1.1	592.3
BB250GFRP2	Shear	268.5	272.7	1.0	499.8	293.0	0.9	586.4

Note: The values of shear capacity of the steel RC beams include the concrete contribution, because although EC2 [23] indicates that the shear capacity is given only by the stirrups contribution, more recent studies and codes [20] mentioned that better estimation can be achieved by adding the concrete contribution, V_c.

All beam specimens failed due to shear in agreement with the design predictions. With the exception of BDHB250GFRP1 and BB250GFRP2, all the GFRP beams had higher failure loads than the non-design values of both codes. The load capacity of BS250GFRP1, BS250GFRP2 and BC250GFRP2 were highly underestimated by the two design codes. ACI 440.1R-06 [2] underestimated the ultimate capacity of BS250GFRP1, BS250GFRP2 and BC250GFRP2 by 60%, 90% and 70%, respectively. FIB 40 [22] underestimated the ultimate capacity of these beams by more than 50%, 70% and 60% respectively for BS250GFRP1, BS250GFRP2 and BC250GFRP2. This high level of underestimation is mainly related to the limit of the strains considered in these codes and a suggestion of improvement is given later in this section.

It was expected that BC250GFRP1 and BS250GFRP1 would have a more similar capacity, but a problem during the test caused premature failure at the beginning of third load-discharge cycle. Nevertheless, the load capacity of BC250GFRP1 was higher than non-design predictions.

Due to the lack of anchorage length of BB250GFRP1, it was expected that the BDHB250GFRP1 would have a higher experimental shear capacity than the capacity of BB250GFRP1, but a shear crack damaged and compromised the end heads of two pairs of GFRP bars, causing the immediate slip of the bars. For this reason, the capacity of BDHB250GFRP1 was only 80% and 70% of the non-design theoretical capacity, from of ACI 440.1R-06 [2] and FIB 40 [22], respectively.

It was foreseen that BB250GFRP2 had higher shear capacity than BB250GFRP1, but the opposite was found. This fact demonstrates that the shear reinforcement solution of two straight bars is not reliable as its behaviour is associated to some randomness related to the crack pattern and to the lack of anchorage length, being even harder to predict the failure

Comparing the shear capacity of the GFRP1 with the reference beams, it can be stated that the capacity of BS250GFRP1 and BC250GFRP1 was 6.2% and 25.3% lower than REF250, respectively, although they were designed to have the same ultimate capacity. The BDHB250GFPR1 had 79% of the capacity of REFB250, while BB250GFRP1 had 114% of the capacity of REFB250, although they have been designed to have the same ultimate shear capacity. The fact that none of the group 2 (GFRP1) beams, with the exception of BB250GFRP1, exceeded the load capacity of the respective reference may be related to the influence of the lower longitudinal stiffness of the GFRP beams.

Focusing on the group 3 (GFRP2) beams it can be mentioned that the ultimate shear capacity of these specimens was higher than the capacity of the references: 18.6% and 12.3% respectively for BS250GFRP2 and BC250GFRP2, and 24.2% and 4.3% for BDHB250GFRP2 and BB250GFRP2.

Comparing the influence on the ultimate shear capacity of increasing the longitudinal stiffness from GFRP1 group to GFRP2, it can be demonstrated that from BS250GFRP1 to BS250GFRP2, BC250GFRP1 to BC250GFRP2, BHDBGFRP1 to BDHBGFRP2, the experimental ultimate capacity increased 27%, 50% and 58% while ACI 440.1R-06 [2] and FIB 40 [22] only predicted an increase of 9% and 8%, respectively, from the longitudinal stiffness GFRP1 to GFRP2. In these codes, the longitudinal stiffness is taken into account in the equations of the concrete contribution to the shear strength, equations (23) and (29). In ACI 440.1R-06 [2], the shear strength provided by the concrete depends directly on the parameter k, which is determined with the longitudinal stiffness (equation(25)). In Figure 43 there is a comparison between the experimental and the theoretical values of the parameter k. Regarding the experimental values of this parameter, a linear equation

is suggested to determine k in the cases were the longitudinal reinforcement ratio is between the 1.5 % and 2.8 %.

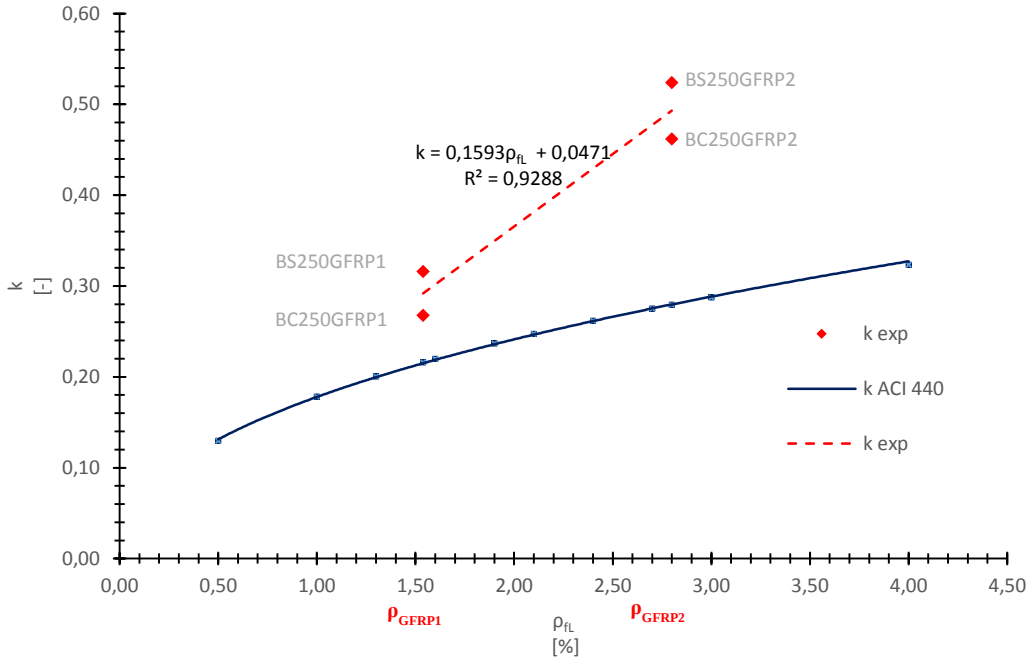

Figure 43 - Comparison between the experimental and the predicted values for the parameter k

Within the group 3, BDHB250GRP2 had a good performance, although with a significant lower resistance value than BS250GFRP2 and BC250GFRP2. This beam also had 20% more shear capacity than BB250GFRP2, suggesting that the heads can really accomplish the function of improving the anchorage length, if the geometrical integrity of the structural element was not committed (as happened in BDHB250GFRP1).

Table 23 shows the design values obtained with ACI 440.1R-06 [2] and FIB 40 [22] and the experimental to predicted ratio. With exception of REFB250 and BDHBGFRP1, which had a disappointing performance explained above, the experimental capacity of the beams ranged from 1.6 to 3.4 times the predicted capacity.

Table 23 – Summary of experimental and design values of shear capacity

Beam	Shear Capacity					
	Experimental		Design Values			
	Load	Type	ACI 440.1R-06 [2] / ACI 318-11 [3]	E/ D	EC2 [23]/ FIB 40 [22]	E/ D
	(kN)		(kN)	(-)	(kN)	(kN)
REF250	426.4	Shear	253.0	1.7	190.9	2.2
REFB250	257.4	Shear	253.0	1.0	190.9	1.3
BS250GFRP1	400.0	Shear	177.2	2.3	151.0	2.6
BS250GFRP2	506.0	Shear	195.7	2.6	151.0	3.4
BC250GFRP1	318.5	Shear	177.2	1.8	151.0	2.1
BC250GFRP2	478.7	Shear	195.7	2.4	151.0	3.2
BDHB250GFRP1	202.2	Shear	177.2	1.1	151.0	1.3
BDHB250GFRP2	319.7	Shear	195.7	1.6	151.0	2.1
BB250GFRP1	293.9	Shear	177.2	1.7	151.0	1.9
BB250GFRP2	268.5	Shear	195.7	1.4	151.0	1.8

* Bending failure
E/D – ratio of Experimental and Design values

In the cases where the closed stirrups were considered, by comparing the experimental ultimate loads with the non-design predictions of the shear capacity, it was verified that codes are very conservative. In the case of ACI 440.1R-06 [2], the differences between the predictions and the experimental values are related to the 4‰ referred as limit to the shear reinforcement strains, which corresponds to 220 MPa in tension. In fact, as shown hereafter, the maximum strains on stirrups of BC and BS beams ranged from 6‰ to almost 10‰ (Figure 64). Table 24 presents the values of the shear capacity for a shear reinforcement strain of 4‰, 6‰ and 7 ‰. For BS and BC beams, better non-design values of predictions can be obtained when considering the value of 7‰ for the strains.

Considering the FIB 40 [22], there are two variables that may be responsible for the difference between the experimental and the prediction values: the angle of 45 degrees for the strut and the limit of 4.5‰ for the reinforcement strain. The failure planes (Figure 44 to Figure 48) suggest that the angle for the strut can be lower, thus Table 24 presents the values considering 30˚, 38˚, and 45˚. Fixing the strains at 4.5‰, the best predictions were obtained with the 30˚, however experimentally the best angle is 38˚. Fixing the angle of 38 degrees, the best predictions were achieved with a strain of 6‰. These predictions' values were very similar to those achieved with ACI 440.1R-06 [2] and

close, but conservative, to the experimental, except for BC250GFRP1. Guadagnini, Pilakoutas, *et al.* [47] had already proposed an increase of the strain limit.

Table 24 – Non-design capacity of the beams considering various strains and angle of strut

Beam	Experimental Load	Non-design Capacity					
		ACI 440.1R-06[2] / ACI 318-11[3]			EC2[23]/FIB 40[22]		
		Shear			Shear		
	(kN)	ε_{fv} =4 ‰	ε_{fv} =6 ‰	ε_{fv} =7 ‰	Θ=30˚	Θ=38˚	Θ=45˚
		(kN)	(kN)	(kN)	(kN)	(kN)	(kN)
REF250	426.4		393.9		454.4	375.5	326.6
REFB250	257.4		391.3		453.1	374.2	325.3
BS250GFRP1	400.0	245.8	317.5	353.3	381.8	316.2	275.6
BC250GFRP1	318.5	261.4	333.1	368.9	390.6	324.9	284.3
BDHB250GFRP1	202.2	251.6	32.3.2	359.1	379.9	314.3	273.7
BB250GFRP1	293.9	250.9	322.6	358.4	379.4	313.8	273.1
BS250GFRP2	506.0	268.5	338.2	373.0	400.4	336.6	297.1
BC250GFRP2	478.7	287.7	357.3	392.2	410.7	346.9	307.4
BDHB250GFRP2	319.7	273.7	343.4	378.3	397.0	333.2	293.7
BB250GFRP2	268.5	272.7	342.4	377.3	396.3	332.4	293.0

2.4.1.2 Cracking pattern

The cracking development with the loading is presented from Figure 44 to Figure 48, to assess the differences in the cracking behaviour.

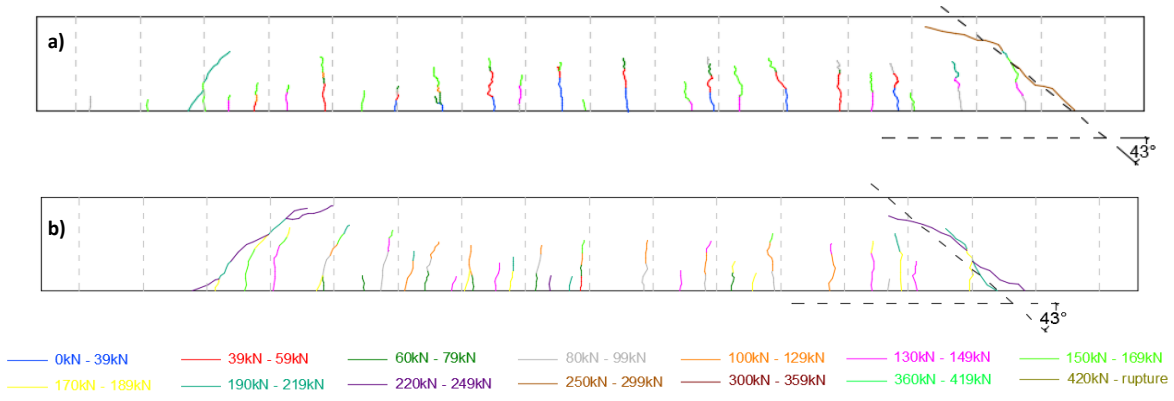

Figure 44 – Cracking pattern of: a) REF250; b) REFB250.

Initially, all beam specimens did not have any cracks. They appeared firstly at the constant moment region, and grew vertically (indicating the absence of shear stresses). With the load increase, other flexural cracks appeared in the shear-span region, initially vertical but then propagating to the loading point. The failure starts with the formation of an inclined crack oriented perpendicular to the direction of the maximum principal stress, and generally, it was the shear crack closest to the support that led to the failure of the beam.

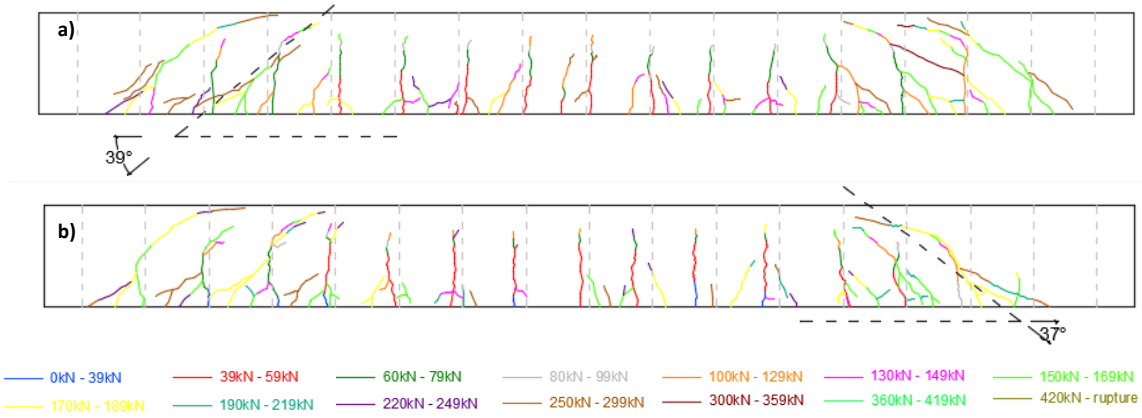

Figure 45 – Cracking pattern of: a) BS250GFRP1; b) BC250GFRP1

The slope of the plane of the failure of the beams that failed due to shear vary from 37 degrees to 43 degrees, being in agreement with the 45 degrees applied in the truss model.

Comparing the cracking pattern between the two different longitudinal stiffness that were considered (GFRP1 and GFRP2) it can be noticed that for the same shear reinforcement layout, beams with higher longitudinal reinforcement failed in general with a less inclined plane. It was also verified that the higher longitudinal stiffness and failure load, the greater the number of shear cracks.

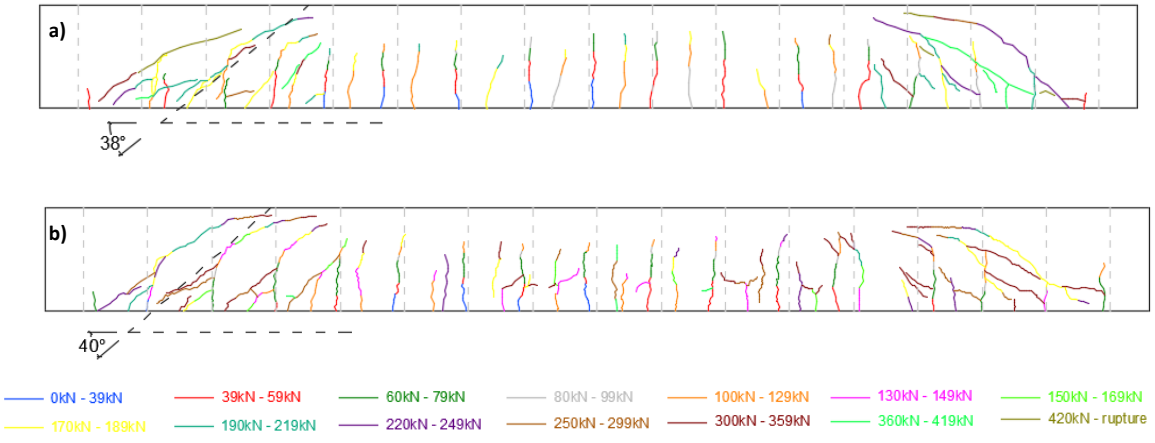

Figure 46 – Cracking pattern of: a) BS250GFRP2; b) BC250GFRP2

For several cases (BS250GFR1, BS250GFR2, BB250GFRP2 and BC250GFRP2) when failure was imminent, horizontal cracks appeared from the bottom of the shear cracks towards the supports. This can be explained by the fact that when the failure is imminent the aggregate interlock is lost at the shear crack, and so that the equilibrium is kept at the section the dowel action in the longitudinal reinforcement has to increase. This increase of the dowel action causes vertical tension stresses which combined with the existing splitting forces due to flexural bond lead to the bond-anchorage failure [98].

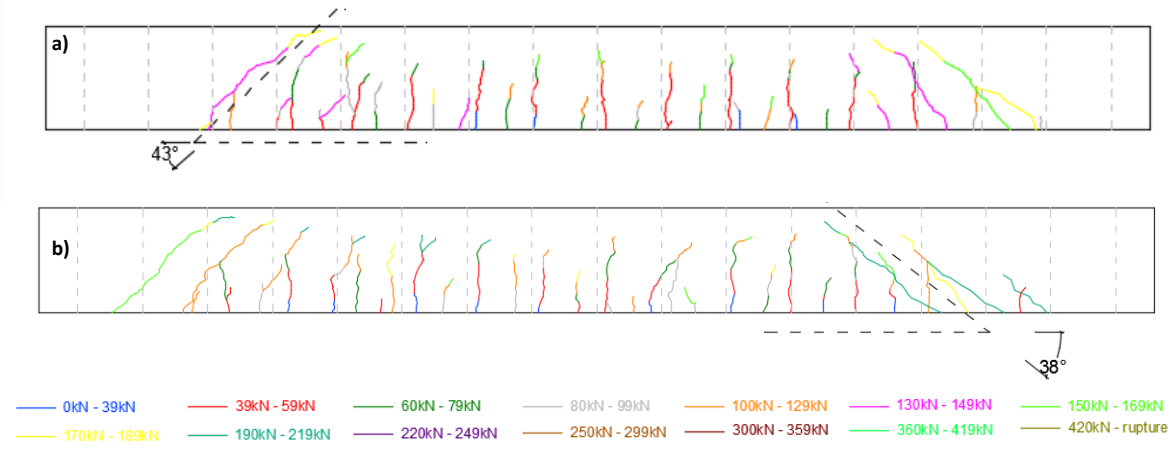

Figure 47 – Cracking pattern of: a) BDHB250GHFRP1; b) BB250GFRP1

Comparing the GFRP beams with the reference beams, it can be stated that the steel reinforced beams had a fixed vertical development pattern of the crack while for GFRP reinforced beams, several oblique ramifications appeared and propagated from the main crack. This can be explained by the differences on the elasticity and bond of the two reinforcements (steel and GFRP).

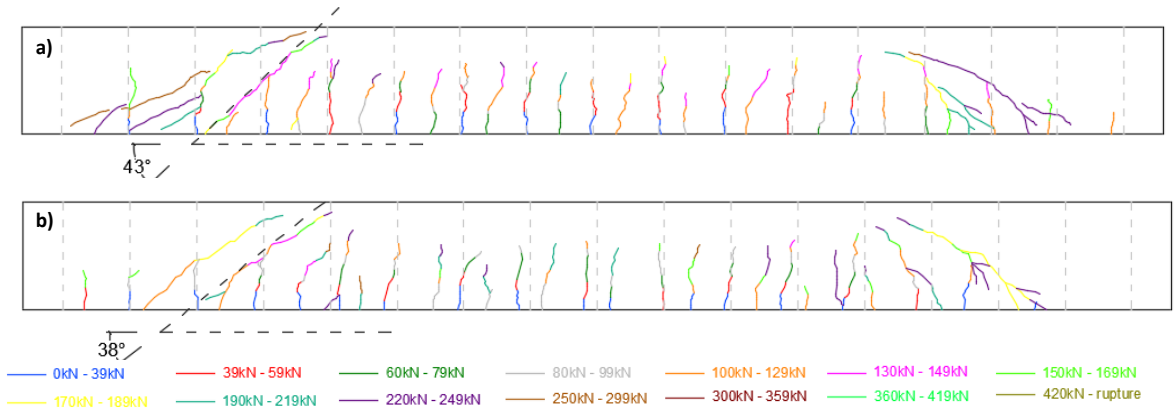

Figure 48 - Cracking pattern of: a) BDHB250GFRP2; b) BB250GFRP2

Another important detail which can be observed is the height of the compression zone (distance between the compression fibre and the neutral axis). The height of the compression zone was smaller in the GFRP1 beams than in the GFRP2 beams: a mean height of 0.095 m and 0.135 m, respectively. The mean height of the reference beams was 0.150 m. This suggests that there is a rise of the neutral axis with the decrease of the longitudinal stiffness.

For the GFRP beams, the increase of the longitudinal stiffness resulted in a reduction of the flexural crack spacing (higher number of cracks). For example, in the BS250GFRP1, the flexural crack spacing was 0.242 m while for BS250GFRP2 it was 0.132 m.

2.4.1.3 Failure modes

Three distinct failure modes occurred:

- Shear diagonal tension failure by shear reinforcement failure in the REF250; REFB250, BC250GFRP1, BDHB250GFRP1, BDHB250GFRP2, BB250GFRP1 and BB250GFRP2 beams (from Figure 49 to Figure 55);
- Shear failure due to the crushing of the concrete rod in the BS250GFRP2 and BC250GFRP2 beams (Figure 56 and Figure 57);
- Shear failure due to the failure of the bond of the longitudinal reinforcement at support of the BS250GFRP1 beam (Figure 58).

The REF250 reference beam had a brittle shear failure mode of several stirrups. Several flexural cracks developed vertically along the span. For loads above 150 kN, cracks located between the loading points and the supports started to incline in the direction of the loading points and the failure occurred with the rupture of the third stirrup from support, followed by the rupture of all the others stirrups along the shear crack and conducting to an almost instantaneous failure of the beam at 426.4 kN (Figure 49 a) and b)). Regarding this stirrup strains it can be stated that the rupture occurred for a strain of approximately 2.8‰, which is the yield strain of the considered steel.

The REFB250 beam failed by the slip/pull-out of the shear reinforcement (Figure 50 a) and b)). Similarly to REF250, for loads above 130 kN, the cracks near the supports started to incline in the direction of the loading points and the failure occurred when the third bar of the shear reinforcement slipped, followed by others along the shear crack, leading to a quick failure of the

beam at 257.4 kN. It was verified by the strain development that these bars did not reach the yield strain.

a) b)

Figure 49 – REF250 beam failure: a) front view of the support; b) broken stirrup

a) b)

Figure 50 – REFB250 beam failure: a) overall view of one of the sides of the support; b) slip of stirrup

The failure of the BC250GFRP1 beam was due to the disintegration of the C-stirrups followed by the pull-out of the longitudinal bars near the support (Figure 51). For loads above 180 kN the cracks on the shear span evolved on the direction of the loading points. This beam failed at the third charge-discharge cycle, but it was previously submitted to 318.5 kN. As showed in Figure 51 b) the helically grooved coating and the ribs of the stirrups were ripped out, and the premature failure seems to be related to the slip between the GFRP and its sheath. This explanation is also validated by looking at the strains of the stirrups: the strains of the failure's side were lower than the strains of the opposite side of the beam (a maximum strain of almost 10‰ was measured on the opposite side of the failure while the maximum strain was approximately 6‰ on the failure's side).

BC250GFRP1

a) **b)**

Figure 51 – BC250GFRP1 beam failure: a) overall view near the support; b) stirrup disintegration

The shear failure of BDHB250GFRP1 and BHDHB250GFRP2 beams was due to the fracture of several end heads of the shear reinforcement bars (Figure 52 and Figure 53). The shear cracks damaged the end heads of GFRP of two pairs of bars at the beam's bottom compromising their function and causing the immediate slip of the bars.

BDHB250GFRP1

a) **b)**

Figure 52 – BDHB250GFRP1 beam failure: a) overall view near the support; b) fractured top and bottom heads

BDHB250GFRP2

a) **b)**

Figure 53 – BDHB250GFRP2 beam failure: a) overall view; b) fractured head

As shown in Figure 54 and Figure 55, the failure of BB250GFRP1 and BB250GFRP2 beams was due to the slip of the shear reinforcement bars. When the cracks on the shear span evolved on the direction of the loading points the shear reinforcement bars slipped along the shear crack causing an increase of the crack width and the pull-out of the longitudinal bars near the support, leading to brittle failure.

Figure 54 – BB250GFRP1 beam failure: a) overall view of the failure; b) pull-out of the shear reinforcement at the bottom

Figure 55 – BB250GFRP2 beam: a) overall view of the support; b) crushing of the concrete rod; d) pull-out of the shear reinforcement on the top

The failure of BS250GFRP2 beam was due to the crushing of the concrete rod between shear cracks at 506 kN (Figure 56 a) and b)). For loads above 200 kN, the cracks on the shear span evolved on the direction of the loading points. Figure 56 b) shows that the closed stirrups also disintegrated at the bottom and on the top of the concrete crushed rod.

a) b)

Figure 56 – BS250GFRP2 beam failure: a) overall view o from one side of the support; b) overall view from the other side of the support

The failure of BC250GFRP2 beam was due to the crushing of the concrete rod between shear cracks (Figure 57). Figure 57 b) shows that the C-stirrups also disintegrated at the bottom at 478.7 kN. After the test, the bottom cover of concrete was removed and it was possible to conclude that there was not pull-out of longitudinal bars.

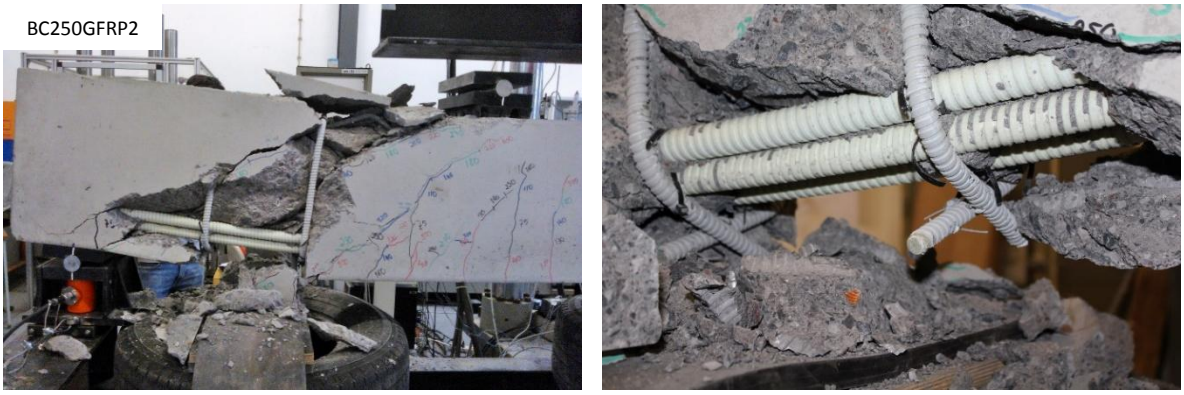

a) b)

Figure 57 – BC250GFRP2 beam failure: a) one side of the support; b) stirrups disintegration

Figure 58 shows the BS250GFRP1 beam failure, which was due to the pull-out of the longitudinal reinforcement at 400 kN, with secondary concrete crushing. In Figure 58 b) the pull-out of the longitudinal reinforcement is shown. The shear cracks appeared for loads near 150 kN and when failure was imminent, horizontal cracks appeared from the bottom of the shear cracks towards the supports. This can be explained by the loss of the aggregate interlock at the shear crack, when the failure is imminent. In order to keep the equilibrium at the section, the dowel action in the longitudinal reinforcement has to increase. The increase of the dowel action causes vertical tension

stresses which combined with the existing splitting forces due to flexural bond can lead to the bond-anchorage failure [98], as happened at 400 kN.

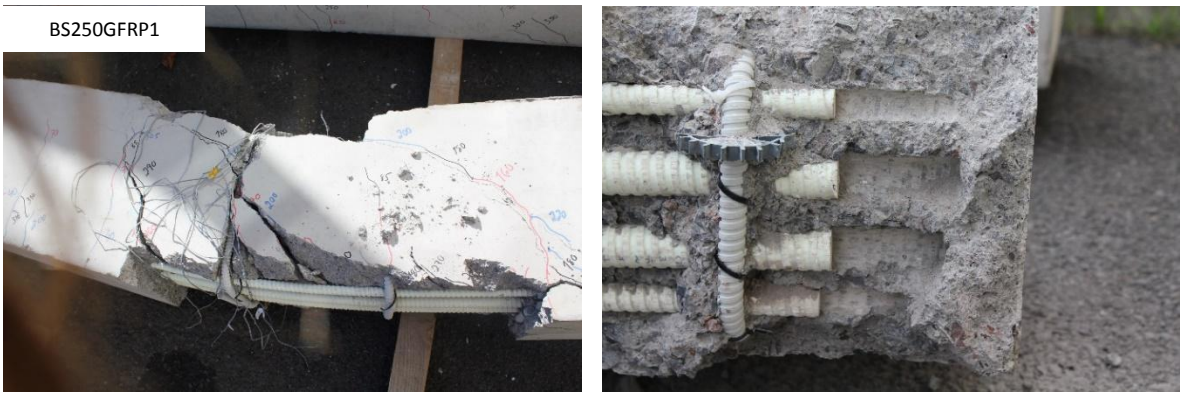

Figure 58 – BS250GFRP1 beam failure: a) overall view near the support; b) slip of longitudinal reinforcement near the support

2.4.1.4 Deflection

The deflection was measured at mid-span and under the two loading points. The mid-span deflection curves are shown in Figure 59, organized by shear reinforcement solution, and in Figure 60 divided by the longitudinal stiffness. The REF250 and REFB250 curves were also plotted over the other curves to immediately compare the behaviour. Each curve represented in these figures is the deflection obtained by the 100 mm LVDT mounted at mid-span. In general, for loads under the load of the cracking moment, all specimens exhibited an initial elastic phase where the load-displacement relation was linear, followed by a cracked phase where the load-displacement relation was still linear but with lower slope.

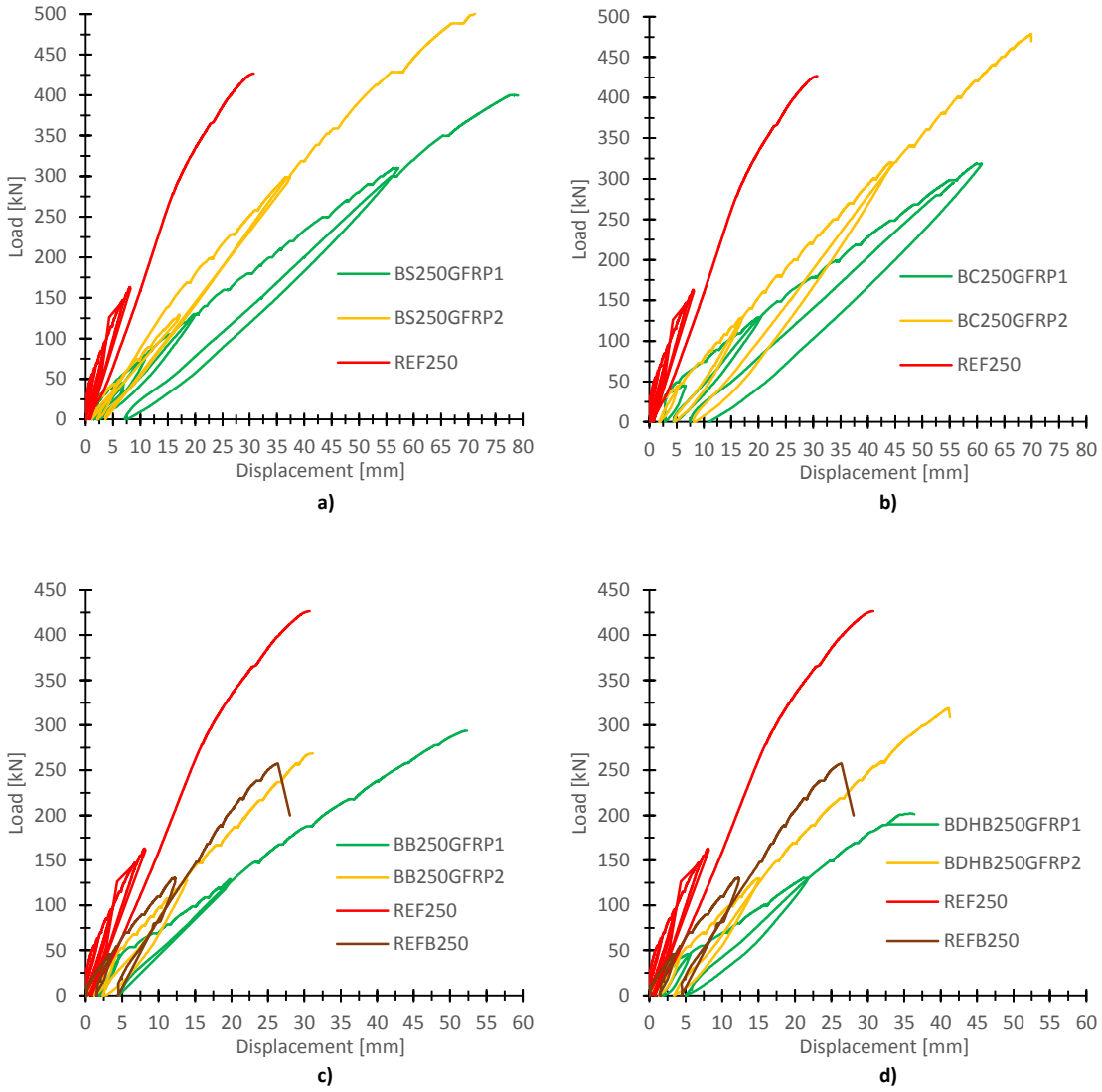

Figure 59 – Load-deflection curves at mid-span: a) BS group beams; b) BC group beams; c) BB group beams; d) BDHB group beams

Concerning Figure 59 a) and fixing a load value of approximately 400 kN, which corresponds to the failure load of BS250GFRP1, the deflection of BS250GFRP2 and BS250GFRP1 was 1.96 and 2.85, respectively, higher than the reference deflection. The behaviour found in Figure 59 b), c) and d) is similar, where the reference REF250 exhibited the lowest displacement followed by GFRP2 beams, and finally by GFRP1 beams.

In Figure 60 it is possible to directly assess the influence of the shear reinforcement solution on the deflection. The load-deflection curves, until the failure, are approximately coincident for the beams with the same longitudinal stiffness, independently of the shear reinforcement solution. As expected, both groups exhibited higher deflections than REF250 as the longitudinal stiffness was one and a half third of the reference beam longitudinal stiffness, respectively for GFRP1 and GFRP2

beams. Strangely, comparing the REF250 with REFB250, it is possible to notice that since the beginning of the loading the deflection of the REF250 was higher than on REFB250, showing lower stiffness when compared with the other steel beam.

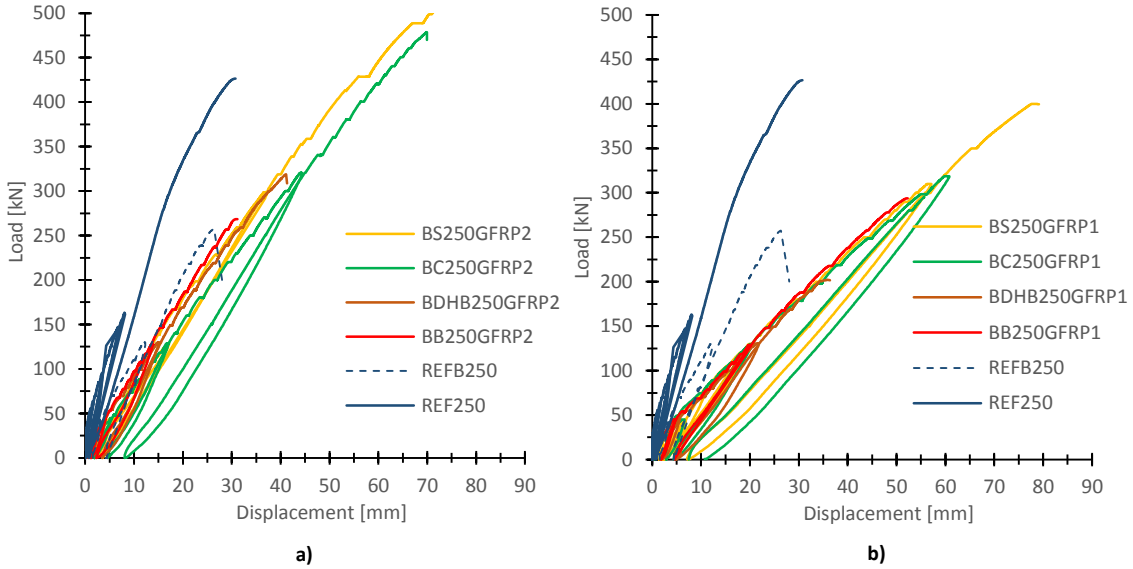

Figure 60 – Load deflection curves at mid-span deflection: a) in the GFRP1 beams; b) in the GFRP2 beams

Table 25 presents the values of the mid-span deflections at service and ultimate loads. The GFRP2 beams were designed to have the same mid-span deflection as the references at the service load (50 kN), but it was found that the deflection was on average 10% higher than the reference beams' deflection. For the GFRP1 beams' group the service deflection goes up to 35% higher than the reference beams. With the load increase these differences are even higher, particularly for GFRP1 beams due to their lowest stiffness. Comparing the service predicted deflections with the experimental deflections, the experimental deflections were on average 25% higher than predicted. For the reference beams: the experimental deflection was 10% lower than predicted for REF250, and the experimental displacement was 36% higher than the predicted for REFB250.

In general, beams with closed stirrups solutions exhibited higher ultimate deflections, and also the highest ultimate loads.

Table 25 – Summary of mid-span deflections at service and ultimate loads

Beam	Flexural stiffness	Mid-span deflection			
		Service			Ultimate
		Exp.	Pred.	Exp /Pred.	Exp.
	(kN)	(mm)	(mm)	(-)	(mm)
REF250	304.5	4.5	5.0	0.90	31.1
REFB250		6.8	5.0	1.36	27.2
BS250GFRP1	83.0	8.0	6.1	1.31	78.0
BC250GFRP1		5.6	6.1	0.92	60.8
BDHB250GFRP1		7.8	6.1	1.28	36.4
BB250GFRP1		5.6	6.1	0.92	52.1
BS250GFRP2	147.0	6.4	5.5	1.16	70.9
BC250GFRP2		6.5	5.5	1.18	69.6
BDHB250GFRP2		5.6	5.5	1.01	41.3
BB250GFRP2		6.8	5.5	1.24	32.0

2.4.1.5 Reinforcement strains

2.4.1.5.1 Mid-span reinforcement tensile strain

The strain values at longitudinal reinforcement at mid-span are presented from Figure 61 to Figure 63. All beam specimens that had a bilinear load-strain relationship with no evidence of yielding of longitudinal reinforcement or concrete crushing. There is also plotted a strain prediction (the "expected" curve), done by the equilibrium of forces in the section and relating the applied load with the reinforcement area. The strains were, in general, in accordance with predictions but for high load values. This enhances the importance of the contribution of the concrete to the tension stiffening at lower load levels when the beams are little cracked. As the load increases, the reinforcement becomes more responsible for supporting the load carrying, as assumed in a simplified form in the predictions. The strain values for the maximum load capacity are presented in Table 26. The variation of the measured values to the predictions is lower than ± 10%.

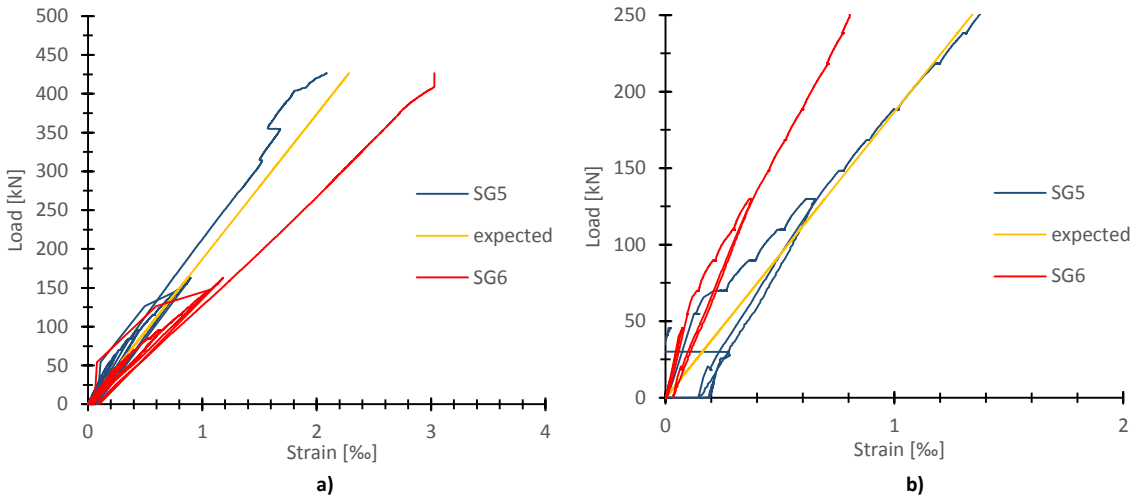

Figure 61 - Strain of tensile reinforcement: a) REF250; b) REFB250

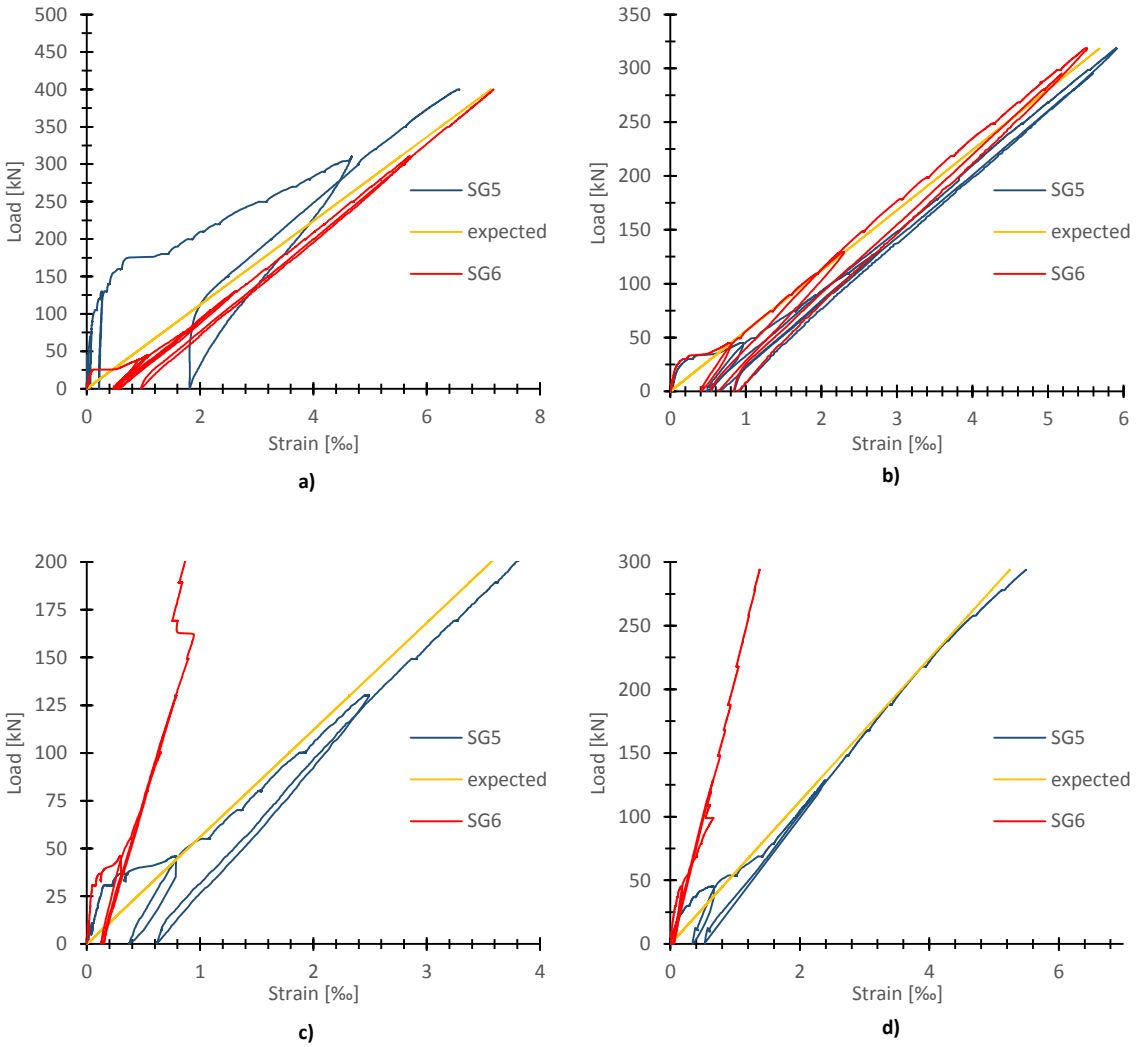

Figure 62 – Strain of tensile reinforcement: a) BS250GFRP1; b) BC250GFRP1; c) BDHB250GFRP1; d) BB250GFRP1

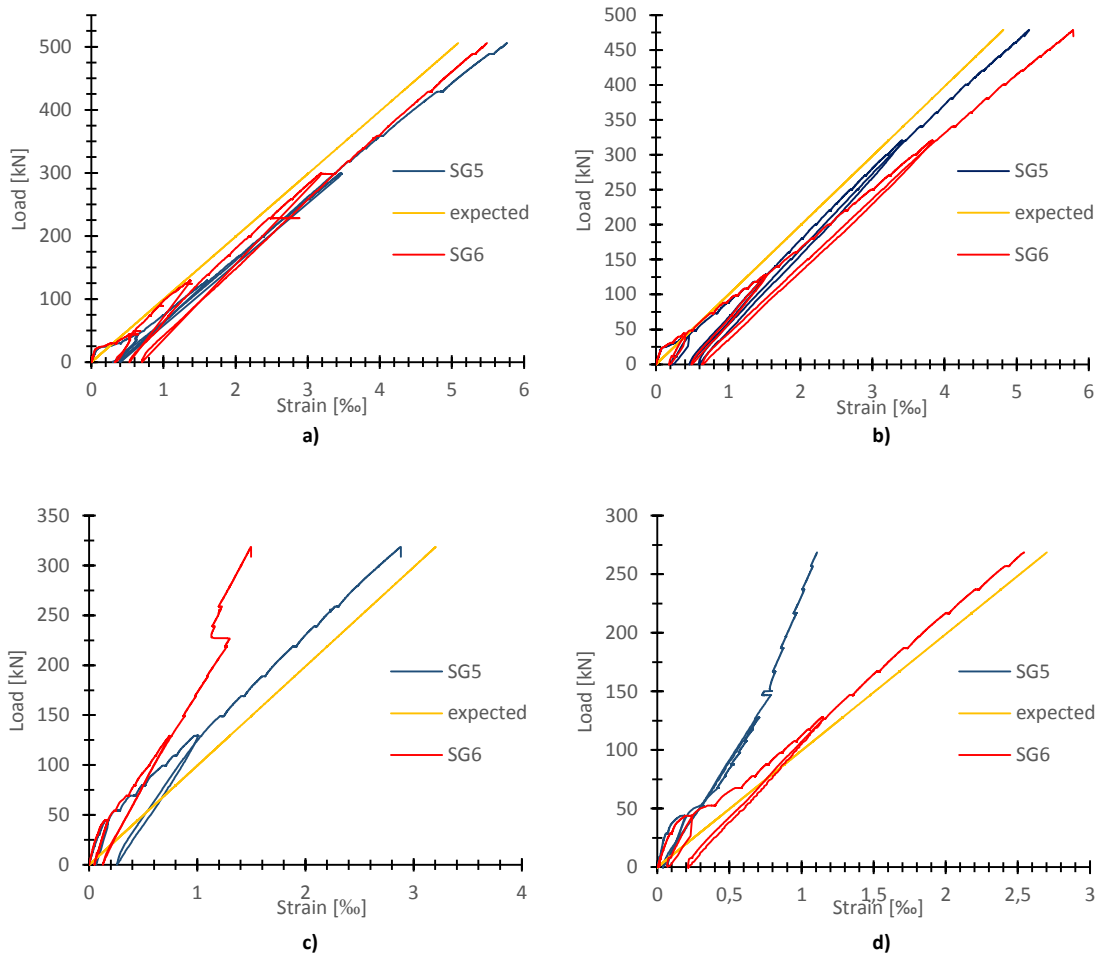

Figure 63 - Strain of tensile reinforcement: a) BS250GFRP2; b) BC250GFRP2; c) BDHB250GFRP2; d) BB250GFRP2

Table 26 – Summary of ultimate strain values

Beam	Ultimate values					
	Mid-span strain			Shear reinforcement strain		
	Exp.	Pred.	Exp /Pred.	Exp.	Pred.	Exp /Pred.
	(‰)	(‰)	(-)	(‰)	(‰)	(-)
REF250	2.53	2.25	1.12	2.74	9.00	0.30
REFB250	1.04	1.30	0.80	2.14	4.00	0.54
BS250GFRP1	6.80	7.15	0.95	6.56	9.40	0.70
BC250GFRP1	5.63	5.50	1.02	9.86*	9.15	1.02
BDHB250GFRP1	3.77	3.54	1.06	3.62	7.20	0.50
BB250GFRP1	5.24	5.09	1.03	5.21	5.20	1.00
BS250GFRP2	5.76	5.02	1.15	8.30	9.40	0.88
BC250GFRP2	5.45	5.10	1.07	7.61	9.15	0.83
BDHB250GFRP2	2.85	3.11	0.92	4.06	7.20	0.56
BB250GFRP2	2.50	2.62	0.92	5.02	5.20	0.97

* not on the failure side. On the failure side the maximum strain was 2.85‰

2.4.1.5.2 Shear reinforcement strain

The maximum shear reinforcement strains for the different beam specimens as well as the predicted values are presented in Table 26.

In Figure 64, the development of the strain at the most stressed stirrup (SG3 or SG8, according to the side of the failure of the beam) is shown, as well as a rough prediction of the strains. The expressed as a function of the applied load, P, the reinforcement spacing, s, the area, A_{fv}, prediction (equation (33)) was and the elasticity modulus, E_{fv}, of the shear reinforcement and the internal lever arm, z.

$$\varepsilon_{fv} = \frac{Ps}{2zE_{fv}A_{fv}} \quad (33)$$

Beams are grouped by the shear reinforcement solution in order to compare the influence of the longitudinal stiffness in the shear strains. In general, near the failure the strain values were close to the predictions. For all beam specimens the development had a bilinear configuration. GFRP1 beams had the higher stirrups strains for the same load value, while beams with the steel longitudinal reinforcement exhibited the lower shear reinforcement strains. Beams with the capacity to better mobilize the shear reinforcement were those with the closed stirrup or C-stirrup, and consequently had a higher shear load capacity.

Corresponding to an average of 4‰ strain in GFRP stirrups, which is the ACI 440.1R-06 [2] limit, the applied forces were 268 kN and 230 kN, respectively for BS250GFRP1 and BS250GFRP2. These values represent, respectively, 67% and 46% of the observed failure loads. For BC250GFRP1 and BC250GFRP2 the applied forces were 200 kN and 301 kN, respectively. Similar results were stated by Ehab A. Ahmed and Brahim [29]. From Figure 64 it can be observed that the strains of shear reinforcement were higher than the ACI 440.1R-06 [2] limit of 4‰ for all beam specimens. Even BC250GFRP1, which exhibited lower strain values on the shear span where the failure occurred, exhibited strains of nearly 9‰ on the opposite side. This shows that the proposed shear reinforcement solutions, with exception of the single vertical bars are capable of being mobilized contributing to the shear strength.

As, between GFRP1 beams and GFRP2 beams, the stirrups strain curves exhibited similar values, it seems that they were not significantly affected by the longitudinal stiffness. However, they are dependent on the shear reinforcement solution.

The maximum shear strains on the beam specimens with the closed stirrups (BS and BC) varied from 7‰ to 10‰, being these solutions the best options in terms of the shear strength.

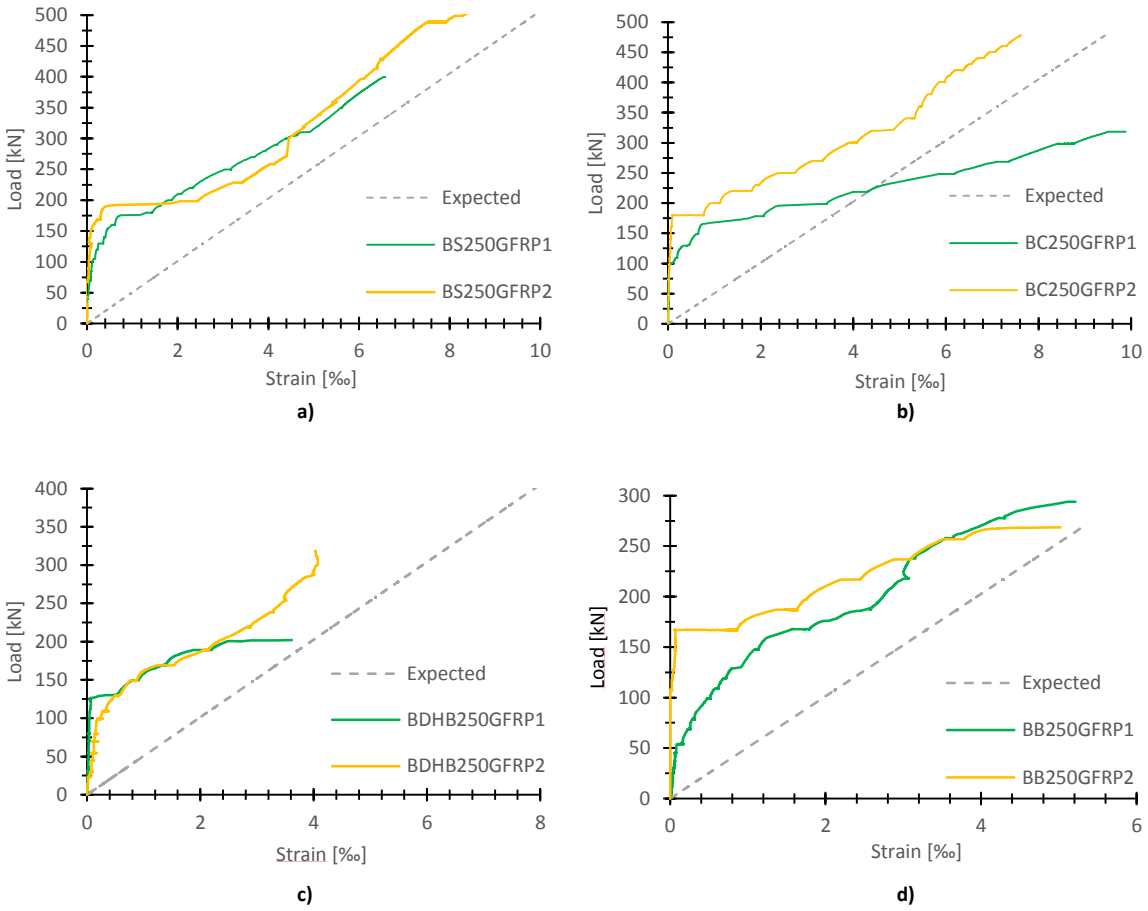

Figure 64 – Shear reinforcement strains for: a) BS- beams; b) BC- beams; c) BDHB- beams; d) BB- beams

2.4.1.6 Shear crack width

In Figure 65 the shear crack variation with the loading is presented. It can be stated that the shear cracks appeared only for load levels above the service load. It seems to be a correlation approximately linear between the crack widths and the applied load of the beams with the same longitudinal stiffness, as shown by the two lines represented. The larger crack widths developed on GFRP1 beams are responsible for the lower shear strength, since the shear mechanisms integrity is called into question.

For REF250, it was not possible to measure the shear cracks during the testing.

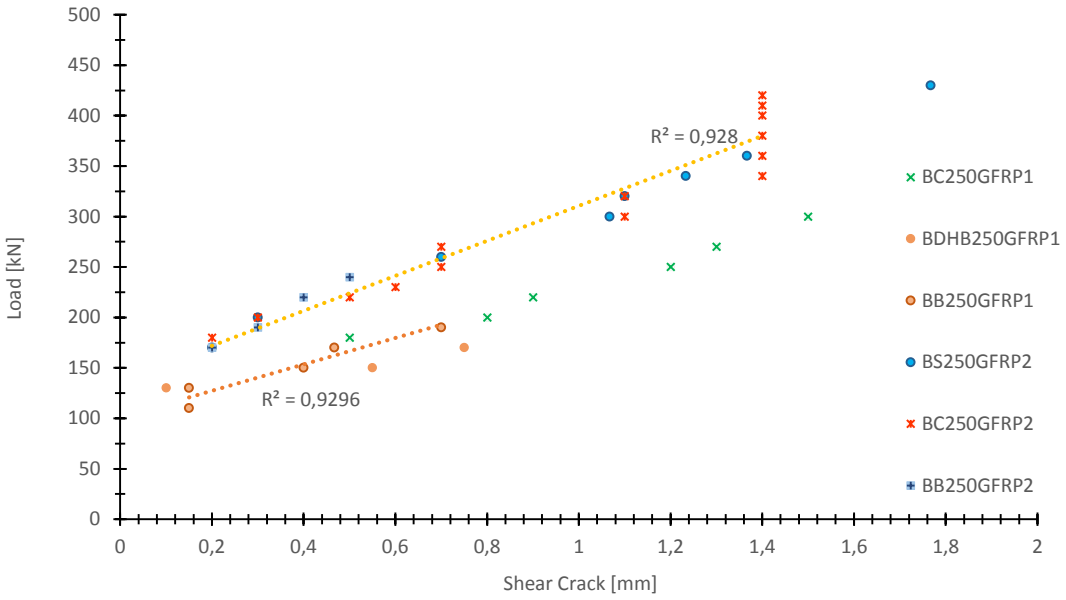

Figure 65 – Shear crack width with the loading

2.4.2 Conclusions

The results of an experimental campaign to test the influence of the longitudinal GFRP bar ratio on the behaviour of RC beams with GFRP shear reinforcement were presented. Two different GFRP longitudinal ratios were considered and tested on four different layouts of GFRP shear reinforcement. The behaviour of GFRP beams was then compared with similar steel RC beams and with predictions of design provisions. The main findings and results of this research can be summarized as follows:

1- The longitudinal stiffness affects the shear capacity of the GFRP beams. Considering beams with the same shear reinforcement solution and amount, increasing the longitudinal stiffness for approximately the double represented gains in the shear capacity from 25% to 50% of the original capacity. This can be explained by the fact that increasing the stiffness, the deflection of the beam specimens and the shear cracks width are lower, and consequently the capacity of mobilizing the shear reinforcement and the integrity of the shear mechanisms is kept for longer. A linear equation - to be applied in the range of the longitudinal reinforcement ratios tested - was suggested, as a modification to ACI 440.1R-06[2] equation, in order to achieved conservative but more rational predictions.

2- Although ACI 440.1R-06[2] and FIB 40 [22], take in consideration the longitudinal stiffness in the concrete contribution to the shear capacity, it was found that this influence is highly underestimated.
3- It was also found that the cracking patterns and failure planes were affected by the longitudinal stiffness. Beams with the higher longitudinal stiffness failed with a less inclined plane and exhibited more shear cracks.
4- The shear reinforcement strains were not significantly affected by the longitudinal stiffness change; however, they were affected by the shear reinforcement solution.
5- Applying ACI 440.1R-06[2] to predict the short-term deflections at service load overestimates this value for some of the beams and underestimates for other beams; however, the experimental values are close to the predictions.
6- Tests highlighted a linear relationship between the shear crack width and the load. However, this relation was found to be dependent of the longitudinal stiffness.
7- The GFRP1 and GFRP2 beam specimens were designed to have a shear strength similar to the reference beams. However, with the exception of the BB250GRP1, none of GFRP1 beams exceeded the load capacity of the respective reference. The GFRP2 beams, with exception of BDHB250GFRP2, had higher shear strength than the references. This shows that the longitudinal stiffness of the GFRP beams had a significant influence on the performance of the GFRP shear reinforcement.
8- Although in general the solutions with closed stirrups (BC and BS beams) exhibited a good performance in both of the longitudinal stiffness cases, the solution with double headed bars exhibited a better performance when it was considered a higher longitudinal stiffness.
9- The solution of using two straight vertical bars as shear reinforcement has proven to be inefficient. The fact that BB250GFRP1 had a shear failure load higher than BB250GFRP2 shows that there is some randomness and uncertainty in the behaviour of this solution (cracks in the right place may cause immediately slip of one of the bars), Therefore, this solution should not be applied.
10- Applying ACI 440.1R-06 [2] to determine the design shear capacity underestimates the beams capacity, particularly in the cases of the solutions with GFRP bent bars. While designing with GFRP bent closed stirrups, it was found that the considered limit of 4‰, could be increased to a value between 6‰ and 7‰, in order to design safe but more economical sections.

2.5 Experimental performance comparison of reinforced concrete beams with different GFRP transverse reinforcement solutions and different longitudinal bar material and ratios

This section outlines the results of 14 of the beam specimens designed and tested in order to study the shear behaviour of GFRP RC beams, and which are described in section 2.1. The main objectives were: to analyse the influence of the longitudinal reinforcement material (steel and GFRP) and of the longitudinal bar ratio on the performance of RC beams with GFRP shear reinforcement; to compare the behaviour with reference beams (entirely steel reinforced); and to establish a comparison between the experimental capacity and several codes and models predictions.

Four different layouts of GFRP shear reinforcement were considered: bent bars forming a closed hoop stirrup; two C-shaped bent bars overlapped to form a closed stirrup; two vertical straight bars and two vertical straight bars.

Beams were divided into 5 groups:

1) The reference beams: REF250 and REFB250 entirely reinforced with steel;
2) 3 BS beams (S - closed GFRP stirrups): BS250, BS250GFRP1 and BS250GFRP2;
3) 3 BC beams (C - two overlapped C-shaped GFRP bent bars): BC250, BC250GFRP1 and BC250GFRP2;
4) 3 BDHB beams (DHB - two double headed GFRP vertical straight bars): BDHB250, BDHB250GFRP1 and BDHB250GFRP2;
5) 3 BB beams (B - two GFRP vertical straight bars): BB250, BB250GFRP1 and BB250GFRP2.

The theoretical shear capacity was maintained constant in all the specimens. Within each group, the beams have the same shear reinforcement but different longitudinal reinforcement materials and ratios. BS250, BC250, BDHB250 and BB250 were steel longitudinal reinforced with the same ratio than the reference beams. Beams designated by GFRP1 were longitudinally reinforced with GFRP but maintaining the same reinforcement ratio and, approximately, the same design capacity of the reference beams. Beams designated by GFRP2 were longitudinally reinforced with GFRP and designed to have a similar deflection at mid-span as the reference beam under service conditions.

Beams were design to fail due to shear and tested under four-point bending until failure. Results are reported in terms of load-deflection, stirrup strains, crack patterns and crack widths.

The tests proved that the solutions with GFRP bent bars are effective as shear reinforcement and that its bending process does not reduce the resistance performance of the material. It was also concluded that the general FRP design guidelines present overly conservative proposals to estimate the shear resistance in the cases where the GFRP bent bars were used as shear reinforcement. The solution with double headed bars exhibited a good performance in the beams with higher longitudinal stiffness, although with lower strength results than the GFRP bent bars solutions, but still conservative. The beams with straight bars as shear reinforcement behaved with a shear resistance lower than predictions, proving to be an inadequate solution. It was also found that the hybrid solution with bent GFRP stirrups and longitudinal steel reinforcement is the best option to combine corrosion resistance, best structural behaviour (having the lower deflection and the higher shear strength) and most economical choice.

2.5.1 Results and discussion

2.5.1.1 Ultimate capacity

All the beam specimens were designed to fail due to shear. The shear capacity of all GFRP shear reinforced beams was calculated considering the expressions and models from Table 27 to Table 29. When designing the beam specimens, only ACI 440.1R-06 [2], FIB 40 [22] and Schöck [84] (which are based on EC2 [23]) formulations were used to calculate the shear strength of GFRP beams with safety factors. These values were designated design predictions. To better determining the shear strength, a second iteration was done where the ultimate strength values of the material properties were considered, and no safety factors were applied and others formulas and models were also analysed. These values were designated non-design values.

For the steel reinforced beams case (REF250 and REFB250), the shear capacity was calculated according to the EC2 [23] and ACI 318-11 [3].

Table 27 – Shear design equations accordingly to ACI 440.1R-06 [2], JSCE design guidelines[35] and FIB 40 [22]

Model	Concrete shear equations		Reinforcement shear equations	
ACI 440.1R-06 [2]	$V_c = \frac{2}{5} k \sqrt{f_c'} b d$	(34)	$V_{fv} = \frac{A_{fv} \sigma_{fv} d}{s}$	(35)
	$k = \sqrt{2\rho_{fl} n_f + (\rho_{fl} n_f)^2} - \rho_{fl} n_f$	(36)	$\sigma_{fv} = 0.004 E_{fv} \leq f_{fb}$	(37)
	$n_f = \frac{E_{fl}}{E_c}$	(38)	$f_{fb} = \frac{\left(\frac{0.05 r_b}{d_b} + 0.3\right)}{1.5} f_{fv} \leq f_{fv}$	(39)

Table 27 – (continuation).

Model	Concrete shear equations		Reinforcement shear equations	
JSCE design guidelines[35]	$V_c = \frac{\beta_d \beta_p \beta_n f_{vcd} bd}{\gamma_b}$	(40)	$V_{fv} = \frac{\frac{A_{fv} E_{fv} \varepsilon_{fv}}{s}}{\gamma_b} \frac{d}{1.15}$	(41)
	$\beta_d = \left(\frac{1000}{d}\right)^{\frac{1}{4}} \leq 1.5$	(42)	$\varepsilon_{fv} = \sqrt{\left(\frac{h}{0.3}\right)^{\frac{-1}{10}} f_c' \frac{\rho_{fl} E_{fl}}{\rho_{fv} E_{fv}}}$	(43)
	$\beta_p = \left(100 \frac{\rho_{fl} E_{fl}}{E_s}\right)^{\frac{1}{3}} \leq 1.5$	(44)		
	$\beta_n = 1$, if there is no axial forces	(45)		
	$f_{vcd} = 0.2(f_c')^{\frac{1}{3}} \leq 0.72MPa$	(46)		
	$\gamma_b = 1.3$	(47)		
FIB 40 [22]	$V_c = 0.12\left(1 + \sqrt{\frac{200}{d}}\right)\left(100 \rho_{fl} \frac{E_{fl}}{E_s} \phi_\varepsilon f'_c\right)^{1/3} bd$	(48)	$V_f = \frac{A_{fl}}{s} f_{fl} z \cot\theta$	(49)
	$\varepsilon_f = 0.0045$	(50)		
	$\phi_\varepsilon = \varepsilon_f / \varepsilon_y$	(51)		

Table 28 – Shear design equations accordingly to CSA S806-02[13]and CSA S6-09 Addendum[65]

Model	Concrete shear equations		Reinforcement shear equations	
CSA S806-02 [13]	$V_c = 0.035 \lambda \varphi_c \left(f_c' \rho_{fl} E_{fl} \frac{V}{M} d\right)^{\frac{1}{3}} bd$	(52)	$V_{fv} = \frac{0.4 \varphi_f A_{fv} f_{fv} d}{s} < 0.6 \varphi_c \sqrt{f_c'} bd$	(53)
	$\lambda = 1$	(54)	$\varphi_f = 0.75$	(55)
	$\varphi_c = 0.6$	(56)		
CSA S6-09 Addendum[65]	$V_c = 2.5 \beta \varphi_c (0.4\sqrt{f_c'}) b d_v$	(57)	$V_{fv} = \frac{\varphi_f A_{fv} \sigma_{fv} d_v cot\theta}{s}$	(58)
	$d_v \geq \begin{cases} 0.9d \\ 0.72h \end{cases}$	(59)	$\varphi_f = \begin{cases} 0.50 \; for \; GFRP \\ 0.75 \; for \; CFRP \end{cases}$	(60)
	$\beta = \frac{1300 \frac{0.4}{1 + 1500 \varepsilon_x}}{1000 + s_{ze}}$	(61)	$\sigma_{fv} = \frac{\left(\frac{0.05 r_b}{d_b} + 0.3\right)}{1.5} f_{fv} \leq 0.004 E_{fv}$	(62)
	$\varepsilon_x = \frac{\frac{M_f}{d} + V_f + 0.5 N_f}{2 E_s A_s} \leq 0.003$	(63)	$\theta = (29 + 7000\varepsilon_x)\left(0.88 + \frac{s_{ze}}{2500}\right)$	(64)
	$s_{ze} = 300mm$	(65)		
	$f_{fv,d} = 130MPa$	(66)	$E\rho_{res} = \sqrt{\left(\rho_{fl} E_{fl}\right)^2 + \left(\rho_{fv} E_{fv}\right)^2}$	(67)

Table 29 – Shear design equations accordingly to CNR DT-203[27], Fico et al. [35], Nehdi et al. [65], Oller et al.[75] and Schöck [84]

Model	Concrete shear equations		Reinforcement shear equations	
CNR DT-203[27]	$V_c = 1.3\sqrt{\frac{E_{fl}}{E_s}}0.25(0.05f_c')k_d(1.2+40\rho_{fl})bd$	(68)	$V_{fv} = \frac{A_{fv}}{s}\frac{f_{fv}}{\gamma_{f,\varphi}\gamma_f}d$	(69)
	$k_d = 1.0$	(70)	$\gamma_{f,\varphi} = 2.0$	(71)
			$\gamma_f = 1.5$	(72)
Fico *et al.* [35]	The same as CNR DT-203[27]	(73)	$V_{fv} = \frac{A_{fv}}{s}f_{fv,b}d$	(74)
			$f_{fv,b} = E_{fv}\varepsilon_{frp,lim}$	(75)
			$\varepsilon_{frp,lim} = 0.0085\ for\ GFRP$	(76)
Nehdi *et al.* [65]	$V_c = 2.1\left(\frac{f_c'\rho_{fl}d}{a}\frac{E_{fl}}{E_s}\right)^{0.23}bd$, if $\left(\frac{a}{d}\right) \geq 2.5$	(77)	$V_{fv} = 0.74\left(\frac{A_{fv}}{bs}\right)^{0.5}f_{fv}bd$	(78)
Oller *et al.*[75]	$V = (V_c + V_w + V_t) = (v_c + v_w + v_t)f_{ct}bd$	(79)	$v_c = \zeta(1.072 - 0.01\alpha)[(0.98 + 0.22v_t)\xi + 0.05]$	(80)
	$v_w = \frac{0.386}{\varepsilon_t}\frac{f_{ct}}{E_c}\left(1+\frac{8G_fE_c}{f_{ct}^2d}\right)$	(81)	$\zeta = 1.2 - 0.2a \geq 0.65$	(82)
	$v_t = 0.85\rho_{fv}f_{fv}$	(83)	$\alpha = \frac{E_{fl}}{E_c}$	(84)
	$f_{fv} = \left(0.05\frac{r_b}{d_b}+0.3\right)f_{fu}$	(85)		
Schöck [84]	$V_{fv} = \frac{A_{fv}}{s}f_{fv,d}z\ \cot\theta$	(86)	$\theta = 50 - \frac{E\rho_{res}}{400}$	(87)
	$f_{fv,d} = 130MPa$	(88)	$E\rho_{res} = \sqrt{(\rho_{fl}E_{fl})^2 + (\rho_{fv}E_{fv})^2}$	(89)

The test results regarding the ultimate capacity of all beams and the corresponding failure modes are presented in Table 30. In order to establish a comparison, it is also indicated the theoretical values of the expected load capacity obtained according to ACI 440.1R-06 [2] / ACI 318-11 [3] and EC2 [23]/FIB 40 [22] . The non-design shear capacity was always estimated as the sum of the concrete and reinforcement contributions ($V = V_c + V_{fv}$) and with the equations summarized in Table 27.

Table 30 – Summary of experimental and predicted ultimate shear and bending capacity with ACI 440.1R-06 [2] / ACI 318 -11[3] and EC2 [23]/FIB 40 [22]

Beam	Non-design Capacity					
	Experimental		ACI 440.1R-06 [2] / ACI 318 [3]		EC2 [23]/FIB 40 [22]	
	Type	Load (kN)	Shear ε_{fv} =4 ‰ (kN)	Bending (kN)	Shear Θ=45 (kN)	Bending (kN)
REF250	Shear	426.4	393.9	546.2	326.6	543.8
REFB250	Shear	257.4	391.3	544.0	325.3	541.5
BS250	Bending	488.2*	335.2	555.4	303.0	553.3
BC250	Bending	490.3*	344.4	562.1	308.0	560.2
BDHB250	Shear	422.3	325.5	542.3	294.8	539.8
BB250	Shear	217.6	327.5	544.2	295.9	541.7
BS250GFRP1	Shear	400.0	245.8	449.9	275.6	527.7
BC250GFRP1	Shear	318.5	261.4	507.5	284.3	595.2
BDHB250GFRP1	Shear	202.2	251.6	437.5	273.7	513.1
BB250GFRP1	Shear	293.9	250.9	434.2	273.1	509.2
BS250GFRP2	Shear	506.0	268.5	527.7	297.1	619.1
BC250GFRP2	Shear	478.7	287.7	598.5	307.4	702.0
BDHB250GFRP2	Shear	319.7	273.7	504.8	293.7	592.3
BB250GFRP2	Shear	268.5	272.7	499.8	293.0	586.4

* - Bending failure

Note: The values of shear capacity of the steel RC beams include the concrete contribution, because although EC2[23] indicates that the shear capacity is given only by the stirrups contribution, more recent studies and codes[20] mentioned that better estimation can be achieved by adding the concrete contribution.

All the beam specimens were designed to fail due to shear, however BS250 and BC250 failed by compression of the concrete at top of mid-span at loads about 85 % of the non-design prediction All the beam specimens were designed to fail due to shear, however BS250 and BC250 failed by compression of the concrete at top of mid-span. The failure occurred at a load value which was 85% of the non-design prediction for the bending capacity of both ACI 440.1R-06 [2] and FIB-40 [22]. To all others beam specimens the experimental ultimate loads were always higher than the bending design capacity.

The bending failure of these beams can be understood considering in the calculation of the bending capacity that the concrete strain was 3.5‰, the ultimate compressive strain, ε_{cu}, and that the strain in the longitudinal reinforcement , ε_{sl}, was 2.8‰, which was the yield strain of the steel considered. This yield strain was determined, with the values of the pure tension tests, as the ratio between the experimental values of the yield strength, f_{sy}, and the elasticity modulus, E_s. An ultimate bending capacity of 477.0 kN is obtained, which is close to the experimental capacity of BS250 and BC250. Moreover, the experimental longitudinal strain development, showed later in Figure 87 supported these calculations.

The shear capacity of both BC250 and BS250 was higher than REF250 in at least 15%, as these two beams failed by concrete crushing at mid-span for a load higher than the failure load of the reference beam.

Although the shear reinforcement ratio was the same between REFB250 and REF250, the shear capacity of REFB250 was approximately 40% lower than the capacity of REF250. This is explained by the lack of the anchorage length of the 2 straight bars. Among the GFRP shear reinforced beams, the same tendency was verified and the solutions with closed stirrups (BS and BC beams) exhibited the highest shear capacities.

Concerning the ultimate loads, BB250, BB250GFRP1 and REFB250 were designed to have the same shear strength. However the ultimate capacity of BB250 was 16% lower, while the ultimate capacity of BB250GFRP1 was 14% higher than REFB250. For the double headed bars GFRP reinforcement the ultimate strength was 2.0 times higher than REFB250.

Within GFRP shear solutions with bent bars (BS and BC beams) it was verified that the closed hoop stirrups conducted to the highest shear capacity. In Figure 66 a comparison between these stirrups after the failure of some of the beams is shown. It was verified that in the C-stirrup there is a tendency to the deformation of the overlapped bottom branches, causing the pull out of the concrete cover (Figure 66 a) and b). This was not verified on the closed hoop stirrup as the overlapped branch was at the top of the beam (Figure 66 c) and d)).

Figure 66 – Comparison between C-stirrups and closed hoop stirrups: a) C-stirrups horizontal branch opening; C-stirrups disintegration; c) closed hoop stirrups behaviour at failure of one of the beams; d) closed hoop stirrups behaviour at failure

The longitudinal reinforcement area and material also had influence in the shear capacity; GFRP1 beams had the lowest shear capacity. BS250GFRP1 had 81.9% and 79.0% the shear capacity of BS250 and BS250GFRP2, respectively. BC250GFRP1 had 64.9% and 66.5% of the shear capacity of BC250 and BC250GFRP2, respectively.

Comparing the experimental ultimate loads of beam specimens with the non-design predictions of the shear capacity it can be stated that, except for BB250 and BDHB250GFRP1, the codes are conservative. In the case of ACI 440.1R-06 [2] the differences between the predictions and the experimental values are related to the 4‰ referred as limit to the shear reinforcement strains, which corresponds in tension to 220 MPa. In fact, as shown hereafter, the maximum strains on stirrups of BC and BS beams ranged from 7‰ to almost 10‰ (Figure 87). Table 31 presents the values of the shear capacity for a shear reinforcement strain of 4‰, 6‰ and 7‰. For the closed stirrups solutions, independently of the longitudinal stiffness, it is possible to increase the strain to 7‰ and maintain conservative predictions. For the solution with double headed bars, in the two higher reinforcement ratios it was possible to obtain good predictions considering the strain limit of 6‰.

Table 31 – Non-design capacity of beams in accordance with ACI 440.1R-06[2] and FIB 40[22] varying the strain limit and the angle

Beam	Non-design capacity								
	Experimental Load	ACI 440.1R-06[2]				FIB 40[22]			
	(kN)	ε_{fv} =4 ‰ (kN)	ε_{fv} =6 ‰ (kN)	ε_{fv} =7 ‰ (kN)	Θ=30 (kN)	Θ=38			Θ=45 (kN)
						ε_{fv} =4.5 ‰ (kN)	ε_{fv} =6 ‰ (kN)	ε_{fv} =7 ‰ (kN)	
BS250	488.2	335.2	406.8	442.6	409.2	343.6	405.5	445.7	303.0
BC250	490.3	344.4	416.0	451.8	414.2	348.6	410.5	451.7	308.0
BDHB250	422.3	325.5	397.1	432.9	400.9	335.4	397.2	438.5	294.8
BB250	217.6	327.5	399.1	434.9	402.0	336.5	398.3	439.6	295.9
BS250GFRP1	400.0	245.8	317.5	353.3	381.8	316.2	391.3	440.1	275.6
BC250GFRP1	318.5	261.4	333.1	368.9	390.6	324.9	400.9	450.2	284.3
BDHB250GFRP1	202.2	251.6	323.2	359.1	379.9	314.3	389.1	437.9	273.7
BB250GFRP1	293.9	250.9	322.6	358.4	379.4	313.8	388.6	437.3	273.1
BS250GFRP2	506.0	268.5	338.2	373.0	400.4	336.6	412.5	461.7	297.1
BC250GFRP2	478.7	287.7	357.3	392.2	410.7	346.9	423.9	473.7	307.4
BDHB250GFRP2	319.7	273.7	343.4	378.3	397.0	333.2	408.8	457.8	293.7
BB250GFRP2	268.5	272.7	342.4	377.3	396.3	332.4	408.0	456.9	293.0

Considering the FIB 40 [22], there are two variables that may be responsible for the difference between the experimental and the prediction values: the angle of 45 degrees for the strut and the limit of 4.5‰ for the reinforcement strain. The failure planes (from Figure 68 to Figure 75) suggest that the angle for the strut can be lower, thus Table 31 has the values considering 30˚, 38˚, and 45˚. Fixing the strains at 4.5‰, the best predictions were obtained with 30˚, however experimentally the best angle was 38˚. It was considered increasing the strains to 6‰ and 7‰ while maintaining the angle of 38˚, and it was verified that the values of predictions were very similar to those achieved with ACI 440.1R-06 [2] and close, but conservative, to the experimental. Other formulations found in literature and listed from Table 27 to Table 29 were also used to calculate the shear strength. Then the results were compared with the experimental capacity (Table 32). In Figure 67 the ratio between the experimental and the predictions is represented to easily compare these values and the different methods.

Table 32 – Ultimate shear capacity accordingly to several models

Beam	Shear capacity									
		Ultimate values								
	Experimental	ACI 440.1R-06[2]	FIB 40[22]	Oller et al.[75]	CSA S6-09 Addendum [65]	CSA S806-02[13, 35]	JCSE guidelines [35]	CNR DT-203[27]	Fico et al.[35]	Nedhi et al.[65]
	(kN)	(kN)	(kN)	(kN)	(kN)	(kN)	(kN)	(kN)	(kN)	(kN)
BS250	488.2	335.2	303.0	465.0	375.6	444.7	432.5	415.1	494.3	545.5
BS250GFRP1	400.0	245.8	275.6	459.3	371.0	358.6	246.9	323.7	403.35	472.5
BS250GFRP2	506.0	268.5	297.1	459.6	371.0	391.5	314.6	346.6	425.7	501.6
BC250	480.3	344.4	308.0	465.0	375.6	444.7	432.5	415.1	494.3	545.5
BC250GFRP1	318.5	261.4	284.3	459.3	37.01	358.6	246.9	323.7	403.35	472.5
BC250GFRP2	478.7	287.7	307.4	459.6	371.0	391.5	314.6	346.6	425.7	501.6
BDHB250	422.3	325.5	294.8	465.0	375.6	444.7	432.5	415.1	494.3	545.5
BDHB250GFRP1	202.2	251.6	273.7	459.3	371.0	358.6	246.9	323.7	403.35	472.5
BDHB250GFRP2	319.7	273.7	293.7	459.6	371.0	391.5	314.6	346.6	425.7	501.6
BB250	217.6	327.5	295.9	465.0	375.6	444.7	432.5	415.1	494.3	545.5
BB250GFRP1	293.9	250.9	273.1	459.3	371.0	358.6	246.9	323.7	403.35	472.5
BB250GFRP2	268.5	272.7	293.0	459.6	371.0	391.5	314.6	346.6	425.7	501.6

Considering the closed stirrups beams (BS and BC), only Nedhi *et al.* [65] formulation provided non-conservative values. On average, the experimental to predicted ratio ranged from 1.0 to 1.2 to Oller *et al.*[75], Fico *et al.* [35], CSA S6-09 Addendum [65], CNR DT-203 [27], and CSA S806-02 [13], JSCE design guidelines[35] yielded more conservative values and the ratio was on average 1.4. For the solutions with the double headed bars, the lowest longitudinal stiffness (BDHB250GFRP1) was overestimated by all the methods.

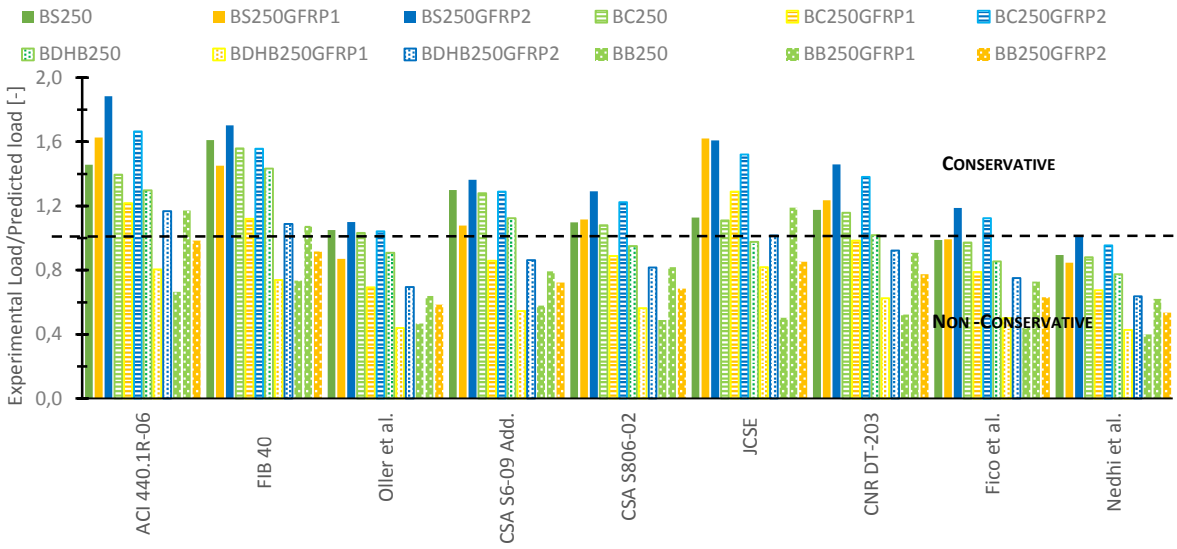

Figure 67 – Comparison of the experimental to predictions ratios for different methods

2.5.1.2 Cracking pattern

The cracking pattern of each beam and the failure plane angle are represented Figure 68 to Figure 74. In terms of development, the cracking patterns were all similar among the specimens. In the beginning of the tests, all beam specimens were uncracked. The first cracks appeared firstly at the constant moment region, and grew vertically, due to the absence of shear stresses. Then several flexural cracks appeared in the shear-span region, propagating to the loading point. It was the shear crack closest to the support that led to the failure of the beam. The slope of the plane of failure of beams that failed due to shear varies from 38˚ to 46˚ being in agreement with the 45 degrees applied in the truss model. Beams with higher longitudinal reinforcement failed in general with a less inclined plane. It was also verified that the higher the longitudinal reinforcement and the failure load, the greater the number of shear cracks.

For BC250 and BS250 the cracking pattern was similar to the one mentioned above, but the concrete at mid-span crushed before the shear failure.

In several cases (BS250GFR1, BS250GFR2, BDHB250, BB250GFRP2 and BC250GFRP2), when the failure was imminent, horizontal cracks appeared from the bottom of the shear cracks towards the supports. This can be explained by the fact that when the failure is imminent the aggregate interlock is lost at the shear crack, the dowel action in the longitudinal reinforcement has to increase, so that the equilibrium is kept at the section. The increase of the dowel action causes vertical tension

stresses which combined with the existing splitting forces due to flexural bond lead to the bond-anchorage failure [98].

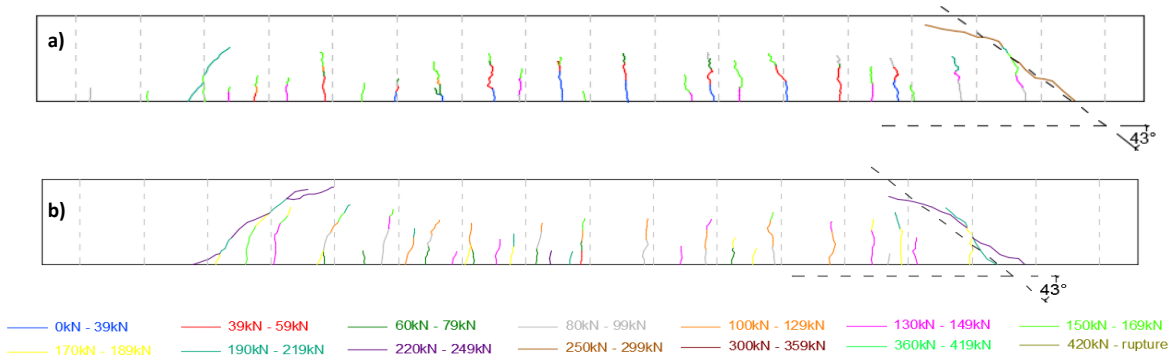

Figure 68 – Cracking pattern of: a) REF250; b) REFB250

Concerning flexural cracks, it can be stated that for GFRP longitudinal reinforced beams, the increase of the reinforcement area resulted in a reduced crack spacing and a higher number of cracks, as expected. BS250GFRP1 flexural crack spacing was 0.242 m while for BS250GFRP2 it was 0.132 m, for BDHB250GFRP1 it was 0.103m while for BDHBGFRP2 it was 0.123 m. Comparing the longitudinal steel reinforced beams with GFRP reinforced, the mean flexural crack spacing for BC250 was 0.112 m while for BC250GFRP1 it was 0.253 m, for BS250 it was 0.109 m while for BS250GFRP1 it was 0.242 m. Thus, it can be stated that for the same amount of reinforcement, steel reinforced beams had a higher number of cracks, with a fixed vertical development pattern while for GFRP reinforced beams, the distance between vertical main cracks was higher, and with the load increase several oblique ramifications appeared and propagated from the main crack. This can be explained by the differences on the elasticity and bond of the two reinforcements (steel and GFRP). Another important data that can be obtained is the height of the compression zone (distance between the compression fibre and the neutral axis). All GFRP1 beam specimens exhibited the smaller compression zones, a mean height of 0.095 m, followed by the GFRP2 beams with 0.135 m and finally steel reinforced beams, with a mean height of 0.150 m. This means that, comparing beams with the same reinforcement area, there was a rise of the neutral axis for GFRP reinforced beams. Also, concerning GFRP reinforced beams, there was a decrease of the neutral axis with the increase of the reinforcement ratio.

It can also be stated that more flexural cracks appeared when the GFRP longitudinal reinforcement ratio increases from GFRP1 to GFRP2.

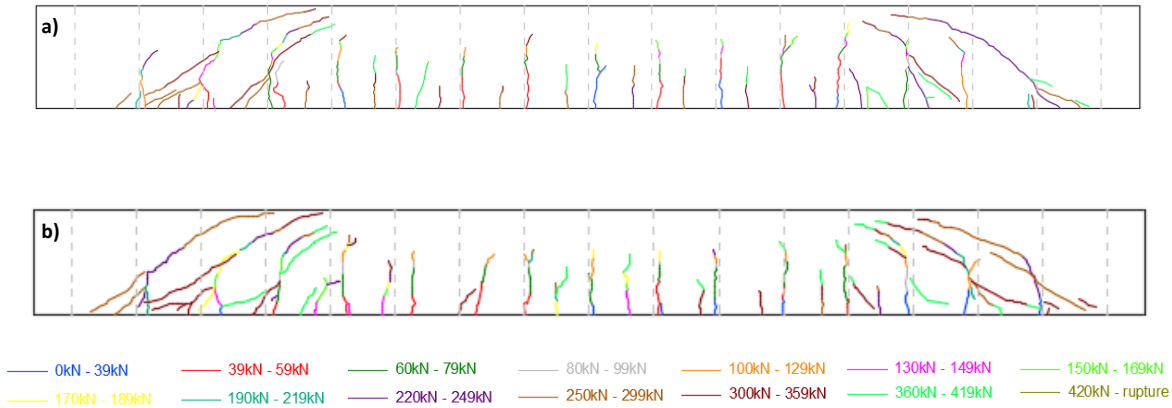

Figure 69 - Cracking pattern of: a) BS250; b) BC250

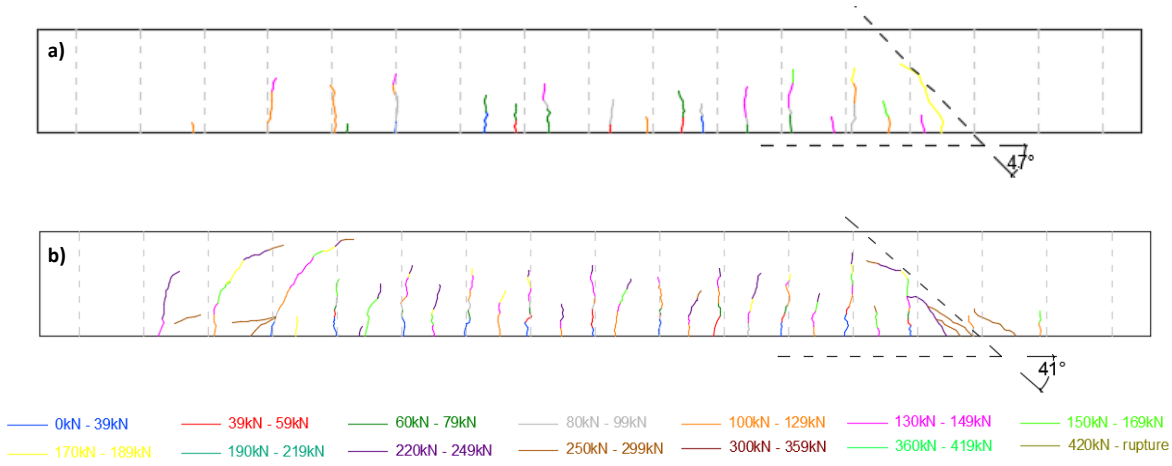

Figure 70 - Cracking pattern of: a) BB250; b) BDHB250

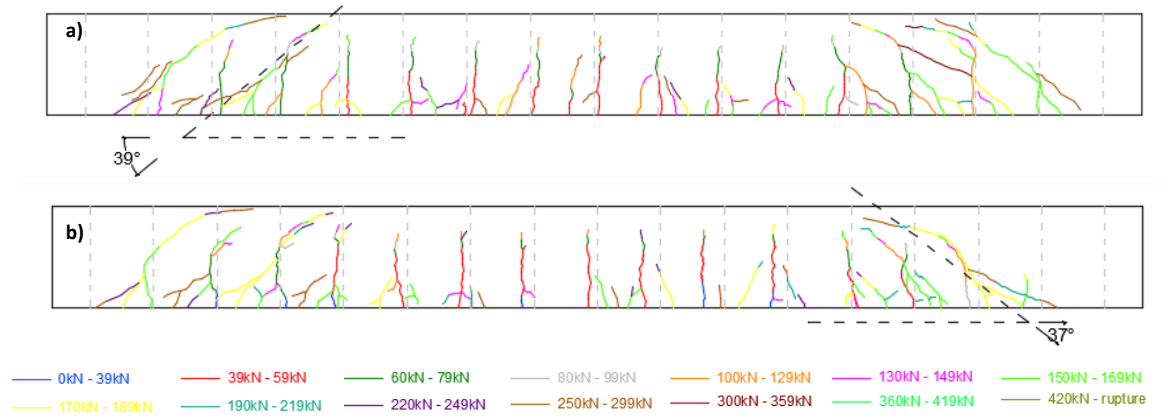

Figure 71 - Cracking pattern of: a) BS250GFRP1; b) BC250GFRP1

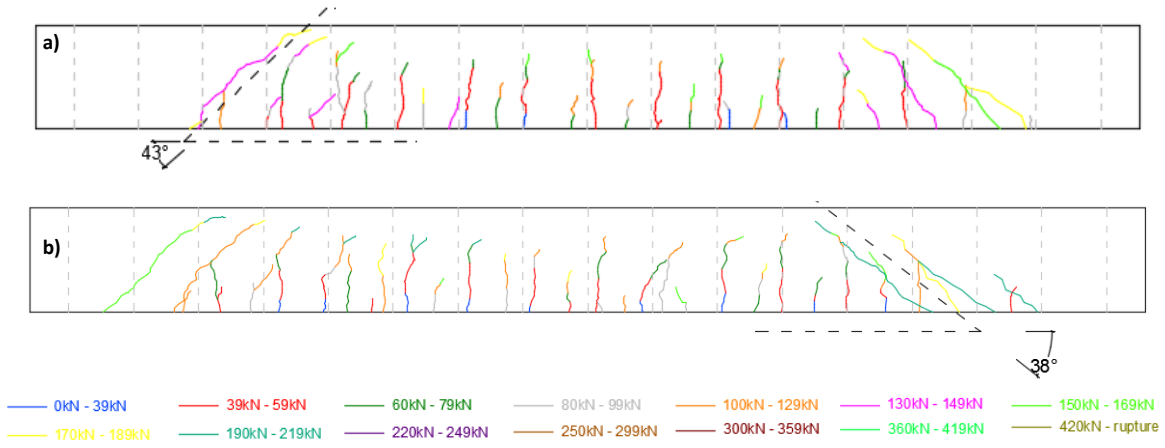

Figure 72 - Cracking pattern of: a) BDHB250GFRP1; b) BB250GFRP1

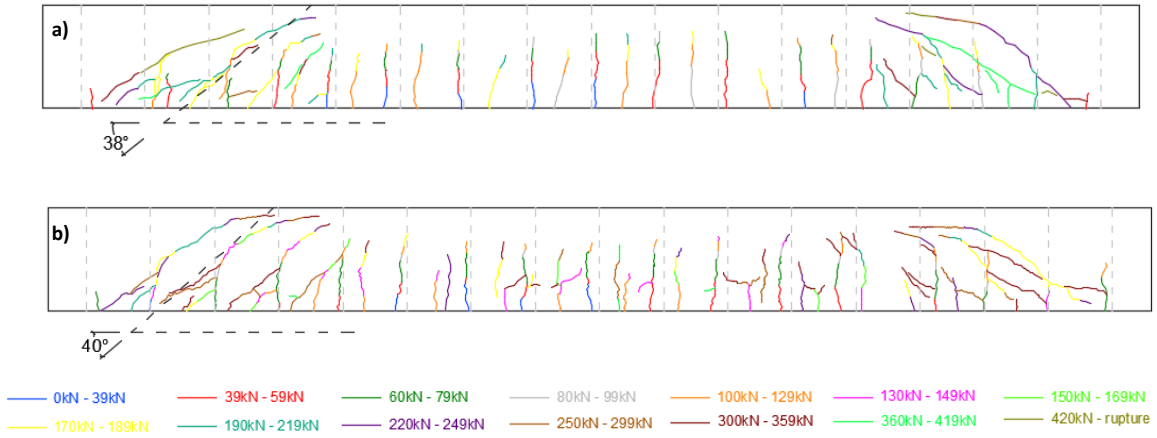

Figure 73 - Cracking pattern of: a) BS250GFRP2; b) BC250GFRP2

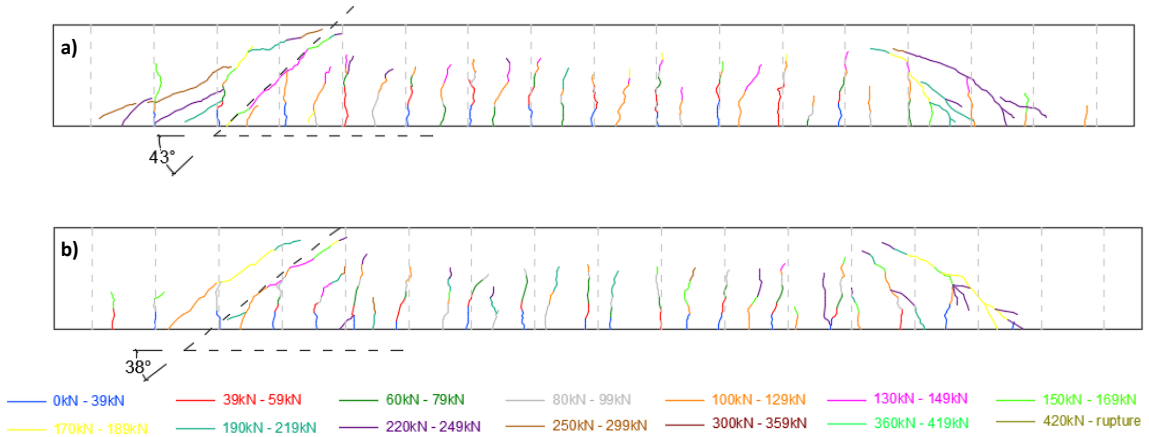

Figure 74 - Cracking pattern of: a) BDHB250GFRP2; b) BB250GFRP2

2.5.1.3 Failure modes

There was no significant difference in the overall behaviour in terms of types of failure when comparing the reference beams with the GFRP beams. The failure modes of all specimens are presented from Figure 75 to Figure 81. In general, four distinct types of failure occurred:

- Bending failure due to concrete crushing at top of mid-span in specimens: BS250 and BC250 (Figure 75);
- Shear diagonal tension failure by shear reinforcement slip or failure of specimens: REF250; REFB250; BC250GFRP1, BDHB250, BDHB250GFRP1, BDHB250GFRP2, BB250, BB250GFRP1 and BB250GFRP2 (Figure 76 to Figure 79);
- Shear failure due to the crushing of the concrete rod in BS250GFRP2 and BC250GFRP2 beams (Figure 80);
- Shear failure due to the failure of the bond of the longitudinal reinforcement at support of BS250GFRP1 (Figure 81).

The failure of BC250 and BS250 was a bending failure which occurred by the crushing of concrete at the top of mid-span. Although for loads above 190 kN several shear cracks appeared in both of the beam specimens, the flexural cracks at mid-span still propagated vertically, and the high levels of deflections caused the crushing of mid-span concrete.

a) b)

Figure 75 – Concrete crushing in: a) BS250; b) BC250

a) b)

Figure 76 - Shear diagonal tension failure in: a) REF250; b) REFB250

a) b)

Figure 77 - Shear diagonal tension failure in: a) BB250; b) BDHB250

a) b)

Figure 78 – Shear diagonal tension failure in: a) BDHB250GFRP1; BDHB250GFRP2

a)

b)

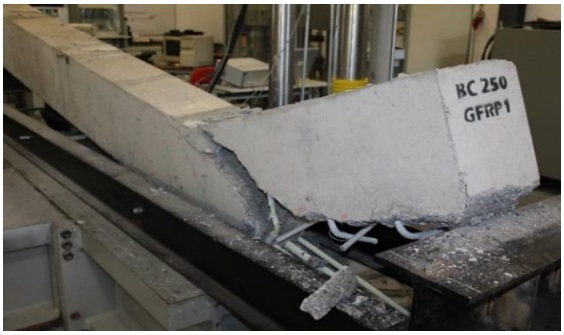

c)

Figure 79 - Shear diagonal tension failure in: a) BB250GFRP1; b) BB250GFRP2; c) BC250GFRP1

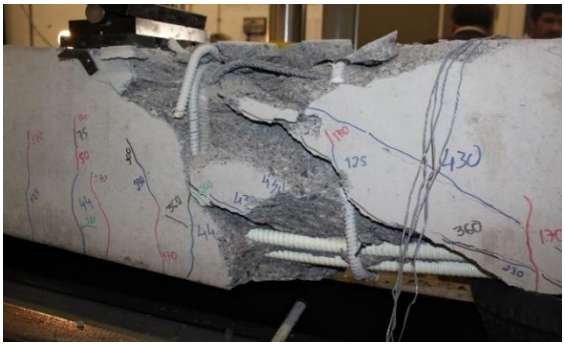

a)

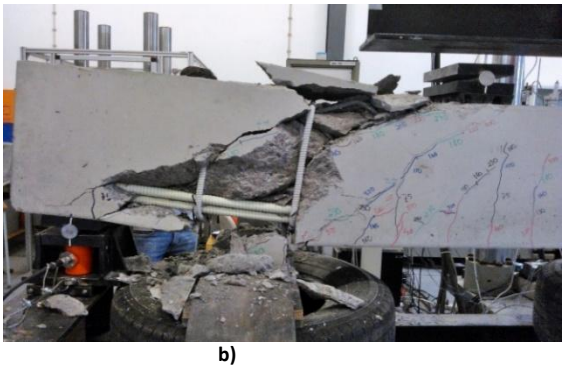

b)

Figure 80 – Shear failure due to the crushing of the concrete rod: a) BS250GFRP2; b) BC250GFRP2

a)

b)

Figure 81 - Shear failure due to the failure of the bond of the longitudinal reinforcement at support of BS250GFRP1 a) overall view; b) slip of the reinforcement at support

The reference beams REF250 and REFB250 had a brittle shear failure mode of several stirrups. Several flexural cracks developed vertically along the span as the load increased. Then the cracks located between the loading points and the supports started to incline in the direction of the loading points. In REF250, the failure occurred with the rupture of one stirrup, followed by the ruptures of all other stirrups along the shear crack; in REFB250 the failure corroded by the slip of one of the shear reinforcement bars, followed by others, leading to an almost instantaneous failure of these beams. The failure of the BB250 beam was similar to the failure of REFB250. In BB250GFRP1 and BB250GFRP2 the failure was also a shear failure due to the slip of the shear reinforcement bars, which also caused the pull-out of the longitudinal bars near the support, leading to brittle failure. The BS250GFRP1 beam exhibited a brittle shear failure due to the pull-out of the longitudinal reinforcement with a secondary concrete crushing.

BDHB250 beam exhibited a shear failure due to the fracture of the end heads of the shear reinforcement. The shear cracks caused the fracture of the end heads of the shear reinforcement along the crack followed by the pull-out of the longitudinal bars, although these bars were bent at supports increasing the embedded length. BDHB250GFRP1 also exhibited a shear failure due to the fracture of the end heads of the shear reinforcement. The shear cracks caused the fracture of the end heads of the shear reinforcement along the crack, followed by a total separation of the beam section at the longitudinal reinforcement level. The BDHB250GFRP2 beam failure was similar to the BB250GFRP2 failure, and due to the fracture of the end heads of the shear reinforcement bars along the shear crack. The failure of the BC250GFRP1 beam was a shear failure due to the disintegration of the C-stirrups followed by the pull-out of the longitudinal bars near the support.

The failure of BC250GFRP2 and BS250GFRP2 beams was a shear failure due to the crushing of the concrete rod between shear cracks. Stirrups also disintegrated at the bottom and on the top of the concrete crushed rod.

2.5.1.4 Deflection

2.5.1.5 Deflection at mid-span

The deflection values in service and ultimate conditions are listed in Table 33. In general, it is possible to state that there is no difference between the deflections of beam specimens for the service load (50 kN). However, with the load increasing on each group the GFRP1 beams exhibited the higher deflections (lower stiffness). Comparing the service predicted deflections (using ACI

440.1R-06 [2]) with the experimental deflections, the experimental deflections were on average 25% higher than predicted deflections. For the reference beams: the experimental deflection of REF250 was 10% lower than predictions, and the experimental displacement for REFB250 was 36% higher than predicted.

The ultimate mid-span deflections are also represented. In general, beams with closed stirrup solutions exhibited higher ultimate deflections, and also the highest ultimate loads.

Table 33 – Summary of mid-span deflections at service and ultimate loads

Beam	Mid-span deflection			
	Service			Ultimate
	Exp.	Pred.	Exp /Pred	Exp.
	(mm)	(mm)	(-)	(mm)
REF250	4.5	5.0	0.90	31.1
REFB250	6.8	5.0	1.36	27.2
BS250	6.2	5.4	1.15	88.0
BS250GFRP1	8.0	6.1	1.31	78.0
BS250GFRP2	6.4	5.5	1.16	70.9
BC250	6.1	5.4	1.13	75.7
BC250GFRP1	5.6	6.1	0.92	60.8
BC250GFRP2	6.5	5.5	1.18	69.6
BDHB250	5.2	5.4	0.96	38.0
BDHB250GFRP1	7.8	6.1	1.28	36.4
BDHB250GFRP2	5.6	5.5	1.01	41.3
BB250	6.1	5.4	1.13	55.0
BB250GFRP1	5.6	6.1	0.92	52.1
BB250GFRP2	6.8	5.5	1.24	32.0

The load-deflection curves at mid-span are shown in Figure 82, divided by the longitudinal reinforcement type in order to assess the behaviour of the different shear reinforcement types in

the same circumstances (same longitudinal reinforcement). The REF250 and REFB250 curves were also plotted over the other curves to immediately compare the behaviour. Each curve represented in Figure 82 is the deflection of the 100 mm LVDT mounted at mid-span. In general, for loads under the load of the cracking moment, all the specimens exhibited an initial elastic phase where the load-displacement relation was linear, followed by a cracked phase where the load-displacement relation was still linear but with lower slope. For all beams, the load-displacement curves developed with only two distinct phases which were approximately linear, with no yielding and no ductile behaviour, with the exception of the beams BS250 and BC250, which failed by mid-span concrete crushing (Figure 82 a)). These two beams' load-deflection curves had a third phase, where the deflection was still increasing for an almost constant load value, corresponding to a yielding phase, and thus exhibiting some ductility. Although the shear capacity varies, the load-deflections curves, until the failure, are approximately coincident for the beams with the same area of longitudinal reinforcement and same area and material of shear reinforcement (independently of the shear reinforcement solution). BS250, BC250, BDHB250 and BB250 exhibited similar behaviour, and on average a service deflection 1.3 times higher than REF250 deflection, after the cracking load (Figure 82 a)). Concerning GFRP1 beams (Figure 82 b)), the stiffness was the lowest and on average, after the cracking load, the deflection was 1.5 times higher than REF250. Concerning GFR2 beams (Figure 82 c)), on average, after the cracking load the deflection was 1.3 times the REF250 deflection. Comparing the REF250 with REFB250, it is possible to notice that since the beginning of the loading the deflection was higher than on REFB250, showing lower stiffness when compared with the other steel beam.

Each curve represented in Figure 82 d) is the average deflection of specimens with the same shear reinforcement in order to directly compare the flexural stiffness of each type of longitudinal reinforcement considered with the references, the REF250 and REFB250. The reference REF250 exhibited higher stiffness followed by the beams with steel longitudinal reinforcement (BS250, BC250, BDHB250 and BB250), followed by GFRP2 beams, and finally by GFRP1 beams.

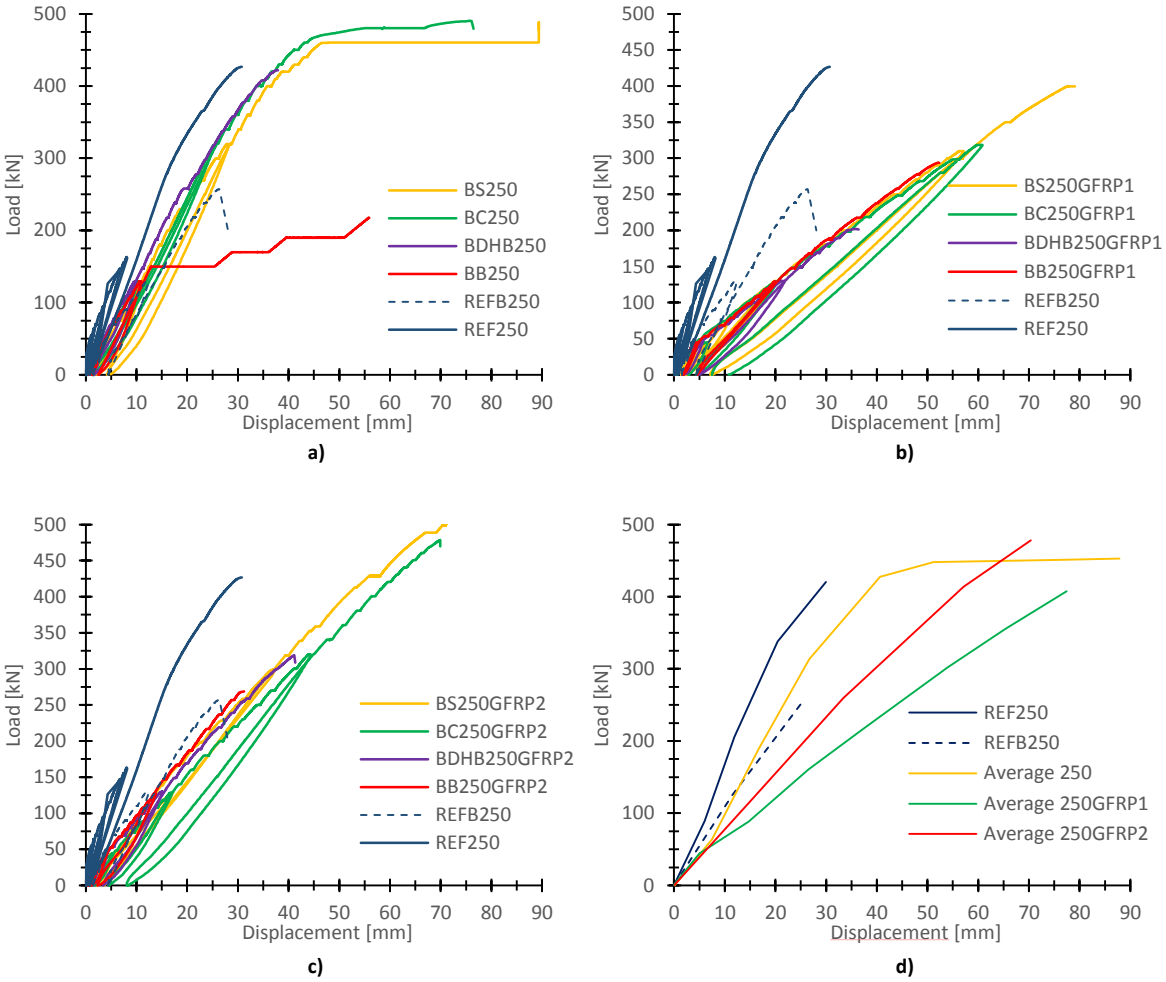

Figure 82 - Load-deflection curves: a) steel 2ϕ16+2ϕ25 reinforced beams; b) GFRP 2ϕ16+2ϕ25 reinforced beams; c) GFRP 5ϕ25 reinforced beams d) average of beams with same longitudinal reinforcement

2.5.1.6 Reinforcement strains

2.5.1.6.1 Longitudinal reinforcement strain

The maximum strains at longitudinal reinforcement at mid-span are presented in Figure 83, by shear reinforcement solution. All beam specimens that failed for shear had a bilinear load-strain relationship with no evidence of yielding of longitudinal reinforcement or concrete crushing. BS250 and BC250 failed due to mid-span concrete crushing (bending failure) and exhibited load-strain relationship with a three-stage development: an elastic first phase until cracking, a second phase non-linear until the yielding and the yielded phase.

Comparing GFRP1 beams with GFRP2 beams, it can be stated that fixing a load value, increasing the reinforcement area decreases the reinforcement strains. Comparing steel reinforced beams BS250, BC250, BB250 and BDHB250 with BS250GFRP1, BC250GFRP1, BB250GFRP1 and BDHB250GFRP1, for the same reinforcement area, GFRP beams had highest reinforcement strains.

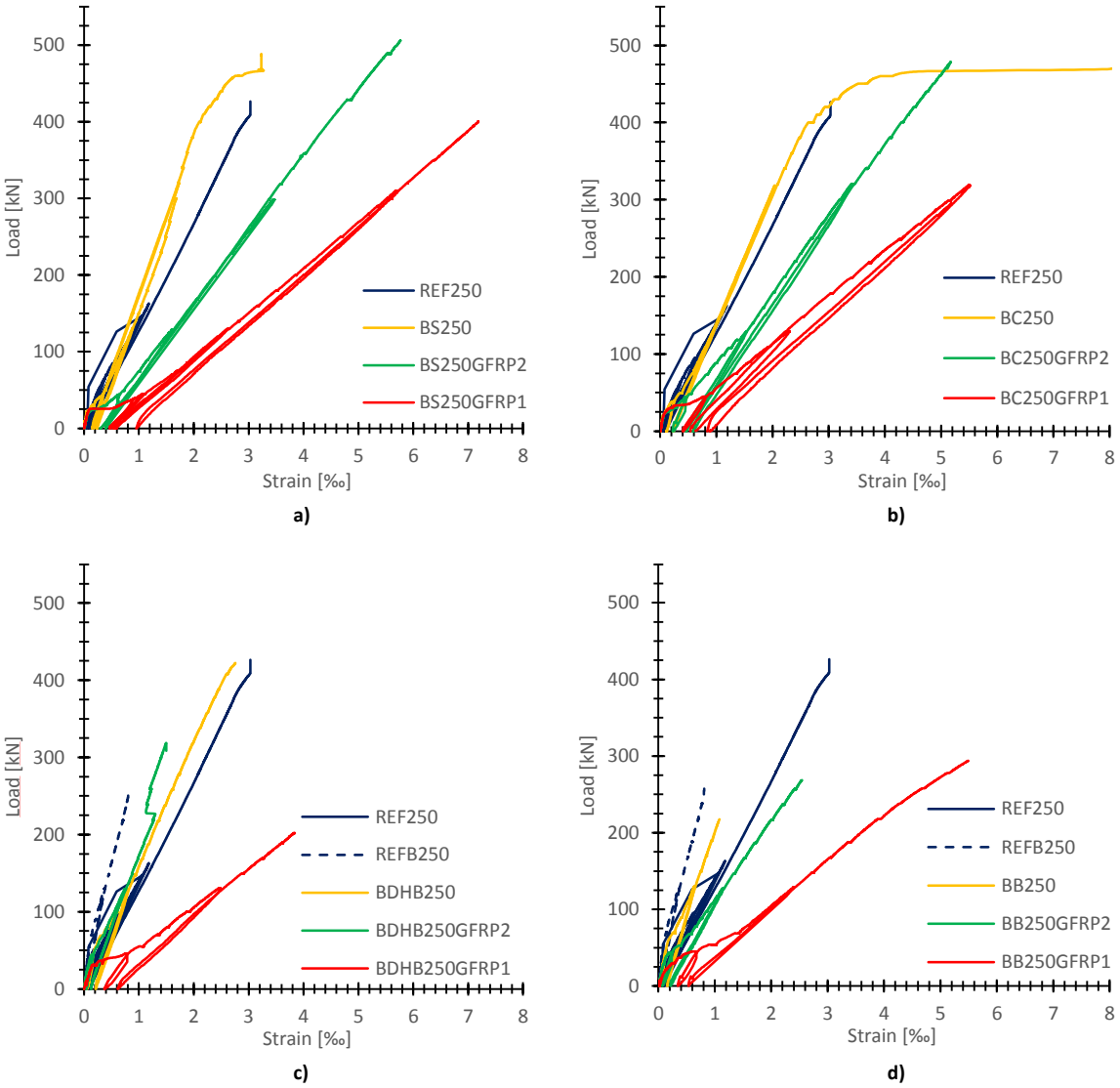

Figure 83 – Longitudinal reinforcement strains at mid-span: a) BS beams; b) BC beams; c) BDHB beams-, d) BB beams

The strain values, for the maximum load capacity, are presented in Table 34. The variation of the measured values to the predictions is lower than ± 10%.

Table 34 – Summary of ultimate strain values

Beam	ρ_{fL} or ρ_{sL}	ρ_{fv} or ρ_{sv}	Ultimate values					
			Mid-span strain			Shear reinforcement strain		
			Exp.	Pred.	Exp /Pred	Exp.	Pred.	Exp /Pred
	(%)	(%)	(‰)	(‰)	(-)	(‰)	(‰)	(-)
REF250	1.40	0.40	2.53	2.25	1.12	2.74	9.00	0.30
REFB250			1.04	1.30	0.80	2.14	4.00	0.54
BS250		0.90	2.08*	2.39	0.87	9.38	9.40	1.00
BS250GFRP1			6.80	7.15	0.95	6.56	9.40	0.70
BS250GFRP2	2.50		5.76	5.02	1.15	8.30	9.40	0.88
BC250	1.40		3.31*	2.50	1.34	6.25	9.15	0.68
BC250GFRP1			5.63	5.50	1.02	9.86+	9.15	1.02
BC250GFRP2	2.50		5.45	5.10	1.07	7.61	9.15	0.83
BDHB250	1.40		2.05	2.25	0.90	6.82	7.20	0.95
BDHB250GFRP1			3.77	3.54	1.06	3.62	7.20	0.50
BDHB250GFRP2	2.50		2.85	3.11	0.92	4.06	7.20	0.56
BB250	1.40		1.08	1.16	0.93	4.00	5.20	0.30
BB250GFRP1			5.24	5.09	1.03	5.21	5.20	1.00
BB250GFRP2	2.50		2.50	2.62	0.92	5.02	5.20	0.97

*- at yielding point

+ On the failure side the maximum strain was 2.85, as showed in Figure 85.

2.5.1.6.2 Shear reinforcement strain

The maximum shear reinforcement strains for the different beam specimens, as well as the predicted values, are presented in Table 34 and the evolution of the shear reinforcement strains near the support (on the side of the failure) during the test is plotted from Figure 84 to Figure 86. The differences in the evolutions of the shear strains with the loading from beam to beam highlight the influence of the crack opening on the stirrups stresses. In general, near the failure the third and the fourth stirrups were the most stressed.

Corresponding to an average of 4‰ strain in GFRP stirrups, which is the ACI 440.1R-06 [2] limit, the applied forces were 305 kN, 268 kN and 230 kN, respectively for BS250, BS250GFRP1 and

BS250GFRP2. These values represent, respectively, 62.5%, 67% and 46% of the observed failure loads. For BC250, BC250GFRP1 and BC250GFRP2 the applied forces were, 360 kN, 200 kN and 301 kN, respectively. These values represent approximately 62% of the ultimate capacity of the beam specimens. Similar results were stated by [29].

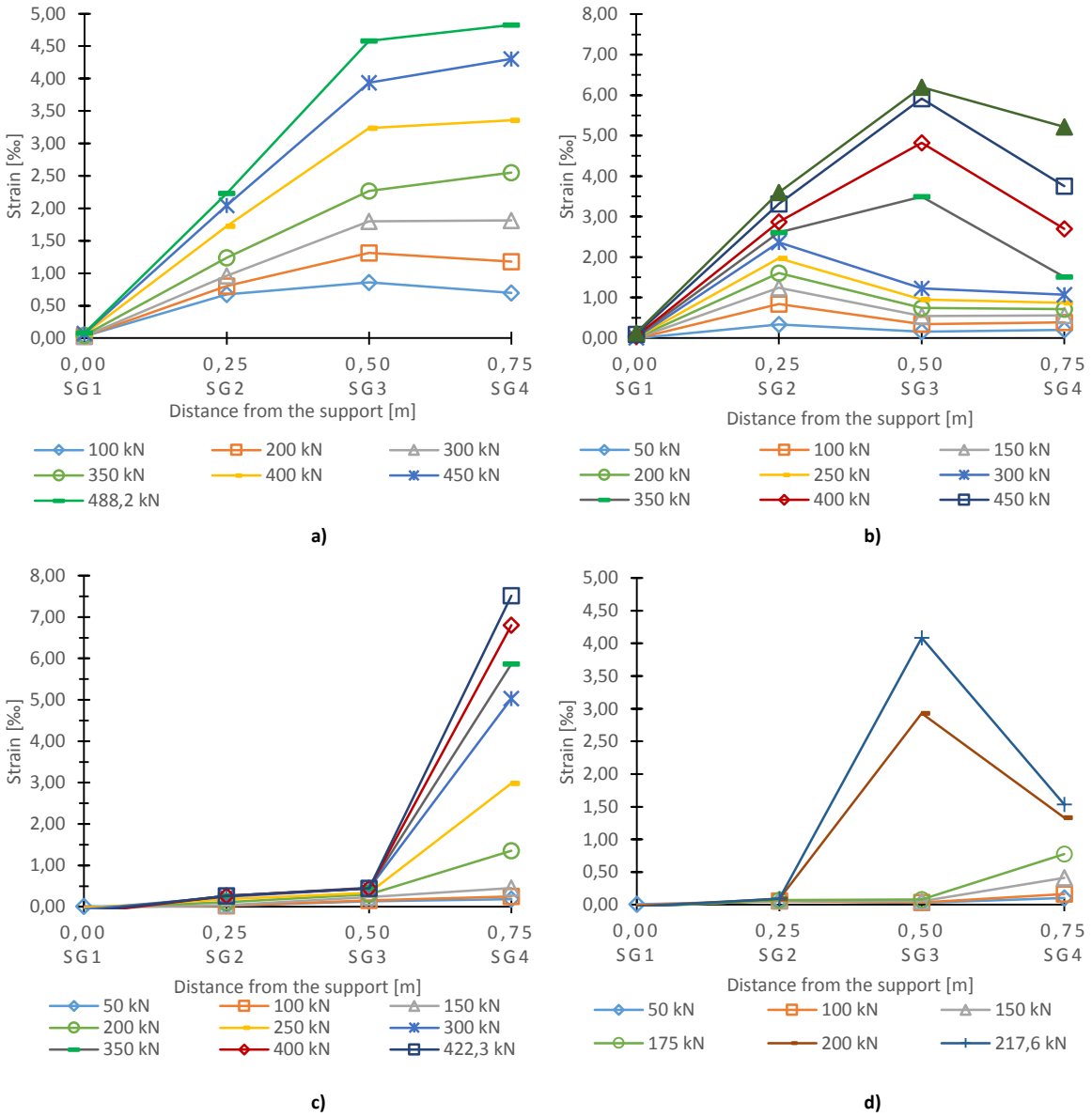

Figure 84 – Distribution of the shear reinforcement strain with the loading: a) BS250; b) BC250; c) BDHB250; d) BB250

It can be observed that the strains of shear reinforcement were higher for all the beams specimens than the ACI 440.1R-06 [2] limit of 4‰, with exception for BB250.

The maximum shear reinforcement strains for the different beam specimens, as well as the predicted values, are presented in Table 34. Figure 87 shows, for each beam, the development of the strain at the most stressed stirrup, as well as a rough prediction of the strains expressed by the

equation (90), as a function of the applied load, P, the reinforcement spacing, s, the area, A_{fv}, and the elasticity modulus, E_{fv}, of the shear reinforcement and the internal lever arm, z.

$$\varepsilon_{fv} = \frac{Ps}{2zE_{fv}A_{fv}} \tag{90}$$

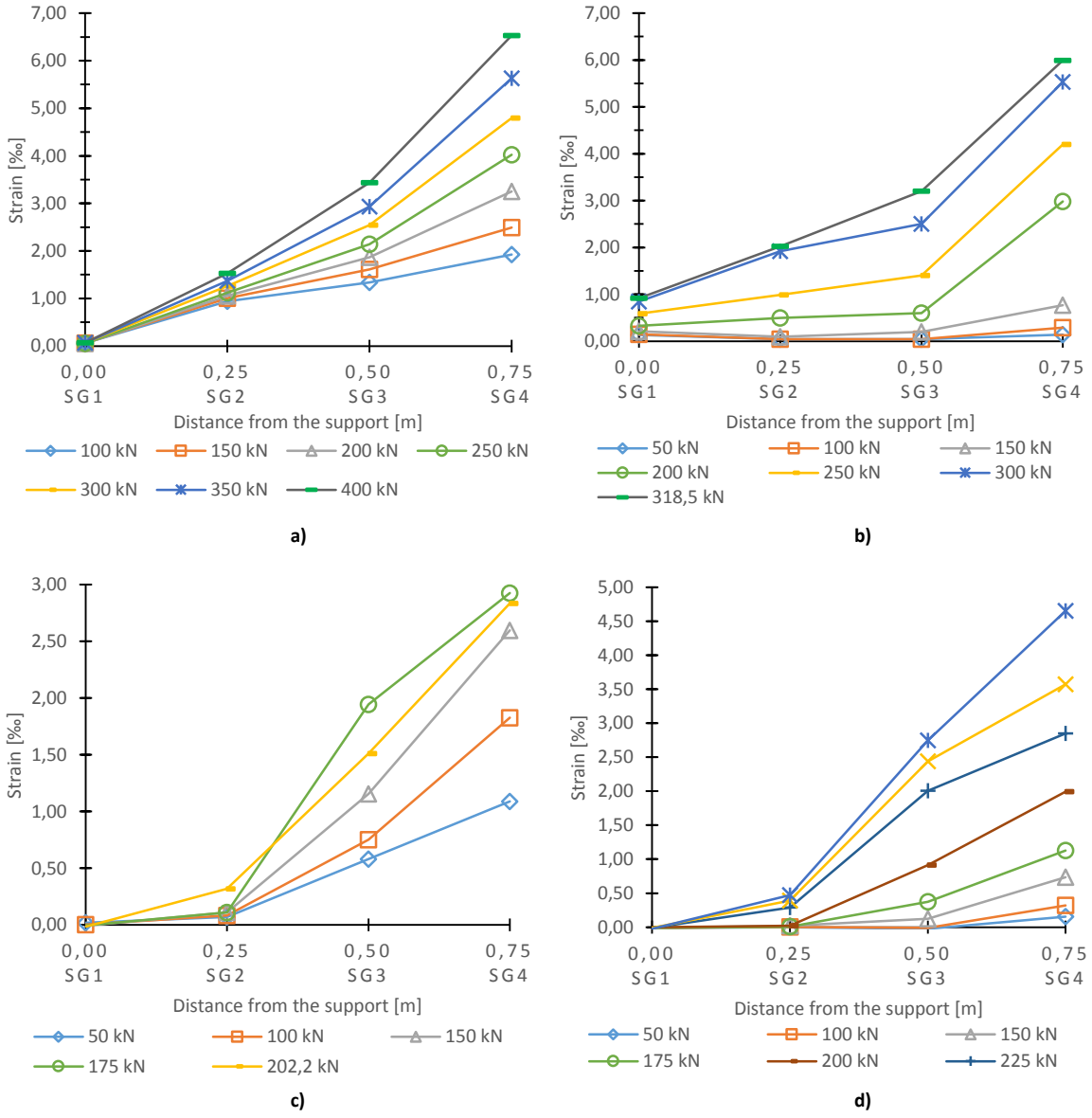

Figure 85 - Distribution of the shear reinforcement strain with the loading: a) BS250GFRP1; b) BC250GFRP1; c) BDHB250GFRP1; d) BB250GFRP1

Figure 88 shows the development of the strain at the most stressed stirrup for each beam. Near the failure the strain values were close to those roughly expected by equation (90). As expected, this behaviour is similar to the typical tension-stiffening effect in tensile RC elements. For all the beam specimens the development had a bilinear configuration. GFRP1 beams had, for the same load value, the higher stirrups strains, while beams with the steel longitudinal reinforcement

exhibited the lower shear reinforcement strains. Beams with the capacity to better mobilize the shear reinforcement were those with the closed stirrup or C-stirrup, and consequently had a higher shear load capacity.

The shear strains on the beam specimens with the closed stirrups (BS and BC) varied from 7‰ to 10‰, with exception of BC250 which exhibited a maximum strain of 6‰, but failed by compression of mid-span concrete, and thus it isn't representative. This shows that these solutions have a higher capacity to mobilizing the shear reinforcement, and for this reason have the highest shear capacity.

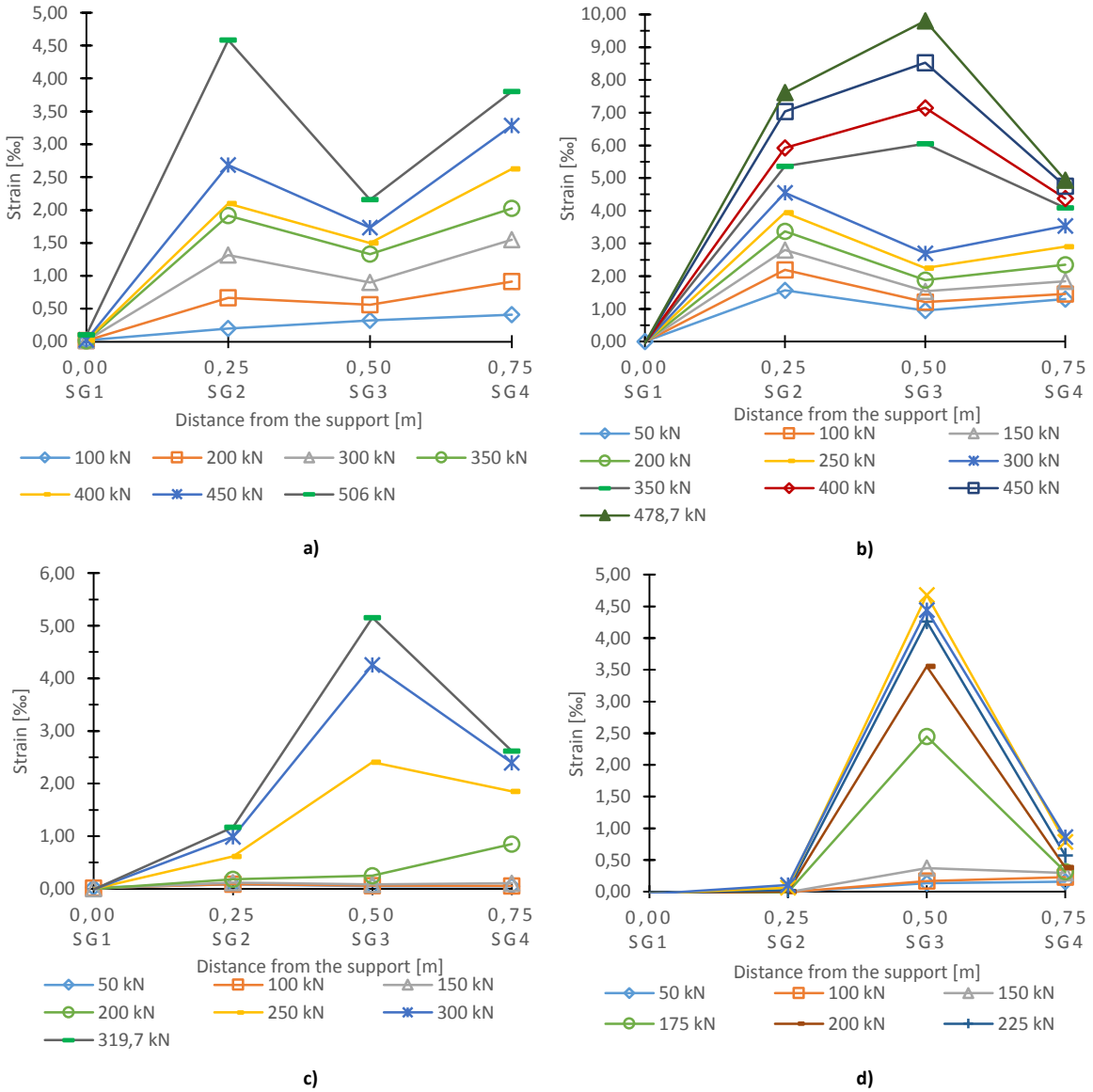

Figure 86 - Distribution of the shear reinforcement strain with the loading: a) BS250GFRP2; b) BC250GFRP2; c) BDHB250GFRP2; d) BB250GFRP2

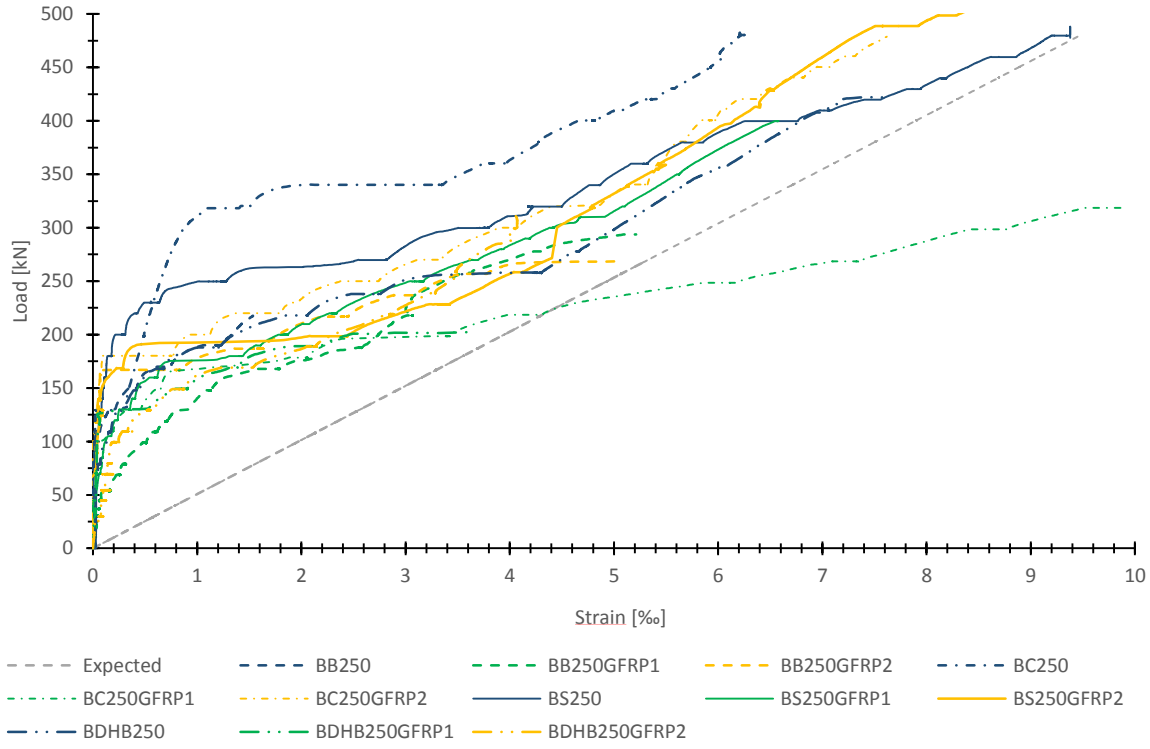

Figure 87 – Maximum shear reinforcement strains development

2.5.1.7 Shear crack width

Figure 88 shows the variation of the shear crack widths with the loading. It can be stated that the shear cracks appeared only for load levels above the service load and that there is a linear correlation (R^2 = 0.8) between the crack widths and the applied load.

The two reference beams, REF250 and REFB250, had the least strain at ultimate load. However, their shear crack width was not the smaller ones, suggesting different bond properties between the two materials. Similar conclusions were found by Ehab A. Ahmed and Brahim [29].

The larger crack widths developed on GFRP reinforced beams are responsible for the lower shear strength, although the characteristics of the shear failure are similar to those of the steel RC beams.

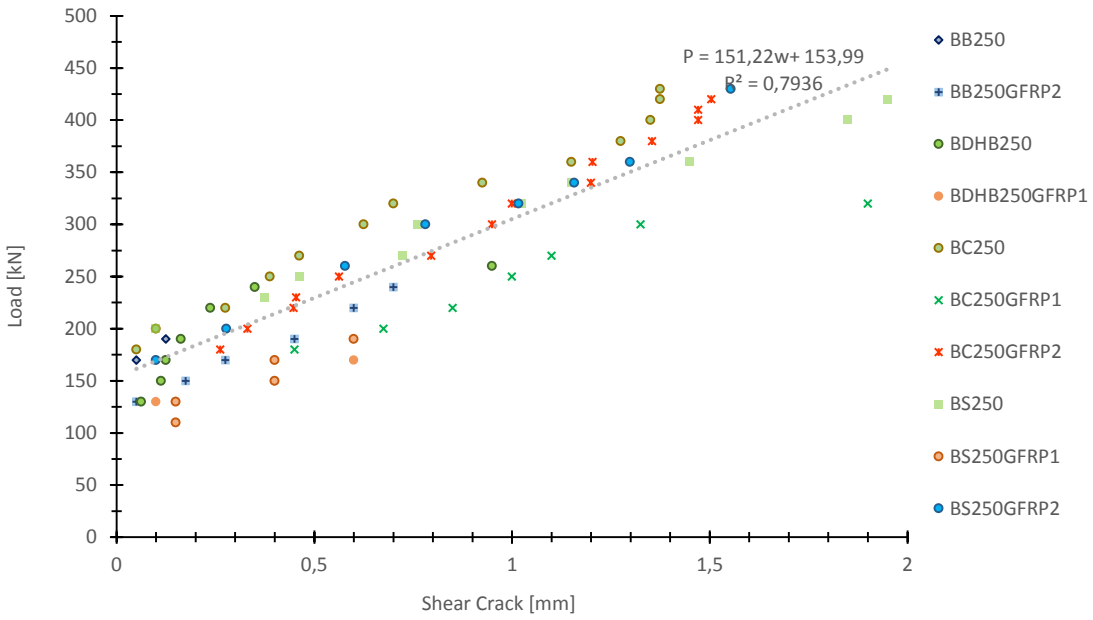

Figure 88 – Variation of the shear crack widths with load

2.5.2 Conclusions

This study proposed and evaluated the performance of four GFRP shear reinforcement solutions by testing and comparing full-scale intermediate length GFRP RC beams with steel RC beams and with design provisions and several model predictions. The results show that the overall behaviour of GFRP shear reinforced beams is similar to steel reinforced beams on cracking pattern and failure mechanisms. More specific findings are:

1- Although all the beam specimens had the same shear reinforcement amount, the four solutions had distinct performances. GFRP bent bars (BS and BC beams) had the highest shear capacity, followed by the double headed bar beams. These results are in agreement with those found on the reference beams: REF250 exhibited a shear capacity two times higher than REFB250, highlighting the importance of the anchorage length provided by the two horizontal branches on the stirrups, which enhances the capacity of the beam to mobilize the shear reinforcement.

2- The longitudinal stiffness (area and material) influenced the shear capacity. The higher the longitudinal stiffness the higher the shear capacity. This can be explained by the fact that increasing the longitudinal stiffness, the deformability of the beam and the crack widths becomes lower, allowing the shear mechanisms to act for longer.

3- BS and BC beams have a similar overall behaviour and close values of shear strength. However, it was verified that C-stirrups have a tendency to the deformation of the overlapped bottom branches causing an earlier failure and also more damages. Despite this, the C-stirrups can be a more flexible solution to use in the field.

4- The double headed bars were an effective solution in the case of the beams longitudinally reinforced with steel and in the case of the GFRP2 beams. The shear failure loads were not as high as the closed stirrups, however the overall behaviour was efficient but affected by the longitudinal stiffness of the beams and by the cracking development, having a disappoint performance in the cases with lower longitudinal stiffness. Although this solution is the easiest to use in the field and it had overcome the different codes predictions, it should only be applied in cases where the integrity of the shear mechanisms is assured (by the high longitudinal stiffness).

5- The solution of using two straight vertical bars as shear reinforcement was proved to be inefficient for having a shear strength lower than predictions. Considering the service load levels, BB beams' behaviour was similar to the other beams. However, by comparing the ultimate loads with the predictions (without safety factors) the shear capacity was overestimated, and thus this solution is inefficient and should not be applied.

6- Both ACI 440.1R-060 [2] and FIB 40 [22] led to conservative non-design predictions, with exception of BB250 and BDHB250GFRP1. The underestimation was particularly high in the GFRP bent bars solutions. In the case of ACI 440.1R-06[2], conservative but better predictions were achieved by increasing the strains in the shear reinforcement to 7‰ for all the longitudinal stiffness considered cases. For the solution with the double headed bars, it was possible to maintain conservative predictions with a limit strain of 6‰, with exception of BDHB250GFRP1. In the case of FIB 40 [22], better predictions were achieved considering an increase of the limit strain to 6‰ and an angle of 38 degrees. These limits were all supported by the experimental values from the beam tests.

7- Applying ACI 440.1R-06[2] to determine the design shear capacity overly underestimated the shear capacity of the beams with bent bars as shear reinforcement, and it was found that for the limit strain considered, beams are about 60-70% of their shear capacity.

8- It was found that CSA S6-09 [65] and CSA S806-02 [13] codes, Oller *et al.* [75] and Fico *et al.* [35] equations provided the best predictions. These conclusions are in agreement with those found by Machial, Alam*, et al.* [65]. However, given the limited number of beam specimens tested, more experimental testing is recommended, varying the stirrups spacing, shear span-to-depth, FRP closed stirrups solutions and concrete strength.

9- The tests highlighted a linear relationship, with a correlation factor r^2 = 0.8 between the shear crack width and the load, which was found to be nearly independent from the shear reinforcement type and from the longitudinal reinforcement.

10- Although applying ACI 440.1R-06[2] to predict the short-term deflections at service load overestimates this value for some of the beams and underestimates to others, the experimental values are close to the predictions.

11- Another interesting finding was the fact that the beams longitudinally reinforced with steel but shear reinforced with GFRP solutions exhibited the best performance. The main reason is the fact that for being longitudinally steel reinforced, the cracks were smaller and the deflection was lower. This contributed for the fact that the integrity of the shear mechanisms was kept for longer, and thus the shear strength was higher. The pertinence of this finding is that these solutions are simultaneously more economical and adequate for the use where the corrosion is the main concern, because the shear reinforcement, as being located outer comparing to the longitudinal reinforcement, is the first to be corroded. Similar findings were mentioned by Johnson and Sheikh [55].

12- To all beams, the angle of the shear failure was in good agreement with the 45 degrees truss model. And generally, the beams failed by the shear crack closest to the support, and the failure plane varied from 37 to 47 degrees. It was found that the beams with higher longitudinal stiffness failed in a less inclined plane.

13- The shear reinforcement strains were influenced by the development of the cracks with the loading, but, in general, the stirrups closer to the loading point were the most stressed at the failure.

It is important to test more specimens longitudinally reinforced with steel but shear reinforced with GFRP stirrups, as this solution seems to have a good performance in terms of ultimate capacity and deformability without being costly.

2.6 Effect of the longitudinal stiffness on the performance of reinforced concrete beams with GFRP stirrups spaced between d/2 and d

This paper reports experimental data on the shear strength of concrete beams reinforced with GFRP closed stirrups spaced between d/2 and d (where d is the depth of the beam). Four large scale beams of rectangular cross section and a total length of 4.30 m were constructed and tested up to failure in 4-point bending over a simply supported clear span of 4.0 m. The test beams include 3 reinforced with GFRP stirrups of 12 mm diameter spaced at 0.250 m and a reference beam reinforced with conventional steel stirrups of 8 mm diameter spaced at 0.250 m. Beams were design to fail due to shear, and both ACI 440.1R-06 [2] and FIB 40 [22] were used to predict the shear strength. It is intended to discuss the viability of a GFRP stirrups spacing higher than the d/2 limit imposed by ACI 440.1R-06 [2] and the effect of the longitudinal stiffness on the performance of the RC beam.

Because these beams are part of an extensive research work of the same authors their designation can be explained as follows: the letter S indicates the GFRP closed stirrups, the number 250 represents the spacing of the stirrups and GFRP1 or GFRP2 indicates two different ratio of GRP longitudinal reinforcement.

Results showed that a higher stirrup spacing limit can be considered and that both predicted ACI 440.1R-06 [2] and FIB 40 [22]shear capacities were highly conservative.

2.6.1 Results and discussion

The beams were tested in four-point bending over a simply supported clear span of 4.0 m and the point loads were located at a distance of 1.0 m from the supports, corresponding to a shear-span ratio (a/d) of 2.67. The load was applied through a 1500 kN capacity actuator. During the test, the loads, the displacements at mid-span and over the loading points, the strains of the longitudinal reinforcement at mid-span, and in four stirrups were measured and recorded using a data acquisition system. More details on the test specimens can be found in section 2.1.

The summary of the test results in terms of shear strength and failure mode, deflection, maximum strains, and angle of the major shear crack are indicated in Table 35. A more detailed analysis of these results is performed in the flowing sections.

Table 35 – Summary of test results

Beam	Failure		Angle of major crack	Maximum Mid-span deflection	Maximum longitudinal reinforcement strain	Maximum stirrup reinforcement strain
	Mode	Load				
		(kN)	(degrees)	(mm)	(‰)	(‰)
REF250	Shear	426.4	43	31.1	2.53	2.74
BS250	Bending	488.2	40	88.0	2.08	9.38
BS250GFRP1	Shear	400.0	39	78.0	6.08	6.56
BS250GFRP2	Shear	506.0	38	70.9	5.76	8.30

2.6.1.1 Capacity and mode of failure

Although the shear crack mechanism were similar among all the beams, the failure mode was different from specimen to specimen. Figure 89 schematically shows the cracking patterns at failure with the shear plane inclination. The test specimens failed at a corresponding applied force of 426.4 kN, 488.2 kN, 400.0 kN, 506.0 kN, respectively for REF250, BS250, BS250GFRP1, BS250GFRP2. The reference REF250 failure was governed by the stirrups strength, and this beam failed due to the shear reinforcement rupture (Figure 90 a)). BS250 reached its flexural capacity prior to the shear capacity. This beam failed unexpectedly by concrete crushing at mid-span location (Figure 90 b)). BS250GFRP2 failed by shear but due to the crushing of the concrete rod (Figure 91 c)) and BS250GFRP1 failed due to shear but due to the failure of the bond of the longitudinal reinforcement at support (Figure 91 a) and b)). The failure of the REF250 was the closest to the support and with the higher angle. Comparing the two beams with GFRP longitudinal reinforcement the inclination of the failure plane was lower in the beam with the higher stiffness. It can also be noticed that the higher the shear failure load, the higher is the number of shear cracks.

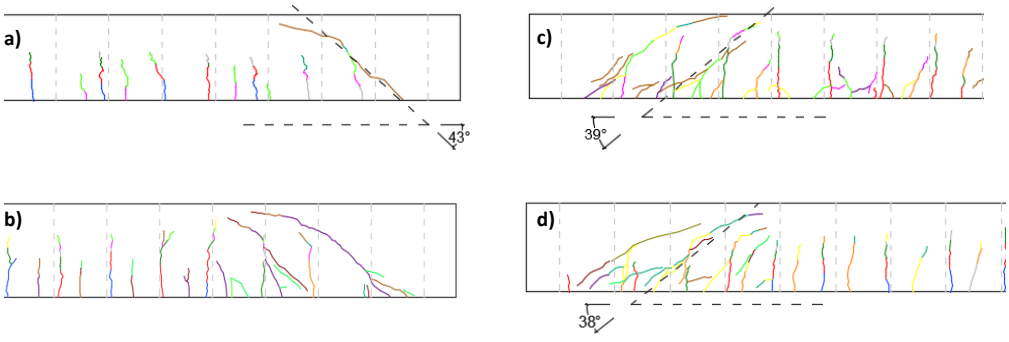

Figure 89 – Cracking pattern at failure for test specimens: a) REF250; b) BS250; c) BS250GFRP1; d) BS250GFRP2

a) b)

Figure 90 –Failure of test specimens: a) REF250; b) BS250

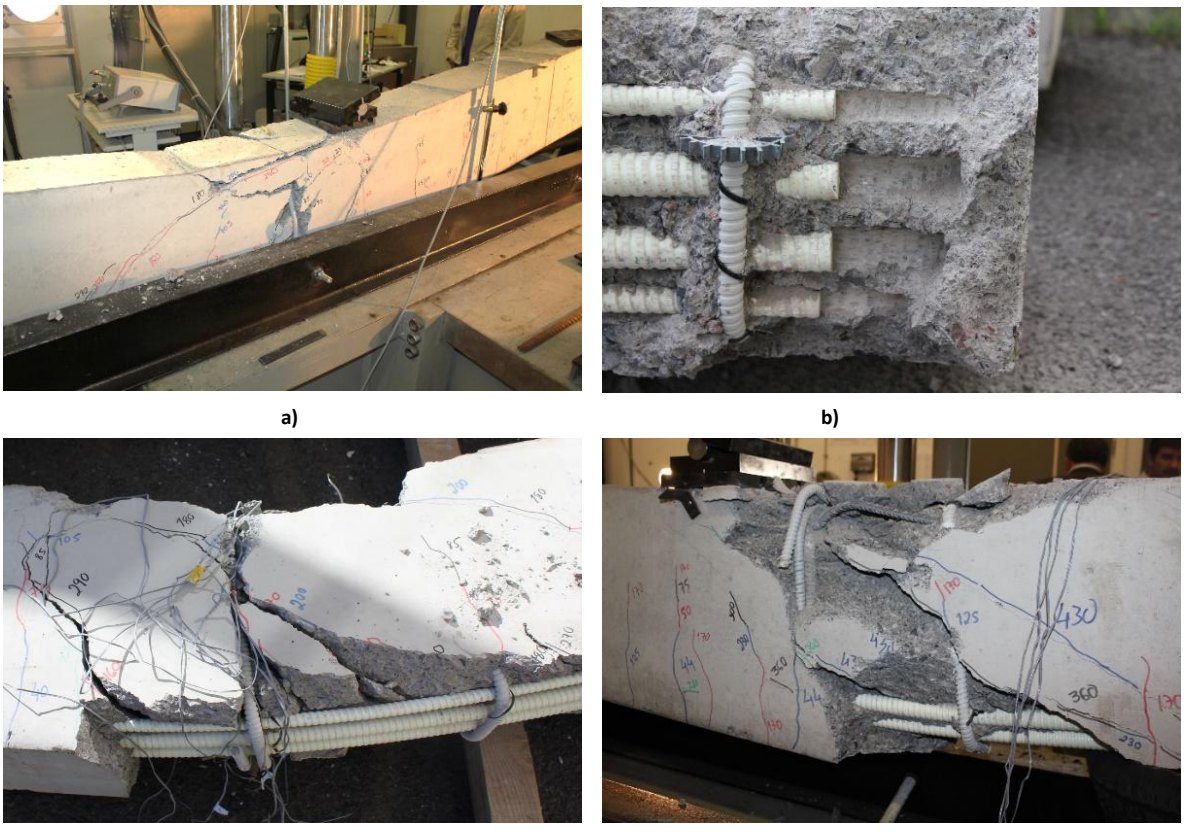

a) b)

c) d)

Figure 91 - Failure of test specimens: a) BS250GFRP1; b) slip of the longitudinal reinforcement in BS250GFRP1; c) stirrups after failure in BS250GFRP1; d) BS250GFRP2

2.6.1.2 Deflection

The applied force –deflection at mid-span is showed in Figure 92. Beams exhibited similar bilinear behaviour with exception of BS250, which exhibited relationship with a three-stage development with a yielded phase. The reference REF250 exhibit higher stiffness followed by the beam with steel longitudinal reinforcement (BS250), followed by GFRP2 beams and finally by GFRP1 beam, which had the highest deflections values.

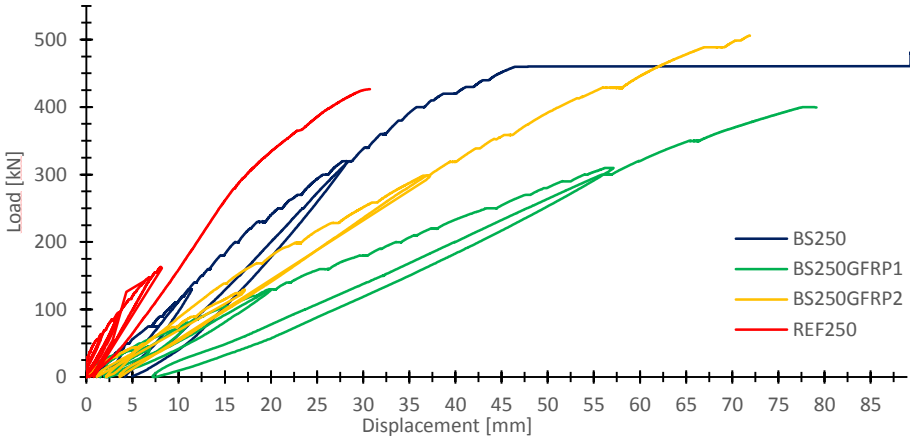

Figure 92 - Force-deflection relationship for the tested beams

2.6.1.3 Flexural strains

The development of the strains of longitudinal reinforcement at mid-span location was similar to the development of the load-deflection, reaching the maximum values listed in Table 35.

2.6.1.4 Strain in stirrups

The maximum strain values in the stirrups are listed in Table 35. The strain varied from stirrup to stirrup and the stirrups closest to the supports had very small strain values in comparison to the remaining stirrups. The maximum strain was measured at stirrups closest to the loading point of the BS250GFRP1 beam. It was found that the strain distribution along the stirrups varied with the longitudinal reinforcement, as supported by Figure 93. All the beams showed similar behaviour at early loading stages. With the load increase, the third and fourth stirrups were the most stressed,

with exception for the BS250GFRP2. This beam has the highest shear strength and the strains were distributed more similarly through the second, third and fourth stirrups, while in the other beams only the third and the fourth stirrups exhibited high strains.

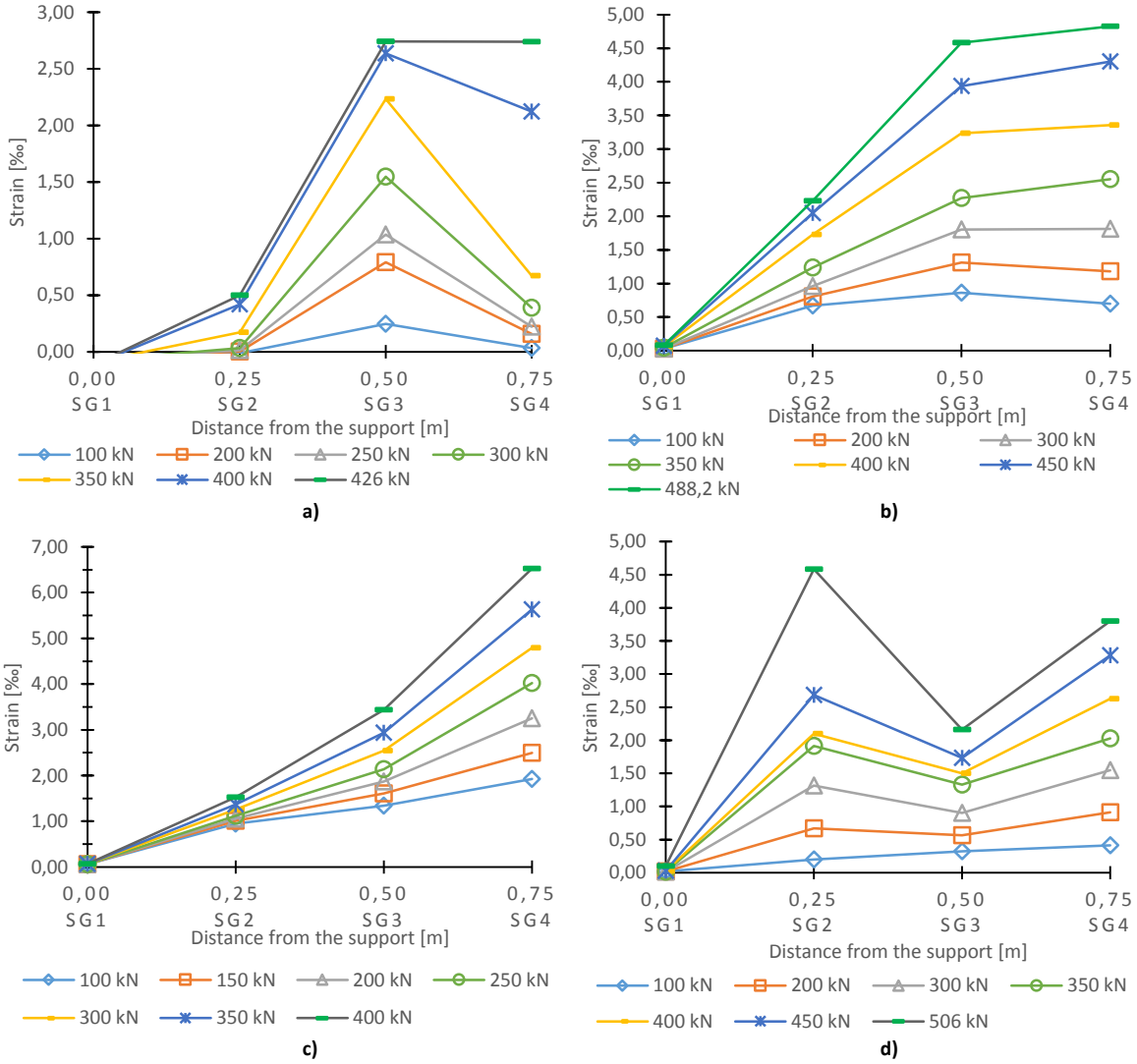

Figure 93 – Development of stirrups strains along the shear span: a) REF250; b) BS250; BS250GFRP1; d) BS250GFRP2

2.6.2 Comparison of experimental results and predicted capacity

2.6.2.1 Shear capacity

The non-design values of the shear capacity of test beams were predicted with the design provisions presented in Table 36 and the results are listed in Table 37. The values calculated considering the characteristic properties of the materials without safety factors were assigned as non-design

values. As showed by the ratio between the experimental and the predicted values, both codes underestimated the shear capacity. The average ratio was 1.66 and 1.59 for ACI 440.1R-06 [2] and FIB 40[22], respectively. The underestimation levels are nearly 50%, for both. Corresponding to an average of 4‰ strain in GFRP stirrups, which is the ACI 440.1R-06 [2] limit, the applied forces were 305kN, 268kN and 230kN, respectively for BS250, BS250GFRP1 and BS250GFRP2. These values represent, respectively, 62.5%, 67% and 46% of the observed failure loads. Similar results were stated by [29].

Table 36 – Shear design equations according to ACI 440.1R-06 [2] and FIB 40 [22]

Model	Concrete shear equations		Reinforcement shear equations	
ACI 440.1R-06 [2]	$V_c = \frac{2}{5} k \sqrt{f_c'} bd$	(91)	$V_{fv} = \frac{A_{fv} \sigma_{fv} d}{s}$	(92)
	$k = \sqrt{2\rho_{fl} n_f + (\rho_{fl} n_f)^2} - \rho_{fl} n_f$	(93)	$\sigma_{fv} = 0.004 E_{fv} \leq f_{fb}$	(94)
	$n_f = \frac{E_{fl}}{E_c}$	(95)	$f_{fb} = \frac{\left(\frac{0.05 r_b}{d_b} + 0.3\right)}{1.5} f_{fv} \leq f_{fv}$	(96)
FIB 40 [22]	$V_c = 0.12 \left(1 + \sqrt{\frac{200}{d}}\right) \left(100 \rho_{fl} \frac{E_{fl}}{E_s} \phi_\varepsilon f'_c\right)^{1/3} bd$	(97)	$V_f = \frac{A_{fl}}{s} f_{fl} z \cot\theta$	(98)
	$\varepsilon_f = 0.0045$	(99)		
	$\phi_\varepsilon = \varepsilon_f / \varepsilon_y$	(100)		

Table 37 – Summary of experimental and predicted ultimate shear and bending capacity with ACI 440.1R-06 [2] / ACI 318-11 [3] and EC2 [23]/FIB 40 [22]

Beam	Type	Experimental	Non-design Capacity			
			ACI 440.1R-06[2] / ACI 318-11[3]		EC2[23]/FIB 40[22]	
		Load	Shear	Experimental / predicted	Shear	Experimental / predicted
		(kN)	ε_{fv} =4 ‰ (kN)	(-)	Θ=45 ε_{fv} =4.5 ‰ (kN)	(-)
REF250	Shear	426.4	393.9	1.08	326.6	1.31
BS250	Bending	488.2*	335.2	1.46	303.0	1.61
BS250GFRP1	Shear	400.0	245.8	1.63	275.6	1.45
BS250GFRP2	Shear	506.0	268.5	1.88.	297.1	1.71

* - Bending failure

Note: The values of shear capacity of the steel RC beams include the concrete contribution, because although EC2[23] indicates that the shear capacity is given only by the stirrups contribution, more recent studies and codes[20] mentioned that better estimation can be achieved by adding the concrete contribution.

2.6.2.2 Maximum spacing of stirrups

According to ACI 440.1R-06 [2], the maximum allowable spacing for the stirrups is 0.5d and according to FIB 40 [22], it is 0.45d in order to ensure that at least one stirrup is crossed by the shear cracks. In the test beams, the stirrups were spaced at 0.67d and there was always at least one stirrup crossed by the shear cracks and the angle of failure was always smaller than 45 degrees (Figure 91 c) and d)). Results showed that less conservative limits can considered, as suggested for traditional RC concrete in EC2 [23], 0.75d.

2.6.3 Conclusions

The experimental results concerning the shear behaviour of full-scale beams reinforced with GFRP stirrups spaced at 0.67d were reported. The main considered variable was the longitudinal reinforcement: a steel reinforcement, and two different ratios of GFRP longitudinal reinforcement. The shear behaviour of the test beams was also compared with the predictions of ACI 440.1R-06 [2] and FIB 40 [22].

The main findings can be summarized as follows:

1- The inclination of the major shear cracks was smaller in the reinforced concrete beams with higher stiffness and longitudinal GFRP reinforcement. In general the inclination angle of the failure plane is in good agreement with the traditional 45-degrees truss model.
2- Both ACI 440.1R-06 [2] and FIB 40 [22] underestimated the shear capacity by more than 40%.
3- The stirrups spacing limit of 0.5d and 0.45d introduced by ACI 440.1R-06 [2] and FIB 40 [22] were proved to be conservative and it was proved that a higher spacing can be considered.

2.7 Influence of the shear reinforcement ratio and the longitudinal stiffness on the behaviour of reinforced concrete beams with GFRP stirrups

This paper reports the results of an experimental campaign of 8 full-scale intermediate length RC beams conducted to test and evaluate the behaviour of bent GFRP bars forming a closed hoop stirrup used as shear reinforcement and the influence of the shear reinforcement ratio.

To accomplish these objectives two different ratios of GFRP shear reinforcement were considered, with stirrups spaced at 0.175 m and 0.250 m and three different longitudinal reinforcements. The beams were divided into four groups according to their longitudinal reinforcement:

1) The reference beams: REF250 and REF175, with stirrups spaced at 0.250 m and 0.175 m, respectively;
2) The BS250 and BS175 beams, with GFRP closed hoop stirrups spaced at 0.250 m and 0.175 m, respectively. These beams were longitudinally reinforced with steel;
3) The BS250GFRP1 and BS175GFRP1 beams, with GFRP closed hoop stirrups spaced at 0.250 m and 0.175 m, respectively. These beams were longitudinally reinforced with GFRP bars, keeping the same area of the reinforcement and approximately the same ultimate capacity of the reference beams;
4) The BS250GFRP2 and BS175GFRP2 beams, with GFRP closed hoop stirrups spaced at 0.250 m and 0.175 m, respectively. These beams were longitudinally reinforced with GFRP bars, maintaining the same deflection of the reference beams.

The beams were designed to fail due to shear and tested in four bending points until failure. The results are reported in terms of load-deflection response, ultimate load carrying, shear and flexural reinforcement strains, crack pattern and shear crack widths.

The tests showed that the solutions are effective and that the application of the general FRP design guidelines, in these cases, is overly conservative. It was also concluded that the best solution tested was the combination of GFRP bent stirrups with steel longitudinal reinforcement, as it had the best structural behaviour (having the lower deflection and the higher shear strength), is the most economical and is also corrosion resistant.

2.7.1 Results and discussion

2.7.1.1 Ultimate capacity

All the beam specimens were designed to fail due to shear. The shear capacity of all GFRP shear reinforced beams was calculated considering the expressions and models from Table 38 to Table 40. When designing the beam specimens, only ACI 440.1R-06 [2] and FIB 40 [22] formulations were used to calculate the shear strength of GFRP beams with safety factors. These values were designated design predictions. To better determine the shear strength, a second iteration was done where the ultimate strength values of the material properties was considered and no safety factors were applied, and other formulas and models were also analysed. These values were designated non-design values.

For the steel reinforced beams case (REF250 and REF175), the shear capacity was calculated according to the EC2 [23] and ACI 318-11 [3].

Table 38 – Shear design equations according to ACI 440.1R-06 [2], JSCE design guidelines[35] and FIB 40 [22]

Model	Concrete shear equations		Reinforcement shear equations	
ACI 440.1R-06 [2]	$V_c = \frac{2}{5} k \sqrt{f_c'} b d$	(101)	$V_{fv} = \frac{A_{fv} \sigma_{fv} d}{s}$	(102)
	$k = \sqrt{2\rho_{fl} n_f + (\rho_{fl} n_f)^2} - \rho_{fl} n_f$	(103)	$\sigma_{fv} = 0.004 E_{fv} \leq f_{fb}$	(104)
	$n_f = \frac{E_{fl}}{E_c}$	(105)	$f_{fb} = \frac{\left(\frac{0.05 r_b}{d_b} + 0.3\right)}{1.5} f_{fv} \leq f_{fv}$	(106)
FIB 40 [22]	$V_c = 0.12 \left(1 + \sqrt{\frac{200}{d}}\right) \left(100 \rho_{fl} \frac{E_{fl}}{E_s} \phi_\varepsilon f'_c\right)^{1/3} b d$	(107)	$V_f = \frac{A_{fl}}{s} f_{fl} z \cot\theta$	(108)
	$\varepsilon_f = 0.0045$	(109)		
	$\phi_\varepsilon = \varepsilon_f / \varepsilon_y$	(110)		

Table 39 – Shear design equations according to CSA S806-02[13] and CSA S6-09 Addendum[65]

Model	Concrete shear equations		Reinforcement shear equations	
CSA S806-02 [13]	$V_c = 0.035\lambda\varphi_c \left(f_c'\rho_{fl}E_{fl}\frac{V}{M}d\right)^{\frac{1}{3}} bd$	(111)	$V_{fv} = \frac{0.4\varphi_f A_{fv} f_{fv} d}{s} < 0.6\varphi_c\sqrt{f_c'}bd$	(112)
	$\lambda = 1$	(113)		
			$\varphi_f = 0.75$	(114)
	$\varphi_c = 0.6$	(115)		
CSA S6-09 Addendum[65]	$V_c = 2.5\beta\varphi_c(0.4\sqrt{f_c'})bd_v$	(116)	$V_{fv} = \frac{\varphi_f A_{fv}\sigma_{fv} d_v cot\theta}{s}$	(117)
	$d_v \geq \begin{cases} 0.9d \\ 0.72h \end{cases}$	(118)	$\varphi_f = \begin{cases} 0.50\ for\ GFRP \\ 0.75\ for\ CFRP \end{cases}$	(119)
	$\beta = \frac{1300\frac{0.4}{1+1500\varepsilon_x}}{1000+s_{ze}}$	(120)	$\sigma_{fv} = \frac{\left(\frac{0.05r_b}{d_b}+0.3\right)}{1.5} f_{fv} \leq 0.004E_{fv}$	(121)
	$\varepsilon_x = \frac{\frac{M_f}{d}+V_f+0.5N_f}{2E_sA_s} \leq 0.003$	(122)		
			$\theta = (29+7000\varepsilon_x)\left(0.88+\frac{s_{ze}}{2500}\right)$	(123)
	$s_{ze} = 300mm$	(124)		
	$f_{fv,d} = 130MPa$	(125)	$E\rho_{res} = \sqrt{(\rho_{fl}E_{fl})^2 + (\rho_{fv}E_{fv})^2}$	(126)

The experimental results of the ultimate capacity of all beams and the corresponding failure modes are presented in Table 41. It is also indicated the theoretical values of the expected load capacity according to ACI 440.1R-06 [2] / ACI 318-11 [3] and EC2 [23]/FIB 40 [22], and estimated as the sum of the concrete and reinforcement contributions ($V = V_c + V_{fv}$) and with the equations summarized in the Table 38.

Table 40 - Shear design equations according to CNR DT-203[27], Fico et al. [35], Nehdi et al. [65], Oller et al.[75] and Schöck [84]

Model	Concrete shear equations		Reinforcement shear equations	
JSCE design guidelines [35]	$V_c = \frac{\beta_d \beta_p \beta_n f_{vcd} bd}{\gamma_b}$	(127)	$V_{fv} = \frac{\frac{A_{fv} E_{fv} \varepsilon_{fv}}{s}}{\gamma_b} \frac{d}{1.15}$	(128)
	$\beta_d = \left(\frac{1000}{d}\right)^{\frac{1}{4}} \leq 1.5$	(129)	$\varepsilon_{fv} = \sqrt{\left(\frac{h}{0.3}\right)^{\frac{-1}{10}} f_c' \frac{\rho_{fl} E_{fl}}{\rho_{fv} E_{fv}}}$	(130)
	$\beta_p = \left(100 \frac{\rho_{fl} E_{fl}}{E_s}\right)^{\frac{1}{3}} \leq 1.5$	(131)		
	$\beta_n = 1$, if there is no axial forces	(132)		
	$f_{vcd} = 0.2(f_c')^{\frac{1}{3}} \leq 0.72MPa$	(133)		
	$\gamma_b = 1.3$	(134)		
CNR DT-203 [27]	$V_c = 1.3 \sqrt{\frac{E_{fl}}{E_s}} 0.25(0.05 f_c') k_d (1.2 + 40\rho_{fl}) bd$	(135)	$V_{fv} = \frac{A_{fv}}{s} \frac{f_{fv}}{\gamma_{f,\varphi} \gamma_f} d$	(136)
	$k_d = 1.0$	(137)	$\gamma_{f,\varphi} = 2.0$	(138)
			$\gamma_f = 1.5$	(139)
Fico *et al.* [35]	The same as CNR DT-203[27]	(140)	$V_{fv} = \frac{A_{fv}}{s} f_{fv,b} d$	(141)
			$f_{fv,b} = E_{fv} \varepsilon_{frp,lim}$	(142)
			$\varepsilon_{frp,lim} = 0.0085 \; for \; GFRP$	(143)
Nehdi *et al.* [65]	$V_c = 2.1 \left(\frac{f_c' \rho_{fl} d}{a} \frac{E_{fl}}{E_s}\right)^{0.23} bd$, if $\left(\frac{a}{d}\right) \geq 2.5$	(144)	$V_{fv} = 0.74 \left(\frac{A_{fv}}{bs}\right)^{0.5} f_{fv} bd$	(145)
Oller *et al.* [75]	$V = (V_c + V_w + V_t) = (\upsilon_c + \upsilon_w + \upsilon_t) f_{ct} bd$	(146)	$\upsilon_c = \zeta(1.072 - 0.01\alpha)[(0.98 + 0.22\upsilon_t)\xi + 0.05]$	(147)
	$\upsilon_w = \frac{0.386 f_{ct}}{\varepsilon_t E_c} \left(1 + \frac{8 G_f E_c}{f_{ct}^2 d}\right)$	(148)	$\zeta = 1.2 - 0.2a \geq 0.65$	(149)
	$\upsilon_t = 0.85 \rho_{fv} f_{fv}$	(150)	$\alpha = \frac{E_{fl}}{E_c}$	(151)
	$f_{fv} = \left(0.05 \frac{r_b}{d_b} + 0.3\right) f_{fu}$	(152)		
Schöck [84]	$V_{fv} = \frac{A_{fv}}{s} f_{fv,d} z \cot\theta$	(153)	$\theta = 50 - \frac{E\rho_{res}}{400}$	(154)
	$f_{fv,d} = 130MPa$	(155)	$E\rho_{res} = \sqrt{(\rho_{fl} E_{fl})^2 + (\rho_{fv} E_{fv})^2}$	(156)

Table 41 – Non-design capacity of the beams

Beam	Experimental	Non-design Capacity						
		ACI 440.1R-06[2] / ACI 318-11[3]			EC2[23]/FIB 40[22]			
	Load	Shear		Bending	Shear			Bending
	(kN)	ε_{fv} =4 ‰ (kN)	ε_{fv} =7 ‰ (kN)	(kN)	Θ=30˚ (kN)	Θ=38˚ (kN)	Θ=45˚ (kN)	(kN)
REF250	426.4	393.9		546.2	454.4	-	-	543.8
REF175	477.0	395.5		547.6	455.2	-	-	545.2
BS250	488.2*	335.2	442.6	555.4	409.2	343.6	303.0	553.3
BS175	468.1*	379.8	532.4	542.9	506.8	413.7	356.1	540.4
BS250GFRP1	400.0	245.8	353.3	449.9	381.8	316.2	275.6	527.7
BS175GFRP1	408.4	315.3	468.8	477.2	493.5	399.8	341.8	559.6
BS250GFRP2	506.0	268.5	373.0	527.7	400.4	336.6	297.1	619.1
BS175GFRP2	500.0	338.0	487.2	560.8	509.8	418.7	362.3	657.8

* Bending failure by concrete crushing at mid-span

Although all the beam specimens were designed to fail due to shear, BS250 and BS175 failed by compression of concrete at top of mid-span, which is a brittle failure mode, inadvisable for steel longitudinal reinforced beams, as mentioned in ACI 318-11 [3]. These two failures can be explained considering in the calculation of the bending capacity that the concrete strain was 3.5‰, the ultimate compressive strain, ε_{cu}, and that the strain in the longitudinal reinforcement , ε_{sl}, was 2.8‰, which was the yield strain of the steel considered. This yield strain was determined, with the values of the pure tension tests, as the ratio between the experimental values of the yield strength, f_{sy}, and the elasticity modulus, E_s. An ultimate bending capacity of 477.0 kN is obtained, which is close to the experimental capacity of BS250 and BC250. Moreover, the experimental longitudinal strain development (Figure 105) supported these calculations.

It can be stated that beams with the lower longitudinal stiffness, GFRP1 beams, exhibited lower shear capacities comparing to their respective reference, although they were designed to have approximately the same shear capacity. This highlights the influence of the longitudinal stiffness in the shear capacity.

Comparing the beams with GFRP shear reinforcement, it can be stated that increasing the ratio of the shear reinforcement did not correspond to an increase of the shear capacity. This is in agreement with the results described by Fico, Prota*, et al.* [35] and, according to these authors, for shear reinforcement ratios over 1%, increasing the shear reinforcement ratio does not increase the shear reinforcement strength. The shear reinforcement ratio is considered to vary linearly with shear strength of shear reinforcement by most codes. However, Machial, Alam*, et al.* [65] also concluded that the stirrup shear strength increases non linearly with the shear reinforcement ratio.

The longitudinal stiffness influenced the shear capacity and the longitudinally steel reinforced, and the GFRP2 beams had the higher shear capacities. This can be explained by the lower deflections and crack widths on these beams, which contribute to the integrity of the shear mechanisms. Similar results were achieved by Admasu and Adam [4], which also refer that the lower shear stiffness of GFRP RC members is partially due to the smaller dowel action caused by the weakness of the bars perpendicularly to the axis

The shear capacity of the beams estimated using ACI 440.1R-06 [2] was more than 40% lower than the experimental shear failure load, due to the limit of the strain (4‰) considered. As showed in Table 41, conservative but more accurate predictions can be achieved when considering a strain limit of 7‰, which was measured experimentally on the stirrups.

Similarly, the shear strength values obtained with FIB 40 [22] were underestimated to all the beams by more than 40%. More accurate predictions can be achieved by varying the angle to 38 degrees, which was the mean angle of the beams failure planes. In Table 42, there are the values of the predictions according to all the other formulations considered. With exception of ACI 440.1R-06 [2] and JCSE guidelines [35], which underestimated all the beam specimens strength, all other formulations overestimated some of the results and underestimated others. The ratio between the experimental and the predicted capacities is presented in Figure 94. The shear capacity of BS250GFRP2 was highly underestimated. And it was also verified that there was tendency to the overestimation of the shear capacity of beams with stirrups spaced at 0.175 m.

Table 42 –Summary of experimental and predicted ultimate shear capacity values

Beam	Shear capacity								
		Ultimate values							
	Experimental	ACI 440.1R-06[2] / ACI 318-11[3]	Oller *et al.*[75]	CSA S6-09 Addendum[65]	CSA S806-02 [13]	JCSE guidelines [35]	CNR DT-203[27]	Fico *et al.*[35]	Nedhi *et al.*[65]
	(kN)	(kN)	(kN)	(kN)	(kN)	(kN)	(kN)	(kN)	(kN)
BS250	488.2	335.2	465.0	375.6	444.7	432.5	415.1	494.3	545.5
BS175	468.1	315.3	563.9	495.0	515.6	442.2	484.5	597.6	586.1
BS250GFRP1	400.0	379.8	459.3	371.0	358.6	246.9	323.7	403.35	472.5
BS175GFRP1	408.4	268.5	596.2	504.3	452.0	285.3	436.0	549.9	531.3
BS250GFRP2	506.0	245.8	459.6	371.0	391.5	314.6	346.6	425.7	501.6
BS175GFRP2	500.0	338.0	596.2	504.3	485.9	364.8	460.8	574.6	561.0

Generally, the overestimation is higher for GFRP2 beams. Nedhi *et al.* [65]formulation yielded non-conservative for all the beam specimens, expect BS250GFRP2. Oller *et al.* [75] formulation overestimate the ultimate capacity of the beam specimens with exception of BS250 and BS250GFRP2. Both CSA S6-09 Addendum [65] and CSA S806-02 [13] theoretical predictions were conservative to all beams with stirrups spaced at 0.250 m and non-conservative to beams specimens with stirrups spaced at 0.175 m. Fico *et al*. [35] formulation yielded theoretical values very close to experimental for beams with stirrups spaced at 0.250 m.

Considering the deviation from the prediction to the experimental value, it can be noticed that the predictions from both CSA S6-09 Addendum [65] and CSA S806-02 [13] had a lower deviation (4% and 3%, on average). All others exhibited a high deviation, suggesting that the models do not adequately reproduce the observed behaviour.

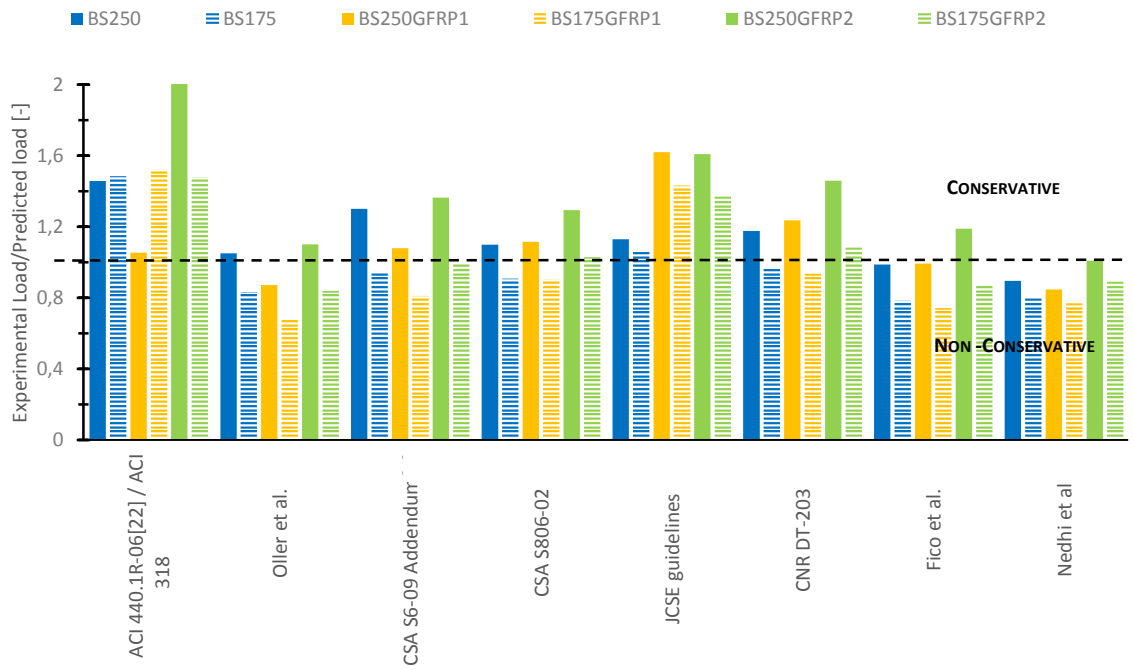

Figure 94 – Experimental to predicted ratio according to the several formulations

2.7.1.2 Failure modes

There was no significant difference in the overall behaviour in terms of cracking pattern and types of failure between the reference beams and the GFRP beams. The failure modes of all specimens are presented from Figure 95 to Figure 102. The propagation of the cracks during the test was marked on one of the faces of the beams and the cracking pattern is presented later from Figure 111 to Figure 114. In general, four distinct types of failure occur:

- Bending failure due to concrete crushing at top of mid-span (BS175 and BS250);
- Shear diagonal tension failure by shear reinforcement failure (REF175, REF250 and BS175GFRP1);
- Shear failure due to the crushing of the concrete strut (BS250GFRP2 and BS175GFRP2);
- Shear failure due to the failure of the bond of the longitudinal reinforcement at support (BS250GFRP1).

The two reference beams failure was similar and due to the failure of several stirrups. For REF175, several flexural cracks developed vertically along the span as the load increased. For loads above 150 kN, the cracks located between the loading points and the supports started to incline in the direction of the loading points (Figure 95 a)). The failure occurs with the rupture of one stirrup,

followed by the ruptures of all the other stirrups along the shear crack (Figure 95 c) and d)), leading to an almost instantaneous failure of the beam at 477.0 kN (Figure 95 b)).

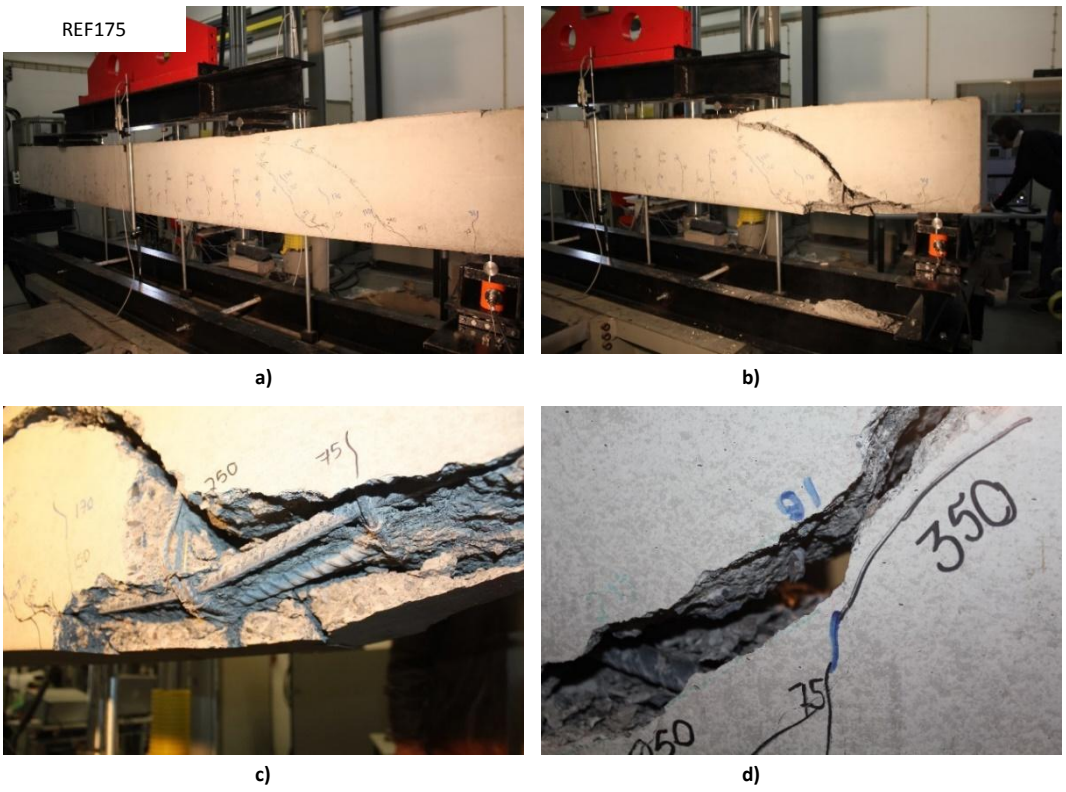

Figure 95 – REF175 beam failure: a) overall view immediately before failure; b) view of the support after failure; c) bottom reinforcement; d) broken stirrup

The failure of REF250 was similar. Several flexural cracks developed vertically along the span as the load increased. For loads above 150 kN, the cracks located between the loading points and the supports started to incline in the direction of the loading points and the failure occurs with the rupture of one stirrup, followed by the rupture of all the other stirrups along the shear crack (Figure 29 c) and d)), leading to an almost instantaneous failure of the beam at 426.4 kN (Figure 29 a) and b)).

BS175 and BS250 failed by the crushing of concrete at the top of mid-span (bending failure), at 468.1 kN and 488.2 kN (Figure 97 and Figure 98), respectively. Although for loads above 190 kN several shear cracks appeared in both of the beam specimens. At mid-span the flexural cracks continued to spread vertically, and given the high ratio of longitudinal steel reinforcement the concrete reached its ultimate strength before steel yields.

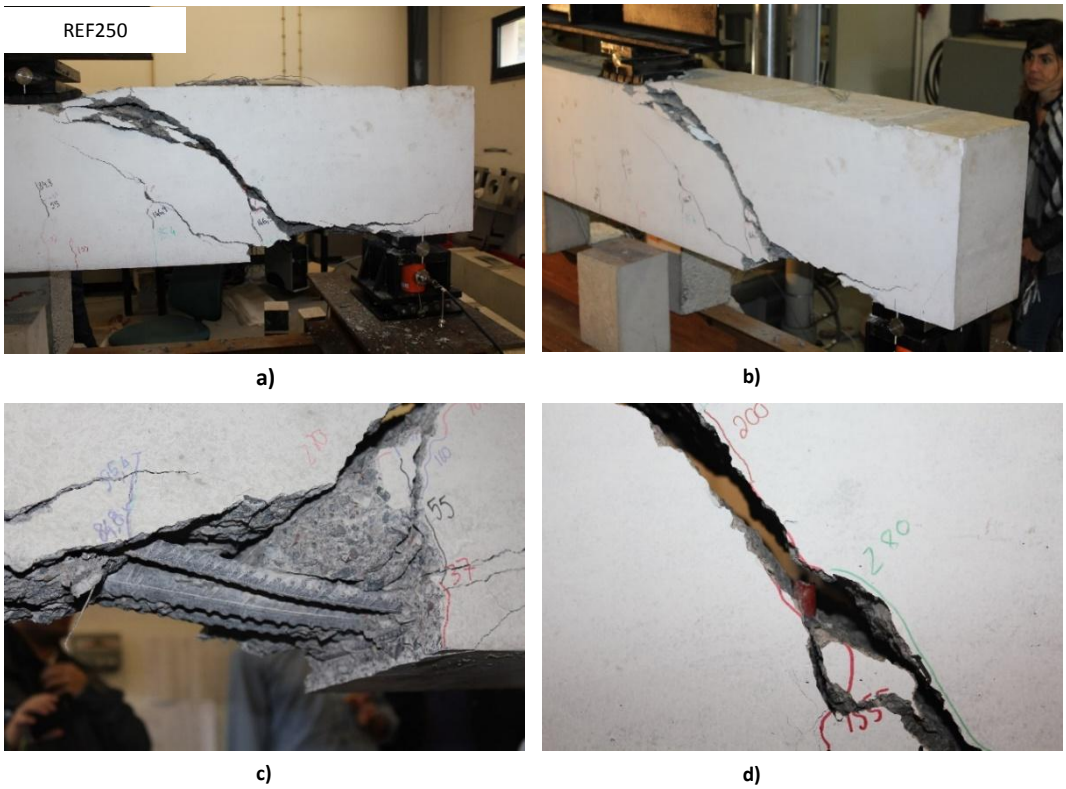

Figure 96 – REF250 beam failure: a) front view of the support; b) overall view of the failure; c) bottom reinforcement; d) broken stirrup

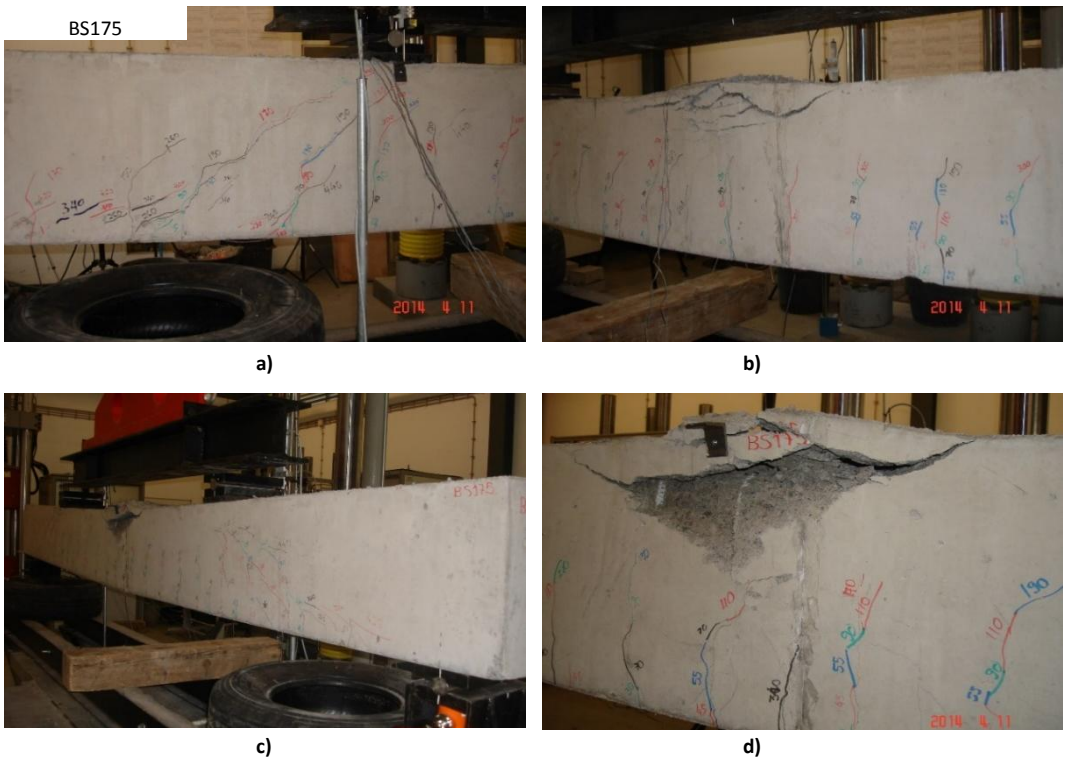

Figure 97 – BS175 beam failure: a) view of shear cracks at failure; b) mid-span; c) overall view; d) top of mid-span

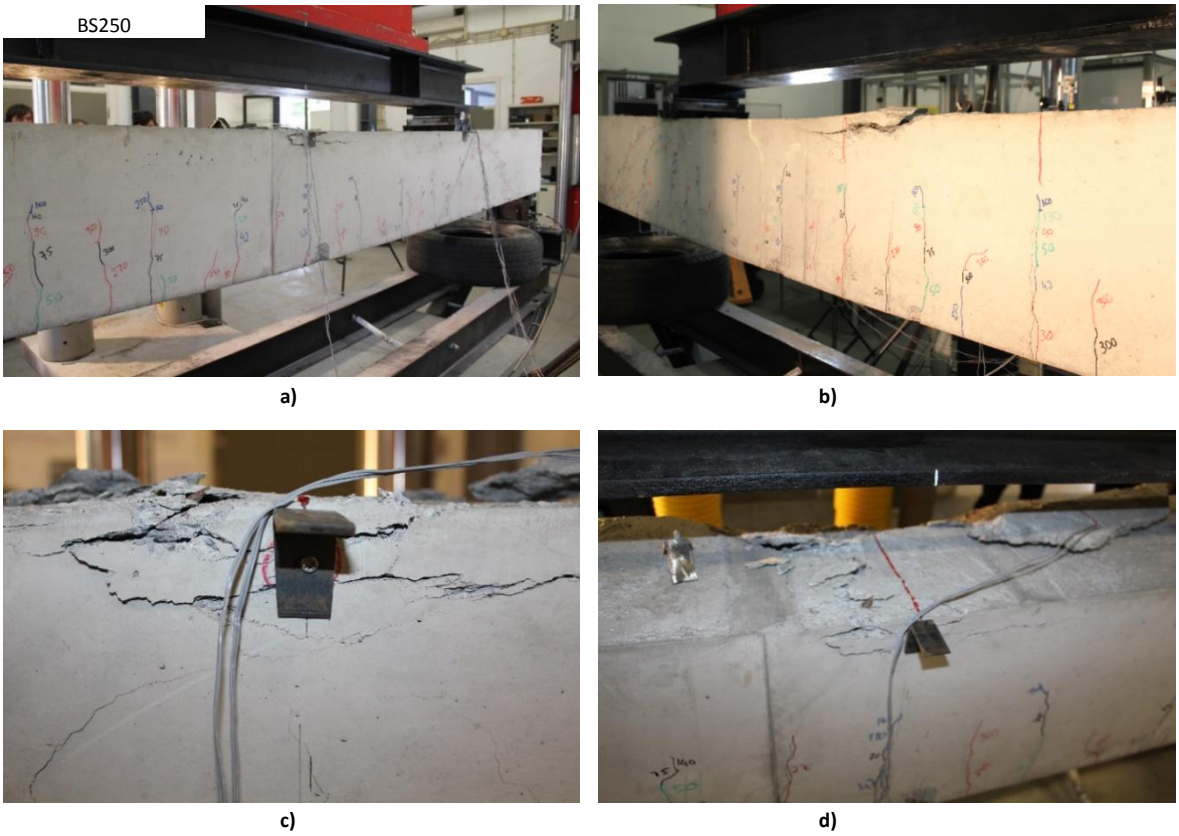

Figure 98 – BS250 beam failure: a) overall view from one side; b) overall view from the other side; c) mid-span; d) top of mid-span

The BS250GFRP1 beam exhibited a brittle shear failure due to the pull-out of the longitudinal reinforcement at 400 kN (Figure 99).The shear cracks appear around 150 kN developing from supports to the loading points. The bond of longitudinal reinforcement failed at 400 kN, and the pull-out of the longitudinal reinforcement is shown in Figure 99 d and f)), which was followed by a secondary concrete crushing Figure 99 e).

The BS175GFRP1 beam failed at 408.4 kN by shear reinforcement failure (Figure 100) with a secondary crushing of the concrete strut. Several stirrups disintegrated and opened, originating delamination of the concrete cover. As already described above regarding the other beam specimens which initially developed the flexural cracks, after 150 kN the first shear cracks propagated from supports to loading points. After testing, it was verified that there was no pull-out of longitudinal reinforcement.

Figure 99 – BS250GFRP1 beam failure: a) shear span before failure; b) overall view before failure; c)overall view after failure; d) shear span after failure; e) shear cracks under loading point; f) slip of longitudinal reinforcement

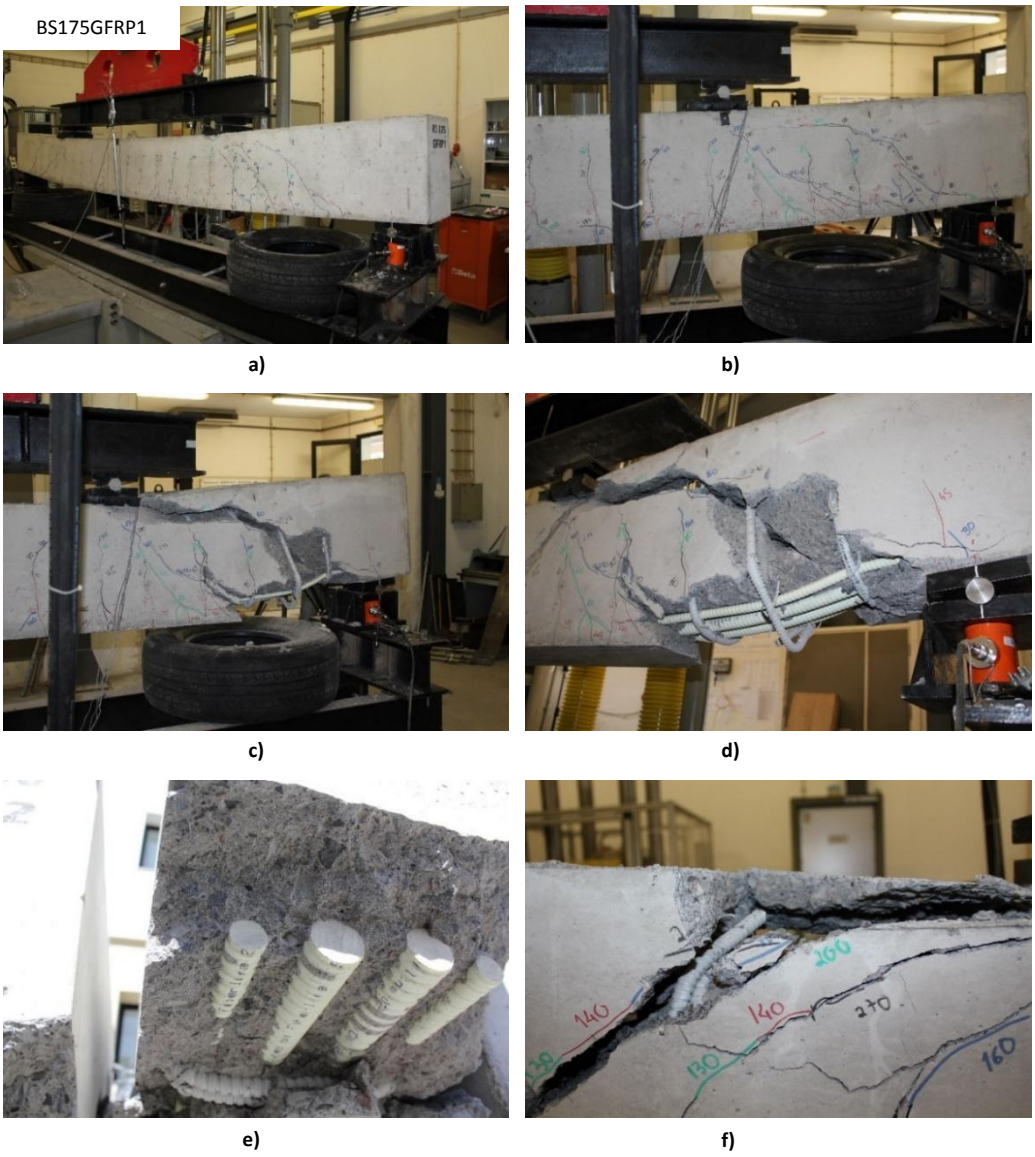

Figure 100 – BS175GFRP1 beam failure: a) overall view before failure; b) shear span before failure; c) shear-span after failure; d) concrete crushing; e) no-slip of longitudinal reinforcement; f) disintegrated stirrup at loading-point

The failure of the BS250GFRP2 beam was a shear failure due to the crushing of the concrete strut between shear cracks at 506 kN (Figure 101). For loads above 200 kN the cracks on the shear span evolved in the direction of the loading points. Figure 101 c) and d) shows that, as a secondary failure mechanism, some of the closed stirrups also disintegrated at the bottom and on the top of the concrete crushed strut.

The failure of the BS175GFRP2 beam was similar to BS250GFRP2, and it was due to the crushing of the concrete strut between shear cracks at 500 kN (Figure 102). For loads above 200 kN the cracks on the shear span evolved in the direction of the loading points. Figure 102 c) and d) shows that, as a secondary failure mechanism, some of the closed stirrups also disintegrated at the bottom and on the top of the concrete crushed strut.

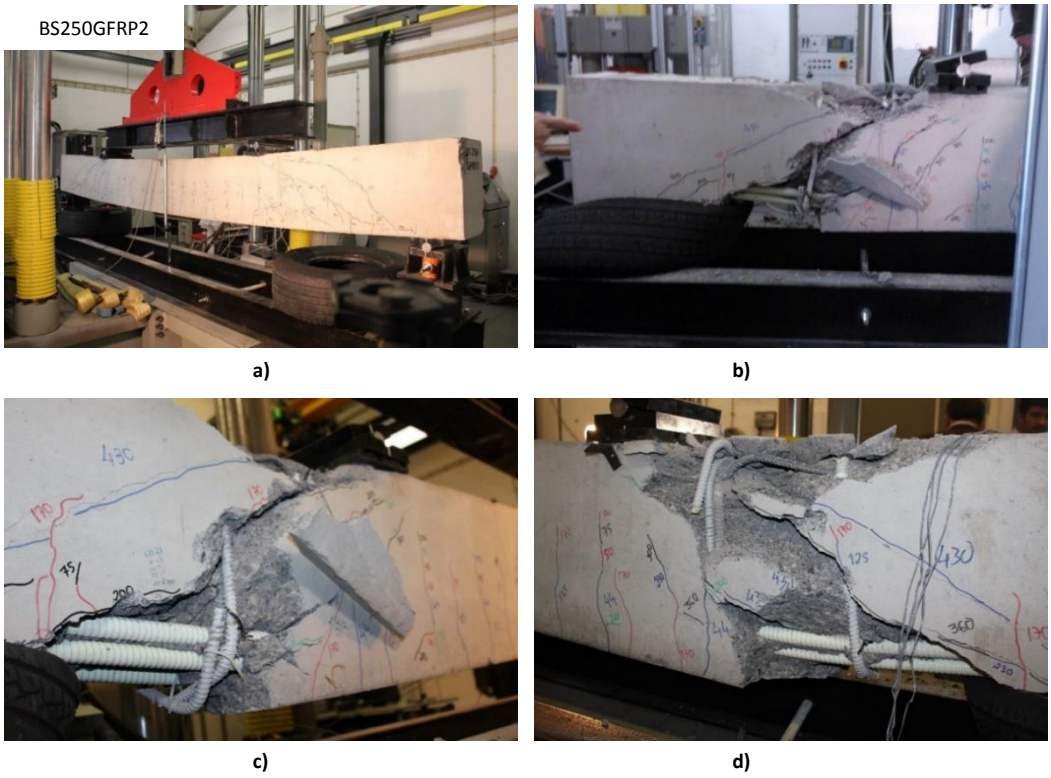

Figure 101 – BS250GFRP2 failure: a) overall view before the testing; b) shear-span after failure; c) stirrup disintegration; d) concrete crushing under the loading point

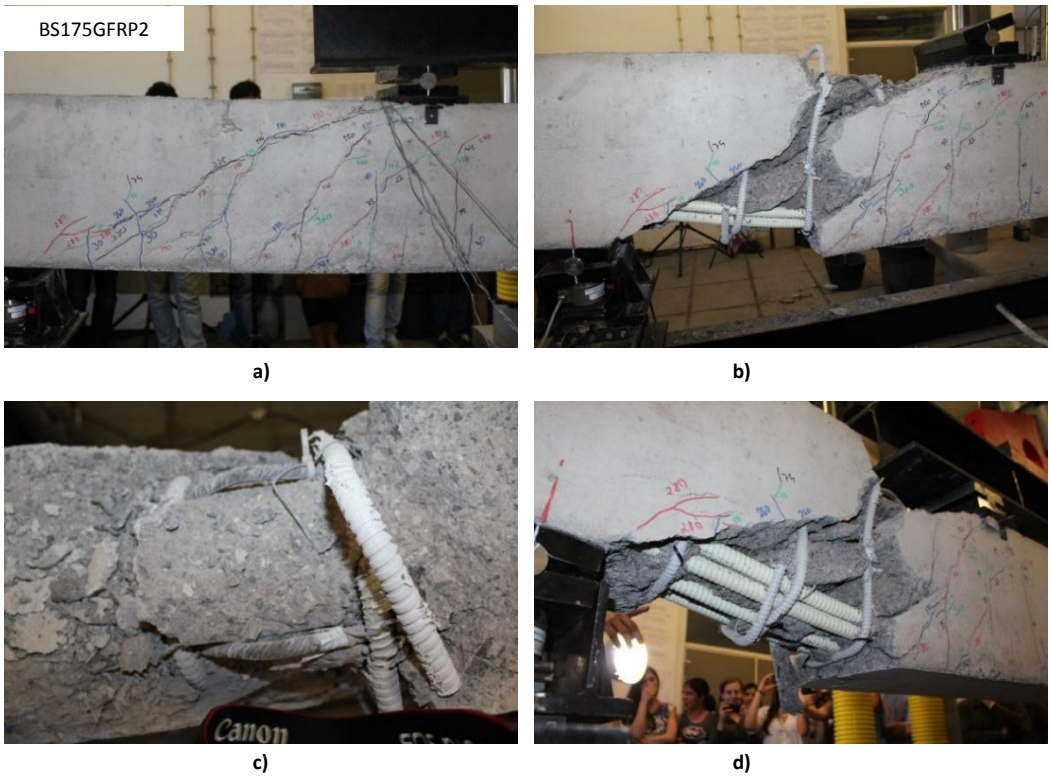

Figure 102 – BS175GFRP2 failure: a) shear-span before failure; b) shear-span after failure; c) concrete crushing over the loading point; d) stirrups disintegrated at bottom

It is important to notice that BS250 and BS250GFRP1 were designed to have the same ultimate load than REF250. However the ultimate capacity of BS250 was 15% higher than the ultimate capacity of REF250 (and failed for bending, which means that the shear capacity was even higher) and the ultimate capacity of BS250GFRP1 was 6% lower than the ultimate capacity of REF250. Concerning the beams with stirrups spaced at 0.175 m, BS175 and BS175GFRP1 had an ultimate capacity of 2% and 14% lower than the ultimate capacity of REF175. BS175 failed for bending and thus its ultimate shear capacity was higher.

2.7.1.3 Mid-span deflection

The load-deflection curves at mid-span are shown in Figure 103. Each curve represented in Figure 103 is the deflection obtained by the 100 mm LVDT mounted at mid-span. To directly compare the flexural stiffness and the overall deflection between beam specimens, the curves were plotted all in the same chart. In general, for loads under the load which corresponds to the cracking moment, all the specimens exhibit an initial elastic phase where the load-displacement relation was linear, followed by a cracked phase where the load-displacement relation was still linear but with lower slope. For all the beams, with exception of BS175 and BS250, the load-displacement curves developed with only two distinct phases which were approximately linear, with no yielding and no ductile behaviour. Even the reference beams with steel longitudinal reinforcement (REF250 and REF175) did not exhibit the yielding phase, as they all had a brittle failure by shear. As soon as the BS175 and BS250 failed for bending, the load-deflection curves had a third phase, where the deflection was still increasing at an almost constant load value, corresponding to a yielding phase, and thus exhibiting some ductility. For BS250, this yielding phase was longer.

Comparing beams according to their longitudinal reinforcement, it can be stated that beams with the same longitudinal reinforcement amount and material, independently of the shear reinforcement, have similar flexural stiffness and almost coincident load-deflection curves. The reference beams and BS250 and BS175 beams have the highest flexural stiffness followed by GFRP2, and finally by GFRP1 beams. BS250 and BS175 exhibit similar behaviour and, on average, a deflection 1.2 times higher than the reference deflection at service. For GFRP2 beams this relation was similar and, on average, 1.2 times higher. For GFRP1 beams the stiffness was the lowest and, the deflection was, on average, 1.5 times higher than the reference.

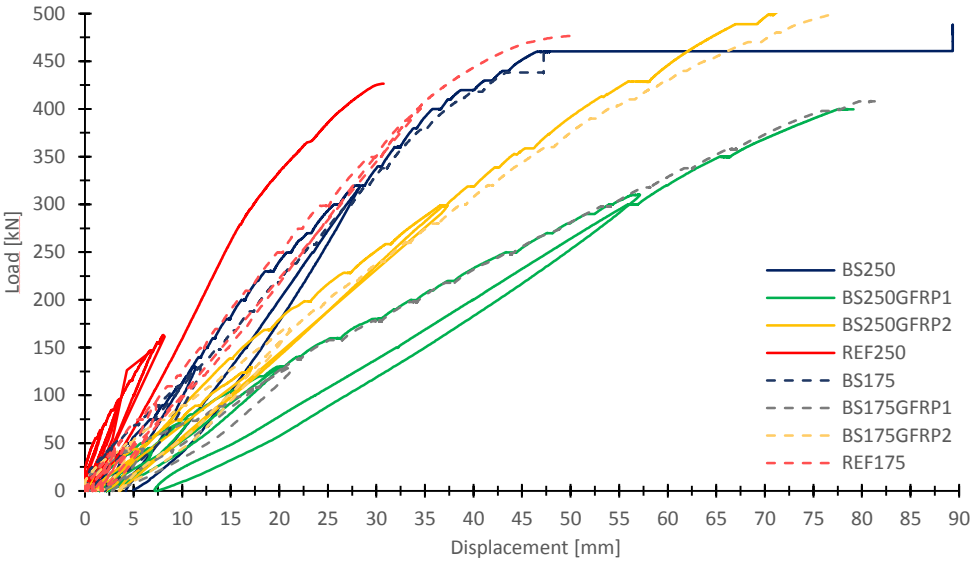

Figure 103 – Load-deflection curves at mid-span location

Considering the change of the slope in the curves, it can be stated that the longitudinal GFRP reinforced beam specimens exhibit a significant reduction of the flexural stiffness after cracking in comparison to the steel reinforced beams. and this was also mentioned by Wegian and Abdalla [96].The Branson's effective moment of inertia was used in order to predict the deflection of a RC beam with GFRP in this work. The comparison between the experimental deflections and the predictions are presented in Table 43.

Table 43 – Summary of deflection values

Beam	ρ_{fL} or ρ_{sL}	Mid-span deflection			
		Service			Ultimate
		Exp.	Pred.	Exp /Pred	Exp.
	(%)	(mm)	(mm)	(-)	(mm)
REF250		4.5	5.0	0.90	31.1
REF175		4.9	5.0	0.98	50.0
BS250		6.2	5.4	1.15	88.0
BS250GFRP1		8.0	6.1	1.31	78.0
BS250GFRP2	2.50	6.4	5.5	1.16	70.9
BS175		5.9	5.4	1.01	47.8
BS175GFRP1	1.40	7.0	6.1	1.14	81.6
BS175GFRP2	2.50	5.7	5.5	1.04	77.9

2.7.1.4 Reinforcement strains

2.7.1.4.1 Mid-span reinforcement strains

The strains of longitudinal reinforcement at mid-span were measured by SG5 and SG6 (Figure 3) and presented, with the respectively strain predictions (expected curve), from Figure 104 to Figure 107. Beam specimens that failed for shear had a bilinear load-strain relationship with no evidence of yielding of longitudinal reinforcement or concrete crushing. BS250 and BS175 that failed due to mid-span concrete crushing (bending failure) had a load-strain relationship with a two-stage development with an elastic and a yielded phase.

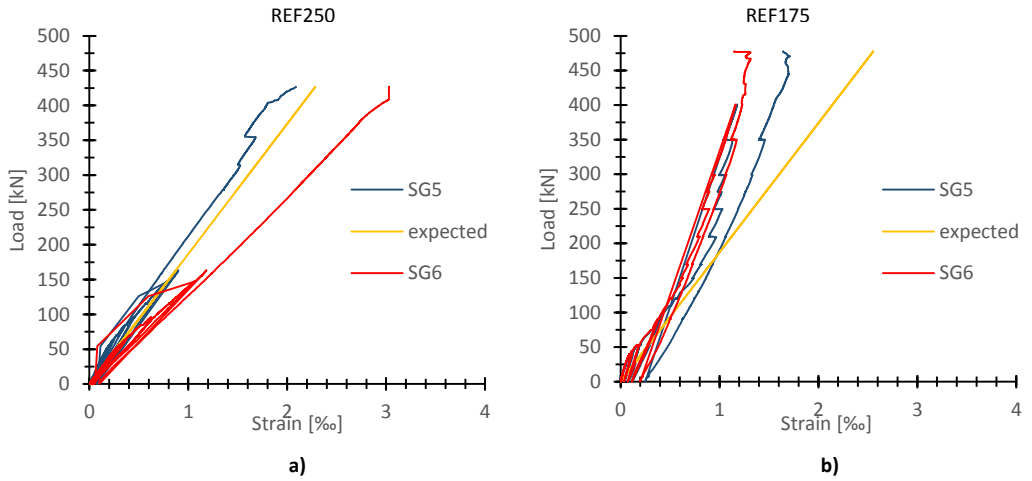

Figure 104 – Longitudinal reinforcement strains: a) REF250; b) REF175

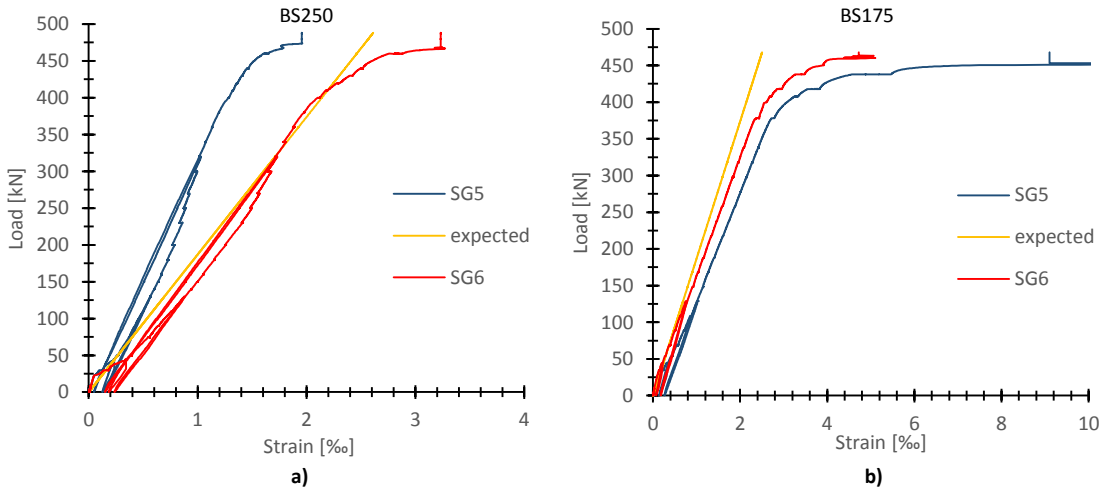

Figure 105 - Longitudinal reinforcement strains: a) BS250; b) BS175

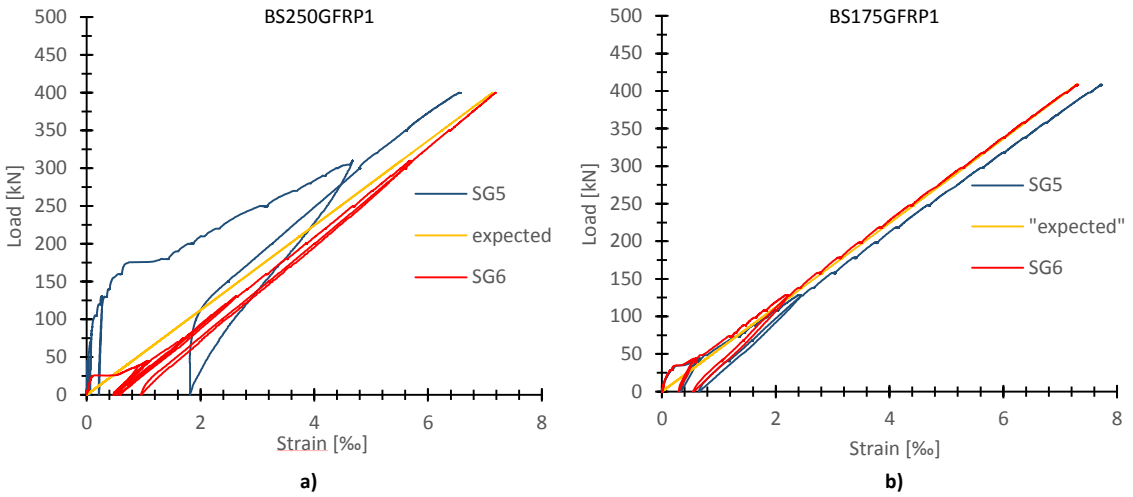

Figure 106 – Longitudinal reinforcement strains: a) BS250GFRP1; b) BS175GFRP2

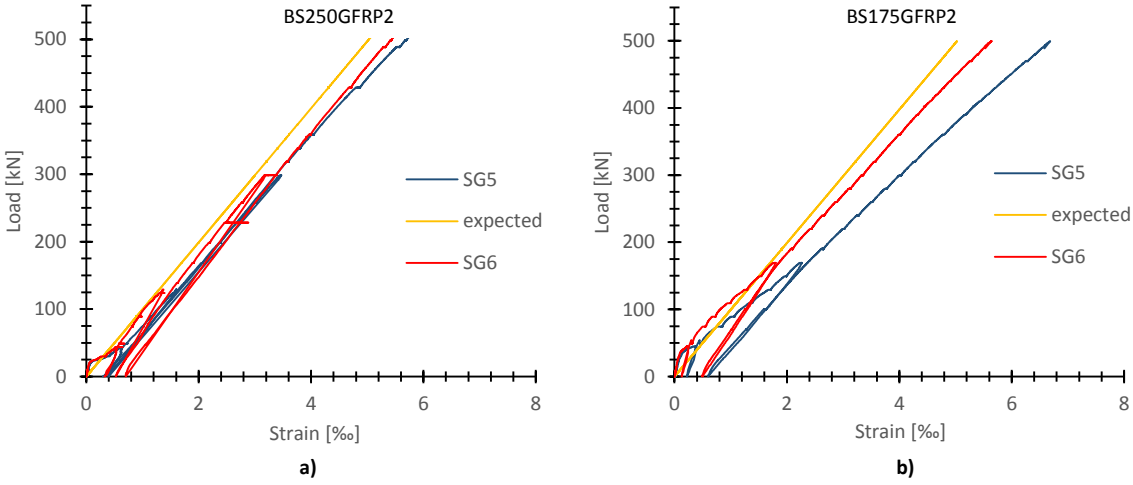

Figure 107 – Longitudinal reinforcement strains: a) BS250GFRP2; b) BS175GFRP2

The values of the strains were, in general, in accordance with predictions for high load values, with the exception of REF175, which had lower strains than predicted. This was expected as the predictions were done assuming that the load carrying was assured by the reinforcement. For lower load values where beams are little cracked, the concrete contribution is important to the load carrying. The strain values, for the maximum load capacity, are presented in Table 44. The average variation of the measured values to the predictions is ± 1%.

Comparing steel reinforced beams BS250 and BS175 (before yielding) with BS250GFRP1 and BS175GFRP1, it can be stated that for the same reinforcement area, GFRP beams had the highest reinforcement strains. These higher strains for the same load level are also related to higher curvatures in GFRP1 beams, which affect and increase deflections and, as consequence, lead to

lower shear strength. By comparing GFRP1 beams with GFRP2 beams, it can be stated that fixing a load value and increasing the reinforcement area decreases the reinforcement strains. Shear reinforcement area and material do not affect the longitudinal reinforcement strains, by comparing all the beams with stirrups spaced at 0.250 m with 0.175 m.

It can also be stated that GFRP longitudinally reinforced beams exhibit higher strains than the steel reinforced beams.

Table 44 – Summary of strain values

Beam	ρ_{fL} or ρ_{sL}	ρ_{fv} or ρ_{sv}	Ultimate values					
			Mid-span strain			Shear reinforcement strain		
			Exp.	Pred.	Exp /Pred	Exp.	Pred.	Exp /Pred
	(%)	(%)	(‰)	(‰)	(-)	(‰)	(‰)	(-)
REF250	1.40	0.40	2.53	2.25	1.12	2.74	9.00	0.30
REF175			1.69	1.30	0.80	2.15	6.00	0.35
BS250		0.90	2.08*	2.39	0.87	9.38	9.40	1.00
BS250GFRP1			6.80	7.15	0.95	6.56	7.80	0.84
BS250GFRP2	2.50		5.76	5.02	1.15	8.30	9.40	0.88
BS175	1.40		3.31*	2.50	1.34	5.53	5.61	0.98
BS175GFRP1			5.63	5.50	1.02	4.75	6.13	0.78
BS175GFRP2	2.50		5.45	5.10	1.07	6.87	6.80	1.01

- - at yielding point

2.7.1.4.2 Shear reinforcement strains

The development of the shear reinforcement strains in the shear span is plotted as a function of the distance from the support in Figure 108 for BS175GFRP2 and in Figure 109 for BS250GFRP2. As the development of the shear reinforcement strains was similar in the other beams it is not presented. It can be noticed that the stirrup near the support have very small strain values in both cases, as expected. The strain distribution along the shear span varies with the loading, being affected by crack development, but with the load increase, the stirrups SG3 and SG4 were the most stressed. It was also verified that the higher strains occurred in the stirrup closer to the mid-span to all the beam specimens.

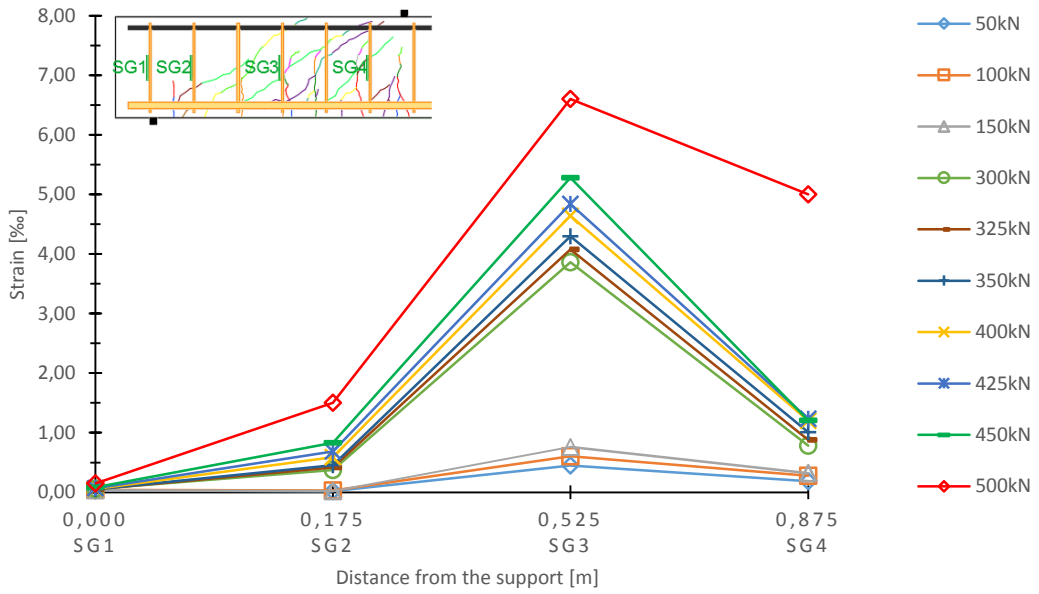

Figure 108 – Shear reinforcement strain distribution along shear span of beam BS175GFRP2

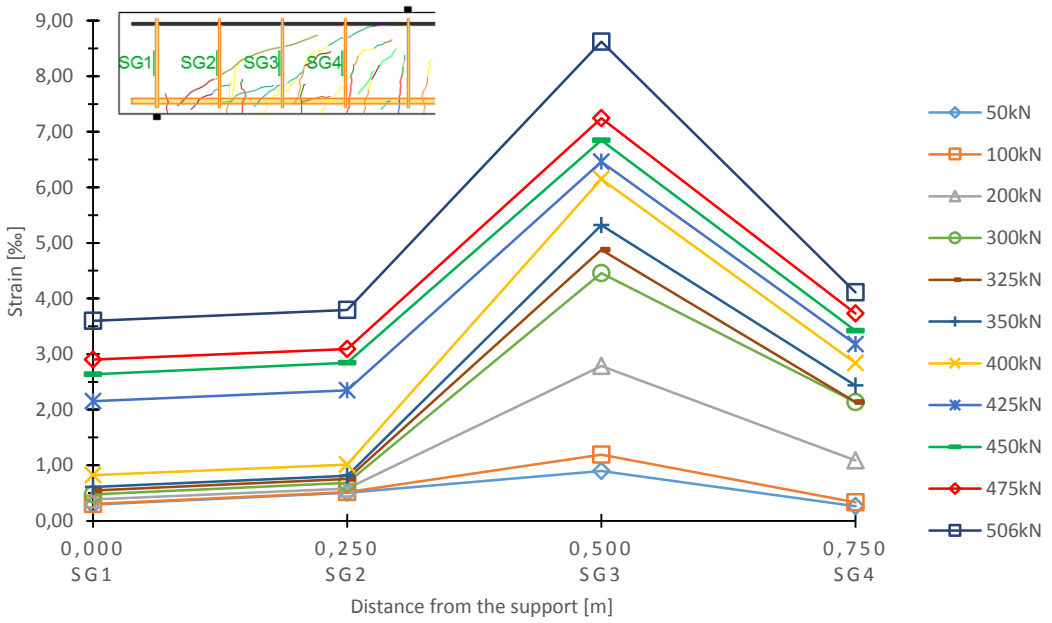

Figure 109 - Shear reinforcement strain distribution along shear span of beam BS250GFRP2

Figure 110 shows, for each beam, the development of the strains at the most stressed stirrup divided by the shear reinforcement spacing: a) for beams with stirrups spaced at 0.250 m and; b) for beams with stirrups with 0.175 m spacing. The expected strain values were also plotted for comparison. Although the expected strain values were roughly expected, in general, the strain

values were close to the predicted near the failure. For all the beam specimens the development had a bilinear configuration. During the major part of the loading, the GFRP1 beams had the higher stirrups strains for the same load value, while beams with the steel longitudinal reinforcement exhibited the lower shear reinforcement strains.

It can be observed that the strains of shear reinforcement were higher than the ACI 440.1R-06 [2] limit of 4‰ for all the beam specimens. And the shear reinforcement strains varied from 6‰ to 10‰.

Corresponding to an average of 4‰ strain in GFRP stirrups, which is the ACI 440.1R-06 [2] limit, the applied forces were 305 kN, 268 kN and 230 kN, respectively for BS250, BS250GFRP1 and BS250GFRP2. These values represent, respectively, 62.5%, 67% and 46% of the observed failure loads. For BS175, BS175GFRP1 and BS175GFRP2 the applied forces were 315 kN, 327 kN and 310 kN, respectively. These values represent approximately 67%, 80% and 62% of the ultimate capacity of the beam specimens. Similar results were stated by [29]. In GFRP1 beams, for having the lower ultimate capacity, the 4‰ strain in GFRP stirrups is related to a load value closer to the ultimate load.

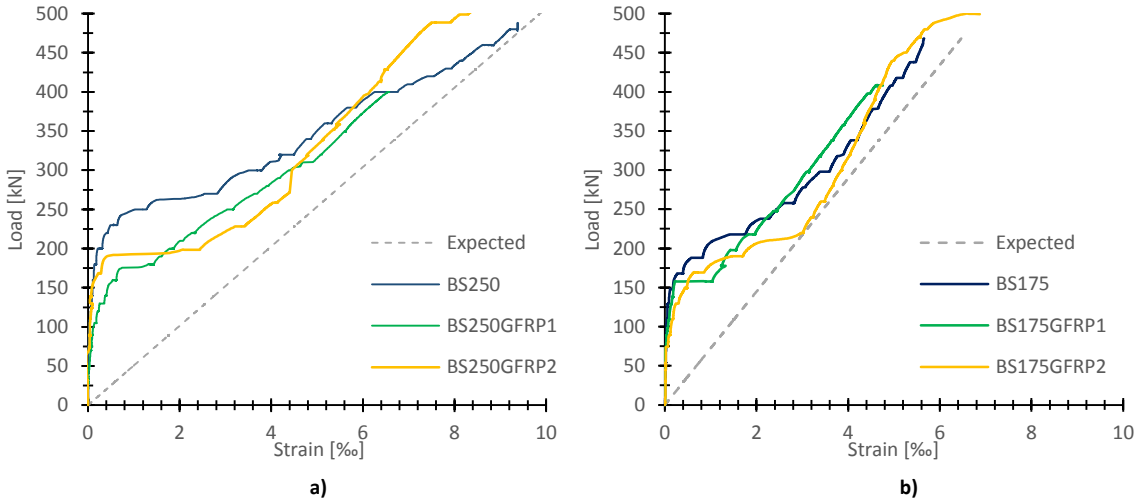

Figure 110 – Strains in shear reinforcement: a) BS250 beams; b) BS175 beams

2.7.1.5 Cracking behaviour

In order to analyse the differences in the cracking behaviour, the crack development was marked in the beams with different colours after each load step. The crack patterns are shown from Figure

111 to Figure 114. Initially, all the beam specimens didn't have any cracks. The cracks appeared firstly at the constant moment region, and grew vertically in the absence of shear stresses. With the load increase, other flexural cracks appeared in the shear-span region. Initially, these cracks propagated vertically but then inclined in the loading point direction. The failure started with the formation of an inclined crack oriented perpendicular to the direction of the maximum principal stress. It can be noticed that generally it was the shear crack closest to the support that led to the failure of the beam. The slat of the plane of the failure of the beams that failed due to shear varies from 38 degrees to 46 degrees being in agreement with the 45 degrees truss model. GFRP2 beams (i.e., beams with higher longitudinal reinforcement area) failed in general with a less inclined plane. It was also verified that the higher the longitudinal reinforcement area and the failure load, the greater the number of shear cracks.

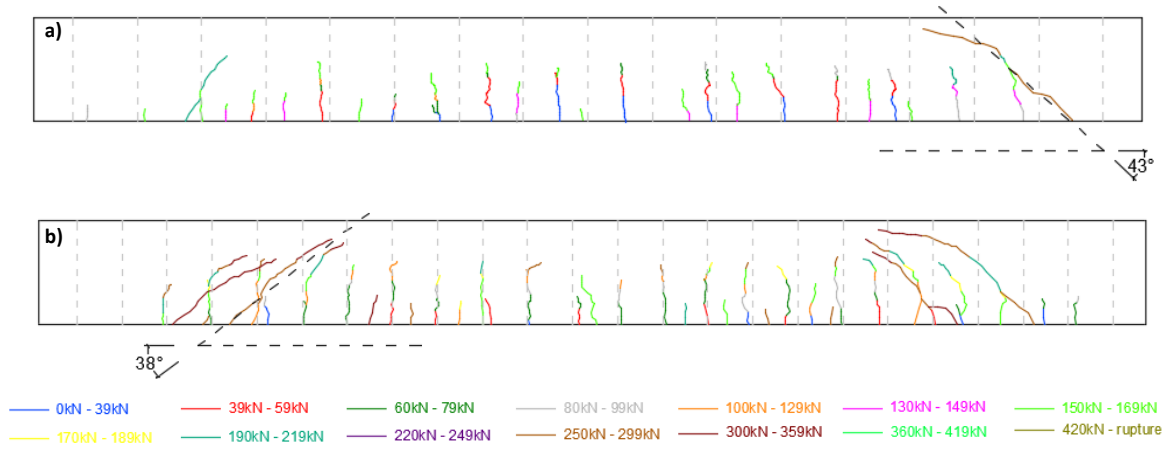

Figure 111 – Cracking pattern of: a) REF250; b) REF175

For the GFRP longitudinally reinforced beams (BS250GFR1, BS250GFR2, BS175GFR1 and BS175GFRP) when the failure was imminent, horizontal cracks appeared from the bottom of the shear cracks towards the supports. This can be explained by the differences between the bond between concrete - GFRP when compared to the bond steel – concrete, and also due to fact that when the failure was imminent the aggregate interlock was lost at the shear crack and in order to maintain the equilibrium at the section the dowel action in the longitudinal reinforcement has to increase. The increase of the dowel action causes vertical tension stresses which combined with the existing splitting forces due to flexural bond lead to the bond/anchorage failure [98].

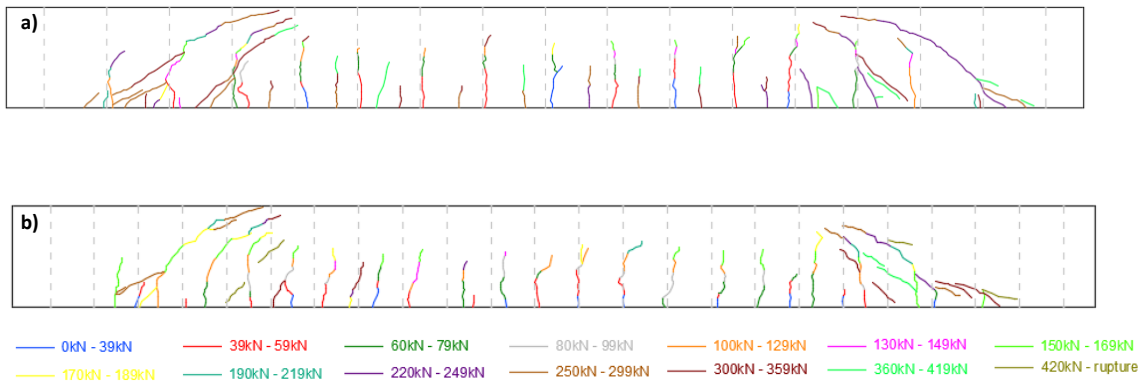

Figure 112 – Cracking pattern of: a) BS250; b) BS175

Concerning flexural cracks, it can be stated that for GFRP longitudinal reinforced beams, the increase of the longitudinal stiffness resulted in a reduced crack spacing and a higher number of cracks. BS250GFRP1 flexural crack spacing was 0.242 m while for BS250GFRP2 it was 0.132 m. Comparing the longitudinal steel reinforced beams with the GFRP reinforced, the mean flexural crack spacing for BS250 was 0.109 m while for BS250GFRP1 it was 0.242 m. Thus, for the same amount of reinforcement, steel reinforced beams had a higher number of cracks, with a fixed vertical development pattern For GFRP reinforced beams, the distance between vertical main cracks was higher and with the load increase several oblique ramifications appeared and propagated from the main crack. Another important achievement is the height of the compression zone (distance between the compression fibre and the neutral axis). All GFRP1 beam specimens exhibited the smaller compression zones (0.100 m for BS250GFRP1 and 0.110 m for BS175GFRP1), followed by the GFRP2 beams (0.111 m for BS250GFRP2 and 0.112 m for BS175GFRP2)and finally steel reinforced beams (0.132 m for BS250 and 0.137 m for BS175). This means that, comparing beams with the same reinforcement area, there was a rise of the neutral axis for GFRP reinforced beams. Also, concerning GFRP reinforced beams there was a decrease of the neutral axis with the rise of the reinforcement ratio.It can also be stated that for the beams longitudinally reinforced with GFRP bars, more flexural cracks appeared, although with smaller widths, due to the increase of the reinforcement area from beams GFRP1 to GFRP2.

Shear cracks appeared at lower load values for GFRP1 and GFRP2 beams in comparison to steel. For example, for REF 250 the first shear cracks appeared between 60 kN and 80 kN, while for BS250GFRP1 and Bs250GFRP2, the first shear cracks appeared for loads between 40 kN and 60 kN. This behaviour may be related to the lower axial stiffness of the longitudinal behaviour, which can lead to a different distribution of internal stresses and a different cracking behaviour and pattern. It can be stated that the higher the shear failure load, the higher the number of shear cracks.

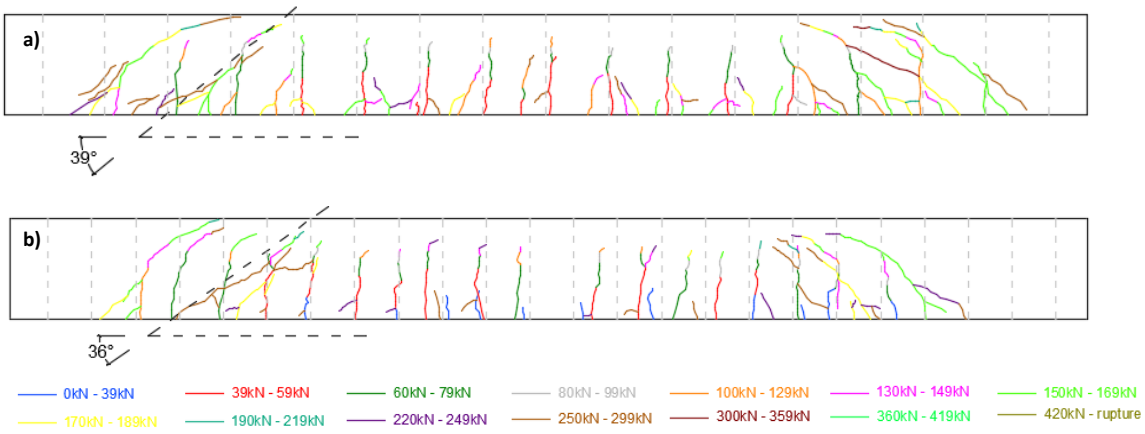

Figure 113 - Cracking pattern of: a) BS250GFRP1; b) BS175GFRP1

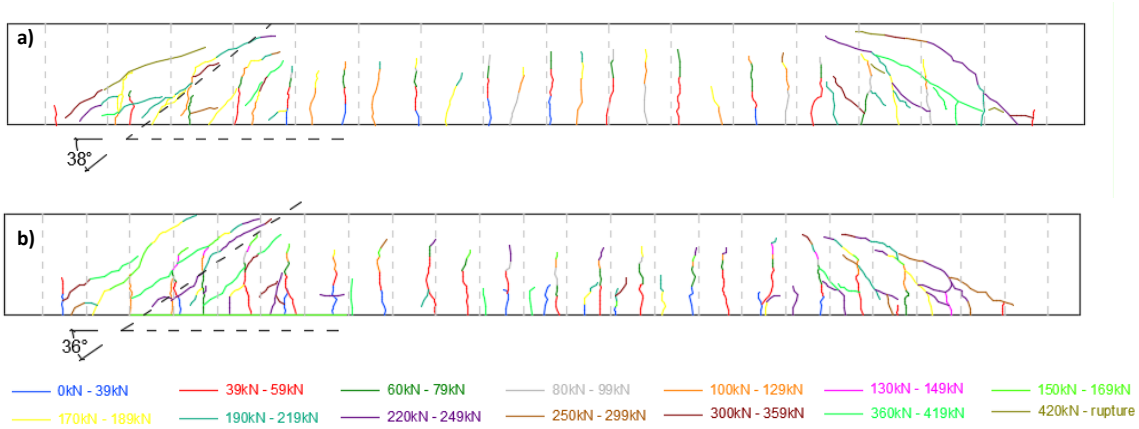

Figure 114 – Cracking pattern of: a) BS250GFRP2; b) BS175GFRP2

2.7.1.6 Shear crack widths

The variation of the shear crack widths with the loading is shown in Figure 115. It can be stated that the shear cracks appeared only for load levels above the service load and that there is a linear pattern between the crack widths and the applied load for the beams with the same stirrup spacing.

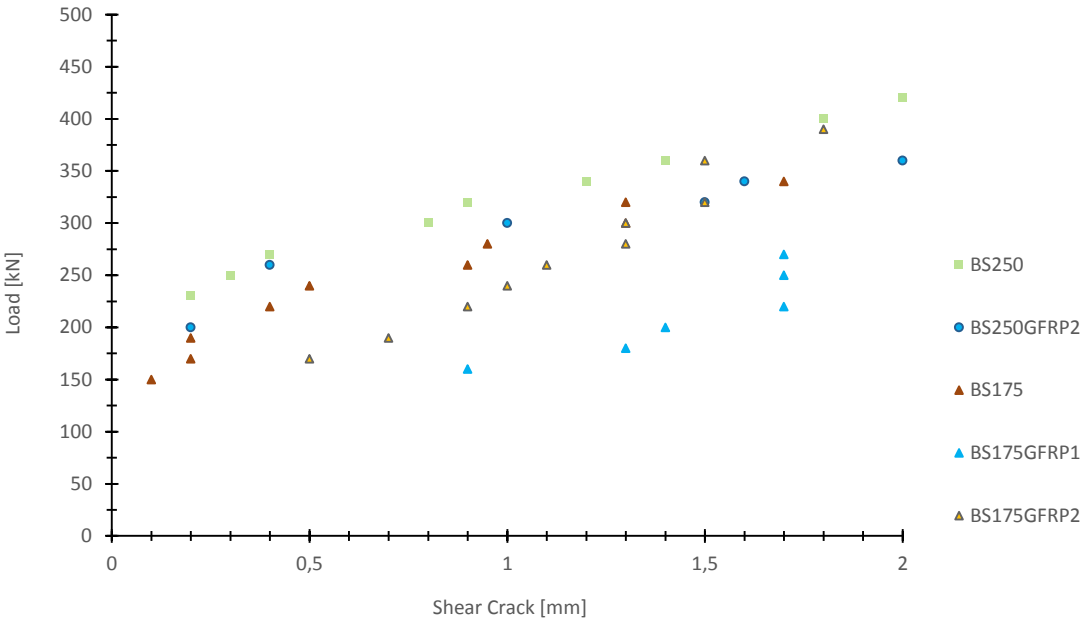

Figure 115 – Variation of the shear crack widths with the load

It can be seen that even for low load levels, the crack width exceeded 0.50 mm, generally assumed as the maximum allowable crack width [2].

Mid-span crack widths were also measured, and it was noticed that the crack width in GFRP longitudinally reinforced beams was higher than on steel reinforced.

2.7.2 Conclusions

This study evaluated the performance of bent GFRP stirrups by testing and comparing full-scale intermediate length GFRP RC beams with steel RC beams and with design provisions and several model predictions, in terms of overall behaviour, parameters affecting shear and shear strength.

The results show that GFRP bent stirrups are an efficient solution as shear reinforcement and that the overall behaviour of GFRP reinforced beams is similar to steel reinforced beams on cracking pattern and failure mechanisms. These findings are consistent with Guadagnini, Pilakoutas*, et al.* [47] experimental study which showed that the main parameters governing the shear behaviour and the failure of FRP RC beam developed in a similar way to steel counterparts. Concerning the GFRP longitudinally reinforced beams, both criteria to design beams with same load capacity (GFRP1 beams) or with the same deflection at service (GFRP2 beams) of the reference beams were satisfied. More specific findings are:

1- ACI 440.1R-06 [2], JSCE design guidelines [35] and FIB40 were found to underestimate the beams ultimate shear strength, conducting to a non-economical section design and problems in terms of congestion of the reinforcement.
2- The underestimation is partially due to the limitation of the stirrups strain or stress considered in these codes. The experimental values indicate that, the limit of stirrups strain quoted for ACI 440.1R-06 [2], correspond to less than a half of the measured maximum stirrup strain. Therefore, increasing the strain limit to 7‰ can be a measure to reduce the underestimation and to achieve a more economical design. Nedhi *et* al. [65] and Oller *et* al.[75] formulations yielded non-conservative of ultimate capacity for several beam specimens and conservative to others. A possible explanation to the dispersion of results can be the fact these models do not capture adequately the real observed behaviour of the beam specimens.
3- From the specimens considered it was demonstrated that the shear strength was influenced by the longitudinal reinforcement amount and type, and by the longitudinal stiffness. For GFRP longitudinal reinforcement, a lower amount of reinforcement, an increase in the crack widths and a reduction of the shear capacity, as well as, keeping the same reinforcement amount but changing from steel to GFRP reinforcements, lead to higher deflections and crack width and lower shear strength. GFRP longitudinal reinforced beams exhibit a significant reduction of the flexural stiffness when compared to steel reinforced beams.
4- It was expected that the shear strength would exhibit a proportional variation with the ratio of shear reinforcement. However, increasing the shear reinforcement ratio from 0.90% on BS250 beams to 1.29% on BS175 beams seems not to increase the shear reinforcement strength, V_f. The shear reinforcement ratio is considered to vary linearly with shear strength of shear reinforcement by most codes. The small shear strength increase that happened from BS250GFRP1 to BS175GFRP1, at 8 kN, can be explained by the fact that smaller stirrup spacing increases the concrete confinement increasing the shear strength of concrete, V_c.
5- As mentioned above, the strain values measured on the shear stirrups were higher than the limits imposed by codes and guides, suggesting that the contribution of the stirrups is underestimated. It seems that the strength of the bent portion of the GFRP stirrups has few influence on the shear contribution of stirrups because the stirrups strains were higher than the strain limit at the bent portion, and the stirrups do not failed at bents.

6- To all beams, the angle of shear failure was in good agreement with the 45 degrees truss model. And generally, the beams failed by the shear crack closest to the support.
7- Although applying ACI 440.1R-06 [2] to predict the short-term deflections at service load overestimates this value for some of the beams and underestimates for others, the experimental values are close to the predictions.
8- Although the cracking pattern of GFRP beams and reference beams was similar, it was noticed that the shear cracks appeared for lower load values on the GFRP longitudinal reinforced beams, when compared with the steel longitudinally reinforced. This demonstrates that the lower axial stiffness of GFRP beams is responsible for a different cracking behaviour of the stresses distribution.
9- Shear crack widths exceeded the maximum allowed value of 0.50 mm according to several recommendations. Although this value is generally imposed for aesthetical reasons it is important to refer that it is also related to the effective development of the shear mechanisms and to the structural integrity of the element.
10- Another interesting finding was the fact that the beams longitudinally reinforced with steel but shear reinforced with GFRP solutions exhibited the best performance. The main reason is the fact that for being longitudinally reinforced with steel, the cracks were smaller and the integrity of the shear mechanisms was kept for longer, and thus the shear strength was higher. The pertinence of this finding is that these solutions are simultaneously economical and adequate for the use where corrosion is the main concern. This is because the shear reinforcement is located outer comparing to the longitudinal reinforcement and, therefore, it is the first to be corroded.

It was concluded that GFRP closed stirrups are a safe and effective alternative to steel stirrups. However, codes and guides are overly conservative of the shear strength of the shear FRP RC beams. Thus, these experimental results emphasized the need for further studies exploring the shear strength.

Chapter 3.

Experimental study of a solution that uses GFRP bars to replace the steel bars of reinforced concrete beams

This chapter describes the part of the experimental campaign whose purpose was to study the behaviour and performance of a rehabilitation solution with GFRP bars. The chapter is based on the scientific manuscript from the author submitted to the Engineering Structures Journal. For this reason, it is organized as the paper and starts with an introduction to the study and its objectives, followed by the experimental program where the specimens and the technique is described. Then results and discussion are presented. Finally some conclusions are drawn.

The corrosion of the steel reinforcement affects drastically the long-term durability of many reinforced concrete (RC) structures in the world, especially the ones near the sea. When this problem is detected at early stages, it is possible and important to repair the structure in order to restore its safety and avoid future hazards and more expensive interventions. The research work described in this paper is inspired on these cases as it proposes a rehabilitation solution to replace the tension steel reinforcement of a RC beam with GFRP bars, which is a material immune to corrosion.

The experimental campaign consisted of six full-scale RC beams subjected to a three-point bending test until failure. The specimens had stirrups without the bottom branch and were casted in two phases to simulate the replacement of the corroded and cracked bottom concrete. Two different GFRP reinforcement ratios were tested to assess the behaviour of the repaired beam regarding its service and ultimate states in comparison with the original beam with steel reinforcement. One of the solutions was able to restore both the deflection and the load capacity of the reference beam.

The joint between the two concrete layers and the absence of the bottom branch of the stirrups did not compromise this performance. The results are presented and discussed in terms of flexural capacity, failure modes, deflection, crack pattern, mid-span crack width and reinforcement strains. It was concluded that the presented rehabilitation solution is easy to implement, can be designed according to general FRP design guidelines, and is able to restore the serviceability and ultimate limit states of the original RC beam.

Keywords: GFRP bars; Full-scale test; Corrosion; Rehabilitation solution; FRP guidelines; Ultimate limit state; Serviceability limit state.

3.1 Introduction

Structural rehabilitation is becoming increasingly important nowadays. The amount of deteriorated structures, the frequency and the costs of rehabilitation interventions motivate the introduction of innovative materials and methods to rehabilitate structures. The service behaviour and the ultimate performance of reinforced concrete (RC) are shortened by the corrosion of steel reinforcement [30, 66]. The volume occupied by the corrosion products is greater than the initial volume of the reinforcement, increasing the tension exerted on the concrete, and consequently causing cracking and delamination. Corrosion of the reinforcement induced by chloride environments has a significant effect on the mechanical behaviour, and the loss of cross-sectional area and bond strength of reinforcement have a very important effect on the bending capacity [103]. Malumbela *et* al. [66] concluded that for a maximum mass loss of the longitudinal reinforcement of 1%, the flexural capacity was reduced by 0.7%. Currently, repairing, rehabilitating and strengthening solutions are being developed and tested using different materials and different layouts. Solutions with steel materials can have limited duration. Fibre Reinforced Polymers (FRPs) have been used in rehabilitation and strengthening of reinforced concrete structures because of their resistance to corrosion, high strength and light weight.

Many experimental studies [9, 15, 79, 97] have been conducted proposing FRP solutions with sheets or laminates which are externally bonded to restore the structural integrity, in cases of theoretical reinforcement mass loss from 5% to 15%. By optimizing the amount and the layout, the bonded FRP sheets are suitable for balancing the strength recovery and failure mode. It is possible to restore the yield and the ultimate capacity with the same or lower deflection than initially. To prevent delamination and debonding, Spadea, Bencardino*, et al.* [88] suggested that the strengthening for

flexure should be accompanied by the strengthening for shear. Thus, the best layout of bonded FRP sheets as reinforcement is a combination of a bonded sheet on the tension side anchored by U-shaped sheets. FRPs for rehabilitation and strengthening are often associated with prestressing techniques [38]. Many studies [38] have been conducted and several techniques are being developed to prestress FRP plates prior to bonding, which has already been proven to be an efficient solution. However these solutions may not be effective when applied to damaged beams with more than 50% mass loss of tensile steel. It is emphasized that additional research is needed for cases where corrosion is severe and part of the reinforcement is missing. Epoxy-bonded FRPs have limitations when applied at high temperatures, because of the rapid deterioration of the properties of the polymer matrix [37]. The use of cement base adhesives can be a solution for the application on structures located in hot regions or when there is a high danger of fire [49].

Rehabilitation solutions using FRP bars are not so frequent. One of the reasons may be that the FRP bar design as reinforcement is still uncommon, although this material has been available on the market for over 15 years in a wide variety of forms (different fibres and surfaces from the smooth or helical to the sand coated). Several factors, such as novelty, production costs, the low modulus of elasticity, the non-ductile behaviour, the different design philosophies, and the need to validate the behaviour, have been responsible for the low levels of its application. Several authors [2, 30] suggest that the analytical procedures developed for the design of reinforced concrete with steel bars in terms of ultimate loads, deflection and crack width are not applicable to the design of reinforced concrete with FRP bars (FRP RC) due to the mechanical property differences. Additionally, the design of FRP RC is generally governed by serviceability. However, the majority of codes and guidelines developed until now [2, 22], use the same equations developed for steel reinforced members, modified to account for the differences between the materials [2, 22]. Several authors [2, 22, 50, 92] have been studying the ultimate and service behaviour of FRP RC. In general, at the ultimate limit state, most of the guides and codes recommend the flexural design according to a compression failure due to its less catastrophic mode [30]. It forces the design of over-reinforced cross-sections, providing a reduction in service load deflections and crack width and lower FRP bars stress. It is suggested that compression failures present better member deformability and gradual member failure than FRP rupture [92].

Among the different fibres used to make FRPs, glass fibres are the most common as they are the least expensive. Glass fibre reinforced polymers (GRFP) can be made of E-glass, S-glass or Alkali resistant glass [22]. The flexural behaviour of GFRP RC beams is bilinear until failure, reducing stiffness after cracking. In serviceability, due to the lower modulus of elasticity of FRPs and to the different bonding properties, larger deflections and crack widths are expected than in steel RC

beams. Several models and approaches for predicting deflections and crack width have been proposed, but some controversy remains. Several authors [101] reported that the deflections of FRP RC can be predicted with the original ACI 318-11 [3] formulas developed for steel reinforced concrete. On the other hand, other experimental analyses [76, 91, 99] pointed out that the modifications proposed in ACI 440.1R-06 [2] relative to ACI 318-11 [3] are needed, achieving more accurate predictions with this approach. Other studies [18] propose different methods. It is also important to state that as the serviceability verification depends on bond and elasticity modulus, a certain equation can predict well the behaviour for one type of FRP bars but not for another of a different material or with a different surface [22, 30, 50]. By increasing the reinforcement ratio and the concrete strength, a larger number of cracks with smaller widths can be achieved.

In the formula to predict the deflection, the Yost *et* al. [56] and Toutanji and Saafi's [50] findings suggest that the effective moment of inertia is overestimated and that it is possible to establish a correlation between the degree of overestimation and the ratio between the reinforcement area and the balanced reinforcement area ($\rho_f/\ \rho_{fb}$): the higher the ratio $\rho_f/\ \rho_{fb}$, the lower the error of the effective moment of inertia value. They also proposed alternative equations for the effective moment of inertia and for deflection.

Furthermore, other studies [30] indicate the use of high strength concrete (HSC) to make better use of FRPs' properties.

Many experimental works of the near surface mounted (NSM) reinforcement technique were done to rehabilitate concrete structures damaged by corrosion[59]. This technique consists in bonding FRP rods with epoxy resins in undamaged areas of concrete cover. Results indicate that it is possible for repaired beams to achieve the same ultimate capacity as the control beam but differing in the failure mode[100] and showing a ductility reduction in comparison with traditional RC beams. However, a significant disadvantage of this technique is that the placing of the NSM rods is highly dependent on the quality of the concrete cover, which is frequently damaged by steel corrosion. If this is the case, this solution cannot be applied.

For all previously referred situations, the research described in this paper is significant since the behaviour of FRP RC beams is still not fully understood. Additionally, rehabilitation or repairing solutions using FRP sheets or textiles, or even the application of FRP bars with NSM, cannot be applied in many cases, such as when the reinforcement mass loss due to corrosion is high, when the concrete cover is extremely damaged or when it is not possible to increase the depth of the section. As a consequence of these facts, the rehabilitation solution in these cases tends to be the replacement of the corroded steel by new steel reinforcement. However, when the deterioration

of the RC structure is due to steel corrosion, the replacement of this material by another that is immune to this problem, such as GFRP, is an additional guaranty for a long-term duration of the rehabilitation solution.

The main objective of the present research is to simulate and assess the behaviour of a rehabilitation intervention using GFRP bars on RC beams, in cases of bottom steel reinforcement highly damaged by corrosion and which forces its total removal. An experimental campaign on six full-scale beams was carried out, with the removal of the corroded steel reinforcement being simulated, and a rehabilitation method was developed and applied using GFRP bars. The rehabilitated beams were subjected to three-point bending tests until failure and the load-deflection response was analysed and compared with a reference beam and with theoretical predictions.

3.2 Experimental program

A total of six full-scale RC beams (one reference and five rehabilitated beams) were cast and tested under three-point bending until failure. The beams were designated according to their characteristics as reference and rehabilitated with steel or GFRP reinforcement. The rehabilitated specimens were concreted in two phases at different dates to simulate the different material layers composed by the original and the rehabilitation concretes with different ages. Several other procedures were also performed to simulate the real conditions when the corroded tension reinforcement has to be removed, such as: use of closed stirrups without the bottom branch to simulate its total destruction due to corrosion; picking the tension surface of the beam to enhance the bonding between the different concrete layers (Figure 116 a)); drilling the intersections with other structural elements (for example columns) to insert a new reinforcement; and filling the holes with resin in the anchorage zone at the end of the longitudinal reinforcement (Figure 116 b) and c)).

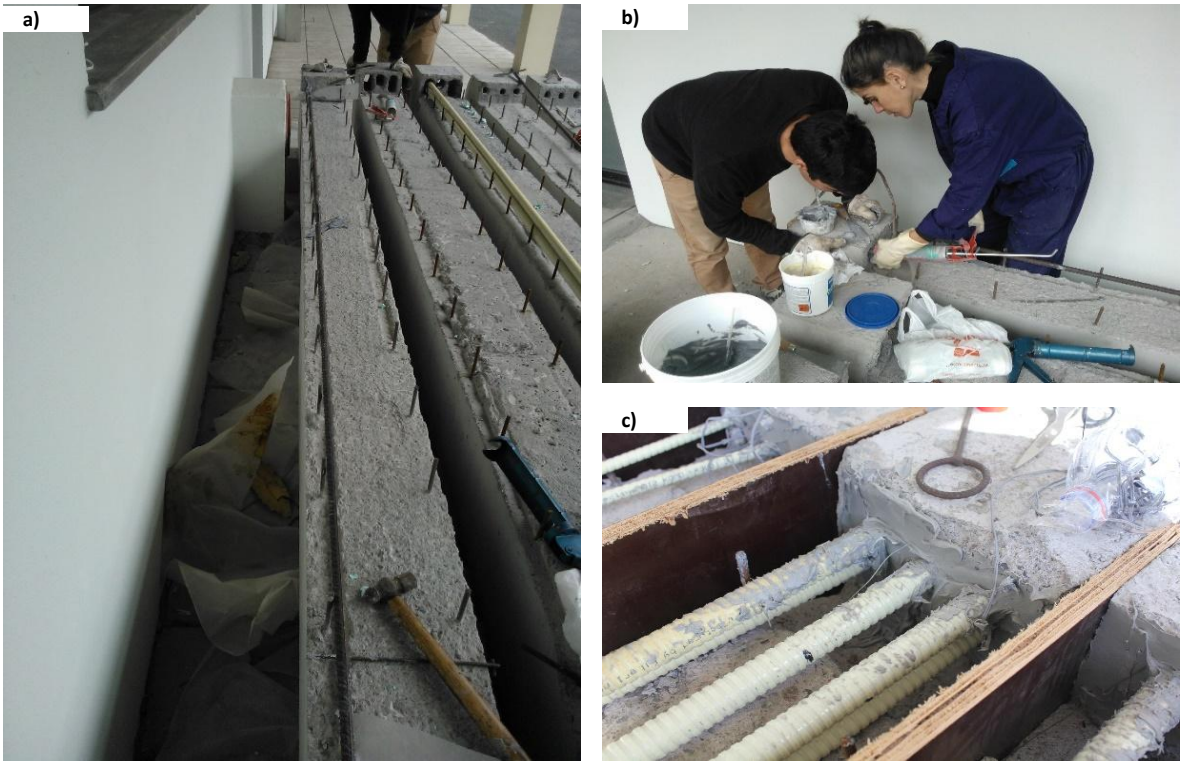

Figure 116 – Procedures to simulate real conditions: a) original layer after surface picking and drilled holes; b) filling the holes with resin; c) anchorage areas after reinforcement insertion and the filling of the holes

3.2.1 Material properties

3.2.1.1 Concrete

The concrete strength for all test specimens was a self-compacting (SCC) C30/37 because it represents a concrete class increasingly used in structures nowadays and besides, a high class of strength minimizes the cases of rupture for concrete crushing and promotes a better use of FRP properties. The concrete composition is presented in Table 45.

Table 45 – Concrete composition according to BETOMADEIRA information

SCC – EN 206-9[51] C30/37 XC4 (P) Cl 0.2 D16 SF2 SR2

Material	Water	Cement	Clinker	Fly Ash	Limestone filler	Additional minority constituents (EN-	Gravel 8/16	Gravel 4/10	Stone dust - AB 0/4	Sand 0/2	G SKy 548 (adjuvant)	Pozolith 390N (adjuvant)
Kg/m^3	185	350	280	100	47.5	22.5	200	575	661	402	5.8	3.5

Table 46 shows the concrete properties. The strength at 28 days of concrete was determined by compression tests of three cubic samples with 0.15m edge and three cylinders with 0.15 m in diameter and 0.30 m high. For additional information about the compression strength, a compression test was made on each beam testing day. The elasticity modulus, E, was also experimentally determined since it is particularly important in SCC because it varies with the lithological type of its aggregates. Although its value tends to increase with increasing compression strength, this increase appears to be lower when fly ash and limestone elements are introduced [73]. At 28 days the expected value for the elasticity modulus of C30/37 was at least 33GPa [1], but tested samples had a lower value.

Table 46 – Concrete properties

Beam designation	Concrete									
	Concrete Age [Days]		Cylinder/cube strength, $f_{cm,28}$ [MPa]		Cylinder strength, f_{cm} [MPa]		Elasticity Modulus, $E_{cm\ 28}$ [GPa]		Elasticity Modulus, E_{cm} [GPa]	
	Original Layer	Rehab Layer	Original Layer	Rehab Layer	Original Layer	Rehab Layer	Original Layer	Rehab Layer	Original Layer	Rehab Layer
REF	253		40.4 / 46.9		47.7		27		29	
REHABSTEEL	281	48	40.4 / 46.9	39.9 / 41.5	47.9	39.9	27	23	29	26
REHABGFRP1A	295	62			48.0	39.9				
REHABGFRP1B	323	90			48.2	39.9				
REHABGFRP2A	282	49			47.9	39.9				
REHABGFRP2B	287	54			48.0	39.9				

3.2.1.2 Steel reinforcement bars

The steel grade of reinforcement used in the reference beams and in compression reinforcement of all beams was A500. In order to determine the mean values of yield stress (f_y), the maximum tensile (f_t) and the elasticity modulus (E), three samples of each diameter used were tested in pure tension, according to standard NP EN ISO 6892-1:2012 [53]. Reinforcement bars of 12 mm and 16 mm were used as longitudinal reinforcement and bars of 8 mm in diameter were used as shear reinforcement in the form of stirrups. The results of pure tension tests are presented in Table 47 and the test set-up is similar to that shown in Figure 118 b).

Table 47 - Yield stress, tensile strength and elasticity modulus of the steel reinforcement bars

Φ [mm]	Yield stress, f_y [MPa]		Tensile strength, f_t [MPa]		Elasticity modulus, E [GPa]	
	Sample	Mean	Sample	Mean	Sample	Mean
8	763.0	670	834.4	743	251.2	230
	603.7		674.5		210.4	
	644.8		717.2		227.4	
12	628.3	605	749.0	721	202.7	209
	540.7		660.7		208.8	
	648.7		762.9		214.0	
16	718.2	682	844.6	820	206.3	218
	648.8		810.8		206.0	
	680.4		805.8		241.9	

3.2.1.3 GFRP reinforcement bars

The type and shape of the GFRP bars used in this experimental study are shown in Figure 117. This reinforcement is a straight bar with a helically grooved surface to increase the bonding to the concrete and headed ends to enhance the anchorage capacity. To compare with the property values presented by the producer, three straight bar samples of each diameter, 12 mm and 25 mm, were tested in pure tension to determine the stress-strain relationship and the tensile strength (f_f).

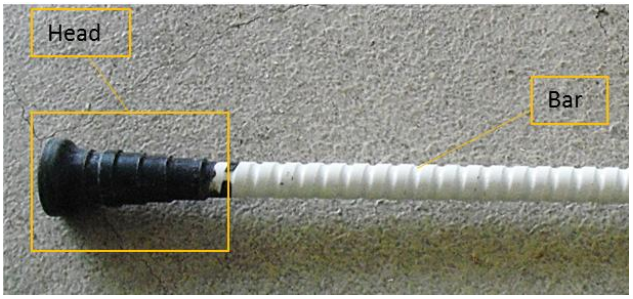

Figure 117 – Sample of GFRP bar with polymeric conic head at the end

The properties of the GFRP bars according to the producer are presented in Table 48.

Table 48 – GFRP bars properties according to the producer [85]

ComBAR	Exterior Diameter	Interior Diameter	Cross-sectional area	Specific mass	Tensile strength, f_f	Elasticity modulus, E_f	Bond Strength, f_{bd}
	[mm]	[mm]	[mm^2]	[Kg/m]	[MPa]	[GPa]	[MPa]
12	13.5	12	113	0.30	1350	60	3.0 (For C30/37)
25	27	25	491	1.22	1100		

The conic end heads are made of polymeric concrete [84] and they are cast at the ends of the straight bars. Their geometry insures minimal tensile splitting forces at the heads, which allows the position of the bar very close to the concrete surface and where it is still possible to develop its full design force. In addition, these heads reduce the required bonding length, lb, of the straight bars [84].

A solution was developed to prevent the crushing of the GFRP bars at the ends due to the clamping forces during the pure tension tests. It consisted of square tubes formed by two welded L-shaped gutters 200 mm long filled with resin at the ends of the testing specimen as shown in Figure 118 a). As shown in Table 49, the thickness and width of the tubes were different for each GFRP bar diameter [43]. This solution had already been tested by Santos [81, 82].

Table 49 – Dimensions of L-shaped gutters according to the diameter of GFRP bar [43]

GFRP bar diameter [mm]	L-shaped gutter steel class	Wall thickness [mm]	Width of L-shaped gutter [mm]
12	S275	3	35
25	S275	5	50

Due to the brittle failure of the GFRP bars in pure tension tests a video extensometer was used instead of the traditional electronic extensometer. Two small metal bars were fixed on the specimens to create two fixed reference points for the video camera image, and their distance was measured in real-time and converted to strains during the test. (Figure 118 b) and c)).

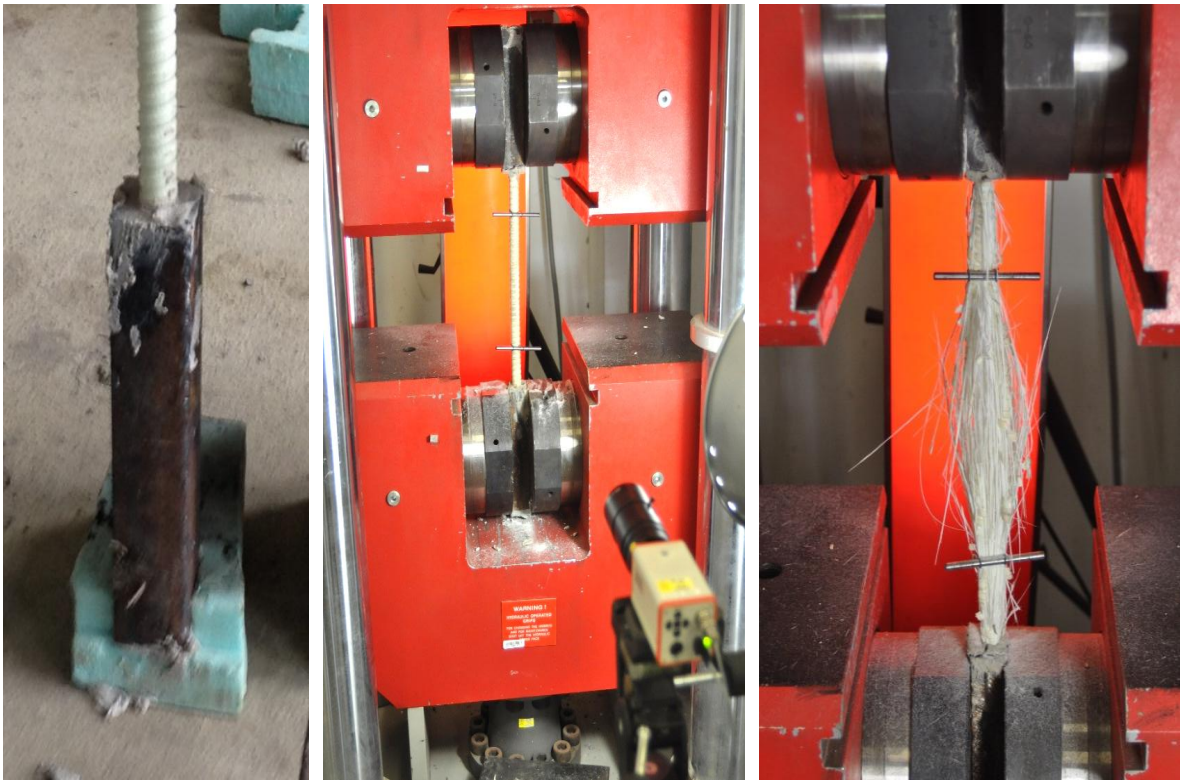

a) b) c)

Figure 118 – Pure tension tests on GFRP bars: a) Solution developed to test GFRP bars in pure tension; b) Test set-up with video extensometer; c) GFRP bar failure

The results of the pure tension tests are presented in Table 50. The obtained values are in agreement with the producer for the 12 mm bars, with the exception of the 25 mm bars' tensile strength, which were lower than expected due to the premature failure at the clamped ends.

Table 50 - Mechanical properties obtained at pure tension test [43].

ComBAR [mm]	Tensile Strength [MPa] [MPa]		Modulus of elasticity [GPa]		Ultimate strain [‰]	
	Sample	Mean	Sample	Mean	Sample	Mean
12	949.6	1200.0	61.8	60.0	15.4	19.0
	1315.3		61.3		21.5	
	1336.8		61.3		21.5	
25	777.3	729.0	59.3	64.0	13.1	11.0
	610.9		68.7		8.9	
	798.5		65.0		12.3	

The Figure 119 represents the stress–strain diagram of the six tested GFRP bars, where it is possible to notice a linear diagram until failure with no yielding.

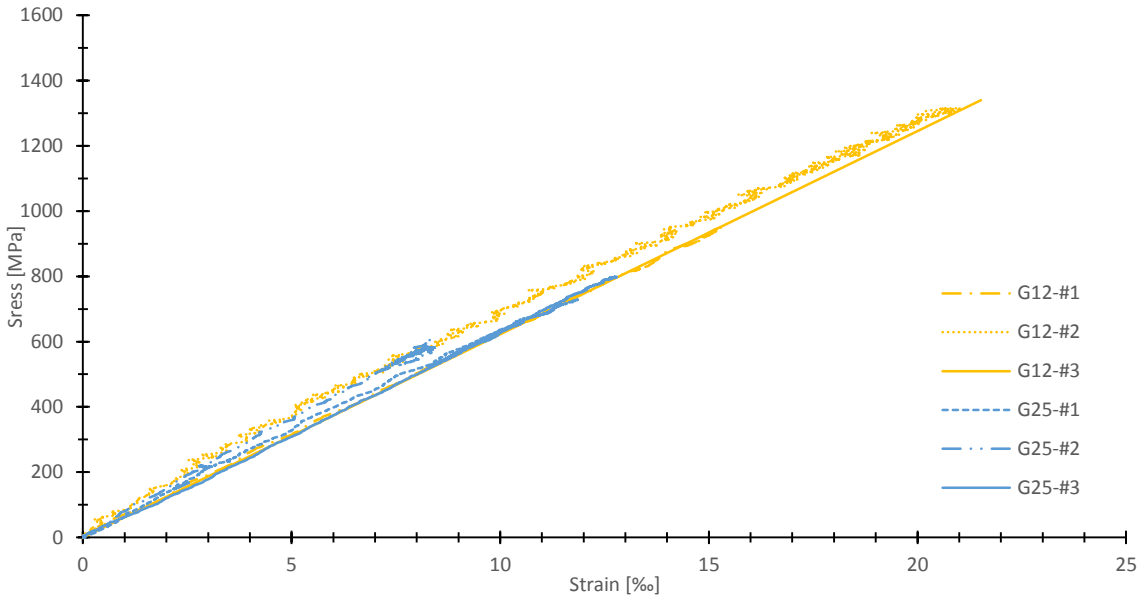

Figure 119 - Stress-strain diagram of the tested GFRP bars [43]

3.2.1.4 Filling resin for the anchorage of the reinforcement in the rehabilitation beams

The material used for the anchorage of the reinforcement in the rehabilitation solution was a two-component epoxy resin with very low shrinkage and with a bond strength to concrete higher than 3 MPa. Small amounts have to be prepared each time and it starts to harden 30 minutes after its mixture at 23°C. Detailed information about the product and its bond characteristics can be found in the manufacturer's technical information [68].

3.2.2 Test set-up

3.2.2.1 Beam specimens

A total of 6 full-scale RC beams were tested under three-point bending until failure. The beam specimens were 4.30 m long with a free span of 4.00 m and a rectangular cross-section of 0.25 x 0.40 m^2. In all specimens, a compressive longitudinal reinforcement was used of two steel bars 12 mm in diameter, a shear reinforcement of 8 mm diameter stirrups with 0.25 m spacing and a

concrete cover of 2.5 cm. Four different types of beams were considered according to their characteristics:

1) 1 RC beam as reference (REF);
2) 1 rehabilitated beam with steel reinforcement (REHABSTEEL) to have similar behaviour as the reference beam;
3) 2 rehabilitated beams with GFRP reinforcement with the same load capacity as the reference beam (REHABGFRP1 A and B);
4) 2 rehabilitated beams with GFRP reinforcement with the same mid-span deflection as the reference beam (REHABGFRP2 A and B).

The REF specimen is a non-deteriorated conventional steel RC beam with two bottom longitudinal 16 mm diameter bars (2ϕ16) to determine the reference behaviour and values of the load capacity and the mid-span deflection to be reproduced by the other five rehabilitated beams. The REF beam was concreted in a single phase, and its stirrups had the conventional closed shape with four branches. The rehabilitated beams were concreted in two phases and their stirrups had only three branches, reproducing a real situation where the bottom branch had already been corroded. This procedure was adopted to evaluate the influence of different concrete layers and the absence of the stirrup bottom branch on the behaviour of the rehabilitated beams.

The REHABSTEEL specimen is a rehabilitated beam with the same cross-section geometry and steel reinforcement as the REF beam and therefore should exhibit similar behaviour. The objective of this beam was to conclude if the rehabilitation solution with the new concrete layer and the absence of the stirrup bottom branch would affect the performance of the rehabilitated beam.

The REHABGFRP1 - A and B specimens are equal rehabilitated beams with three bottom GFRP longitudinal 12 mm diameter bars (3ϕ12) designed to have the same ultimate load as the REF beam, keeping the cross-section geometry. Due to the lower modulus of elasticity of the GFRP material in comparison with steel, it is not possible to obtain the same deflection in these beams as in the REF beam. In fact, considering that the steel reinforcement area of the REF beam is 18.6% higher and its modulus of elasticity is 3.6 times higher, a significantly higher deflection is expected in the REHABGFRP1 beams.

The most efficient solution to design a rehabilitated beam with GFRP bars with the same load capacity and deflection as the reference beam is to increase the height of the cross-section. However there are two main problems with this solution. It must be possible from an architectural point of view and most importantly it may have some deficiencies in its shear behaviour due to the fact that the stirrups vertical branches become too short, only overcome by a shear strengthening

which would largely complicate the solution. Another possibility within the solution of increasing the height of the beam is to keep the longitudinal bars in the original position at the bottom of the stirrups vertical branches, meaning that the rehabilitated beam would have a higher concrete cover. Nevertheless, none of these possibilities were tested because it was decided in this research work to keep the original geometry of the specimen, which was the easiest and the best solution to avoid compromising the shear behaviour of the rehabilitated beam.

Because of this issue, the REHABGFRP2 - A and B specimens are equal rehabilitated beams with the same cross-section geometry as the REF beam and five bottom GFRP longitudinal 25 mm diameter bars (5ϕ25) designed to have the same service mid-span deflection.

A schematic representation of the test set-up and the different cross-sections are shown in Figure 120, Table 51 presents information about all reinforcement in all beams and a detailed description of the tests instrumentation used is presented below. Due to the three-point bending test configuration and the 4.0 m span, it is possible to conclude that the ratio between the applied load and the bending moment is one.

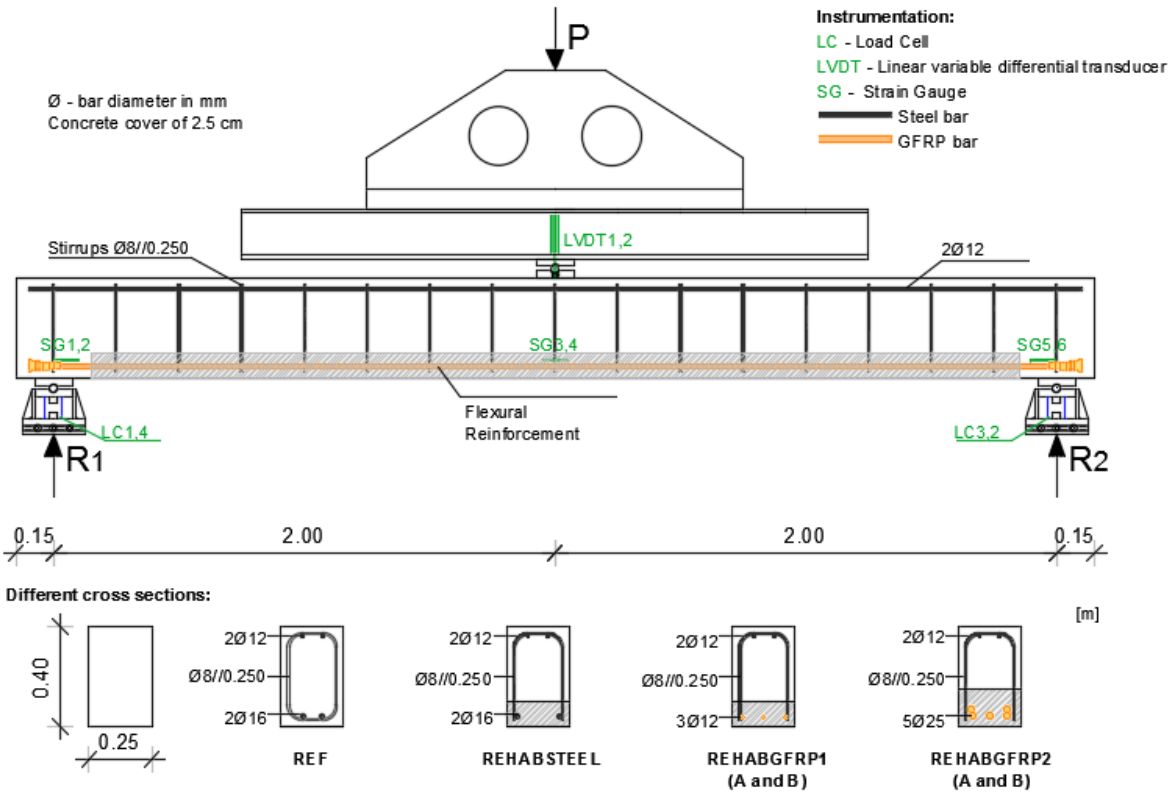

Figure 120 – Test set-up and specimens configuration

Table 51 – Beams reinforcement

Beam Designation	Tension Reinforcement			Compression Reinforcement			Transversal Reinforcement		
	Type	Bars	ρ (%)	Type	Bars	P (%)	Type	Bars	P (%)
REF	Steel	2ϕ[1]16 4.02cm²	0.40						
REHABSTEEl									
REHABGFRP1 A	GFRP	3ϕ12 3.39cm²	0.34	Steel	2ϕ12 2.26cm²	0.226	Steel	ϕ8//0.250[2]	0.40
REHABGFRP1 B									
REHABGFRP2 A		5ϕ25 24.54cm²	2.50						
REHABGFRP2 B									

1 – ϕ is the bar diameter in millimetres
2 - ϕ8//0.250 means two branches of 8mm stirrups spaced at 25cm

3.2.2.2 Tests instrumentation

The instrumentation used during the loading tests is indicated in Figure 120 and Figure 121. At each support there were two load cells (Figure 122 b) (LC1 and LC4; LC2 and LC3), each one with 200 kN load capacity, to monitor the reaction forces). Their sum of values is the applied load. Two linear variable differential transducers (LVDT1 and LVDT2) Figure 122 c) with a maximum capacity of 100 mm were installed on each beam at the mid-span to measure the deflection. These sensors were placed on both sides and on top of the beams, as shown in Figure 121, to prevent them being damaged during the tests.

The tension reinforcement bars were instrumented with six glued strain gauges (SG1 to SG6) to monitor the strains at mid-span and at each support (two at each location) According to the manufacturer, the used strain gauges are indicated for general use and are made of a single element, a foil of the elements copper and nickel with a length of 5 mm. The maximum strain capacity is of the order of 21±1‰, the gauge factor (GF) is 2.13±1% and the resistance is 120±0.3Ω[90].

The crack widths were measured manually using a monocular lens with an accuracy of 0.05mm (Figure 122 a).

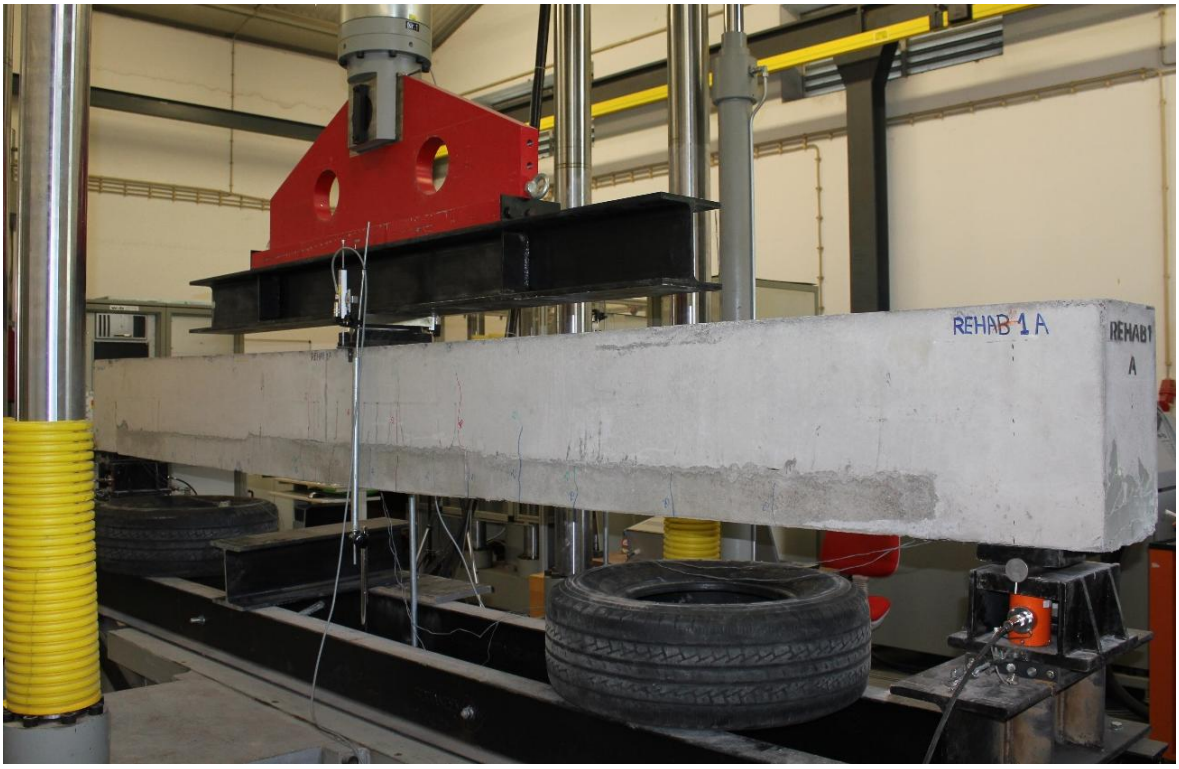

Figure 121 –Beam test set-up

(a) **(b)** **(c)**

Figure 122 – Instrumentation used in the tests: a) Lens used for the crack width measure; b) Load-cell; c) LVDT

3.2.2.3 *The production of the beam specimens and the rehabilitation procedure*

To simulate the real situation where the corroded steel tension reinforcement has to be removed, the beam specimens were concreted in two phases. The main steps of the production of the beam specimens and their rehabilitation procedure are presented and summarized in Figure 123.

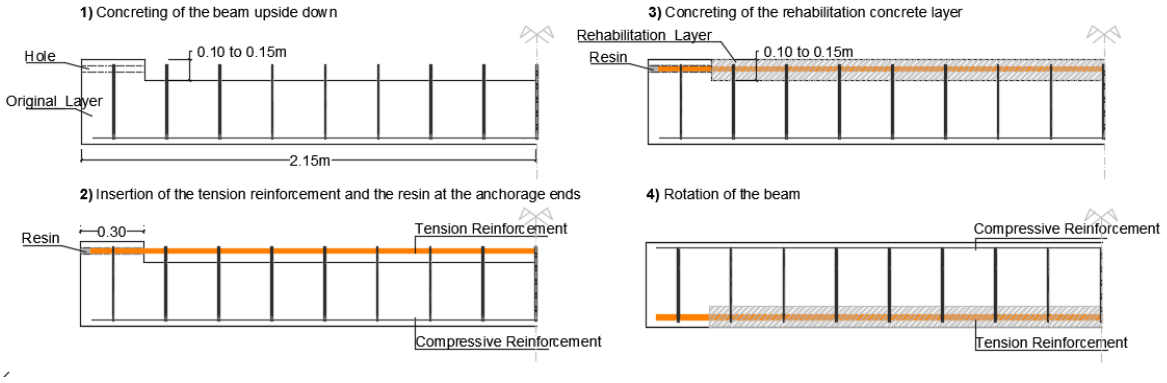

Figure 123 - Steps of the beam specimen production and its rehabilitation procedure: 1 – Concreting of the first layer; 2 – Insertion of the GFRP tension reinforcement; 3 – Concreting of the second layer; 4 – Rotation of the beam

The beams were produced at LREC[1] in an upside-down position in order to facilitate the operations to simulate the rehabilitation procedure. In the first phase of their production the specimens were concreted from the top until the tension reinforcement level. The support areas were fully concreted in this phase to simulate the intersection with an existent 0.30 x 0.25m^2 column. The main stages of this phase are presented in Figure 124. The formworks were filled with concrete until it reached the desired level, which was 0.10 m from the top for REHABSTEEL and REHABGFRP1 and 0.15 m for REHABGFRP2. These values were considered to ensure that the new reinforcement would be properly covered by the rehabilitation concrete layer. Then moulds were positioned at the ends of the beams and these areas were filled with concrete until the top. These negatives were introduced in the specimens to avoid the drilling of the holes of the corroded reinforcement, which had to be made in a real situation.

[1] LREC - Regional Laboratory of Civil Engineering

Figure 124 - First stage of the specimen's production: a) filling the formworks with concrete until it reaches the tension reinforcement level; b) insertion of the negatives at the supports; c) filling with concrete the support areas

The mould was removed after the hardening of the concrete, the holes for the new reinforcement were enlarged and the surface was chiped with a pneumatic hammer. The tension reinforcement bars were introduced and the holes were sealed with a two-component epoxy resin. After mixing the components the resin was applied with a silicone spray to prevent voids. After this, the rehabilitation layer was concreted in such a way as to ensure the proper cover of the reinforcement. These stages are presented in Figure 125. Before testing, the beams were rotated to the correct position (Figure 123).

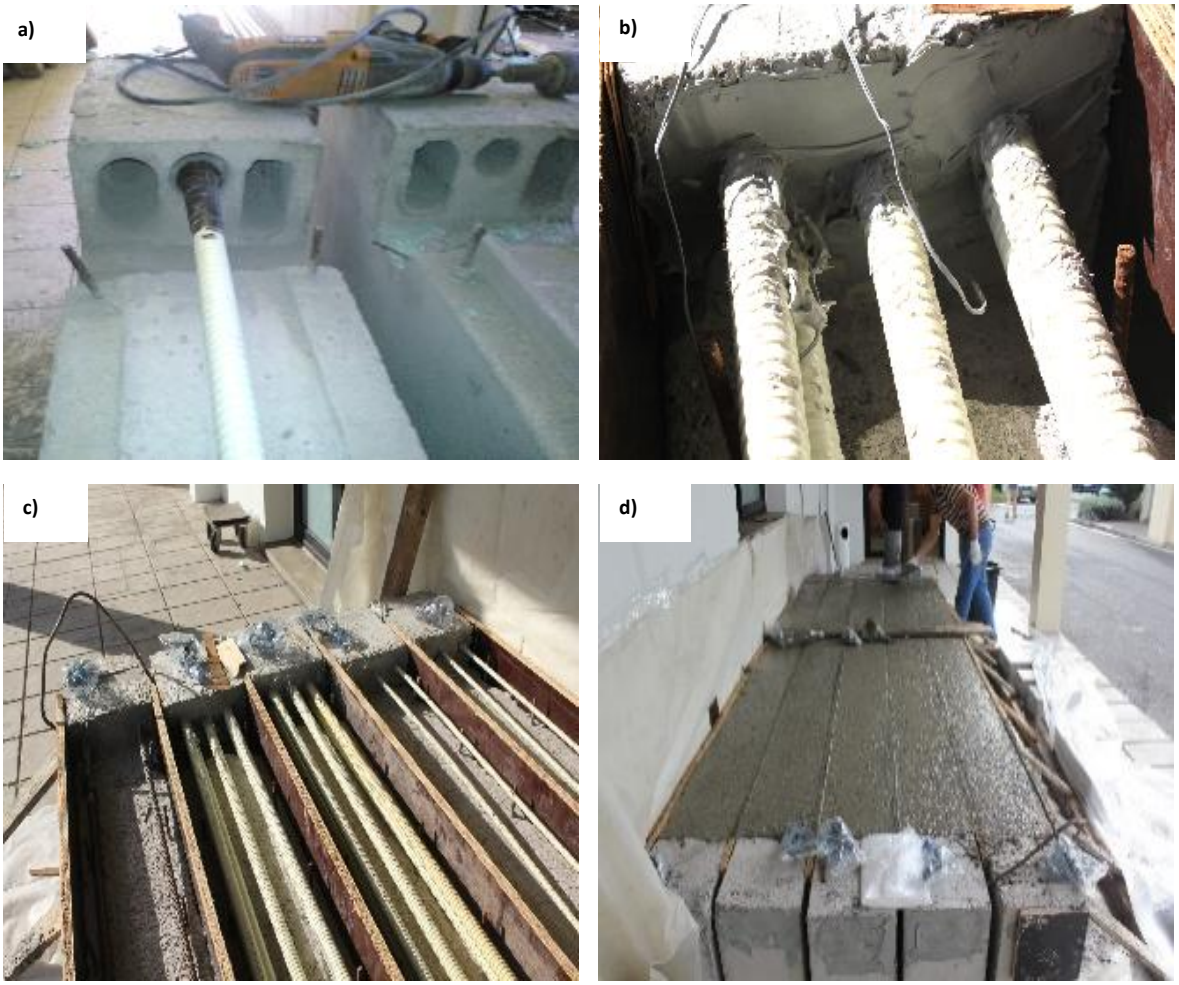

Figure 125- Steps of the rehabilitation stage: a) enlargement of the holes, concrete surface pricking and reinforcement insertion; b) and c) sealing of the anchorage holes; d) rehabilitation layer concreting

3.2.2.4 Tests loading history

All beam specimens were tested in a three-point bending test, with a free span of 4.0 m and the load was applied using a 1500 kN hydraulic actuator. The actuator, the load cells, the strain gauges and the LVDTS were connected to a data acquisition system to continuously monitor and record the values. The loading was controlled by force and its history up to failure was divided into 5 kN steps to allow a beam inspection at the predicted load values of the different stages of the beam's behaviour: the cracking load, the mean and the design values of the yielding and failure loads. Pictures were taken and the development of the cracking pattern was visually observed and marked on the side of each beam. The crack width was controlled on cracks near mid-span. In each test, three total unloading were considered to assess the deflection recover ability of the beam. The first was at 10 kN and full recovery was predicted since at this value the beams were not expected to be cracked. The second and third discharges were near the predicted values of the cracking and the

service loads respectively of each specimen. The cracking load was also determined from the loss of stiffness on the load-deflection relationships obtained from the tests. The service load of each beam was considered to be 30% of its flexural capacity, as suggested by some researchers [30]

3.2.3 Results and discussion

3.2.3.1 Theoretical predictions

Before the tests a theoretical prediction of the cracking moment, the failure moment and the mid-span deflection values for each beam was made based on the ACI 440.1R-06 [2], FIB-40 [22] and EC2 [23]. The equations used for the theoretical predictions of the test results and for a design point of view are indicated in the following sections. The obtained values are presented in the tables within the experimental results in section 3.2 to establish a comparison.

3.2.3.2 Cracking moment

An actual beam needing rehabilitation due to the corrosion of the steel reinforcement is already cracked due to this problem and due to the service load. However, in the present research work it was assumed that the steel corrosion only occurred at the bottom of the beam, which is usually the most exposed side to the aggressive environment, and therefore the consequent concrete delamination did not occur in the whole element. Since the removed tensile concrete height was 0,10 m and 0,15 m, which corresponds to 25% and 37,5% of the beam total height respectively, it is supposed that all the cracked concrete is located in this area in the majority of the cases that are worth being repaired. Therefore, it is assumed that the repaired beam begins its performance from an uncracked state and the cracking moment is the boundary between this state and the cracked state.

The cracking moments are directly related to the concrete's tensile strength and were estimated using Equation (157) from ACI 440.1R [2], where f_c' is the compressive strength of concrete [MPa], $I_g$is the cross-section gross moment of inertia [mm^4], h is the cross-section depth [mm] and M_{cr} is the cracking moment [Nm].

$$M_{cr} = \frac{2 \cdot \left(0.62\sqrt{f_c'}\right) I_g}{h} \quad (157)$$

The cracking moments [Nm] can also be estimated with Equation (158).

$$M_{cr} = f_{ctm} \frac{bh^2}{6} \quad (158)$$

Where f_{ctm} is the mean tensile strength [Pa], b and h are respectively the width and depth [m].

3.2.3.3 Flexural capacity

The GFRP RC beams were designed for a bending failure mode by concrete crushing under the over-reinforcement criterion. This is the usual design concept for concrete reinforced with FRP according to ACI 440.1R-06 [2]. Several authors [22, 40, 50] have studied the bending behaviour, and observed that the concrete crushing failure provides a better energy absorption, better member deformability, more gradual failure, lower deflections and crack widths and a relatively more ductile failure. The balanced failure is the case when the strains in the concrete and in the GFRP bars reach their limits simultaneously and the balanced reinforcement ratio is the limit between the compression and tension failure. This is why the reinforcement ratio, ρ_f, calculated from Equation (159) is compared with the balanced reinforcement ratio, ρ_{fb}, which in the ACI 440.1R-06 [2] is given by Equation (160), where A_f is the reinforcement area [mm^2], b is the width of the rectangular cross-section [mm], d is the distance from the extreme compression fibre to the centroid of the tension reinforcement [mm] and β_1 is a coefficient obtained by Equation (161). The variables f_c', ε_{cu}, f_{fu}, and E_f, are respectively the concrete compressive strength [MPa], the concrete ultimate strain, the ultimate FRP tensile strength [MPa] and the FRP modulus of elasticity [MPa]. With the same principle, Pilakoutas *et* al. [77] derived Equation (162) from EC2 [23]:

$$\rho_f = \frac{A_f}{bd} \quad (159)$$

$$\rho_{fb} = 0.85 \cdot \beta_1 \frac{f_c'}{f_{fu}} \frac{E_f \varepsilon_{cu}}{E_f \varepsilon_{cu} + f_{fu}} \quad (160)$$

$$\beta_1 = \begin{cases} 0.85 + \left[\frac{-0.05}{7}(f_c' - 28)\right] \; for \; f_c' \geq 28MPa \\ 0.85 \; for \; f_c' < 28MPa \end{cases} \quad (161)$$

$$\rho_{fb} = \frac{0.81(f_{cm})\varepsilon_{cu}}{f_{fk}\left(\frac{f_{fk}}{E_f} + \varepsilon_{cu}\right)} \quad (162)$$

where f_{cm} is the mean value of concrete compressive strength [MPa] and f_{fk} is the tensile strength characteristic value of the FRP reinforcement [MPa].

The minimum reinforcement ratio required for a compression failure must be higher than the balanced ratio. Compression failures are in the form of crushing and spalling of the concrete near the mid-span or beneath the load points [40].

The ACI 440.1R-06 [2] uses Equation (163) to calculate the moment capacity (nominal moment), M_n, of a rectangular concrete cross-section. For failure due to concrete crushing the moment capacity is given in terms of FRP reinforcement,

$$M_n = \rho_f f_f \left(1 - 0.59\frac{\rho_f f_f}{f_c'}\right) bd^2 \tag{163}$$

where f_f is the FRP reinforcement tensile stress [MPa] obtained from Equation (164),

$$f_f = \left(\sqrt{\frac{\left(E_f \varepsilon_{cu}\right)^2}{4} + \frac{0.85\beta_1 f_c'}{\rho_f} E_f \varepsilon_{cu}} - 0.5 E_f \varepsilon_{cu}\right) \leq f_{fu} \tag{164}$$

where f_{fu} is the FRP reinforcement design tensile stress, considering reductions for service environment [MPa], obtained by the product of the environmental factor [-], C_E, and the guaranteed tensile strength of an FRP bar, [MPa], ${f_{fu}}^*$.

The FIB 40 [22] suggests that in the case of concrete failure, the ultimate moment resistance, M_u, can be obtained by Equation (165),

$$M_u = f_{cd} bd^2 \left(0.8\frac{\varepsilon_{cu}}{\varepsilon_f + \varepsilon_{cu}}\right)\left(1 - \frac{0.8}{2}\frac{\varepsilon_{cu}}{\varepsilon_f + \varepsilon_{cu}}\right) for\ f_{ck} \leq 50MPa \tag{165}$$

where f_{cd} is the concrete compressive strength design value [MPa] and ε_f is the FRP reinforcement tensile strain [MPa], which is given by Equation (12).

$$\varepsilon_f = \frac{-\varepsilon_{cu}\sqrt{\varepsilon_{cu}^2 + \frac{3.2 f_{cd}\varepsilon_{cu}}{\rho_f E_f}}}{2} \tag{166}$$

The flexural capacity of the conventional RC beams with steel reinforcement (REF and REHABSTEEL) was obtained according to the EC2 [1, 23].

3.2.3.4 Deflection

To predict the deflection of a RC beam with GFRP bars, several studies [22, 76] proposed modifying the inertia with Branson's equation with the introduction of some modification factors. Others suggest an equivalent moment of inertia derived from the curvature calculations [2, 22]. Theoretical predictions in the present work were calculated using Branson's effective moment of inertia equation (167), I_e, modified by the factor β_d of the ACI 440.1R-06 [2], where M_{cr} is the cracking moment [kNm] and M_a is the moment [kNm] for the considered load.

$$I_e = \left(\frac{M_{cr}}{M_a}\right)^3 \beta_d I_g + \left[1 - \left(\frac{M_{cr}}{M_a}\right)^3\right] I_{cr} \leq I_g \tag{167}$$

$$\beta_d = 0.2\left(\frac{\rho_f}{\rho_{fb}}\right) \leq 1.0 \tag{168}$$

To predict the deflection of a steel RC beam the ACI 318-11 [3] formulation was used.

3.2.3.5 Mid-span strain

The bar strains at the mid-span of the beams were predicted with equation (169) as a function of: the bending moment, *M* [kN.m], the bar cross-section area, *A* [m^2], the modulus of elasticity, *E* [GPa], and the *d* [m]. This formula is obtained from the equilibrium equations of the cross-section. With a free span length of L = 4.0m, the bending moment at mid-span is equal to the applied load, P, according to: M = P * L / 4 = P.

$$\varepsilon = \frac{M}{0.9dAE} \tag{169}$$

3.2.4 Experimental results

3.2.4.1 Cracking moment and deflection at service load

During each test the first crack was visually observed and the corresponding value was recorded, which was also confirmed by the load-displacement relationships when a stiffness loss was

detected. The comparison between the experimental results and the theoretical predictions are listed in Table 52. In general, the cracking moments ranged from 24 kNm to 33 kNm with an average value of 28.7 kNm. Comparing the mean cracking moments between the REHAB beam specimens, it is possible to see that the REHABGFRP1 had a slightly lower value than the REHABGFRP2, which can be a result of its lower longitudinal reinforcement.

Figure 126 shows the ratio between the experimental-to-predicted values of the deflection at service load. The results of the deflection at service load are also presented in Table 52. It is possible to conclude that the main objective of the REHABGFRP2 beams was achieved, which was having the same deflection as the reference beam (REF) (5.00 mm), since the REHABGFRP2A beam presented almost the same value (5.15 mm) and the average of both beams was 5.84 mm. As expected, the average deflection of the REHABGFRP1 beams was 9.8 mm which was almost twice of the REF beam.

Table 52 – Summary of the experimental-to-predicted values of the cracking moment and the deflection at service load

Beam	Cracking Moment, M_{cr}					Service Load $0.30M_u$	Service Deflection, δ		
	Experimental	EC2 [23]	$M_{cr}^{exp}/M_{cr}^{pred}$	ACI [2]	$M_{cr}^{exp}/M_{cr}^{pred}$		Experimental	ACI [2]	$\delta^{exp}/\delta^{pred}$
	[kN.m]	[kN.m]		[kN.m]		[kN]	[mm]	[mm]	
REF	29.75		0.93		1.05		5.00		1.15
						30.00		5.25 4.34	
REHABSTEEL	25.47		0.80		0.90		5.50		1.27
REHABGFRP1A	24.32		0.76		0.86		10.65		1.69
		32.00		28.33		30.00		9.80 6.32	
REHABGFRP1B	32.00		1.00		1.13		8.93		1.41
REHABGFRP2A	32.99		1.03		1.16		5.15		1.19
						30.00*		5.84 4.32	
REHABGFRP2B	27.82		0.87		0.98		6.52		1.50

* The value that corresponds to 0.30Mu of the REHABGFRP2A and B is 50.00kN. However the 30kN was considered because the design condition of these beams was to have the same deflection as the REFREHAB at its service load

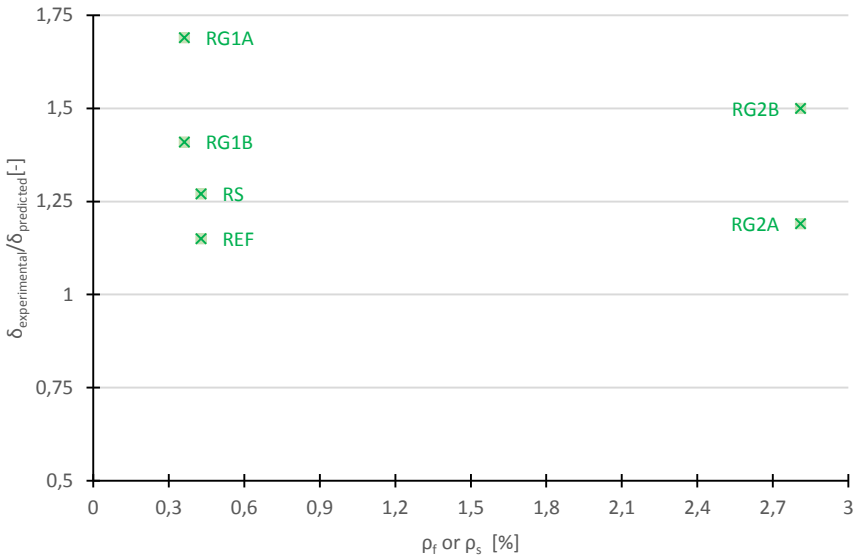

Figure 126 - Ratio between the experimental and the predicted values in function of deflection. Where REF – REF beam; RS – REHABSTEEL; RG1A – REHABGFRP1A; RG1B – REHABGFRP1B; RG2A – REHABGFRP2A; RG2B – REHABGFRP2B

3.2.4.2 Flexural capacity and failure modes

The REHABGFRP beams were designed as over-reinforced to fail by concrete crushing, whereas the REF and the REHABSTEEL beams were designed as under-reinforced to fail by steel yielding.

Concerning the beams with bottom longitudinal steel reinforcement, the REHABSTEEL beam presented a load-carrying capacity (89.81 kN) only 4.5% lower than the REF beam (94.06 kN), which proves that the rehabilitation solution works and is not affected by the new concrete layer.

The main objective of the REHABGFRP1 beams was achieved, which was having the same load capacity as the reference beam (REF) (94.06 kN), since the REHABGFRP1A beam presented the exact same value (94.03 kN) and the average of both REHABGFRP1A and B beams (89.94 kN) was only 4.4% lower.

Comparing the rehabilitated beams with GFRP bars (REHABGFRP1 and REHABGFRP2), the ρ increase of approximately eight times, from 0.362% to 2.810% corresponded to an average increase of 215.5% in load capacity, from 89.94 kNm to 193.85 kNm. On the other hand, as demonstrated in the previous section, the REHABGFRP2 beams achieved their design objective of having the same deflection as the reference beam.

Table 53 –Summary of the experimental and the predicted ultimate moments for the tests with the corresponding design values

Beam	ρ_{fb}	ρ_f or ρ_s	Experimental			Predicted				Design			
						ACI [2]		FIB 40 [22] / EC2 [23]*		ACI [2]		FIB 40 [22]/ EC2 [23]*	
			M_u	M_{Mean}	δ	M_u	exp/ pred	M_u	exp/ pred	M_u	exp/ pred	M_u	exp/ pred
	%	%	[kNm]	[kNm]	[mm]	[kNm]		[kNm]		[kNm]		[kNm]	
REF	(-)	0.429	94.1	91.9	90.5	89.4	1.05	88.7	1.06	(-)	(-)	(-)	(-)
REHABSTEEL			89.8		98.9		1.00		1.01	(-)	(-)	(-)	(-)
REHABGFRP1A	0.27	0.362	94.0	89.9	89.3	87.4	1.08	92.1	1.02	70.8	1.33	58.3	1.61
REHABGFRP1B			85.9		66.0		0.98		0.93		1.21		1.47
REHABGFRP2A	0.26	2.81	181.5	193.9	59.1	205.2	0.94	208.6	0.87	136.2	1.33	125.7	1.44
REHABGFRP2B			206.2		67.0		1.00		0.99		1.51		1.64

* It was used the formulas of the EC2 [23] or the FIB40, whether the prediction/design result was for the reinforced concrete beam with steel or GFRP bars, respectively.

The loading capacity of the rehabilitated beams with GFRP bars was also predicted according to ACI 440.1R-06 [2] and FIB 40 [22] (proposed modifications to EC2 [23] and the results are presented in Table 53. The experimental to predicted values ratio using FIB 40 [22] was non-conservative for REHABGFRP1B and for REHABGFRP2A (Figure 127), whereas the ACI 440.1R-06 [2] predictions were conservative. One reason for the differences between ACI 440.1R-06[2] and FIB 40 [22] predictions is the fact that the ultimate concrete compression strain is considered as 3.0‰ and 3.5‰, respectively [30].

The ultimate loads from a design point of view, considering the safety factors, are shown in Table 53. In general, it is possible to conclude that the beams had an ultimate capacity on tests that ranged from 1.2 to 1.5 times the design ultimate load value of ACI 440.1R-06 [2] and from 1.4 to 1.7 times the design ultimate load value of FIB 40 [22].

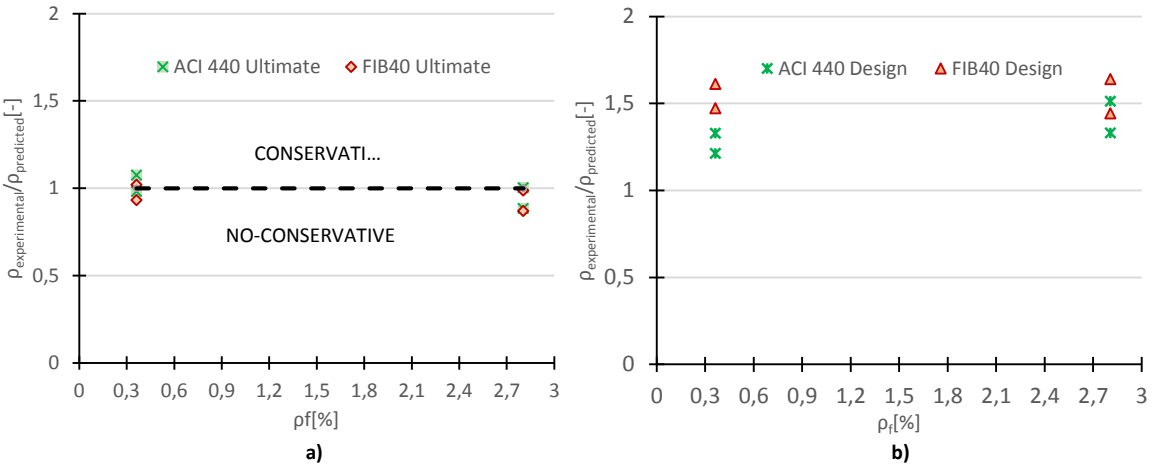

Figure 127 - GFRP beams ratio between the experimental and the predicted values as a function of: a) Experimental ultimate moment; b) Design moment

The crack propagation of the beams during the tests was marked on one of the faces and reproduced in Figure 128. All specimens presented bending failure modes and a detailed description is indicated in Table 54, complemented with some test pictures, shown from Figure 129 to Figure 134.

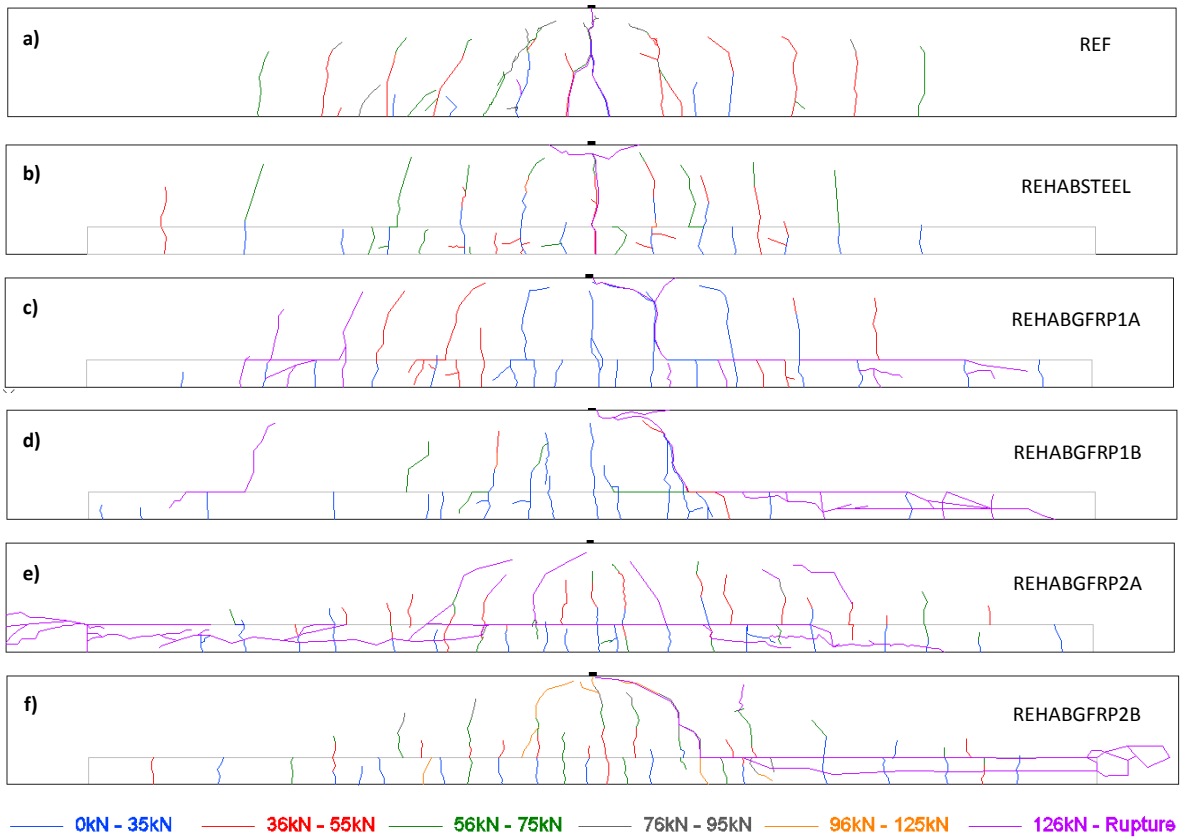

Figure 128 –Main cracking at failure: a) REF; b) REHABSTEEL; c) REHABGFRP1A; d) REHABGFRP1B; e) REHABGFRP2A; f) REHABGFRP2B

The reference beam REF had a failure mode caused by the yielding and breaking of the bottom steel reinforcement at mid-span (Figure 129). Several flexural cracks developed along the span (Figure 128a)). Although these cracks were initially vertical, they started to incline in the direction of the load-point with the failure approach (Figure 129a)). The failure occurred after the two central cracks reached the load-point (Figure 129 (b)).

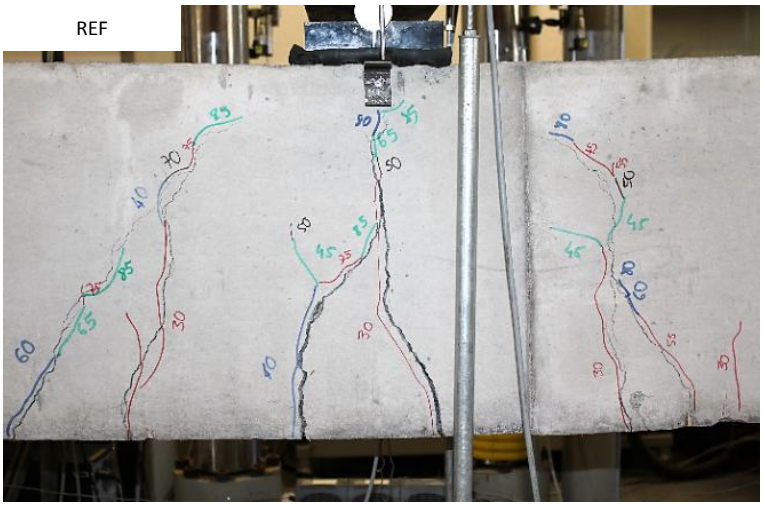

a)

b)

Figure 129 - REF beam failure: a) immediately before; b) after

The REHABSTEEL beam had a similar failure mode to the REF beam, with the yielding of the bottom steel reinforcement at mid-span region but followed by the crushing of the top concrete in compression (Figure 130). The crack pattern was similar to the REF beam, differing in the fact that, close to mid-span, the cracks also developed horizontally at mid-height of bottom concrete

suggesting some slip of the tension reinforcement (Figure 128 b)). No visible slip or separation between the two concrete layers occurred in this beam (Figure 130 b), c) and d)).

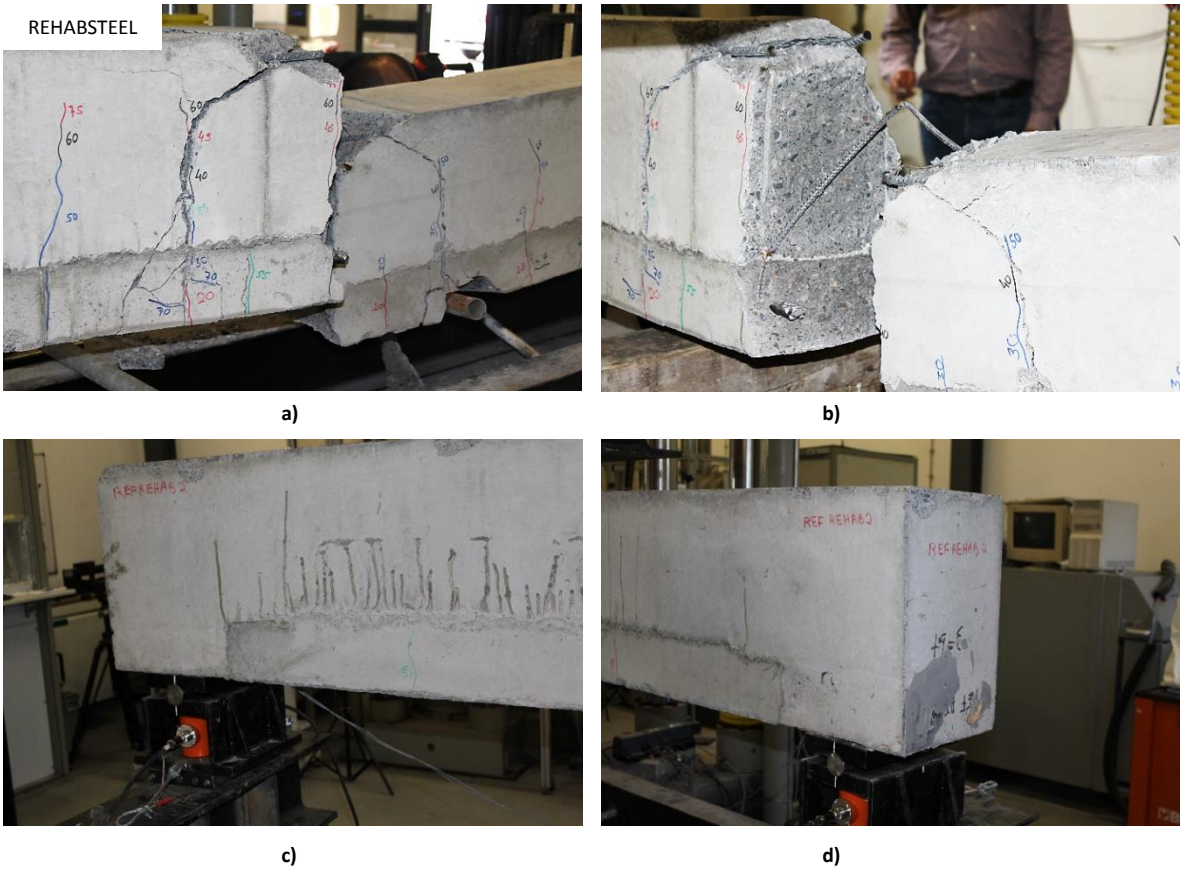

Figure 130 – REHABSTEEL beam failure: a) at mid-span; b) mid-span cross section detail; c) left support; d) right support

Both REHABGFRP1A and B beams had similar behaviour until failure. The cracks appeared along the entire span, propagating from the bottom concrete layer to the other in the direction of the load point. Horizontal cracks at the bottom reinforcement level started to appear with the load increase. A partial separation between the two concrete layers was also detected, which started at the mid-span zone and propagated into the support direction (Figure 128 c) and d)). In these two cases, the failure was caused by the crushing of the top concrete in compression at the load point, followed by the separation of the concrete layers which caused some spalling of the bottom concrete layer (Figure 131 and Figure 132).

Figure 131 – REHABGFRP1A beam failure: a) general view; b) mid-span detail; c) left support; d) right support

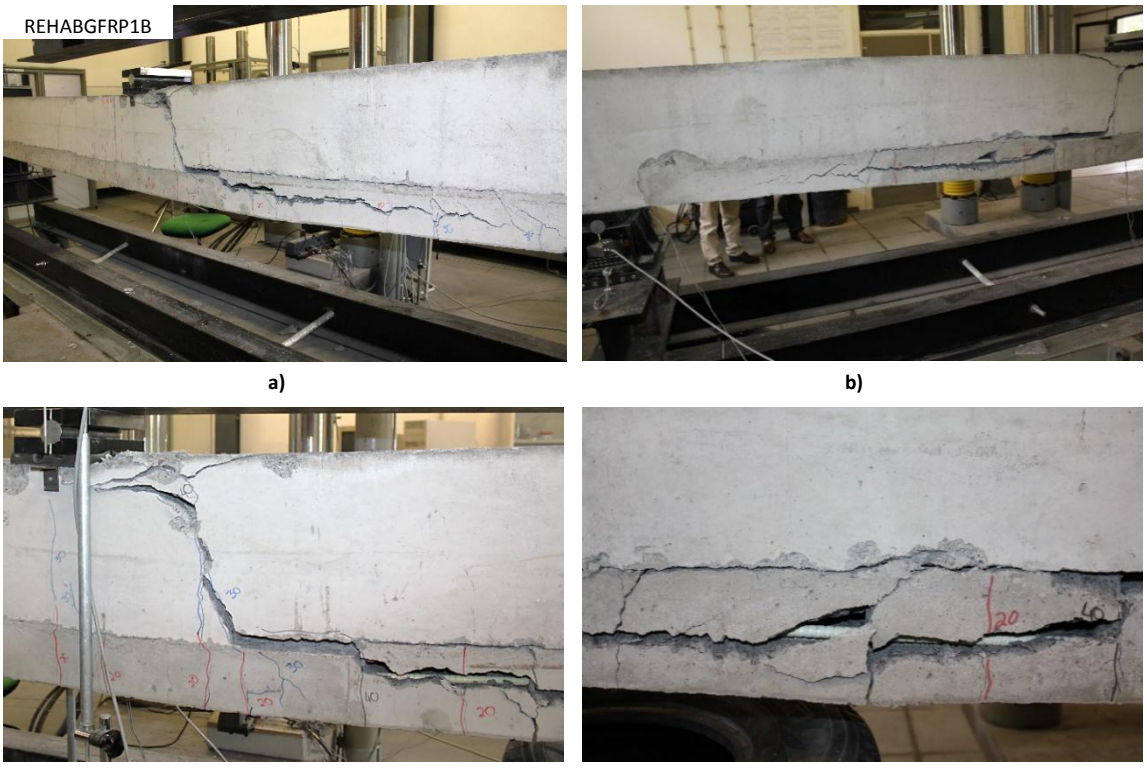

Figure 132 – REHABGFRP1B: a) front general view; b) back general view mid-span detail d) concrete layers detail

The REHABGFRP2A and B beams also had a similar crack pattern and behaviour until failure. As the load increased, horizontal cracks at the tension reinforcement level and the separation between the two concrete layers were detected. These two phenomena started at the mid-span zone and progressed to the supports, which contributed to the failure (Figure 128 e) and f)). The failure occurred mainly due to the slip of the tension GFRP bars at the support areas. Debonding and spalling of the new concrete was also observed at mid-span and supports (Figure 133 and Figure 134). Despite the global slip at failure between the reinforcement and the concrete, no visible debonding between the GFRP bars and the resin at the supports area was found. The resin stayed bonded to the reinforcement and slipped from the concrete (Figure 133 d)).

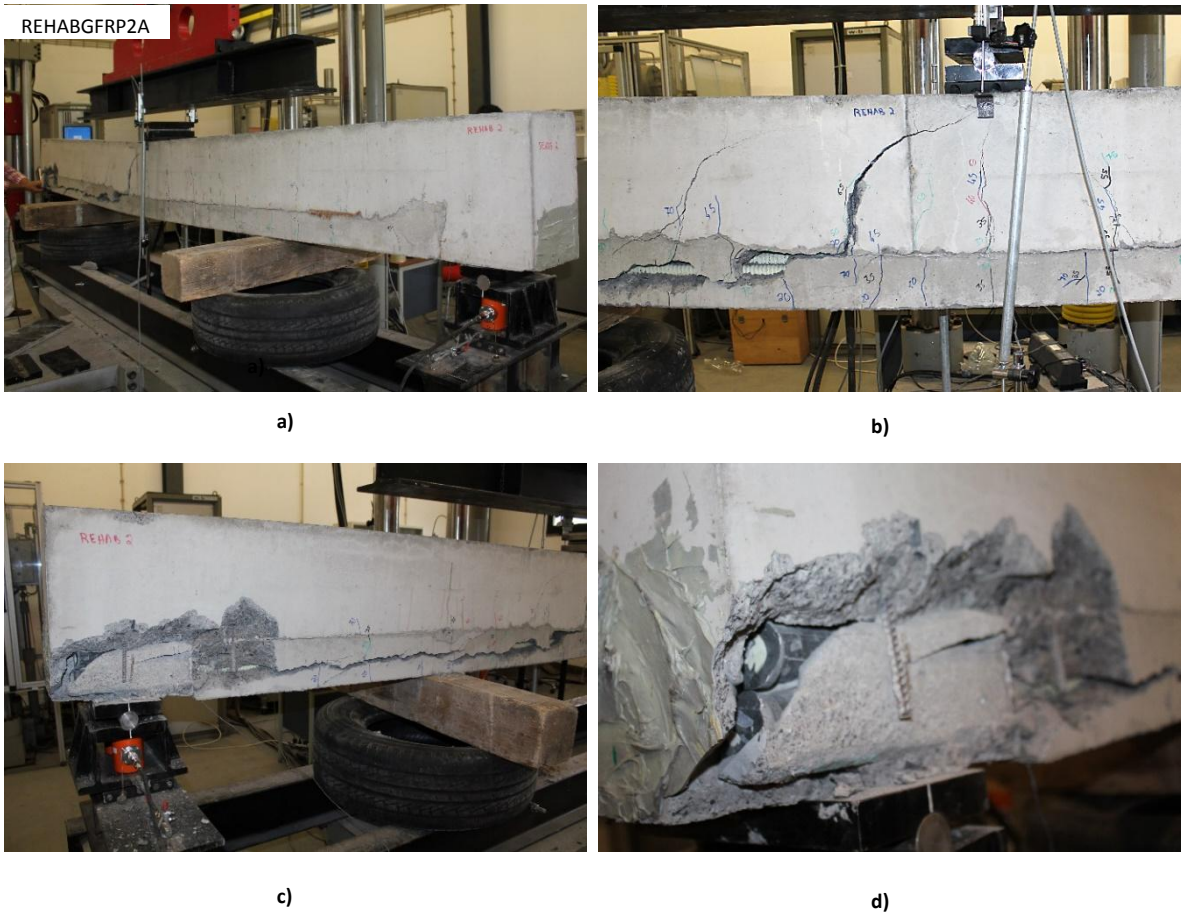

Figure 133 - REHABGFRP2A: a) general view b) mid-span detail; c) support detail; d) reinforcement slip detail

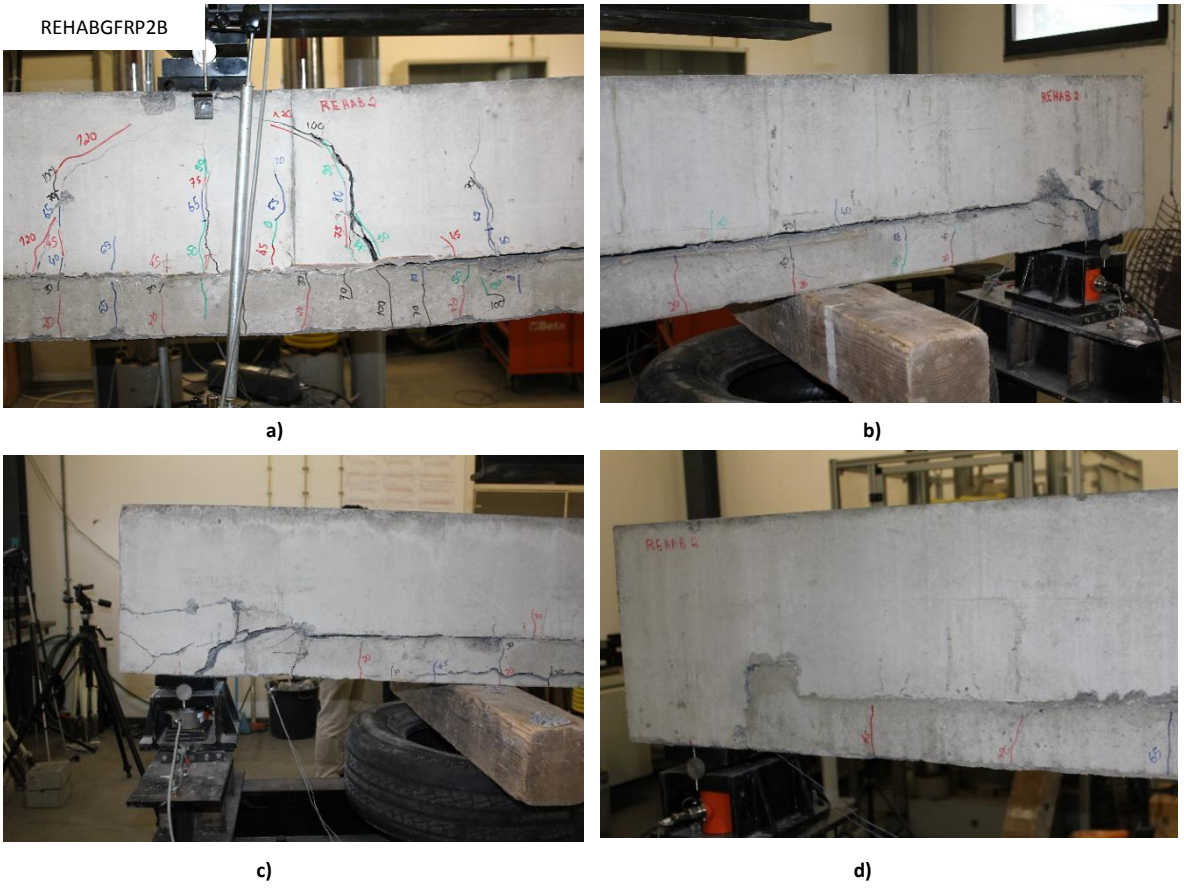

Figure 134 - REHABGFRP2B: a) mid-span detail; b) right support front detail; c) right support back detail; d) left support detail

A failure due to the slip of the tension reinforcement highlights the lack of anchorage length. However, it is important to mention that despite the failure occurred due to the slip of the tension GFRP bars at the supports, it did not compromise the desired behaviour and bending capacity. These two beams supported a load 2.5 times greater than the original beam, and this means that as a rehabilitation solution they will never be subjected to this loading level, except if this solution is also a strengthening solution to increase the bending capacity. To the level of load corresponding to the reference beam, the support areas were in perfect condition. This is shown in Figure 128 e) and f), where it is possible to state by the colour scaling that the support areas only started to be affected for a load higher than 126 kN. This is also evident in Figure 135**,** as the support strains only increased for loads above 150 kN.

Table 54 – Description of failure modes

Beam	Experimental Failure Mode
REF	Yielding of tension steel
REHABSTEEL	Yielding of tension steel and concrete crushing
REHABGFRP1A	Compression concrete crushing and debonding of new concrete in central tension zone
REHABGFRP1B	Compression concrete crushing and debonding of new concrete in central tension zone
REHABGFRP2A	Tension GFRP bars split and debonding and spalling of new concrete in mid-span and supports
REHABGFRP2B	Tension GFRP bars split and debonding and spalling of new concrete in mid-span and supports

3.2.4.3 Tensile reinforcement strain

In order to study the bottom longitudinal reinforcement strains at the supports and at the mid-span, two strain gauges were glued to two bars at these positions of each beam. The load-strain relationships at the mid-span and at the supports are presented in the Figure 135 and Figure 136. The curves present the mean strains of the two strain gauges at each monitored cross-section.

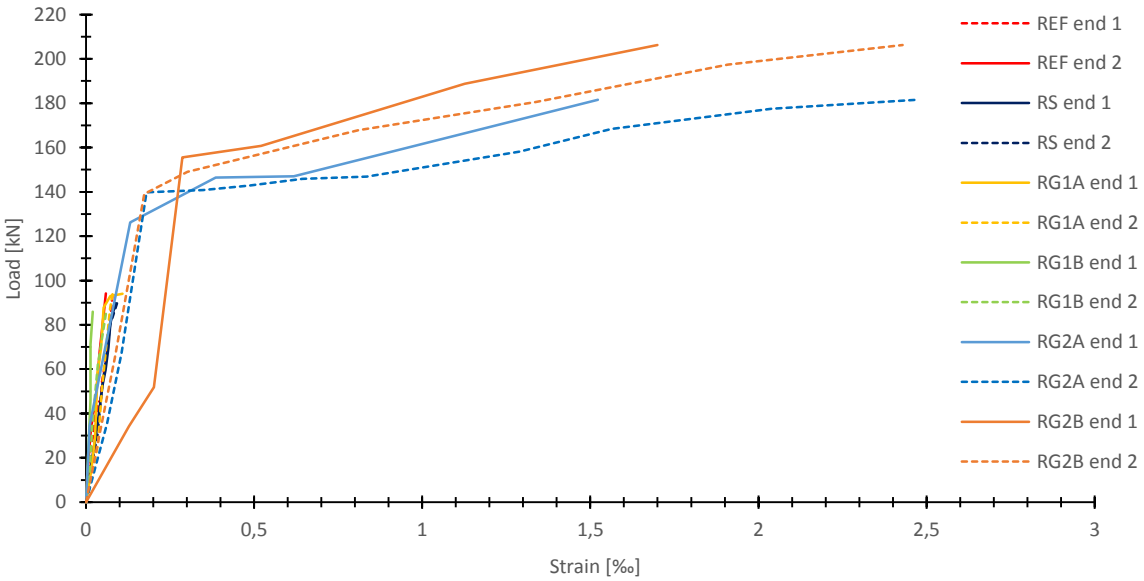

Figure 135 – Bottom reinforcement mean tensile strain of each beam at the supports (end 1 and 2)

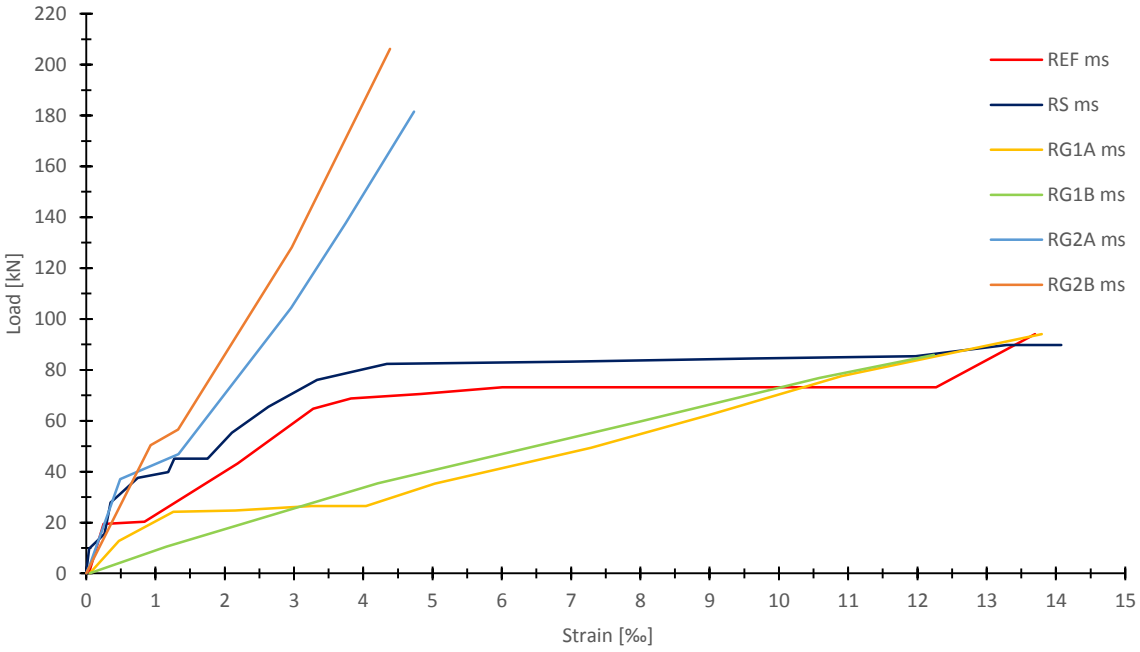

Figure 136 – Bottom reinforcement mean tensile strain of each beam at the mid-span (ms)

The tensile strains at the mid-span of the steel reinforced beams (REF and REHABSTEEL) presented a three stage behaviour development until failure: the elastic, the cracked and the yielded stages. On the other hand, the GFRP reinforced beams only presented the elastic and the cracked stages.

At maximum load capacity, the mean value of strains at mid-span for REHABGFRP1A and for REHABGFRP1B were, respectively, 12.28‰ and 12.48‰. Theoretical strains were of 12.51‰ and 13.41‰ respectively for REHABGFRP1A and for REHABGFRP1B at mid-span for the maximum load.

Although for REHABGFRP2A and REHABGFRP2B there was a strain gauge glued on the centre rebar and the other on the outside rebar, the strain values were similar and the mean maximum value was 3.75‰ at the maximum load capacity for REHABGFRP2A and 4.35‰ for REHABGFRP2B. Theoretical strains were of 3.66‰ and 4.16‰ respectively for REHABGFRP2A and for REHABGFRP2B.

Comparing REHABGFRP1A and B and REHABGFRP2A and B relationships, it is possible to see that increasing the GFRP ratio decreases the strain in GFRP reinforcement for the same load level. REF, REHABSTEEL, REHABGFRP1 A and B had similar maximum load capacity and reinforcement area, and in general exhibit similar strains. Strains in REHABGFRP2 A and B were significantly lower than in REF and REHABSTEEL, although for regulations, they would have the same behaviour for deflections.

At the considered service load representing 30% of the ultimate load capacity, mid-span reinforcement average strain, at first load cycle, was 2.40‰ for REF and REHABSTEEL beams, 4.02‰ for REHABGFRP1A and 3.45‰ for REHABGFRP1B, and 0.40‰ for REHABGFRP2. The higher the reinforcement ratio the lower the reinforcement strains will be. Predicted values were of 4.37‰ and 0.6‰, respectively for REHABGFRP1 and REHABGFRP2.

For REF, there is a significant growth of the strains at 20 kN. This effect was not verified for REHABSTEEL. This difference in behaviour can be explained by the fact that measured strains are point values from a specific location of the reinforcement. If the strains were measured over a crack, the values will be affected by the "localized" increase in the reinforcement strain.

At the supports of the steel reinforced beams, the maximum strain was 0.12‰ at maximum load capacity. For REHABGFRP1A and REHABGFRP1B the maximum strain value was 0.15‰. For REHABGFRP2A and REHABGFRP2B from 150 kN of load, strain values had a faster increase, which is noticeable by the change in the slope of the curve. Although this change gives the curve a yielding appearance graphically, it corresponds to the detachment of the concrete near the supports. It is important to state that this load level corresponds to the short-term load (F_{head}) which according to the manufacturer can be anchored by the end heads [84]. The maximum strain value was 3.35%. The high level of strains at the supports shows insufficient anchorage length of the bars, resulting in the failure of the support zones of these two beams when the concrete is not able to bond the high force developed at the end of the GFRP bars. The mean of reinforcement strain at supports from the side of beam that failed is indicated in Table 55. For these values the total anchorage load (F) was calculated. Subtracting the short-term load from this load (F_{head}) which can be anchored by the end heads, and considering the value of bond given by the manufacturer, the anchorage length needed to prevent the failure was calculated at 0,32 m.

Table 55 – Mean load and anchorage length at failure side of REHABGFRP2 beams

Beam	Mean strain, ε	Total Load, F	Anchorage length, lb
	(‰)	(kN)	(m)
REHABGFRP2 A	2.48	390.00	0.31
REHABGFRP2 B	2.56	401.30	0.32

3.2.4.4 Deflection behaviour

The load-deflection at mid-span curves are shown in Figure 137 and Figure 138. Figure 137 shows a comparison between the four groups.

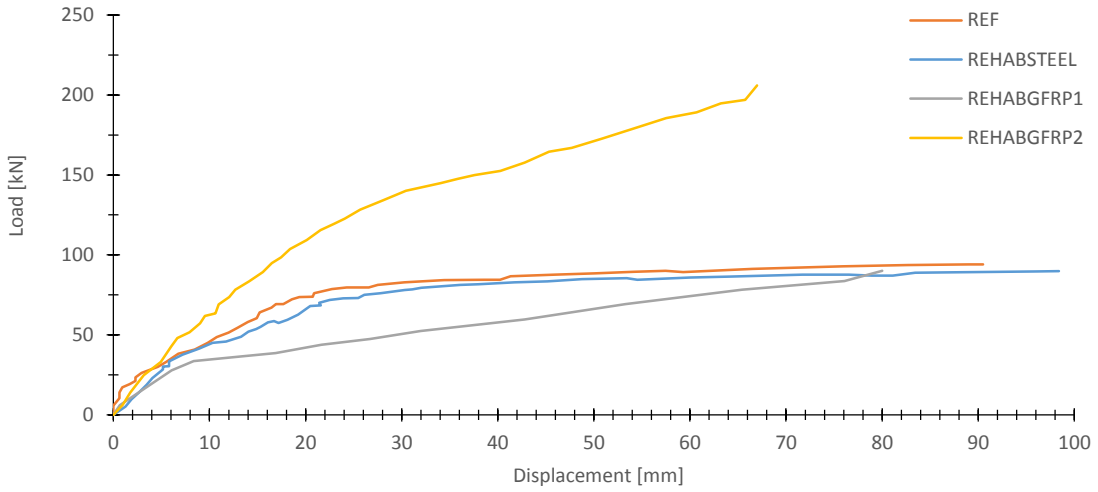

Figure 137 – Load-deflection curves at mid-span for all beams

Each curve of Figure 138 represents the average deflection obtained from the two LVDTs mounted at mid-span for each beam. These curves allow the evaluation of the flexural stiffness at the various stages of the beams until failure during the tests. The steel reinforced beams, REF and REHABSTEEL, presented similar behaviour, which can be summarized in three different stages. An elastic first phase where the relationship between the load and the mid-span displacement was linear, followed by a cracked phase where the load-displacement relation was approximately linear but with a lower slope, and a third phase, which is the steel yielding phase, characterized by a rapid increase in the deflection until failure (Figure 138 a)). Although the two curves were similar, REHABSTEEL had slightly lower flexural stiffness after the first loading cycle, a lower yielding loading point and 4.5% lower maximum load capacity. This difference can be explained by the existence of a new layer of concrete and a possible slip between these layers. The failure mode is also shown in Figure 128.

The development of the load-displacement at mid-span curves of the REHABGFRP1A and REHABGFRP1B beams was different from the reference beams with only two distinct and approximately linear phases and no ductile behaviour. In the first elastic stage of the beams, the relationship between the load and the deflection was linear. Then the slope of the curve decreased as a consequence of the cracking, but the relationship continued to be linear until failure.

The REHABGFRP2A and REHABGFRP2B beams had identical behaviour to the REHABGFRP1 beams. The major difference was that the transition point between the two stages was not so easily identified, since this transition was progressive, giving a non-linear aspect to the curves.

From Figure 137, it is possible to notice qualitatively that a change in the reinforcement ratio changes the load-displacement behaviour. The lower the GFRP ratio, the higher the mid-span deflection.

Values of deflections at service load are shown in Table 52. Although the deflection of the REHABGFRP2 beams were higher than the REF beam, as expected the difference between the two values is lower than 10.0%, with similar deflection values for the groups, suggesting adequacy of the prediction formulas used in both cases [2]. Although the reinforcement ratio and the ultimate capacity were close between REF and REHABGFRP1 groups, GFRP reinforced beams exhibited 1.86 times higher deflection at service. These differences are due to the lower elasticity modulus of GFRP when compared to steel (about one third). The ACI 440.1R-06 [2] underestimates the mid-span deflections. For REHABGFRP1 the experimental deflections were on average 55.0% higher than predicted, and for REHABGFRP2 34.5%. Although this is a short-term deflection, assuming that the long-term deflection is three times higher than this value and comparing with the service limit of span/240, which corresponds to 16.7mm, only the reference beams and REHABGFRP2 verified the limit. This shows that service can have a greater effect than ultimate limit states when designing RC structures with GFRP reinforcement.

Deflections at ultimate limit load carrying capacity were also measured (Table 53). The REF had the highest ultimate deflection, as expected due to the ductile property of the steel reinforcement, followed by the REHABGFRP1 group and then the REHABGFRP2 group, both with no ductile behaviour.

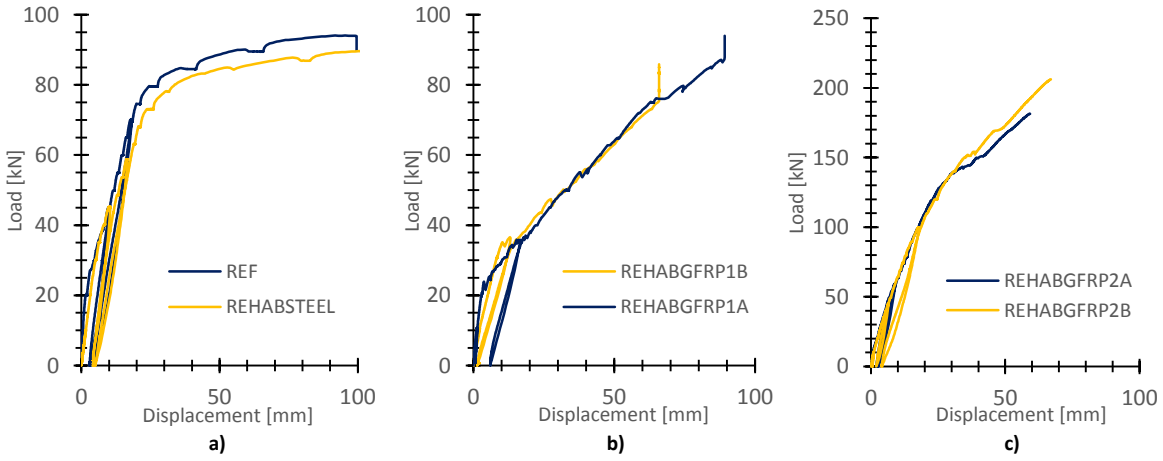

Figure 138 - Load-Deflection at mid-span: (a) REF and REHABSTEEL; (b) REHABGFRP1 A and B; (c) REHABGFRP2 A and B

3.2.4.5 Crack development

In order to analyse the differences of the distance between cracks and their width and length until failure, the crack development was marked on the beams with different colours after each load step. The crack pattern of all beams until failure is reproduced in Figure 128.

The beams were initially uncracked before testing. The flexural cracks started to appear after reaching the cracking load. In general, the first cracks were vertical and developed closely to the mid-span, where the bending moment had the maximum value. As the load progressively increased, the cracks appeared along the entire span, starting vertically or at a slight angle and then taking the load-point direction. All cracks increased in width and length until the failure of the beam.

Looking at Figure 128, the increase in ρ_f resulted in a higher number of cracks and reduced the crack spacing. Similar behaviour was also reported by Amr El-Nemr and Brahim [30]. The mean crack spacing for REF was 0.172 m. For the rehabilitated beams, the distance between the cracks was different in the two concrete layers, with more cracks in the bottom layer (Table 56). REHABGFRP1A, REHABGFRP1B and REHABSTEEL had similar mean crack spacing. The crack spacing on the original concrete layer was approximately two times the spacing on the rehab layer. On REHABGFRP2A and B there was a better propagation of the cracks from the second layer to the first layer crack, since the crack spacing between layers was small.

Table 56 – The mean spacing between cracks of beams

Beam	Crack spacing (m)		Height of compression zone at failure (m)
	Original Layer	Rehab Layer	
REF	0.172	(-)	0.103
REHABSTEEL	0.221	0.137	0.064
REHABGFRP1A	0.218	0.109	0.058
REHABGFRP1B	0.231	0.138	0.063
REHABGFRP2A	0.151	0.141	0.105
REHABGFRP2B	0.164	0.144	0.121

Another important information that can be extracted from Figure 128 is the distance between the top compression fibre and the cracks top. At failure, due to the high curvature of the mid-span cross-sections, this measure is approximately the position of the neutral axis or, in other words, the height of the compression zone. The results are shown in Table 56 and were determined by measuring the height of all the mid-span flexural cracks and subtracting their mean value to the height of the section. Comparing REF and REHABSTEEL, the existence of two concrete layers caused

a height lessening of the compression zone. This means that there was a rise of the neutral axis in the rehabilitated beams. REHABSTEEL and REHABGFRP1A and REHABGFRP1B had similar distances. REHABGFRP2A and REHABGFRP2B also had similar values, which comparing with REHABGFRP1A and REHABGFRP1B are two times higher. It also important to mention that these values were similar to predictions done with ACI 440.1R-06[2] formulation, which were of 0.050 m for REHABGFRP1 and 0.092 m for REHABGFRP2.

3.2.4.6 Mid-span crack width

To monitor the crack width evolution at mid-span, a crack near the mid-span was chosen and its width was measured with a monocular lens with a metric scale. The crack width at each load step is shown in Figure 139. For the same load value, the REHABGFRP1 A and B had the largest cracks followed by the two reference beams REF and REHABSTEEL. The REHABGFRP2 A and B beams presented the smallest cracks. The increase of the GFRP reinforcement ratio decreases the crack widths. Between the two RC beams with steel reinforcement, the crack width was larger in the REHABSTEEL than in the REF, which may be a consequence of the fact that the REHABSTEEL was concreted in two layers. The cracking width limit of steel reinforced concrete is associated with the need for corrosion protection of the bars and with an aesthetic consideration. As the GFRP bars are immune to corrosion, the codes and guides allow larger crack width limits because this issue is only related to the aesthetic appearance. The ACI 440.1R-06 [2] recommends a flexural crack width of 0.50 mm and 0.70 mm at service for exterior and interior conditions respectively.

The crack width of the steel beams at service load ranged from 0.10 mm to 0.20 mm, the REHAB1 beams from 0.40 mm to 0.60 mm and the REHAB2 from 0.05 mm to 0.10 mm. One of the REHAB1 specimens exceeded the limit of 0.50 mm for the exterior conditions, but the crack width of the REHAB2 group is far from this limit.

It is also important to mention that as crack width is related to the reinforcement strains, other codes [22, 30] suggest controlling the crack width by considering a maximum limit for the reinforcement strain of 2‰ at service. In the REHABGFRP1 beams, the load that corresponds to this strain is the service load of 30 kN, whereas in the REHABGFRP2 beams this load is about 70 kN. These results suggest that the maximum limit for the reinforcement strain can be an effective way to control the crack width.

Although the collected data related to the crack width was limited, it seems to be in agreement with other studies [40] that suggest that in some compression failure cases of structures reinforced with GFRP bars there is a reduction in the rate of the crack width increase with the load increase. This phenomenon can be explained by the increase in the neutral axis depth to satisfy the force equilibrium, which has a crack closure effect. This effect is presented in Figure 139 in the REHABGFRP1 beams.

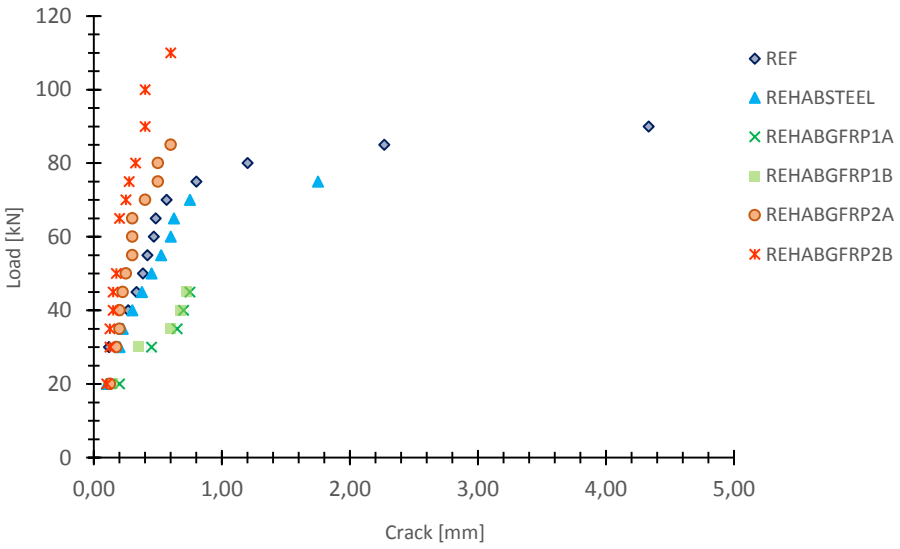

Figure 139 - Width progression of the bottom mid-span crack of the beam with load increase

Figure 140 a) shows the relationship between the reinforcement strain at mid-span and the crack width. For the same crack width value, the strains were higher in the REHABGFRP1 beam specimens due to the lower reinforcement ratio. There is a high dispersion of values between beams.

The interaction between crack width and deflection is shown in Figure 140 b). In this case, the differences are not so visible, and it is possible to relate the deflection to crack width. This shows that the deflection control is more related to crack, and for each 1 mm of crack width there is a corresponding 24.77 mm of mid-span deflection. However, for a certain mid-span deflection the mid-span crack width was lower for REHABGFRP2 beam specimens.

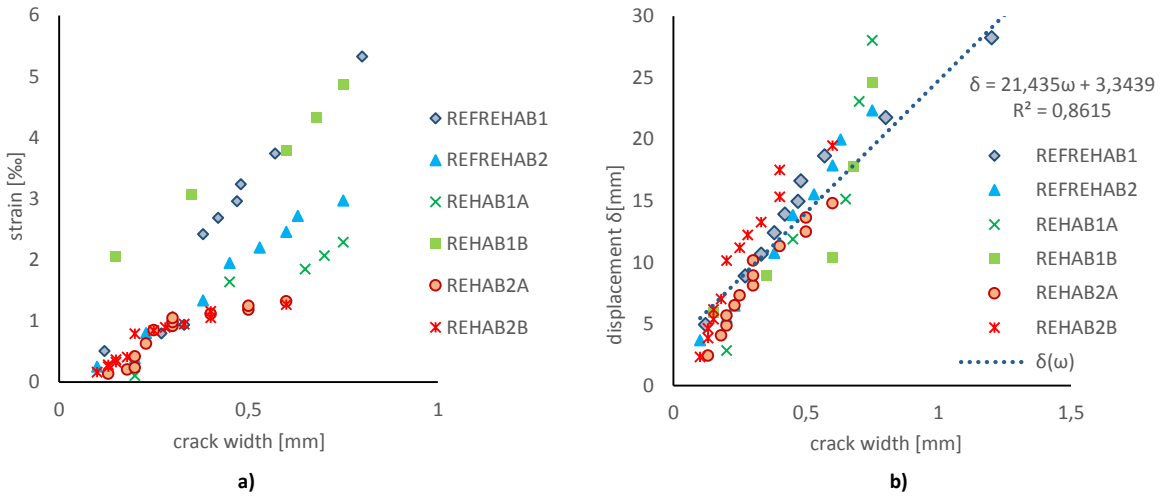

Figure 140 - a). Variation of mid-span reinforcement strain width the mid-span crack width. b). Variation of mid-span deflection with mid-span crack width

3.3 Conclusions

This study proposed, tested and evaluated an efficient and easy to implement rehabilitation procedure that uses GFRP bars to replace the tension steel bars of deteriorated reinforced concrete beams. It is an ideal technique to repair and improve the long-term durability of the existing marine steel reinforced concrete structures with corrosion problems. The conclusions are based on the results of an experimental campaign performed with full-scale reinforced concrete beam specimens casted in two phases to simulate the replacement of the corroded and cracked concrete. Two different GFRP reinforcement ratios were tested in order to assess the behaviour of the repaired beam regarding its service and ultimate states in comparison with the original beam with steel reinforcement. The main findings of this research can be summarized as follows:

1- Although a new concrete layer with a more flexible tensile reinforcement has been introduced to the rehabilitated specimens, the construction joint was not the cause of the failure and did not compromise the serviceability and ultimate limit states of the beams.
2- Good result predictions were obtained with the formulas of the EC2[23] / FIB40[22] and ACI 440.1R-06 [2], which indicates that these documents can be used to design this solution.
3- The absence of the stirrups' bottom branch due to a possible corrosion did not compromise the shear behaviour of the rehabilitated beams.

4- The criterion to design a rehabilitated beam with the same load capacity or with the same deflection at service load as the reference RC beam with conventional steel reinforcement was satisfied. One of the proposed repaired solutions was able to keep both the deflection and the ultimate load capacity of the original beam.
5- The rehabilitated beams with GFRP bars exhibited a bilinear behaviour until failure in terms of load-deflection as expected since the ductile performance of the reference beam with steel reinforcement is not possible to replicate due to the GFRP material linear elastic property until failure.
6- The conic heads at the end of the GFRP bars inserted in the concrete holes filled with epoxy resin were sufficient to ensure their anchorage at the ends of the beams.

Chapter 4.

Numerical Simulation

Although this was mainly an experimental work, the numerical simulation and modelling is important to understand some experimental issues regarding the specimen's behaviour and allowed to extrapolate some results of non-tested possibilities and applications examples.

The commercial software ATENA, a non-linear finite element (FE) program, was used to model some of the tested specimens to see if the FE program was able to simulate the tested beams, especially the rehabilitated beams. By validating the FE model with test results it is expected that the extrapolations are reliable.

GFRP is considered an alternative to steel due to its high tensile strength and corrosion immunity. However, the low axial stiffness and the different bond properties make the use of the traditional design equations difficult. The numerical simulations can help improving the design guidelines and knowledge in the field of the GFRP RC. However, limited numerical models that have been developed and exist in the literature [8].

The linear and nonlinear behaviour of all materials was adequately modelled by appropriate constitutive laws. As a good agreement between the tests and the model results was achieved, the FE program based on the same principles was used to model other examples. The results are discussed and compared with the FE model and the test results.

4.1 Non-linear finite element program, ATENA

This section describes in short the main elements and the theoretical basis of ATENA FE program needed to accomplish the desired analysis.

For the non-linear finite element analysis, the software ATENA was used because it is a FE program developed for the analysis of reinforced concrete structures and several researches have validated its objectivity by experimental simulation and practical applications [36, 46, 83] .

There are several finite elements available in ATENA for 2D and 3 D analyses. For the 2D case of the models constructed in this study, the used elements are quadrilateral isoparametric with linear or quadratic interpolation functions. The integration is performed with the Gauss method.

The constitutive model used for the concrete material is based on the smeared crack concept, the nonlinear elasticity and the material damage approach and it is known as SBETA material.

In the smeared crack model, cracks are smeared over a distinct area, a finite element or an integration point of the finite element. Discontinuities such as compression failure zones and discrete cracks are simulated by strain localization in a continuous displacement field and introduced directly into the numerical model [25].

Stress-strain relationship of the concrete is shown in Figure 141, which can be used for all types of concrete from normal to high strength [44]. For compressive loading before the peak stress (f_{cm}) it is represented by a non-linear function and after the peak stress by a linear softening until ε_{cu}. The pre-peak relation is based on the MC90 [21] that enables the use of several curve forms. In tension the stress-strain relation is represent by a linear loading before the cracking stress (f_{ctm}) and after cracking, follows an exponential softening [25].

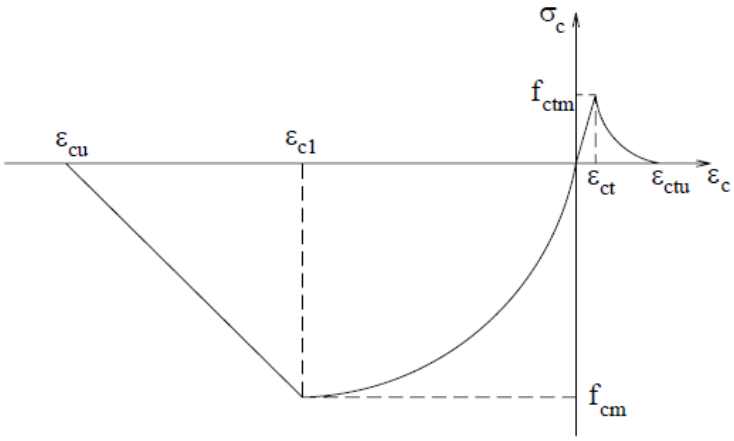

Figure 141 – Unixaial stress-strain relationship for concrete [25]

After the cracking, the constitutive relation in the SBETA model is combined with the crack band to model crack propagation based on a crack-opening law and the fracture energy. Concrete without cracks is considered as isotropic while concrete with cracks as orthotropic. Two models, the fixed crack model and the rotated crack model, can be used to define the material axes of cracked

concrete, but, in both models the crack is formed when the principal stress exceeds the tensile stress. The main difference between these two models is that in the fixed crack model the crack direction and the material axes are defined by the principal stress direction at the beginning of the cracking and remains the same upon continued loading, while in the rotated crack model the crack direction always coincides with the principal strain direction, which means that the cracks rotate during the analysis [38]. Coronelli [26] stated that although the rotated crack model is computational simpler and accurate, the fixed crack model is similar to reality.

The crack opening is defined by a curve of stress-crack width which is related to three parameters: the tensile strength, the fracture energy and the shape of the softening curve. Where the fracture energy of concrete, G_F, is defined as the energy that is required to propagate a tensile crack of unit area, which according to MC2010 [20] can be estimated from the mean compressive strength of concrete, f_{cm}, as mentioned in Equation (170):

$$G_F = 73{f_{cm}}^{0.18} \quad (170)$$

By using the crack band model in the SBETA material, it is possible to obtain mesh-independent and reduced effects of the sizes, shape and orientation of the finite elements and the cracks results of in the load-deflection curves.

Shear is important in the cracked concrete especially when the fixed crack model is used, due to the shear stress in the crack plane, which represents the physical phenomena of aggregate interlock and dowel action of reinforcement in the crack plane. In the SBETA material the shear modulus is reduced with the growing strain normal to the crack, simulating the reduction of the shear stiffness due to the crack opening.

The reinforcement can be modelled as smeared or as discrete – in the form of reinforcing bars by one-dimensional truss elements embedded in the concrete. These elements can be used to model straight or radial reinforcement. The constitutive law can be a linear, bilinear or multi-linear stress-strain diagram. The mesh of FE is generated independently of the position of the reinforcing bars therefore the nodes of the bars elements do not have to be coincident with the concrete element nodes.

It is also possible to simulate and consider a bond stress-slip relationship. In these cases, bond elements, formulated cinematically, are generated between the concrete and the reinforcement bars and the bond slip deformations are introduced as additional degrees of freedom in the bars.

Another important element in ATENA is the interface which models the contact between two surfaces. It can be modelled so that there is no interaction or that there is a full interaction. In this

second case, it is possible to attribute a tensile strength to the interaction, and frictional properties such as cohesion and friction coefficient.

The FE mesh is generated automatically, and isoparametric plane quadrilateral FE with 4 integration points is used [25].

The analyses are made by the definition of load cases and analysis steps, where it is possible to apply a load or to impose a displacement by increments. The conceptual non-linear equation of the FE method is indicated in Equation (171).

$$K(a) \cdot \Delta a = q - f(a) \quad (171)$$

where

- $K(a)$ is the stiffness matrix
- a are the deformations in the structure before the load increment;
- Δa is the deformation increment due to load increment;
- q is the vector of the total applied joint loads;
- $f(a)$ is the vector of the internal joint forces;

At the beginning of each step the Equation (171) is out-of-balance and it has to be solved iteratively due to its non-linearity. This obeys to the definition of convergence criteria for the deformation change, out-of-balance forces and out of balance energy.

Two numerical methods can be used to solve the equilibrium equations: the Newton-Raphson or the arc-length method. In both cases, the line search method to speed-up the convergence can be used simultaneously.

4.2 Reinforced concrete beams with GFRP shear reinforcement

4.2.1 Simulation of tested beams

Considering the two reference beams, REF250 and REF175, and the beams with closed hoop GFRP stirrups (BS250, BS175, BS250GFRP1, BS175GFRP1, BS250GFRP2 and BS175GFRP2), a total of 8 beams were created. As the analysis was two-dimensional it was not possible to model the other

shear reinforcement solutions. The results are presented in this section by load-displacement curves and the comparison between the experimental curves and the numerical curves is done in order to evaluate the agreement between the modelling and the test results.

In ATENA, after the geometric definition of the nodes, the macro-elements that constituted the FE model were defined. In these models, 5 macro-elements were needed as indicated in Figure 142. Macro-elements 5 is the concrete element, and macro-elements from 1 to 4 are steel plate elements. These last elements were modelled with a similar dimension of the one used in the experimental tests, and represent the four loading points of the beam specimens. The steel plate elements were modelled as a plane stress elastic isotropic material. An elasticity modulus of 210 GPa was used. Interface elements ("2D interface") were introduced in the boundary lines between these elements and the concrete beam. These interface elements had a high stiffness in compression but no stiffness in tension, so that the rotation is allowed avoiding stress concentrations and numerical problems.

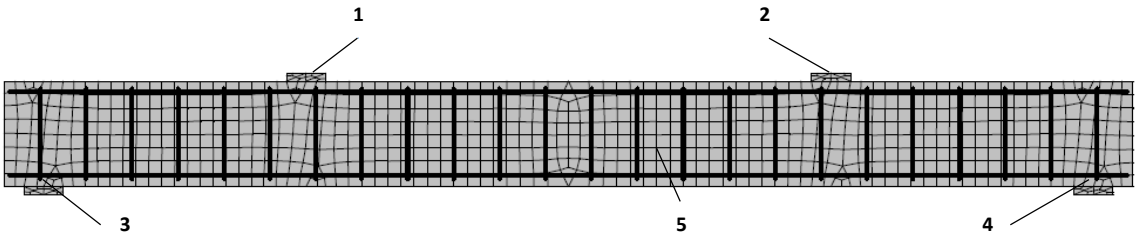

Figure 142 – Macro-elements and FE mesh

The concrete was modelled with SBETA material and with the mechanical properties measured in the experimental tests. For shear behaviour a fixed crack model was used, with variable shear retention factor and linear tension-compression interaction. The crack direction is fixed during the loading and is given by the principal stress direction at the moment of the initiation of the crack.

All the reinforcement bars were simulated as discrete bar elements embedded in the concrete FE and with perfect connection (Figure 142). The constitutive stress-strain relationship used for all steel reinforcement elements was bilinear. The yielding stress and elasticity modulus used were different for each bar diameter and were defined according to the experimental values of the samples tested and which were related in 2.1.1. For GFRP reinforcement bars, it was considered a linear stress-strain relationship with an elasticity modulus of 55 GPa for the bent stirrups case and 60 GPa for the straight GFRP bars.

It was considered a FE mesh where the finite elements have a maximum dimension of 0,05 m because it was concluded that decreasing the mesh size beyond 0.05 m increased the run time significantly and did not result in significant changes in the results.

In the beams with steel reinforcement the Newton-Raphson method in simultaneous with the line search method were used in all the analyses. In the GFRP beams, the arc-length was used due to its robustness and stability. The load steps defined were increasing imposed displacements at the loading points.

For loads above 450 kN the model was not able to reproduce the real behaviour of REF175 and overestimated the ultimate capacity by 13% (Figure 143). This error was the highest among all modelled beams. There is a good agreement between the load-deflection curve of the numerical model and the experimental one of the beam REF250 (Figure 144) and the difference in the ultimate capacity was of 9.4%.

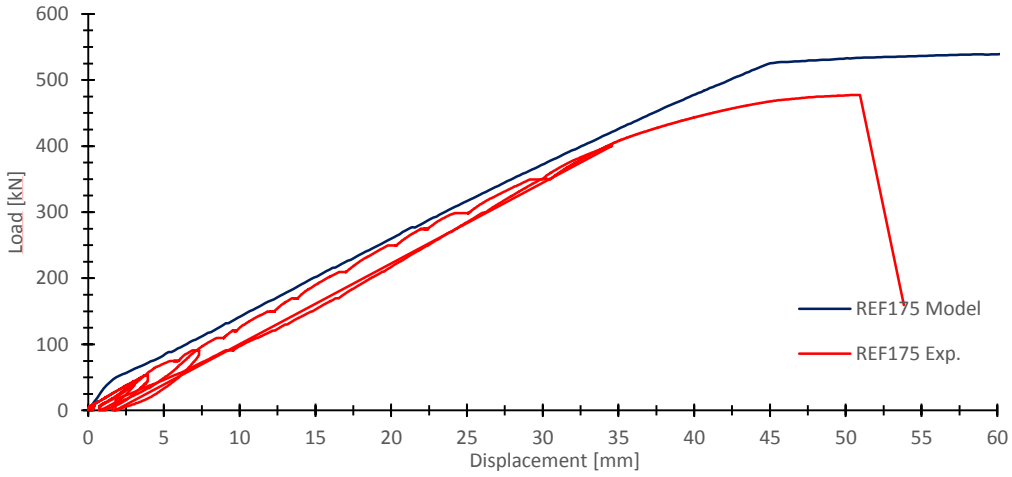

Figure 143 – Load-deflection curves of REF175

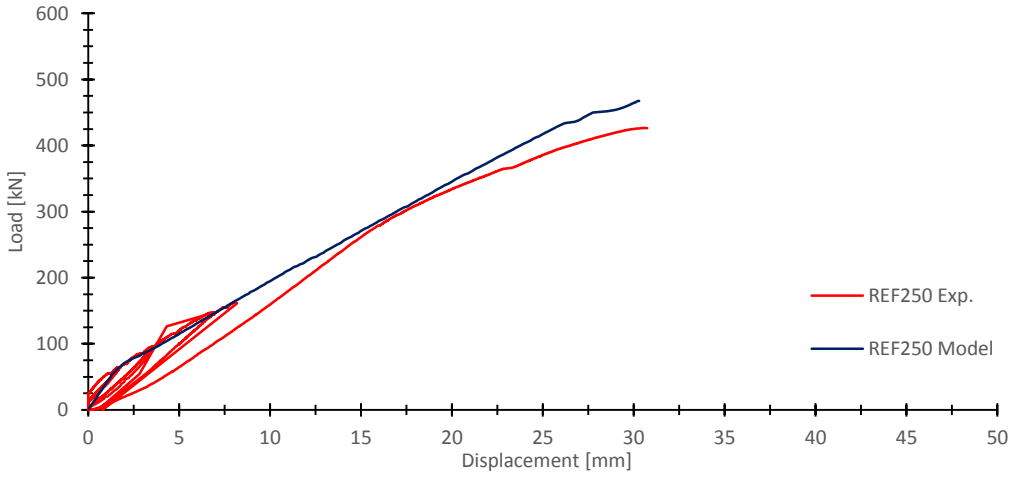

Figure 144 – Load-deflection curves for REF250

In Figure 145 there is a comparison between the crack patterns of beams REF175 and REF250 obtained in the numerical models and in the experimental tests. The spacing of the flexural cracks, and the orientation of the shear cracks are consistent between the models and the tests. In the tests these two beams failed by the shear reinforcement rupture. In the model, the failure was due to the loss of convergence, however before this step some steel stirrups have yielded. Near the failure, several stirrups of the model exhibited stresses higher than the yielding stress of the 8 mm diameter bars, 670 MPa. These stirrups stress curves of the FE model are in agreement with the failure picture (Figure 146 a) and b)).

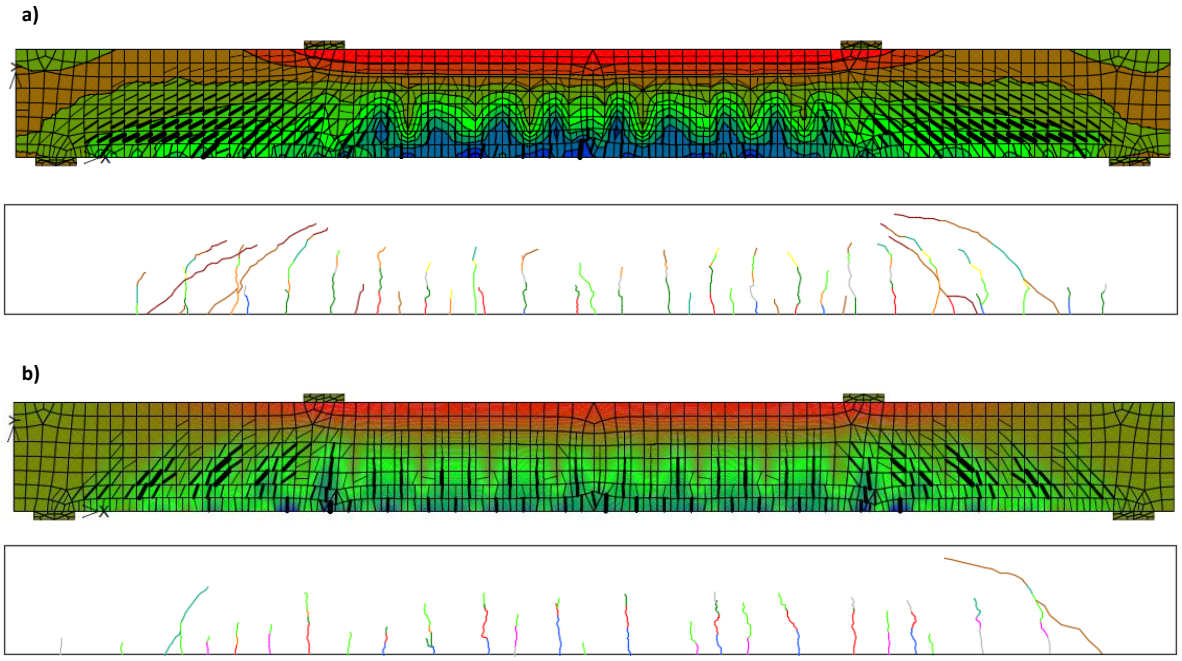

Figure 145 – Comparison between the crack patterns obtained in the models near the failure and in the experimental tests: a) REF175; b) REF250

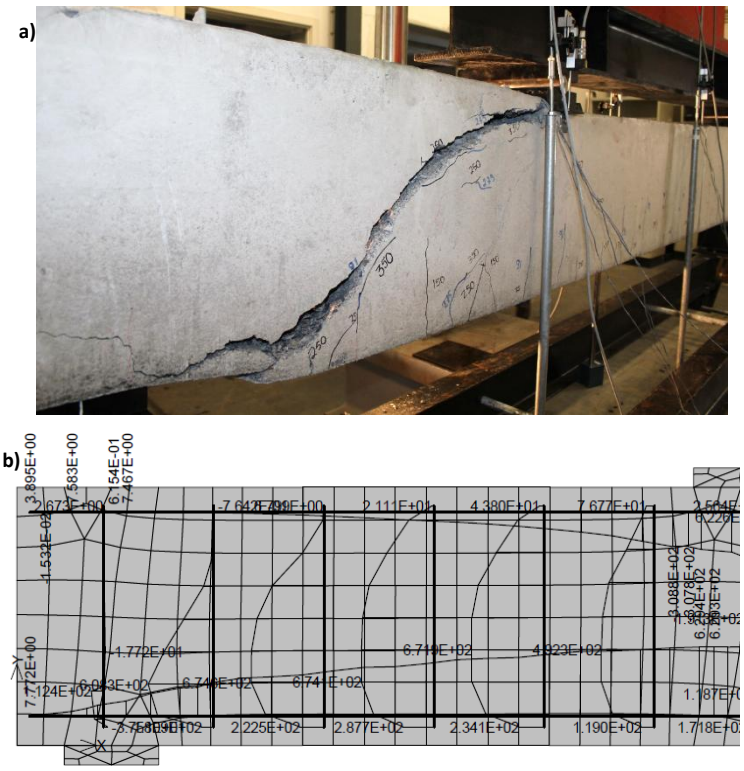

Figure 146 – a) REF175 failure; b) Reinforcement stress obtained in the numerical model before the failure

As the values of the deflections measured in the tests exceed the 50 mm in many cases, in this thesis it was only considered the 100 mm LVDT values. The 50 mm LVDT has a higher accuracy in measuring the lower values of deflection, as consequence sometimes there is a difference of 5 mm between the values measured between these two LVDTs. As in many cases the curves of the FE models are closer to the 50 mm LVDT (Figure 147 and Figure 148) it is possible that the values of deflections presented in the other chapters of this thesis are greater than the actual values.

Figure 147 and Figure 148 show the comparison of the load-deflection curves of the beam specimens BS175 and BS250, respectively. There is plotted the experimental curves of both the 50 mm capacity LVDT and the 100 mm LVDT. The 50 mm LVDT curves were in both cases closer to the FE model' curves. In the case of BS175 there was good agreement between both the values of ultimate load and deflection from the model and the experimental values. For BS250 the model underestimate the actual capacity by 11.9%. It was possible to verify the crushing of concrete at mid-span that causes the bending failure of these two specimens (cracks at the finite elements at mid-span in Figure 149 and Figure 150).

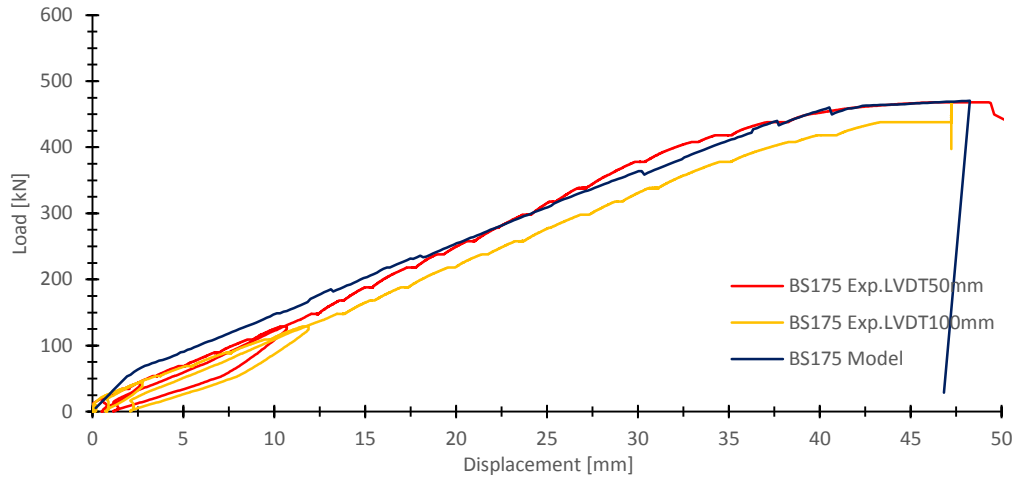

Figure 147 – Load-deflection curves of BS175

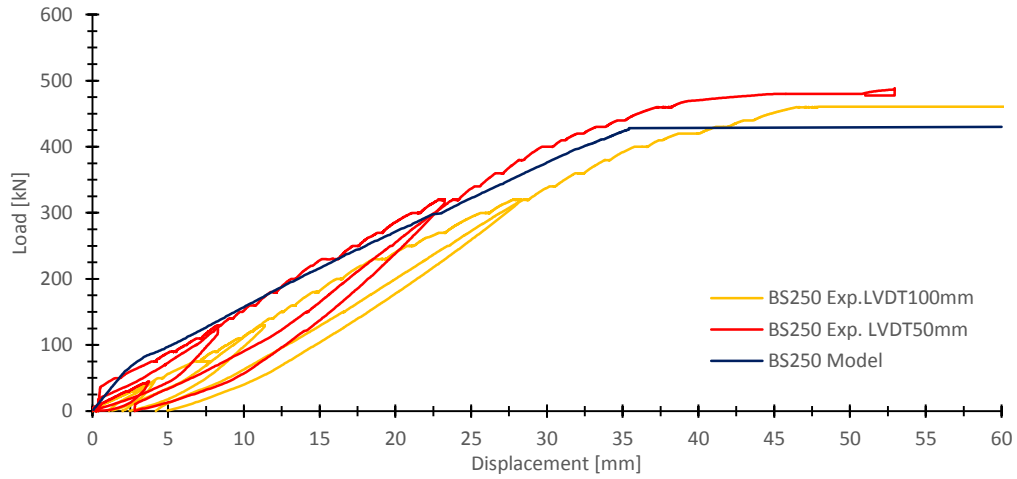

Figure 148 – Load-deflection curves of BS250

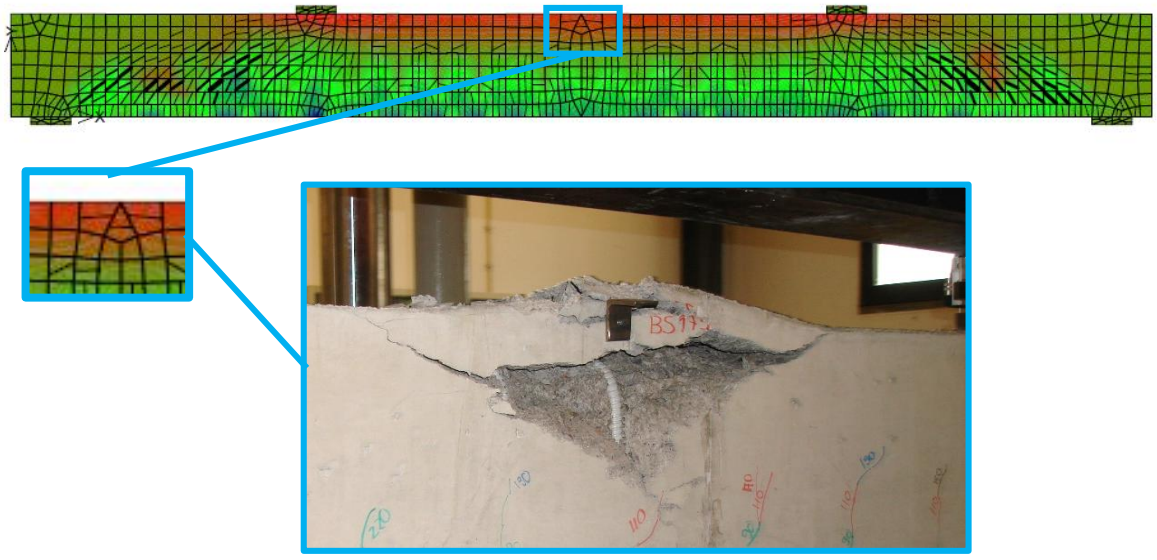

Figure 149 – Comparison of the FE model and the actual failure of BS175

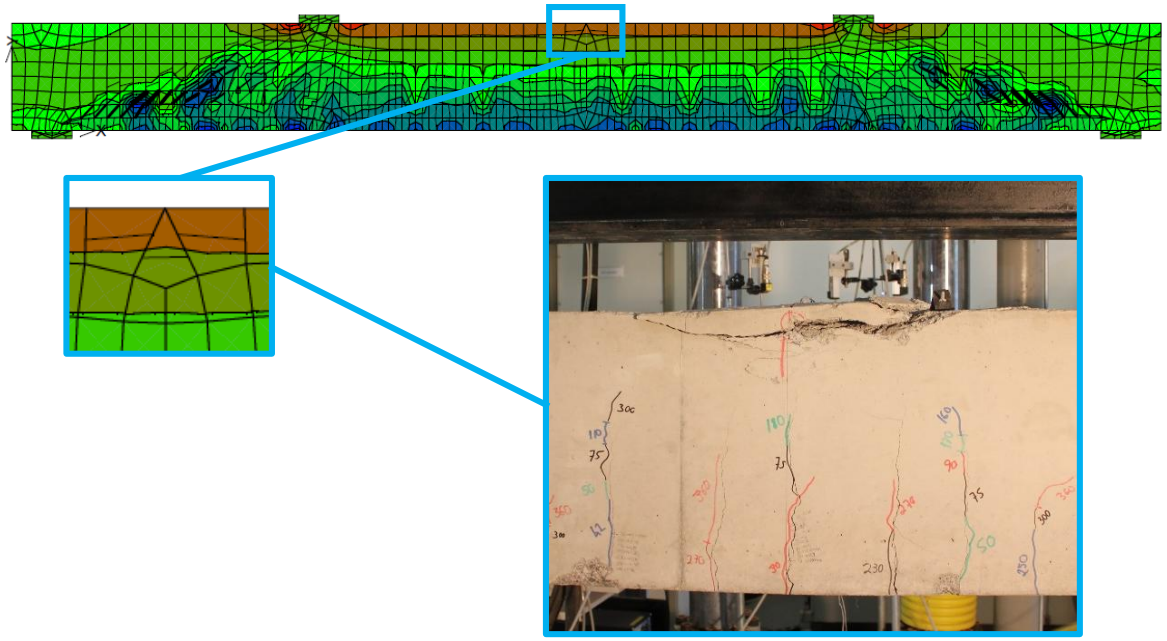

Figure 150 - Comparison of the FE model and the actual failure of BS250

From Figure 151 to Figure 154 it is presented the comparison between the model's load deflection curve and the test curve of BS250GFRP1, BS250GFRP2, BS175GFRP1 and BS175GFRP2, respectively. In general, the curves of the FE models are closer to the curve of the 50 mm LVDT.

In the FE model of these beams the failure was due to the loss of the convergence. The shear reinforcement strains at this step are higher or similar to the experimental strain at failure, for this reason it was admitted that the failure has occured, and that it was due to stirrups rupture.

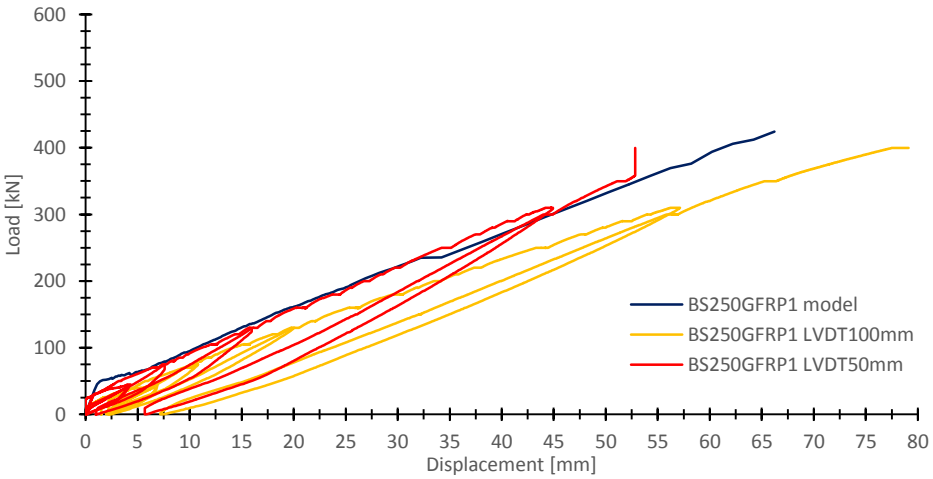

Figure 151 – Load deflection curves of BS250GFRP1

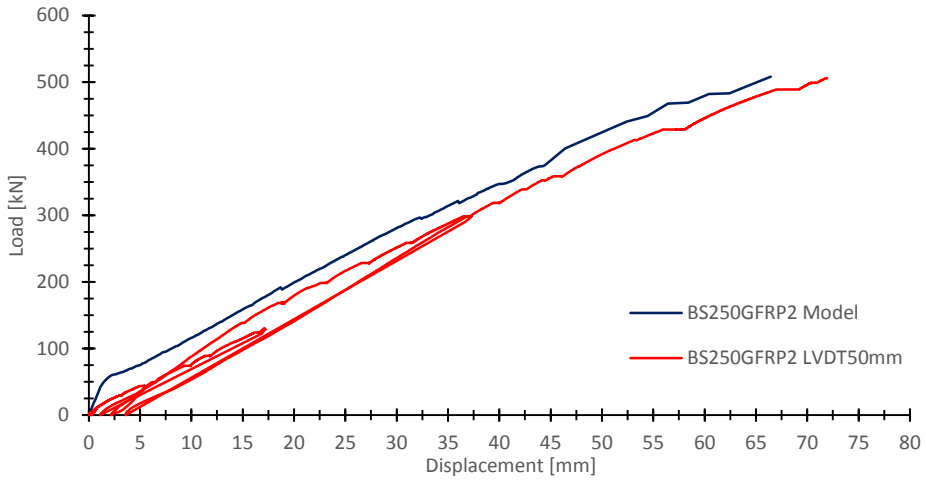

Figure 152 -– Load deflection curves of BS250GFRP2

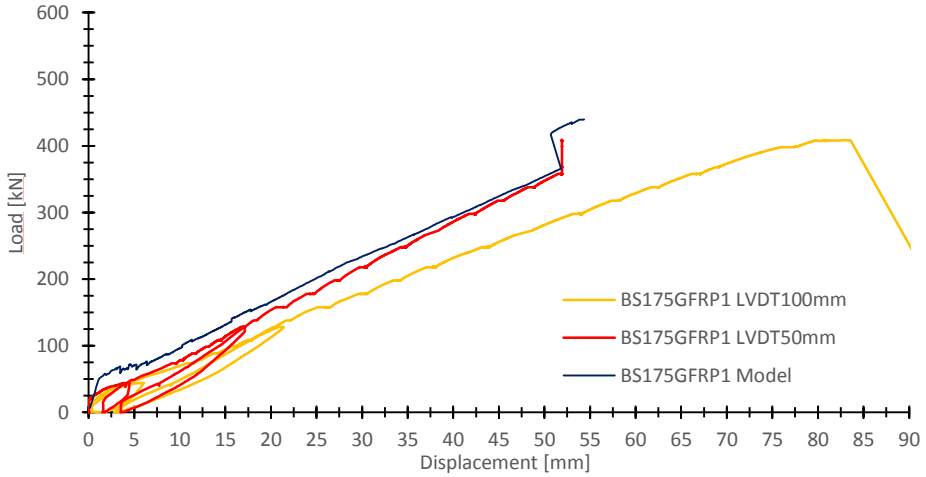

Figure 153 - Load deflection curves of BS175GFRP1

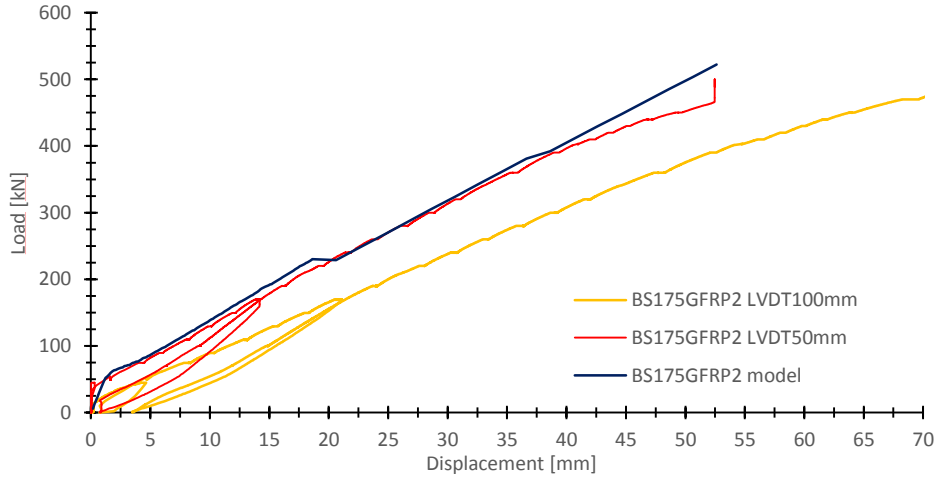

Figure 154 - Load deflection curves of BS175GFRP2

The models were able to predict the reduction of the stiffness after cracking, but in almost all the cases, the elastic phase is stiffer in the model than in the real case. The FE model was not able to simulate exactly the initial elastic stage of the beams. The heterogeneity of the concrete and the fact that a self-compacting concrete was used may be possible reasons for these differences.

The difference between the predictions of the FE Model and the experimental is shown in Table 57. Several reasons may explain these differences, such as: some imperfections in the monitoring during the tests, the fact that in the models the reinforcement was considered perfectly bonded to the concrete.

Table 57 – Comparison of the experimental and numerical ultimate loads

	Ultimate load		
	FE model	Test	Difference
Beam	(kN)	(kN)	(%)
REF250	466.4	426.4	9.4
REF175	539.0	477.0	13.0
BS250	430.0	488.2	11.9
BS175	470.4	468.1	0.5
BS250GFRP1	423.9	400.0	6.0
BS175GFRP1	439.8	408.4	7.7
BS250GFRP2	507.2	506.0	0.2
BS175GFRP2	522.4	500.0	4.5

Despite some differences, is possible to conclude that in general each FE model was able to simulate the results of the respective real tested beams.

4.2.2 Parametric study

After the validation of the FE model through the comparison with the experimental data, a second part of the numerical investigation consisted on the realization of a parametric study made in order to draw further conclusions. The discussed parameters are: 1 – Two additional shear reinforcement spacing; 2 – Closed GFRP stirrups of 8 mm diameter, similar to the steel reinforced reference beams.

The C30/37 typical properties were considered. It was considered the typical A500 grade for the steel reinforcement, with a yield strength of 500 MPa and a bilinear stress-strain relationship. The GFRP reinforcement bars were modelled with a linear stress strain relationship and with an elasticity modulus of 60 GPa.

4.2.2.1 Beam reinforced with 8 mm GFRP stirrups

A beam identical to the REF250 was considered, but with GFRP stirrups of 8 mm diameter, which was designated by BS250-8. The considered GFRP stirrups had identical mechanical properties to the 12 mm. The main reasons for this comparison were: 1) the manufacturer of the GFRP bars only produce GFRP bent bars for a diameter higher than 12 mm. 2) according to the codes used for design it only achieved an equivalent shear capacity considering the 12 mm stirrups.

The FE model failed due to shear since the shear reinforcement exhibited strains higher than 8‰. The ultimate load of BS250-8 was 406 kN, while REF250 failed at 426,4 kN.

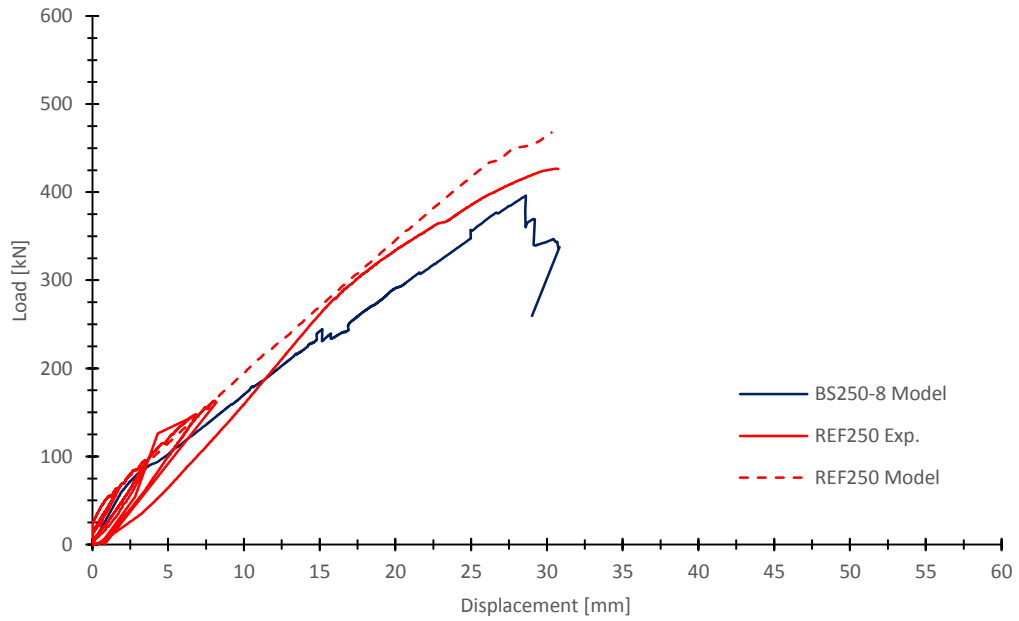

Figure 155 - Behaviour comparison between the REF250 and BS250-8 mm

Despite the fact that the simulated beam exhibited a 4.5% lower load capacity than the reference beam, the overall behaviour was similar. It is possible to conclude that solutions with 8 mm diameter stirrups were possible.

4.2.2.2 *Shear reinforcement ratio*

Two additional stirrups spacing were considered: 1) GFRP 12 mm stirrups spaced at 0.150 m which is smaller than those tested and corresponds to 0.4 d (BS150 beam); 2) GFRP 12 mm stirrups spaced at 0.280 m which is higher than those tested and corresponds to 0.75 d (BS280 beam).

Figure 156 shows the comparison between the load-deflections of BS150, BS175, BS250 and BS280. The behaviour was similar in all the cases. As the BS150, BS175 and BS250 failed by bending it was not possible to clarify and quantify the influence of the shear reinforcement ratio the ultimate shear capacity.

The FE model of the beam with stirrups spaced at 0.75 d suggest that the it is possible to extend the maximum spacing of 0.5 d indicated by ACI 440.1R-06 [2] to the 0.75 d indicated in EC2 [23] for traditional steel reinforcement.

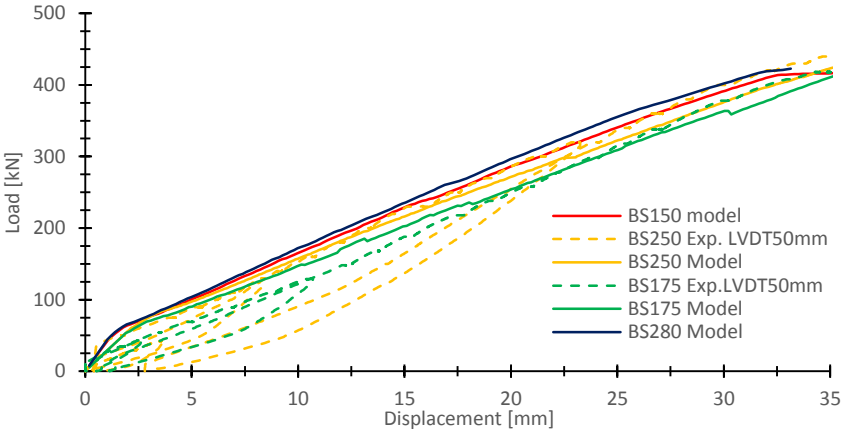

Figure 156 – Comparison between BS150, BS175, BS250 and BS250

4.2.2.3 *Longitudinal reinforcement ratio*

In section 2.4 it was concluded that the longitudinal reinforcement ratio has an important influence in the shear capacity. As experimentally only two different GFRP longitudinal reinforcement ratios were tested, it was not possible to clarify if the relation between the longitudinal reinforcement ratio and the shear capacity is linear. Considering the same GFRP shear reinforcement – closed stirrups of 12 mm diameter with 0.250 m of spacing - three different GFRP longitudinal ratios were simulated, 2.80%, 1.58% and 0.86%. The beams failed due to shear and the load – deflection curves

are represented in Figure 157. In general it can be stated that increasing the longitudinal reinforcement ratio increases the shear capacity.

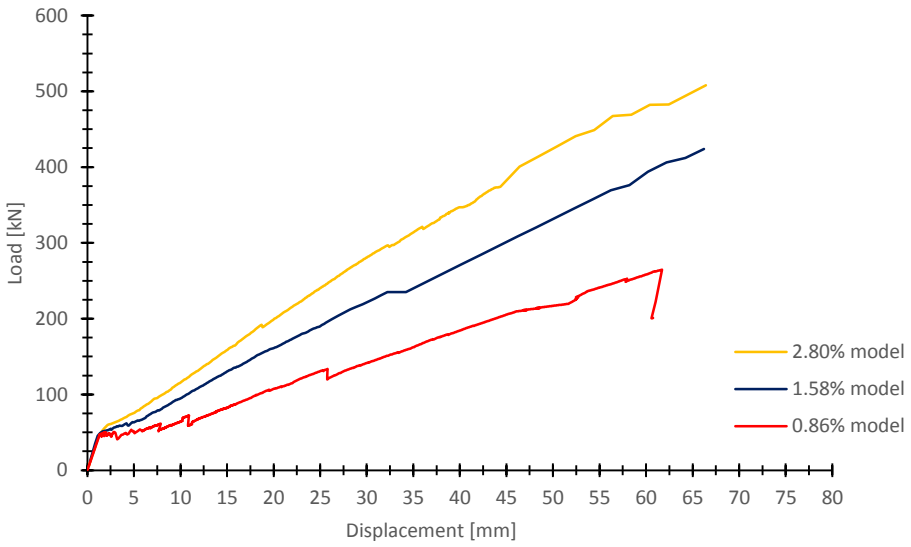

Figure 157 – Load-displacement curves for different GFRP longitudinal reinforcement ratios

In Figure 158 it is represented the values of the shear capacity for the different GFRP longitudinal reinforcement ratios considered. The relationship is not linear. For lower values of the longitudinal reinforcement, increasing the longitudinal reinforcement ratio corresponds to a sharp increase in the shear capacity. As the longitudinal reinforcement ratio increases, the increase in the shear capacity is lower.

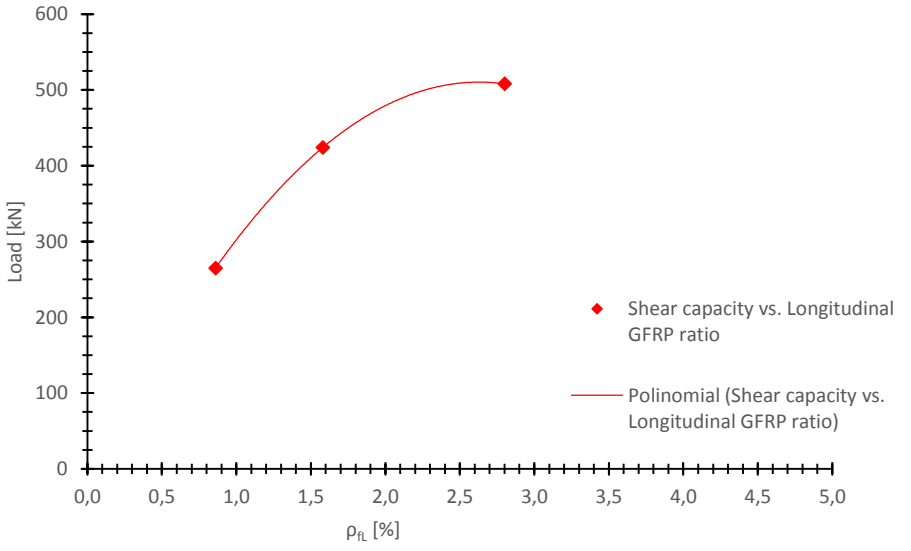

Figure 158 – Shear capacity vs. GFRP longitudinal reinforcement ratio

4.3 GFRP longitudinally rehabilitated beams

Both the steel beams, REF and REHABSTEEL, and the GFRP beams REHABGFRP1 and REHABGFRP2 were modelled. The results are presented in this section by load-displacement curves and the comparison between the experimental curves and the numerical curves is done in order to evaluate the agreement between the modelling and the test results.

In these models, 5 macro-elements were needed as indicated in Figure 142. Macro-element 5 is the concrete element, and macro-elements from 1 to 4 are steel plate elements. These last elements were modelled with a similar dimension of the one used in the experimental tests, and represent the four loading points of the beam specimens. The steel plate elements were modelled as a plane stress elastic isotropic material. An elasticity modulus of 210 GPa was used. Interface elements ("2D interface") were introduced in the boundary lines between these elements and the concrete beam. These interface elements had a high stiffness in compression but no stiffness in tension, so that the rotation is allowed avoiding stress concentrations and numerical problems.

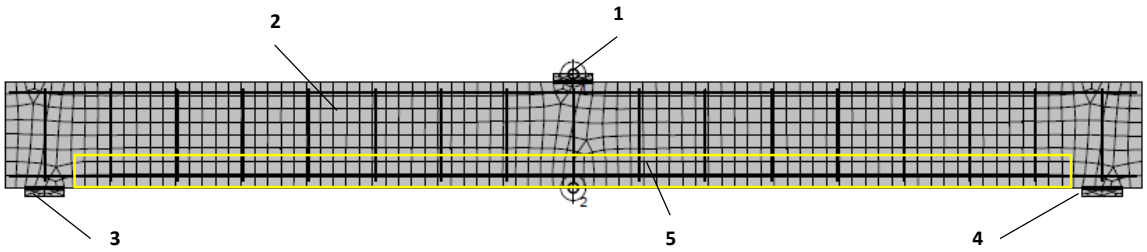

Figure 159 – Macro-elements and FE mesh

The concrete was modelled with SBETA material and with the mechanical properties measured in the experimental tests. For shear behaviour a fixed crack model was used, with variable shear retention factor and linear tension-compression interaction. The crack direction is fixed during the loading and is given by the principal stress direction at the moment of the initiation of the crack.

All reinforcement bars were simulated as discrete bar elements embedded in the concrete FE and with perfect connection. The constitutive stress-strain relationship used for all steel reinforcement elements was bilinear. The yielding stress and elasticity modulus used were different for each bar diameter and were defined according to the experimental values of the samples tested and which were related in 2.1.1. For GFRP reinforcement bars, it was considered a linear stress-strain relationship with an elasticity modulus of 60 GPa for the straight GFRP bars.

It was considered a FE mesh with a dimension of the FE of 0,05 m.

The Newton-Raphson method in simultaneous with the line search method were used in all the analyses. The load steps defined were increasing imposed displacements at the loading points.

The load-deflection at mid-span between the models and the respective results of the tested beams are compared and present from Figure 160 to Figure 164. Figure 164 shows the cracking pattern of REHAB beams FE model. This pattern shows the cracks at the interface of the two concrete layers verified in the experimental tests (Figure 163).

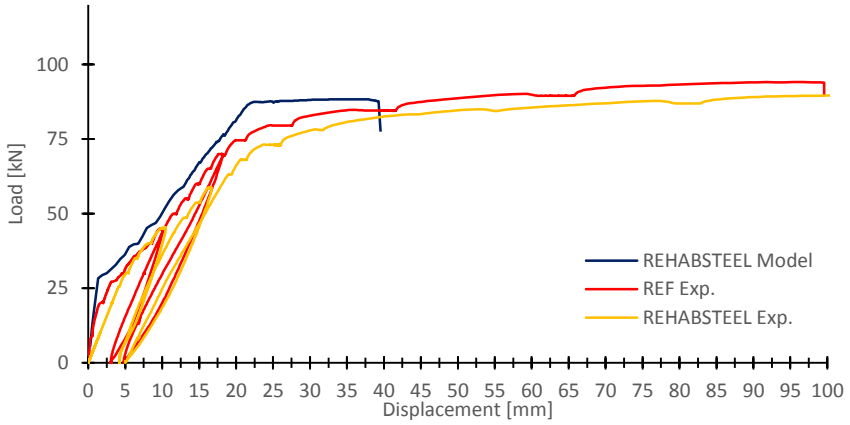

Figure 160 - Behaviour comparison between the REF, REHABSTEEL and the FE model

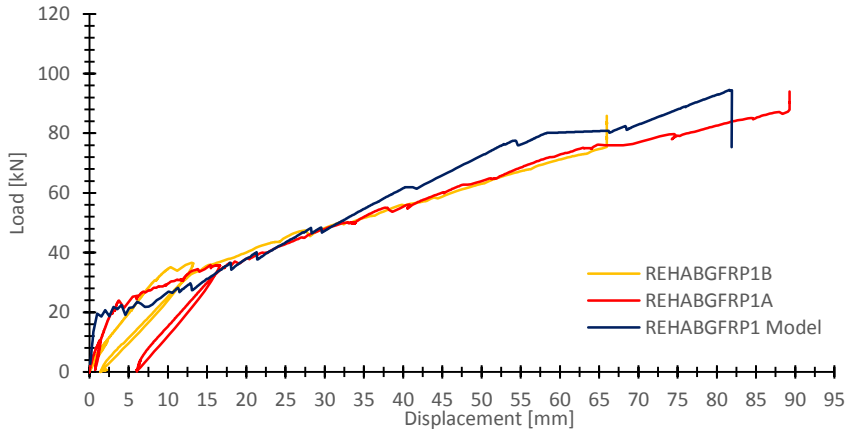

Figure 161 - Behaviour comparison between the REHABGFRPGFRP1A, REHABGFRP1B and the FE model

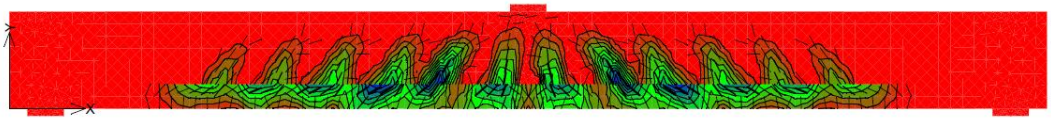

Figure 162 – FE model crack pattern of REHAB beams

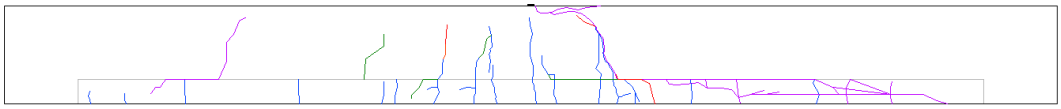

Figure 163 – Experimental crack pattern of REHAB beams

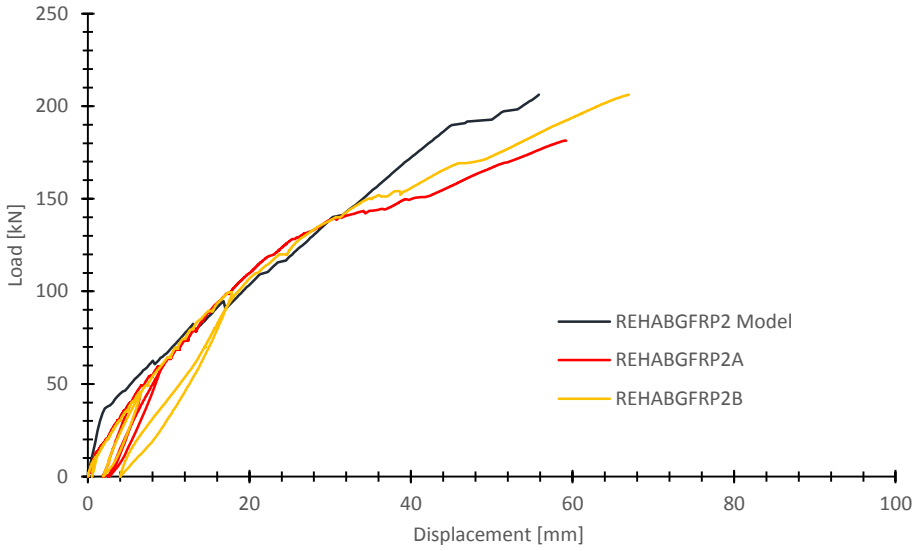

Figure 164 - Behaviour comparison between the REHABGFRP2A, REHABGFRP2B and the FE model

In all considered cases the model was able to predict the real behavior in terms of ultimate loads and in terms of deflections (with exception of REHABSTEEL), as showed in Table 58.

Table 58 – Comparison between the experimental and numerical values

	Ultimate load			Ultimate deflection		
	FE model	Test	Diference	FE model	Test	Diference
Beam	(kN)	(kN)	(%)	(mm)	(mm)	(%)
REF	88.8	94.1	5.6	99.0	90.5	9.4
REHABSTEEL	88.8	89.8	1.1	99.0	41.0	141.0
REHABGFRP1A	94.5	94.0	0.5	81.9	89.3	8.3
REHABGFRP1B	94.5	85.9	10.1	81.9	66.0	24.2
REHABGFRP2A	206.1	181.5	13.6	55.9	59.1	5.4
REHABGFRP2B	206.1	206.2	0.1	55.9	67.0	16.5

4.4 Conclusions

The following can be concluded based on the findings of the study:

1- The constructed models of the beams with GFRP shear reinforcement were able to predict the behaviour in terms of load-deflection curve with reasonable accuracy. The failure modes obtained in the FE model were also consistent with the experimental, with exception of BS2520GFRP1. The model was not able to reproduce the splitting of the longitudinal reinforcement.

2- The FE model deflection values were closer to the values measured by the 50 mm LVDT. As in all the chapters of this thesis, the values considered were those measured by the 100 mm, therefore, it is possible that the deflections are overestimated and higher than the real ones.

3- From the parametric study related to the GFRP shear reinforced beams it was concluded that the beams reinforced with GFRP stirrups with 8 mm diameter have an identical behaviour, capacity and failure modes to the reference steel beam. This is an important conclusion because it may indicate that there is a direct correspondence between the stirrups of these two materials, which may be useful when designing.

4- By simulating the 0,75 d spacing, it was concluded that it is possible to extend the limit of 0.5 d for maximum stirrups spacing indicated by ACI 440.1R-06 [2] to the maximum proposed in the EC2 [23] for traditional RC, 0.75 d.

5- The shear capacity depends on the longitudinal reinforcement ratio. After modelling several GFRP longitudinal reinforcement ratios it was concluded that, the increase rate of shear capacity was lower than a linear relationship with the longitudinal reinforcement.

6- The FE model was able to reproduce the behaviour of the rehabilitated beams in terms of load-deflection curves, crack pattern and deflections. Thus, this model can be used to simulate other solutions, namely a rehabilitated beam where both deflection and ultimate capacity of the reference were assured by increasing the total height of the beam instead of increasing the reinforcement area.

Chapter 5.

Conclusions, final remarks and future research

The main objective of this research work was to provide a contribution to the scientific knowledge in two different main domains of the FRP RC: the performance of RC beams with GFRP shear reinforcement and the rehabilitation of steel RC elements through the replacement of the deteriorated reinforcement by GFRP bars. In order to achieve this goal an experimental campaign was carried out with 24 full-scale RC beams with GFRP and steel reinforcement. An additional numerical analysis using finite element models of the tested specimens was made to enhance and confirm the findings and to enable further conclusions based on extrapolated models of non-tested beam cases.

This chapter presents general conclusions and final comments to this thesis. It starts with a summary of the conclusions followed by final remarks. It ends with some proposals for future research to continue this line of work, based on the achieved experience.

5.1 Conclusions

All the conclusions of the present research regarding a specific subject are described in detail at the end of the corresponding section within the previous chapters. Therefore, the current section is only a summary of the conclusions as it shortly reports the main findings of the scientific work.

Concerning the study of RC beams with different layouts of GFRP shear reinforcement it was concluded that:

1- Both tested solutions with GFRP bent bars (closed hoop stirrups and two C bars forming a closed stirrup) were efficient and the crack pattern and failure mechanisms of the beams with GFRP stirrups were similar to the ones with steel closed stirrups. In both cases the bent of the bar was not responsible for the failure mechanism.
2- Some shear failure modes showed that the anchorage length of the bent solutions should be at the top of the beam and not at the bottom because it has a tendency to open. Therefore, in this particular issue, the closed hoop stirrup is a better solution than the two C bars, which inevitably has an anchorage at the bottom.
3- The solution of using two vertical double headed GFRP bars has the advantage of being easy to assemble but its performance as shear reinforcement of a RC beam was not very reliable. It was proved that it is significantly affected by the longitudinal stiffness of the beam. In the cases of high deflections, when a crack crossed over a head and damaged it, the anchorage of the bar was reduced and its ability to support load was compromised, which contributed to the premature failure of the beam.
4- The simple straight bars alternative proved to be an inadequate solution due to the lack of anchorage length
5- The longitudinal stiffness of the RC beams had a significant influence on the shear strength of all tested solutions. A lower stiffness is related to higher deflections and tends to increase the crack widths and to reduce the shear strength. The inclination of the failure plane in the beams with lower stiffness was found to be higher. Consequently, the shear cracks crossed less stirrups, reducing the shear strength.
6- The hybrid specimens with GFRP shear reinforcement and steel longitudinal reinforcement exhibited a better performance than the ones with GFRP longitudinal bars. The explanation to this fact is the higher stiffness of the steel material that contributed for smaller deflections and smaller cracks in the beams. Therefore, the integrity of the shear resistance mechanisms was kept for higher loads and as a consequence the shear strength increased. Although this hybrid solution is not entirely immune to corrosion, it has the advantage of being less expensive and at the same time more durable in aggressive environments than the conventional steel RC structures as the outer and more exposed reinforcement is made of GFRP.
7- It was found that the estimated values for the concrete contribution according to ACI 440.1R-06 [2] tended to be lower than the obtained in the tests. Therefore, it was proposed an adjustment to the ACI 440.1R-06 [2] formula to the concrete shear contribution (V_c). This

adjustment was done introducing a linear equation to the estimation of the parameter k based on the experimental results.

8- It was demonstrated that a lower spacing of the closed GFRP stirrups resulted in the increase of the cracking angle with the horizontal he tests showed that the stirrups spacing can be higher than the maximum of 0,5d allowed by ACI 440.1R-06 [2] or than the 0.45d referred by FIB40[22].

9- Both ACI 440.1R-06 [2] and FIB40[22] documents for the design of RC structures with GFRP reinforcement underestimated in general the shear strength of the tested beams. The cases with evident shear failure mode reached higher strain values in the GFRP shear reinforcement than the suggested according to these two codes. In order to calibrate the formulas and to adjust them to the tests results, it was proposed a correction to the strain limit and to the strut angle values used in both ACI 440.1R-06 [2] and FIB40[22] formulas. This fact has a direct consequence in the design of the RC beams with GFRP shear reinforcement as it implies an increase of its shear strength. Furthermore, this fact allows a more economical although effective design.

10- The formulas of ACI 440.1R-06[2] to determine the short-term deflections at service load predicted with good accuracy the values monitored in the tests.

11- The tests did not confirm a shear strength directly proportional to the shear reinforcement ratio as proposed by most codes.

Based on the experimental study of the proposed solution to rehabilitate deteriorated RC beams due to steel corrosion by replacing it with GFRP bars, the following main conclusions were drawn:

1- The rehabilitation procedure was viable, not difficult to implement and the solution proved to be efficient in restoring the load capacity and the deflection of the original steel RC beam. The main constructive difficulties were related to the insertion of the GFRP bars at the supports due to the dimensions of the conic heads, particularly in the case of the 25 mm diameter bar.

2- Despite the lower modulus of elasticity of the GFRP in comparison to steel, one of the tested rehabilitated solution was able to restore both the serviceability and ultimate capacity of the original beam.

3- The absence of the bottom branch of the steel stirrups, eventually destroyed by corrosion, did not compromise the shear performance of the rehabilitated beams. Thus, there is no need for shear strengthening, which simplifies this rehabilitation proposal.

4- The construction joint between the two concrete layers was not the failure cause and did not compromise the serviceability and ultimate limit states of the rehabilitated beams.
5- Even though there were some doubts about the performance of the GFRP bar ends, the tests proved that their conic heads inserted in the concrete holes at the supports filled with epoxy resin were sufficient to ensure the anchorage of the bars.
6- The rehabilitated solution was designed according to the existing RC design code EC2 [23] and the FRP design guidelines FIB40 [22] and ACI 440.1R-06 [2]. These documents are sufficient and there is no need for additional formulas since good result predictions were obtained, which makes it possible for engineers to implement this technique in actual structures.
7- This technique has the advantage of solving the steel corrosion problem of a RC structural element subjected to bending until the end of its design working life due to the immunity to this phenomenon of the GFRP material. Therefore, it is a solution with lower costs in the long term when compared to some of the traditional rehabilitation techniques to solve the steel corrosion issue, which are expensive and have limited warranty of success, hence limited durability.

Finally, the finite element analysis enabled the following additional conclusions that complement the conclusions of the experimental tests:

1- The beams reinforced with GFRP stirrups with 8 mm diameter have an identical behaviour, capacity and failure modes to the reference steel beam. This is an important conclusion because it may indicate that there is a direct correspondence between the stirrups of these two materials.
2- From the models were the GFRP stirrups were spaced at 0,75 d, it was concluded that it is possible to extend the limit of 0.5 d for maximum stirrups spacing indicated by ACI 440.1R-06 [2] to the maximum indicated in the EC2 [23] for traditional RC, 0.75 d.
3- By testing several GFRP longitudinal reinforcement ratios, it was concluded that although the shear capacity depends on the longitudinal reinforcement ratio, the rate of increase of the shear capacity decreases as the longitudinal reinforcement ratio increases.

5.2 Final remarks

The current scientific work demonstrated that the use of GFRP bars is a viable alternative to the use of steel, not only as shear reinforcement of RC beams to be constructed but also as a rehabilitation solution to replace steel reinforcement in deteriorated RC beams. The immunity to corrosion of the GFRP material makes it highly competitive from an economic perspective in long-term durability when compared to steel in RC structures in general and in marine RC structures in particular.

One of the well-known causes for its delay in wide use in civil engineering structures is some lack of knowledge about its behaviour in RC structures and the absence of codes to guide the engineers in the design. This work contributed to increase the scientific knowledge of the RC structures with GFRP reinforcement and proposed improvements and adjustments to the design formulas of the existing guidelines.

Since the present work is based on tests with full-scale specimens, their performances are a faithful representation of the actual RC structures behaviour. Hence, the conclusions and the proposals reported are reliable and can be directly applied to real cases.

5.3 Future Research

The results reported in this thesis are related to rectangular cross-section beams of intermediate length. Given the limited number of beam specimens tested, and the issues found during the tests more experimental testing is suggested below.

Concerning the study of RC beams with different layouts of GFRP shear reinforcement several issues remained to clarify and / or justify further investigation namely:

1- As shear mechanisms and failures are a complicated phenomenon by occurring under combined stresses resulting from applied shear force and bending moment, more experimental testing is needed exploring other situations in order to increase the database of the beam specimens and develop and adapt the existing models and equations.
2- It is important to test more specimens longitudinally reinforced with steel but shear reinforced with GFRP stirrups, as this solution seems to have a good performance in terms of ultimate capacity and deformability without being costly.
3- The C-stirrups were proved to be an interesting solution. However, inevitably they have an anchorage length at the bottom of the beam, which in several failure modes exhibited a

tendency to open. In future tests, additional strain gauges should be placed near these bottom branches of the stirrups to measure the strains and the level of stress that causes this disintegration and consequently the shear failure. It is important to quantify the stirrup stress.

4- The double headed bars as shear reinforcement are the easiest solution to implement in the field. But the tests showed that this solution is only effective in some cases of flexural stiffness. Further research, considering other more longitudinal reinforcement ratios should be done in order to quantify and stablish a boundary in terms of longitudinal stiffness where this solution can be applied.
5- By testing several beams with GFRP stirrups spaced at 0.67 d, it was showed that stirrup spacing higher than the 0.5 d suggested by ACI was possible. The numerical models indicate that this limit can be extended to 0.75 d indicated in EC2 [23] for traditional reinforced concrete. However, in future research it is important to validate this conclusion experimentally.
6- Varying shear span-to-depth is also important to extend the main conclusions of this work.

Regarding the rehabilitation technique future research should consider:

1- It was proven that it is possible to keep both the deflection and the ultimate load capacity of the original beam by considering a high ratio of the GFRP reinforcement. Testing a solution where the rehabilitated beams restore the serviceability and the ultimate capacity of the original beams by increasing the height of the beams. In this solution it is also important to study if the shear behaviour would not be affected since the stirrups would be shorter than the beam.
2- It was only considered a longitudinal GFRP reinforcement with double headed bars. But it was also verified that the dimensions of the heads can make the insertion of the bars more difficult. This issue can compromise the application of this solution in several practical cases where there is few space. Testing the solution with GFRP bars without the end heads is important.

References

1. 1992-1-1, N.E., *Eurocode 2: Design of Concrete Structures - Part 1-1: General Rules and Rules for Building.* European Committee for Standardization (CEN), 2010.
2. ACI, *ACI 440.1R-06 Guide for the design and Construction of structural concrete reinforced with FRP Bars*. 2006, American Concrete Institute: Farmington Hills, U.S.A.
3. ACI, *ACI 318-11 Building Code Requirements for structural concrete*. 2011.
4. Admasu, S.D. and S.L. Adam, *Shear in Concrete Beams Reinforced with High-Performance Steel.* ACI Structural Journal, 2015. **112**(06).
5. Ahmed, E.*, et al.*, *Bend Strength of FRP Stirrups: Comparison and Evaluation of Testing Methods.* Journal of Composites for Construction, 2010. **14**(1): p. 3-10.
6. Ahmed, E.A., E.F. El-Salakawy, and B. Benmokrane, *Fibre-reinforced polymer composite shear reinforcement: performance evaluation in concrete beams and code prediction.* Canadian Journal of Civil Engineering, 2010. **37**(8): p. 1057-1070.
7. Ahmed, E.A.*, et al.*, *Bend Strength of FRP Stirrups: Comparison and Evaluation of Testing Methods.* Journal of Composites for Construction, 2010. **14**(1): p. 3-10.
8. Al-Rahmani, A. and F.H. Abed. *Numerical investigation of hybrid FRP reinforced beams*. in *Modeling, Simulation and Applied Optimization (ICMSAO), 2013 5th International Conference on*. 2013.
9. Al-Saidy, A.H.*, et al.*, *Structural performance of corroded RC beams repaired with CFRP sheets.* Composite Structures, 2010. **92**(8): p. 1931-1938.
10. Alsayed, S.H., *Flexural behaviour of concrete beams reinforced with GFRP bars.* Cement and Concrete Composites, 1998. **20**(1): p. 1-11.
11. Ashour, A.F., *Flexural and shear capacities of concrete beams reinforced with GFRP bars.* Construction and Building Materials, 2006. **20**(10): p. 1005-1015.
12. Ashour, A.F. and I.F. Kara, *Size effect on shear strength of FRP reinforced concrete beams.* Composites Part B: Engineering, 2014. **60**(0): p. 612-620.
13. Association, C.S., *CSA S806-02 Design and construction of building structures with fibre-reinforced polymers*. 2002: Canada.
14. B. Benmokrane, B.T. and Chaallal, *Bond Strength and Load Distribution of Composite GFRP Reinforcing Bars in Concrete.* ACI Materials Journal, 1996. **93**(3).
15. Badawi, M. and K. Soudki, *CFRP Repair of RC Beams with Shear-Span and Full-Span Corrosions.* Journal of Composites for Construction, 2010. **14**(3): p. 323-335.
16. Bakis, C.*, et al.*, *Fiber-Reinforced Polymer Composites for Construction - State-of-the-Art Review.* Journal of Composites for Construction, 2002. **Vol. 6, n.º2**: p. 14.
17. Bakis, C.E.*, et al.*, *Fiber-Reinforced Polymer Composites for Construction--State-of-the-Art Review*. 2002.
18. Bischoff, P.H.a.S., A., *Effective Moment of Inertia for Calculating Concrete Members Containing Steel Reinforcement Fiber-Reinforced Polymer Reinforcement.* ACI Structural Journal, 2007. **104(1)**: p. 68-76.
19. Cantwell, W.J., *The Fracture Behavior of Glass Fiber/Recycled PET Composites.* Journal of Reinforced Plastics and Composites, 1999. **18**(4): p. 373-387.
20. CEB-FIB, *Model Code 2010*. 2012, International Federation for Structural Concrete (fib): Switzerland.
21. CEB-FIP, *Model Code 1990 - Design Code.* 1991.
22. CEB-FIP, *Bulletin n. 40 - FRP reinforcement in RC structures - Design and use of fibre reinforced polymer reinforcement (FRP) in reinforced concrete structures*. 2007, International Federation for Structural Concrete (FIB).

23. CEN, *NP EN 1992-1-1 - Eurocode 2: Design of Concrete Structures - Part 1-1: General Rules and Rules for Building*, in *European Committee for Standardization (CEN)*. 2010, European Committee for Standardization (CEN).
24. Ceroni, F.*, et al.*, *Durability issues of FRP rebars in reinforced concrete members.* Cement and Concrete Composites, 2006. **28**(10): p. 857-868.
25. Cervenka, V.C., Jan; Jendele, Libor, *ATENA Program Documentation Part 1: Theory*. 2016, Cervenka Consulting Prague, Czech Republic.
26. Coronelli, D.M., M., *Modeling of shear behaviour in reinfroced concrete beams.* ACI Structural Journal, 2006. **103**(n.3): p. 372-382.
27. Council, N.R., *CNR-DT 203/2006 Guide for the Design and Construction of Concrete Structures Reinforced with Fiber-Reinforced Polymer Bars*. 2006, CNR: Rome - Italy.
28. David Trejo, P.G. and K. Jeong Joo, *Long-Term Performance of Glass Fiber-Reinforced Polymer Reinforcement Embedded in Concrete.* ACI Structural Journal, 2011. **108**(06).
29. Ehab A. Ahmed, E.F.E.-S. and B. Brahim, *Performance Evaluation of Glass Fiber-Reinforced Polymer Shear Reinforcement for Concrete Beams.* ACI Structural Journal, 2010. **107**(01).
30. El-Nemr, A., E.A. Ahmed, and B. Brahim, *Flexural Behavior and Serviceability of Normal- and High-Strength Concrete Beams Reinforced with Glass Fiber-Reinforced Polymer Bars.* ACI Structural Journal, 2013. **110**(06).
31. El-Sayed, A.K. and K. Soudki, *Evaluation of Shear Design Equations of Concrete Beams with FRP Reinforcement.* Journal of Composites for Construction, 2011. **15**(1): p. 9-20.
32. Elgabbas, F., E.A. Ahmed, and B. Benmokrane, *Physical and mechanical characteristics of new basalt-FRP bars for reinforcing concrete structures.* Construction and Building Materials, 2015. **95**: p. 623-635.
33. Elgabbas, F., E.A. Ahmed, and B. Benmokrane, *Physical and mechanical characteristics of new basalt-FRP bars for reinforcing concrete structures*. 2015.
34. Fares, E.T. and S. Hamid, *Environmental Effects on the Mechanical Properties of the E-Glass FRP Rebars.* ACI Materials Journal, 1998. **95**(2).
35. Fico, R., A. Prota, and G. Manfredi, *Assessment of Eurocode-like design equations for the shear capacity of FRP RC members.* Composites Part B: Engineering, 2008. **39**(5): p. 792-806.
36. Firmo, J.P., M.R.T. Arruda, and J.R. Correia, *Contribution to the understanding of the mechanical behaviour of CFRP-strengthened RC beams subjected to fire: Experimental and numerical assessment.* Composites Part B: Engineering, 2014. **66**: p. 15-24.
37. Firmo, J.P., J.R. Correia, and P. França, *Fire behaviour of reinforced concrete beams strengthened with CFRP laminates: Protection systems with insulation of the anchorage zones.* Composites Part B: Engineering, 2012. **43**(3): p. 1545-1556.
38. França, P.M.M., *Reinforced Concrete Beams Strengthened with Presstressed CFRP Laminates, PhD Thesis*. 2007, Universidade Técnica de Lisboa -Instituto Superior Técnico.
39. Gangarao, H.V.S.T., Narenda; Vijay, P.V., *Reinforced Concrete Design with FRP Composites*, ed. C. Press. 2007.
40. Gangarao, P.V.V.H.V.S., *Bending behavior and defomability of Glass Fiber-Reinfroced Polymer Reinforced Concrete Members.* ACI Structural Journal, 2001.
41. Ghosh, P. and N.R. Bose, *FRP composites based on different types of glass fibers and matrix resins: A comparative study.* Journal of Applied Polymer Science, 1995. **58**(12): p. 2177-2184.
42. Golafshani, E.M., A. Rahai, and M.H. Sebt, *Artificial neural network and genetic programming for predicting the bond strength of GFRP bars in concrete.* Materials and Structures, 2015. **48**(5): p. 1581-1602.
43. Gonçalves, J.F.G., *Aderência de Varões GFRP no betão*, in *Centro de Ciências Exactas e da Engenharia*. 2014, Universidade da Madeira: Funchal, Portugal. p. 135.

44. Gouda, A. and E. El-Salakawy, *Finite Element Modeling of GFRP-Reinforced Concrete Interior Slab-Column Connections Subjected to Moment Transfer.* Fibers, 2015. **3**(4): p. 411.
45. Grace , N.*, et al.*, *Behavior and Ductility of Simple and Continous FRP Reinforced Beams.* Journal of Composites for Construction, 1998. **Volume 4, n.º 2**
46. Gribniak, V., V. Cervenka, and G. Kaklauskas, *Deflection prediction of reinforced concrete beams by design codes and computer simulation.* Engineering Structures, 2013. **56**: p. 2175-2186.
47. Guadagnini, M., K. Pilakoutas, and P. Waldron, *Shear Resistance of FRP RC Beams: Experimental Study.* Journal of Composites for Construction, 2006. **10**(6): p. 464-473.
48. Hany Jawaheri, Z. and N. Antonio, *Reliability Analysis of Concrete Beams Internally Reinforced with Fiber-Reinforced Polymer Bars.* ACI Structural Journal, 2013. **110**(06).
49. Hashemi, S. and R. Al-Mahaidi, *Experimental and finite element analysis of flexural behavior of FRP-strengthened RC beams using cement-based adhesives.* Construction and Building Materials, 2012. **26**(1): p. 268-273.
50. Houssam, A.T. and S. Mohamed, *Flexural Behavior of Concrete Beams Reinforced with Glass Fiber-Reinforced Polymer (GFRP) Bars.* ACI Structural Journal, 2000. **97**(5).
51. IPQ, *EN 206-9:2010 Concrete. Additional rules for self-compacting concrete (SCC)*. 2010, IPQ - Instituto Português da Qualidade: Portugal. p. 30.
52. IPQ, *NP EN 12390-3: "Ensaios do betão endurecido; Parte 3: Resistência à compressão de provetes"*. 2011, IPQ
53. IPQ, *NP EN ISO 6892: Materiais metálicos. Ensaio de Tração Parte 1: método de ensaio à temperatura ambiente*. 2012.
54. IPQ, *NP EN 12390-13: "Ensaios do betão endurecido; Parte 13: Determinação do módulo de elasticidade secante à compressão;"*2014, IPQ - Instituto Português da Qualidade.
55. Johnson, D.T. and S.A. Sheikh, *Performance of bent stirrup and headed glass fibre reinforced polymer bars in concrete structures1.* Canadian Journal of Civil Engineering, 2013. **40**(11): p. 1082-1090.
56. Joseph Robert Yost, S.P.G. and W.D. David, *Effective Moment of Inertia for Glass Fiber-Reinforced Polymer-Reinforced Concrete Beams.* Structural Journal, 2003. **100**(6).
57. Kara, I.F., *Prediction of shear strength of FRP-reinforced concrete beams without stirrups based on genetic programming.* Advances in Engineering Software, 2011. **42**(6): p. 295-304.
58. Keller, T., *Use of Fibre Reinforced Polymers in Bridge Construction*, ed. I.A.f.B.a.S.E. (IABSE). 2003, Zurich.
59. Kreit, A.*, et al.*, *Repairing corroded RC beam with near-surface mounted CFRP rods.* Materials and Structures, 2011. **44**(7): p. 1205-1217.
60. Lee, S. and C. Lee, *Prediction of shear strength of FRP-reinforced concrete flexural members without stirrups using artificial neural networks.* Engineering Structures, 2014. **61**(0): p. 99-112.
61. Lees, J.M., *Fibre-reinforced polymers in reinforced and prestressed concrete applications: moving forward.* Progress in Structural Engineering and Materials, 2001. **3**(2): p. 122-131.
62. Lignola, G.P.*, et al.*, *Probabilistic design equations for the shear capacity of RC members with FRP internal shear reinforcement.* Composites Part B: Engineering, 2014. **67**: p. 199-208.
63. Lisa, V. and S. Shamim, *Investigation of Bond Properties of Alternate Anchorage Schemes for Glass Fiber-Reinforced Polymer Bars.* ACI Structural Journal, 2015. **112**(1).
64. M. R. Ehsani, H.S., S. Tao, *Bond of Hooked GFRP Rebars to Concrete.* ACI Materials Journal, 1995. **92**(4).
65. Machial, R., M.S. Alam, and A. Rteil, *Revisiting the shear design equations for concrete beams reinforced with FRP rebar and stirrup.* Materials and Structures, 2012. **45**(11): p. 1593-1612.

66. Malumbela, G., M. Alexander, and P. Moyo, *Variation of steel loss and its effect on the ultimate flexural capacity of RC beams corroded and repaired under load.* Construction and Building Materials, 2010. **24**(6): p. 1051-1059.
67. Malvar, L.J., *Tensile and Bond Properties of GFRP Reinfrocing Bars.* ACI Materials Journal, 1995. **92**(3).
68. Mapei, *Adesilex PG1 - Two component thixotropic epoxic adhesives for structural bonding*. 2013, Lusomapei S.A.: Milan.
69. Marí, A.*, et al.*, *Shear design of FRP reinforced concrete beams without transverse reinforcement.* Composites Part B: Engineering, 2014. **57**(0): p. 228-241.
70. Matos, B.*, et al.*, *Structural response of hyperstatic concrete beams reinforced with GFRP bars: Effect of increasing concrete confinement.* Composite Structures, 2012. **94**(3): p. 1200-1210.
71. Michael, A.C. and S. Shamim, *Behavior of shear-critical RC beams strengthened with FRP-experimentation.* Structural Journal, 2014. **111**(6).
72. Nayera Mohamed, A.S.F.B.B. and W.N. Kenneth, *Drift Capacity Design of Shear Walls Reinforced with GFRP Bars.* Structural Journal, 2014. **111**(6).
73. Nogichi, T.*, et al.*, *A Practical Equation for Elastic Modulus of Concrete.* ACI Structural Journal, 2009. **V.106, No. 5**: p. 7.
74. Olivito, R.S. and F.A. Zuccarello, *On the Shear Behaviour of Concrete Beams Reinforced by Carbon Fibre-Reinforced Polymer Bars: An Experimental Investigation by Means of Acoustic Emission Technique.* 2010. **46**(5): p. 470-481.
75. Oller, E.*, et al.*, *Shear design of reinforced concrete beams with FRP longitudinal and transverse reinforcement.* Composites Part B: Engineering, 2015. **74**: p. 104-122.
76. Pecce, M., Manfredi, G., and Consenza, E. , *Experimental Response and Code Models of GFRP RC Beams in Bendino.* ASCE Journal of Composites for Construction, 2000. **4**(n. 4): p. 182-190.
77. Pilakoutas, K., Neocleous, K., Barnes, B. and O'Neil , E.F., *Design philosophy issues of fibres reinforced polymer reinforced concrete structures.* Journal of Composites for Construction, 1997. **6(3)**: p. 154-161.
78. Portnov, G.*, et al.*, *FRP Reinforcing bars - designs and methods of manufacture (Review of Patents)*. 2013.
79. Quantrill, R.J. and L.C. Hollaway, *The flexural rehabilitation of reinforced concrete beams by the use of prestressed advanced composite plates.* Composites Science and Technology, 1998. **58**(8): p. 1259-1275.
80. Ramôa, J.A., Inês; Sá, Mário; Branco, Fernando; Gonilha, José; Garrido, Mário;, *Pontes em plásticos reforçados com fibras (FRP) e em betão-FRP*, in *1ª Jornadas de Materiais na Construção*. 2011: FEUP - Porto.
81. Santos, P., *Avaliação Experimental do Comportamento de Vigas Contínuas com secção em T de Betão Armado com Varões de GFRP, M. Sc. Dissertation*. 2010, UMa - Madeira University Madeira (in Portuguese).
82. Santos, P.*, et al.*, *Ductility and moment redistribution capacity of multi-span T-section concrete beams reinforced with GFRP bars.* Construction and Building Materials, 2013. **49**(0): p. 949-961.
83. Santos, P.*, et al.*, *Ductility and moment redistribution capacity of multi-span T-section concrete beams reinforced with GFRP bars.* Construction and Building Materials, 2013. **49**: p. 949-961.
84. Schoeck, *Schoeck Combar*. 2013.
85. Schoeck, *Schöck's website*. 2014, Schoeck.
86. Shehata, E., R. Morphy, and S. Rizkalla, *Fibre reinforced polymer shear reinforcement for concrete members: behaviour and design guidelines.* Canadian Journal of Civil Engineering, 2000. **27**(5): p. 859-872.

87. Soudki, K.A., *FRP reinforcement for prestressed concrete structures.* Progress in Structural Engineering and Materials, 1998. **1**(2): p. 135-142.
88. Spadea, G*., et al.*, *Structural effectiveness of FRP materials in strengthening RC beams.* Engineering Structures, 2015. **99**: p. 631-641.
89. Stratford, T.a.B., C., *Shear Analysis of Concrete with Brittle Reinforcement.* Journal of Composites for Construction, 2003. **7**(4): p. 323-330.
90. TML, *Strain gauge performance characteristics*. 2016.
91. Toutanji, H.a.D., Y., *Deflection and Crack-Width prediction of Concrete Beams reinforced with Glass FRP rods.* Journal of Construction and Building Materials, 2003. **17**: p. 69-74.
92. Vijay, P.V. and V.S.G. Hota, *Bending Behavior and Deformability of Glass Fiber-Reinforced Polymer Reinforced Concrete Members.* Structural Journal, 2001. **98**(6).
93. Wang, H. and A. Belarbi, *Flexural durability of FRP bars embedded in fiber-reinforced-concrete.* Construction and Building Materials, 2013. **44**: p. 541-550.
94. Wang, X*., et al.*, *The influence of fiber type and conformation on the damping property of FRP composite.* Journal of Wuhan University of Technology (Material Science Edition), 2012(3): p. 450.
95. Wang, X*., et al.*, *Shear behavior of basalt fiber reinforced polymer (FRP) and hybrid FRP rods as shear resistance members.* Construction and Building Materials, 2014. **73**: p. 781-789.
96. Wegian, F.M. and H.A. Abdalla, *Shear capacity of concrete beams reinforced with fiber reinforced polymers.* Composite Structures, 2005. **71**(1): p. 130-138.
97. Xie, J.-h. and R.-l. Hu, *Experimental study on rehabilitation of corrosion-damaged reinforced concrete beams with carbon fiber reinforced polymer.* Construction and Building Materials, 2013. **38**(0): p. 708-716.
98. Yost, J.R., S.P. Gross, and D.W. Dinehart, *Shear Strength of Normal Strength Concrete Beams Reinforced with Deformed GFRP Bars.* Journal of Composites for Construction, 2001. **5**(4): p. 268.
99. Yost, J.R., Gross, S.P and Dinehart, D. W., *Efective Moment of Inertia for Glass Fiber-reinforced Polymer-reinforced Concrete Beams.* ACI Structural Journal, 2003. **100(6)**: p. 732-739.
100. Zhang, H., L. He, and G. Li, *Bond failure performances between near-surface mounted FRP bars and concrete for flexural strengthening concrete structures*. 2015.
101. Zhao, W., Pilakoutas, K. and Waldron, P. . *FRP Reinforced Concrete: Calculations for Deflections*. in *Proceedings of the 3rd Symposium on Non-metallic (FRP) reinforcement for concrete structures (FRPRCS-3)*. 1997.
102. Zhou, A. *Stiffness and Strength of Fiber Reinforced Polymer Composites Bridge Deck Systems, PhD Thesis in Engineering Mechanics*. 2002.
103. Zhu, W*., et al.*, *Effect of corrosion of reinforcement on the mechanical behaviour of highly corroded RC beams.* Engineering Structures, 2013. **56**(0): p. 544-554.